Spring 4-15-2014

Axonal Damage in Repetitive Concussive Traumatic Brain Injury: Characterization and Contributing Factors

Rachel Bennett
Washington University in St. Louis

WASHINGTON UNIVERSITY IN ST. LOUIS

Department of Biology and Biomedical Sciences
Neurosciences

Dissertation Examination Committee:
David Brody, Chair
Marc Diamond
Aaron DiAntonio
Robyn Klein
Steven Mennerick

Axonal Damage in Repetitive Concussive Traumatic Brain Injury: Characterization and Contributing Factors

by

Rachel Elise Bennett

A dissertation presented to the
Graduate School of Arts and Sciences
of Washington University in
partial fulfillment of the
requirements for the degree
of Doctor of Philosophy

May 2014

St. Louis, Missouri

TABLE OF CONTENTS

LIST OF FIGURES

LIST OF TABLES

ACKNOWLEDGEMENTS

I would like to acknowledge several individuals who have contributed to this work during my six years as a graduate student and without whom this would not have been possible. Foremost, I would like to thank my mentor Dr. David Brody, who has encouraged my scientific growth, supported my choices outside the lab, and been an incredible source of guidance during my graduate studies. I know that not all experiments turned out as planned and that many questions are left unanswered—I hope that this work will be a useful starting off point for future researchers in your lab.

I would also like to thank my thesis committee members for their honest opinions and for pushing me to think more deeply about my research. I am particularly thankful to Steven Mennerick who taught me how to perform slice electrophysiology and who graciously allowed me to spend time in his lab as I worked with this technique for more than a year.

I am especially grateful to the current and former members of the Brody lab who have kept me grounded throughout my graduate work. In particular, I would like to thank Hien Tran and Yoshitsuga Shitaka for their work in developing methods and analysis techniques for the repetitive concussion injury model. Their preliminary findings laid the foundation for the following studies.

I also want to express my deep appreciation to Christine Mac Donald for sharing her expertise in diffusion tensor imaging and for her willingness to help me even when it meant staying in lab until 3 in the morning. For her contributions to MRI acquisition and analysis, Dr. MacDonald shares co-authorship for the work in Chapter 3 which was published in the Neuroscience Letters in 2012.

I would also like to thank Thomas Esparza for his sense of humor, troubleshooting advice, and for his hard work breeding 3xTG-ApoE mice. Both Thomas' help and that of co-authors Hal Lewis, Eddie Kim, Christine MacDonald, and Patrick Sullivan (Duke University)

made possible the studies in Chapter 7. This research was published in the Journal of Neuropathology and Experimental Neurology in 2013.

I am also extremely grateful to Krikor Dikranian and Marilyn Levy for showing me how to prepare samples for electron microscopy and for their patient assistance in this method. Truly you are both artists and I have so much more to learn from you.

Finally I would like to thank Jean-Pierre Julien (Laval University) for graciously sharing the CD11b-TK mouse line with us.

This work would not have been possible without financial support from NIH F31-NS076047 (Bennett), NIH R01 NS065069 (Brody), a Burroughs Wellcome Career Award in the Biomedical Sciences (Brody), NIH K08-NS049237 (Brody), Health South Research Grant (Brody), and an NIH Neuroscience Blueprint Core Grant to Washington University (P30 NS057105).

DEDICATION

To my husband Andy and my son Calvin, who have shown me unconditional love and support throughout this experience.

ABSTRACT OF THE DISSERTATION

Axonal Damage in Repetitive Concussive Traumatic Brain Injury:

Characterization and Contributing Factors

by

Rachel Elise Bennett

Doctor of Philosophy in Biology and Biomedical Sciences

Neurosciences

Washington University in St. Louis, 2014

Professor David Brody, Chair

There are an estimated 1.6-3.8 million concussions in the United States annually. Individuals who experience a single concussion are at low risk for long-term consequences. However, there is mounting evidence that experiencing multiple concussions can lead to persistent symptoms, cognitive impairment, and increased risk for neurodegenerative disease. The underlying pathophysiology of concussions is not well understood.

To study the mechanisms that lead to these long-term consequences, a mouse model of repetitive concussive traumatic brain injury (rcTBI) was developed. Initial studies sought to characterize the histological and functional changes that occur after two closed-skull impacts in mouse. Similar to human traumatic brain injury, rcTBI produced axonal injury evident by amyloid precursor protein, neurofilament, and silver staining abnormalities in the absence of gross structural changes or cell loss. Microglia and astrocytes both became activated and were prominent in injured white matter by 7 days. Behaviorally, injury resulted in acute Morris Water Maze deficits that were not completely recovered by 7 weeks post-injury. Functionally, the velocity of axonal compound action potentials was slowed in both myelinated and unmyelinated axons. These alterations were accompanied by changes in white matter that were detectable by *in vivo* diffusion tensor magnetic resonance imaging (MRI). At 7 days post-injury, mean

diffusivity and the diffusion of water parallel to axons in the corpus callosum and external capsule was reduced. However, these parameters did not correlate with increases in silver staining or microglial activation and indicate a need to develop better histological methods for assessing axonal injury after mild trauma. Future experiments will be conducted to quantify axonal injury by array tomography, a method outlined here briefly.

The second goal of this work was to determine what factors might contribute to axonal injury in concussion. Specifically, the hypothesis that microglia may increase axonal injury acutely following rcTBI was tested. The CD11b-TK mouse line, a valganciclovir-inducible model of microglial depletion, was used to reduce microglia within the corpus callosum and external capsule by 35%. Quantification of silver staining determined that this had no effect on axonal injury at 7 or 21 days after rcTBI. Further reduction by 56% also did not alter axonal injury detectable by silver staining, APP or neurofilament labeling, or by electron microscopy. We additionally tested several pharmacological compounds to determine whether they could reduce the microglial response. None of the compounds tested—including minocycline, (RS)-2-Chloro-5-hydroxyphenylglycine (CHPG), brilliant blue g (BBG), and microRNA-124 (miRNA-124)—were able to reduce the number of iba-1-positive microglia present in the corpus callosum after injury, which were quantified by stereology. Silver staining was unaffected. Use of the targeted toxin, Mac-1-Saporin, was found to dramatically reduce microglial number but also result in non-specific neuronal loss days 7 after rcTBI. Collectively, these experiments indicate that microglia appear to play a neutral role in regards to axonal injury acutely after repeat concussion. To test the role of microglia in the long-term, additional tools to manipulate the microglial response will need to be developed.

Last, the contribution of Apolipoprotein E to axonal injury after moderate-severe traumatic brain injury was assessed in a transgenic mouse model carrying three human familial AD mutations ($PS1_{M146V}$, tau_{P301L}, and APP_{SWE}). The Apolipoprotein E4 (*APOE4*) genotype is a risk factor for poor outcome following traumatic brain injury, especially in young patients. By

analogy to *APOE4's* effects on the risk of Alzheimer's disease, one hypothesis is that *APOE* genotype influences amyloid-beta (Aβ) and tau deposition following injury. Surprisingly, the amount of amyloid-beta and tau as measured by stereology was similar between mice possessing the *APOE2, 3,* or *4* allele. However, *APOE4* mice had significantly greater numbers of APP-positive axons. These results suggest that the *APOE4* genotype may have a primary effect on the severity of axonal injury in the setting of acute traumatic brain injury.

Altogether, this work presents the characterization of a mouse model of repetitive concussive traumatic brain injury that can be utilized to determine what factors contribute to pathophysiological changes and to aid in the design of future therapeutics.

CHAPTER 1

Introduction

1.1 TRAUMATIC BRAIN INJURY

Annually, there are more than 2.4 million traumatic brain injuries (TBI) in the US alone, producing an estimated lifetime total cost of $60 billion to the economy (Coronado, et al. 2011; Coronado, et al. 2012). Of these, 75% of all TBIs may be mild TBIs, or concussions, costing nearly $17 billion (Centers for Disease Control and Prevention 2003). Leading causes of traumatic brain injuries are falls, motor vehicle accidents, and direct head impact during work, sports, or recreational activities (Coronado et al. 2011). Children and young adults 10-19 years old are particularly prone to mild TBI and concussion, and account for 71% of all sports and recreational TBI emergency department (ED) visits and hospitalizations (Gilchrist, et al. 2011). Of these, 70% are males. Overall, it is difficult to estimate the total number of mild TBIs including concussions that occur each year in the United States given that not all are severe enough to result in ED visits or hospitalizations, though estimates range from 1.6-3.8 million annually (Thurman, et al. 1998; Langlois, et al. 2006). Thus, the burden of TBI and concussion is considerable, and identification of new therapeutic strategies is imperative.

TBIs can be classified along a spectrum of mild to moderate to severe brain injury, though exact clinical definitions are the subject of debate. Traditionally, clinicians use the Glasgow Coma Score (GCS) to assess level of coma and consciousness (Teasdale, et al. 1974). Scores of 3-8 indicate a severe traumatic brain injury and are often the result of motor vehicle accidents or penetrating skull injuries that are characterized by contusions to the brain, hemorrhage, vasogenic and cytotoxic edema, and can be accompanied by skull fracture. Moderate brain injuries may have some or all of the characteristics of severe injury and GCS

scores ranging between 9-12 (Rimel, et al. 1982). In both severe and moderate brain injury, abnormalities are typically evident by computed tomography (CT) scan or magnetic resonance imaging (MRI). Finally, mild brain injuries and concussion, a form of mild TBI, are characterized by alterations to mental status as a result of acceleration/deceleration forces or a direct impact to the head or body (McCrory, et al. 2009). Injury may be present with or without small contusions, hemorrhages, and a <30-minute loss of consciousness. GCS scores range from 13-15 and CT or conventional MRI abnormalities are most often absent (Rimel et al. 1982; Newton, et al. 1992; Mittl, et al. 1994; Iverson, et al. 2000; Bazarian, et al. 2006).

1.2 CONSEQUENCES OF TRAUMATIC BRAIN INJURY

Long-term changes associated with traumatic brain injury have a broad range and likely depend on the specific injuries sustained by each individual. In some, TBI appears to accelerate age-related cognitive decline (Moretti, et al. 2012). In others, TBI may contribute to the development of Alzheimer's disease, which is supported by both retrospective and prospective studies that point to moderate-severe TBI as a leading environmental risk factor for AD (Mortimer, et al. 1991; Plassman, et al. 2000; Fleminger, et al. 2003). A recent study using uniform data sets from the National Alzheimer's Coordinating Centers (NACC) determined that individuals who suffer from traumatic brain injury (TBI) with persistent symptoms are more 3 times more likely than individuals with no history of TBI to develop dementia of the Alzheimer's type (Sayed, et al. 2013). Additionally, a number of psychiatric disorders are associated with moderate-severe traumatic brain injury including schizophrenia and depression, particularly among young individuals injured at 11-15 years of age (Orlovska, et al. 2013). These long-term effects appear to be distinct from changes associated with mild TBI.

Immediately after a concussion, headache, inability to focus, dizziness, and sleep disturbances are frequent complaints (McCrory et al. 2009). Generally, 91% of individuals will be asymptomatic after 1 week (McCrea, et al. 2003). However, in some, symptoms persist for

months or years and as many as 20% or more of these may not return to work within a year of injury (van der Naalt, et al. 1999; Iverson 2005; Nolin, et al. 2006; Daneshvar, et al. 2011). In particular, concussed athletes who return to play within a week and experience a second concussion are at greater risk for persistent symptoms and worse outcome (Guskiewicz, et al. 2003). Increased risk of second impact syndrome is also a concern, a rare condition which involves severe, usually fatal, brain injury despite a minor impact (Saunders, et al. 1984; Cantu 1998). Further, individuals who have experienced multiple concussions in their lifetime are at risk for developing Chronic Traumatic Encephalopathy (CTE), a disorder characterized by accumulation of the protein tau particularly around blood vessels and at the depths of sulci, and by alterations in behavior often resulting in violent or aggressive mood swings and increased risk-taking (McKee, et al. 2013b). CTE is best characterized in boxers (*i.e.* dementia pugilistica), but there is increasing awareness of incidence in football players, wrestlers, and hockey players as well as military servicemen (Corsellis, et al. 1973; Roberts, et al. 1990; Omalu, et al. 2005; Omalu, et al. 2006; McKee, et al. 2009; Goldstein, et al. 2012; McKee et al. 2013b). What specific pathological features give rise to persistent symptoms and, potentially, to CTE following concussions are unknown.

1.3 AXONAL PATHOPHYSIOLOGY IN TRAUMATIC BRAIN INJURY

While severe injuries deform brain tissue leading to gross structural alterations, cell loss, and compromise blood brain barrier integrity, mild injuries appear to be disruptive to axons. To understand the biomechanical forces acting on the brain, some of the earliest studies of TBI were conducted using gelatin models of brain tissue subjected to angular acceleration (Holbourn 1943). Later, experiments conducted in both gelatin models and in primates determined that rapid rotational acceleration of the head results in sheer strain forces that are sufficient to produce axonal injury in the absence of other pathologic abnormalities (Gennarelli, et al. 1982; Margulies, et al. 1990). Optic nerve stretch experiments provide further evidence

that these forces lead primarily to cytoskeletal changes with loss of axonal microtubules and neurofilaments immediately after injury (Maxwell, et al. 1997). Cell culture models have also supported this idea, demonstrating that stretching results in microtubule breakage and leads to axonal degeneration (Smith, et al. 1999; Tang-Schomer, et al. 2010; Tang-Schomer, et al. 2012). In these studies, severing of even a single microtubule bundle can result in the accumulation of proteins and organelles normally transported down the length of the axon (Tang-Schomer et al. 2012).

Other events also take place immediately following axonal injury that can compromise axon integrity and ultimately lead to neurodegeneration. Mechanical injury disrupts ionic homeostasis, leading to high extracellular potassium (K^+), excitatory glutamate release, and intracellular calcium (Ca^{2+}) influx (Giza, et al. 2001). This reduces local ATP concentrations as cells attempt to restore ionic homeostasis. These changes in turn activate caspases, calpains, phosphatases, and kinases that can cleave sodium channel proteins, alter neurofilament spacing, and induce mitochondrial swelling in the minutes to hours following injury (Maxwell, et al. 1995; Okonkwo, et al. 1998; Iwata, et al. 2004; Saatman, et al. 2010).

Histologically, damaged axons are typically visualized by labeling with amyloid precursor protein (APP) which is normally carried by fast axonal transport along the length of the axon but can be found in stereotypical axonal swellings after both severe or mild traumatic brain injury (Gentleman, et al. 1993; Blumbergs, et al. 1994; Graham, et al. 1995). These swellings usually have a beads-on-the-string or tadpole-shaped morphology and can be seen in the brain within hours of injury and up to months or even years after the initial insult (Sherriff, et al. 1994; Chen, et al. 2009; Johnson, et al. 2013a). At these later time points, it is unclear whether axonal swellings belong to axons that were injured during the initial insult and have not resolved or whether they are newly injured axons arising from some secondary process of degeneration. In addition to APP, axonal disruption has also been visualized by silver staining and using

antibodies to neurofilament heavy and light chain proteins (Oppenheimer 1968; Strich 1970; Gennarelli et al. 1982; Yaghmai, et al. 1992; Grady, et al. 1993).

Specific to concussion, few histological studies exist due to the non-fatal nature of the injury. However, a classic study revealed silver staining abnormalities and microglial activation in the brains of concussed individuals (Oppenheimer 1968). Another study found APP-positive axonal injury in the white matter tracts of five concussed individuals who died 2-99 days post-injury of other causes (Blumbergs et al. 1994). More recently, McKee and colleagues have observed several cases of CTE where axonal injury was evident by SMI-32, an antibody to neurofilament, indicating a persistent injury to axons that may be a cause or an effect of CTE (McKee et al. 2009; Goldstein et al. 2012). Additional evidence for axonal injury in concussion comes from diffusion tensor MRI studies that have confirmed white matter injury in small cohorts of athletes (Lipton, et al. 2008; Niogi, et al. 2008; Wilde, et al. 2008). Interestingly, in these studies, changes evident by MRI correlated with post-concussive symptoms. Last, animal studies have also been key to our understanding of concussion. Studies in mice, rats, and pigs have confirmed that axonal injury arises as a result of concussive impacts (Laurer, et al. 2001; DeFord, et al. 2002; Creeley, et al. 2004; Raghupathi, et al. 2004; Friess, et al. 2007). Neuronal loss is minimal in these injury models and gliosis appears to be a second common pathological event.

1.4 SUMMARY

Altogether, there is growing realization of the costs of traumatic brain injuries—and of concussion in particular—to society. Better understanding of the pathological events that take place after concussion is key to developing therapeutics that will minimize long-term disabilities. As axonal disruption is evident across the spectrum of TBI at both acute and chronic timepoints, axon injury may provide the substrate for persistent symptoms and pathological change in TBI

patients. My thesis work sought to better understand concussion by focusing on axonal injury. Overall, the goals of this research were to 1) Evaluate an experimental model of concussion in mouse 2) Determine how axons are affected by repetitive concussive injury and 3) Evaluate factors that may contribute to axonal injury including the microglial response and expression of the Apolipoprotein E4 allele.

CHAPTER 2

Modeling Repetitive Concussion in Mouse

2.1 INTRODUCTION

Mild repetitive brain injuries are a growing health concern, particularly among children and adolescents participating in sports. Males participating in high school football for example, experience concussive injuries at a rate of 0.47 per 1000 athlete exposures and nearly 20% will experience recurrent concussions (Gessel, et al. 2007). Prospective studies in high school and collegiate athletes have determined that experiencing multiple concussive impacts can lead to cognitive deficits in these individuals (Collins, et al. 2002; Guskiewicz et al. 2003; Iverson, et al. 2004) . The cognitive effects of concussions are best described in boxers, where as many as 17% may develop persistent symptoms that may be associated with Chronic Traumatic Encephalopathy, a devastating neurodegenerative disease (Roberts et al. 1990; McKee et al. 2009). However, despite the increased incidence of concussion and the growing number of individuals suffering from multiple concussions, little is known about the effects of these injuries on the brain.

To better understand the underlying mechanisms of adverse effects, several groups have developed mouse and rat models of concussive injury. Most models use one of three methods of injury 1) weight drop 2) fluid percussion injury or 3) pneumatic/electromagnetic impact. In weight drop injury models in both rats and mice, the head is typically fixed in a stereotaxic frame and a 15-150g weight is dropped from the height of 30-60 cm onto the fixed or unfixed head of the anesthetized animal (Marmarou, et al. 1994; Tang, et al. 1997a, b; Han, et al. 2000; DeFord et al. 2002; Zohar, et al. 2003; Milman, et al. 2005; Tashlykov, et al. 2007; Israelsson, et al. 2009; Meehan, et al. 2012; Mannix, et al. 2013). This injury model was

originally developed by Marmarou and colleagues to induce moderate-severe brain injury in rats but has since been adapted to produce mild injuries in mice (1994). However, skull fracture is common and the exact number of impacts is variable as the weight can "bounce" several times on the animal's head before coming to a rest.

In fluid percussion injury, a craniotomy is performed and a skull cap attached to a fluid reservoir is glued in place. Dixon et al. originally adapted this technique to produce traumatic brain injury in rats (1987). To produce injury water is rapidly injected, and the physical force of the fluid striking the brain causes injury. Several groups have utilized this technique to study "mild" and repetitive brain injuries but fundamentally, this invasive technique is not likely to truly represent uncomplicated concussive injury (Spain, et al. 2010; Cao, et al. 2012; Shultz, et al. 2012; Selwyn, et al. 2013) .

Other groups have used pneumatic or electromagnetic devices in recent years to impact the skull (Laurer et al. 2001; Uryu, et al. 2002; Longhi, et al. 2005; Creed, et al. 2011; Hylin, et al. 2013). These devices produce single, rapid impacts to the skull and injury severity can be altered by adjusting the depth of impact or the number of impacts delivered to a single animal. Though the head is fixed, these injuries likely represent the most analogous injuries to human concussion available in rodents. However, certain aspects of human concussion are unlikely to be represented in these lissencephalic animals.

Injuries in large animals such as pigs use a separate device that rapidly rotates the head to produce injury (Raghupathi et al. 2004; Friess et al. 2007). Similarly, the classic studies of Gennarelli and colleagues where macaques were subjected to rapid head acceleration also model concussive forces (Gennarelli et al. 1982). For face validity, experimental models in pigs and primates resemble human mild TBI the closest, recapitulating the biomechanical forces that act upon the brain to produce injury. However, ethical and practical concerns limit the use of these animals in widespread concussion research.

Literature regarding experimental concussion models in rat and mouse to date has been summarized in Table A1 of the Appendix. Altogether, in rat and mouse models of concussion, one clear limitation of previous studies is the high rate of contusions and skull fractures that are produced. Thus, many studies of "concussive" or mild TBI are performed in models of complicated mild TBI, which represents a small overall fraction of human clinical TBI cases. Of the injury models that do resemble uncomplicated concussion in that there are no fractures or gross lesions to the brain, single injuries are reported to result in subtle, transient changes in behavior and APP immunohistochemistry while 2 or more repetitive injuries resulted in more persistent injury and impaired performance on behavioral tasks (Laurer et al. 2001; DeFord et al. 2002; Creeley et al. 2004; Longhi et al. 2005). Indeed, studies have reported striking behavioral alterations after injury despite relatively little pathology as seen by immunohistochemistry (Laurer et al. 2001; DeFord et al. 2002; Creeley et al. 2004). However, few studies have investigated axonal pathology despite its prevalence in human TBI including concussion (Oppenheimer 1968; Blumbergs et al. 1994; Johnson, et al. 2013b). Thus, it is possible that the disparity between histological abnormalities and behavioral performance may be due either to a lack of sensitive assays for axonal injury or it may be that concussive injury results in electrophysiological changes and not structural alterations. This work sought to test these hypotheses in a mouse model of repetitive closed-skull injury—a model that does not produce gross brain lesions and uses young 6-8 week old wild-type mice. Several histological methods were employed to visualize injury induced changes and compound action potentials were measured in the corpus callosum to characterize axonal injury.

2.2 METHODS

Animals

Male C57Bl/6j wild-type mice (Jackson, cat# 000664) 6 to 8 weeks of age were used for all experiments. Mice were fed food and water ad libitum and housed under a 12-hour light dark cycle. All experiments were approved by the Washington University Animal Studies Committee.

Electromagnetic Repetitive Closed-Skull TBI

Mice were randomly assigned to either rcTBI or sham injuries so that each cage of 5 mice contained both groups. Anesthesia was induced using 5% isoflurane and the mouse was placed in a stereotaxic frame with rounded Kopf head holders (David Kopf Instruments). Isofluorane was then maintained at 2% for the duration of the experiment using a nose cone. Body temperature was controlled at 37℃ using a fee dback temperature controller (Cell Microcontrols). Heads were shaved, swabbed with betadine, and a midline skin incision was made to expose the skull.

Impacts were performed using an electromagnetic impactor fitted with a custom tip (Figure 2.1). To construct the impactor tip, rubber spheres were purchased from Precision Associates, Inc. (molded ball 0.375 diameter, 50 Duro salmon silicon) and cut in half. The cut side was glued to the base of a 9mm steel impactor tip. The impactor was lowered at a 20° angle so that the tip was just touching the skull at -1.8 mm bregma, -3.0 mm to midline. A hand lens was used to verify the position and an impact was performed at a depth of -3.3 mm (5.0 m/s, 100 ms dwell time). Immediately after injury, mice were removed from head bars and anesthesia until normal breathing was restored. Skin was then sutured closed, antibiotic ointment was applied, and mice were allowed to recover on a warming pad before being returned to their cages. 24 hours following the initial impact, a second, identical injury was performed. Skull fractures were not common using this rubber tip (<3%), but all mice with skull

fractures were excluded from experiments. Sham-injured mice underwent the same surgical procedures but did not receive impacts

Behavioral Testing using the Morris Water Maze

All experiments were performed blinded to injury group identity and all mice had indistinguishable sutures on their heads. The water maze used was 109 cm in diameter and the platform was 11 cm in diameter. Hidden platform testing began 48 hours after the second injury and was performed on 4 days with 4 1 minute trials per day. A probe trial was conducted on day 4 after the final hidden platform test. For the probe, the platform was removed and the location of the mouse was tracked for 30 seconds. Following the probe, a visible platform test was also conducted by placing the platform in a new location so that is slightly above the water and marked with a pole. Mice were given 1 minute to find the visible platform.

Histopathology

Mice were killed by isofluorane overdose followed by cardiac perfusion with ice-cold phosphate-buffered saline containing 0.3% heparin. Brains were removed and fixed in 4% paraformaldehyde for 24 hours and equilibrated in 30% sucrose for at least 24 hours. A freezing microtome was used to cut 50 µm coronal slices beginning at the anterior portion of the corpus callosum ending at the posterior portion of the hippocampus. For all histological analysis, sections were sampled every 400 µm.

Cresyl violet staining was performed to assess tissue for contusion and cell loss. For amyloid-precursor protein and NF200, immunohistochemistry was performed as previously described (Mac Donald, et al. 2007a; Mac Donald, et al. 2007b). In brief sections were rinsed in Tris-buffered saline (TBS) twice, incubated in 0.03% H202 in TBS for 10 minutes, rinsed twice in TBS, and then blocked for 1 hour in normal goat serum in TBS containing 0.25% Triton-X (TBS-X). Following blocking, sections went into rabbit anti-APP (1:1000, Invitrogen), rabbit anti-

NF200 (1:20,000, Sigma Aldrich), mouse anti-SMI-32 (1:1000, abcam), rabbit anti-iba-1 (1:1000, Wako), chicken anti-gfap (1:1000, Millipore), or rabbit anti-cleaved capase 3 (1:1000, Cell Signaling) and sections were incubated overnight at 4℃ with gentle shaking. For SMI-32, after blocking, sections were incubated in 1:10 goat anti-mouse Fab IgG (Jackson Immunoresearch) in TBS for 30 minutes. Sections were then rinsed twice in TBS and incubated overnight in SMI-32. After the overnight incubation, sections are rinsed with TBS twice, incubated for 1 hour in goat anti-rabbit (APP, NF200, cleaved caspase 3, iba-1; Vector Laboratories), anti-chicken (gfap) or anti-mouse (SMI-32). After incubation with secondary antibodies, sections were rinsed again, then incubated in streptavidin-horseradish peroxidase (1:400, Vector Labs) for 1 hour. Labeling was visualized with 3-3‘diaminobenzidine tetrahydrochloride (DAB; Sigma Aldrich), sections were mounted on slides, and coverslipped with Cytoseal XYL (Thermo Scientific). For mouse anti-RM014, sections were blocked in 1:10 mouse serum in TBS-X. RM014 antibody was prepared by incubating it with biotinylated goat anti-mouse Fab IgG (Jackson ImmunoResearch) at room temperature for 20 minutes. The antibody-biotin IgG complex was then diluted in blocking solution at a working concentration of 1:1000 and applied to sections overnight. Immunohistochemistry was then performed as described above with the omission of the secondary antibody.

Silver staining was performed using the FD NeuroSilver Kit II (FD NeuroTechnologies) according to the manufacturer's instructions with the following modifications. Sections were post-fixed again for 5 days in 4% PFA before staining and were only incubated in solution C once for 2-minutes. Brain sections were stained in batches so that all batches contained animals from both injury groups to avoid bias due to variability in staining intensity between batches.

Quantitative Analyses of Histopathology

All histopathological analysis was performed blinded to injury status. For silver staining measurements, section images were captured using the Nanozoomer Whole Slide Imaging System (Olympus). 3-4 sections from each mouse beginning with the anterior-most section containing both blades of the dentate gyrus were included in densitometric analysis. These sections spanned approximately bregma -1.1 to -2.3 mm (24). The ipsilateral corpus callosum and external capsule were defined as the area from midline extending laterally to a horizontal line dividing the hippocampus and thalamus. ImageJ (NIH, Bethesda, MD) was used for quantitation of the staining and was expressed in arbitrary units, ranging from 0 (minimum) to 255 (maximum).

Stereological quantification was performed using StereoInvestigator version 8.2 software (MBF Bioscience). The optical fractionator method was employed for quantification of total numbers of Iba1-positive cells with activated microglial morphology per mm^3 of tissue. Details on these stereological methods have been described (22). Briefly, 4 sections per mouse (each separated by 400 μm) were used for ipsilateral cortex and thalamus and sections per mouse were used for estimations in corpus callosum. A grid of 180 μm × 180 μm and a counting frame of 80 μm × 80 μm were used. Gunderson coefficients of error were less than 0.1.

Electrophysiology

Separate mice were injured or underwent sham procedures for electrophysiology experiments. Artificial cerebrospinal fluid (aCSF) was prepared fresh daily (120 mM NaCl, 3.5 mM KCl, 26 mM $NaHCO_3$, 1.25 NaH_2PO_4, 10 mM Glucose). Slicing solution was prepared by adding 0.5 mM $CaCl_2$ and 7 mM $MgCl_2$ to aCSF. Holding solution was prepared by adding 2.5 mM $CaCl_2$ and 1.3 mM $MgCl_2$ to aCSF. All solutions were sterile filtered and bubbled with carbogen (95% oxygen, 5% CO2) for 1 hour prior to use.

To prepare 300 μm slices for electrophysiology, mice were deeply anesthetized with isofluorane and sacrificed by decapitation. Heads were immediately immersed in ice cold slicing solution. Brains were carefully dissected and rinsed in slicing solution before razor blades were used to trim away the anterior and posterior regions of the brain leaving a coronally sectioned block of tissue corresponding approximately to 0 to -3.5 mm bregma. Cyanoacrylate glue was used to secure the posterior trimmed face of the tissue block to the pedestal of the Leica VT1200 vibratome, which was immersed in slicing solution with gentle bubbling. Sections were cut with a blade oscillation amplitude of 1.1 mm and forward speed of 0.06 mm/s. 3-4 sections were cut per animal and transferred by pipette to an incubation chamber containing holding solution at 32-34℃ with constant bubbling. Slices were allowed to equilibrate for 1-4 hours before recording.

During recording, slices were continuously perfused with room temperature oxygenated holding solution. An upright Nikon Eclipse E600FN microscope and digital camera controlled by Metamorph software was used to image slices and determine electrode positioning. A stimulating electrode with a tip diameter of 100 μm was made from 1.5 mm outer diameter borosilicate theta glass. Recording electrodes with tip resistances of ~2 MΩ were made from 1.2 mm outer diameter borosilicate glass. All recordings were acquired using a MultiClamp 700B amplifier (Molecular Devices) and MultiClamp 700B Commander software. Data was collected at 3000 samples/sweep/signal (15 ms), with a 2 kHz sampling interval and were digitized using a Digidata 1322A 16-bit A/D converter (Molecular Devices). Stimulating currents 100 μs in duration were produced using a WPI A365 stimulus isolator (World Precision Instruments).

For measurement of compound action potentials electrodes were placed 1 mm apart in corpus callosum on opposite sides of midline with the stimulating electrode ipsilateral to injury. Electrode depth was adjusted to achieve maximum signal per slice. Input-output curves of CAP amplitude were acquired by making 8 sweeps and the stimulus intensity was adjusted from

0 mA to 4 mA in 0.5 mA steps. The maximum amplitude was calculated by averaging CAP amplitude values at 3-4 mA. Amplitude measures were made by drawing a line from connecting the peaks of the CAP response and measuring perpendicularly from this line to the trough of the CAP to determine the height in mV. Following amplitude measurements, refractoriness was determined by varying the interpulse interval from 8 ms down to 1.5 ms in 0.5 ms steps. Half maximum stimulus intensities were used for all refractoriness measures. Refractoriness was determined by subtracting a control response (single stimulus) from the paired-pulse response and dividing this by the control response. This value was multiplied by 100%. To measure axonal velocity, half maximum CAP recordings were made moving the recording electrode 1.5 mm, 1 mm, or 0.5 mm away from the stimulating electrode. The latency from the stimulus artifact to the peak of the action potential was measured and plotted versus the distance between electrodes. The slope of the line was used to determine the velocity in ms^{-1}.

Statistical Methods

All analyses were performed using Statistica 6.0 (StatSoft, Tulsa, OK). Shapiro-Wilks normality tests were performed to determine if data fit Gaussian distributions. In cases where data were found to be non-normally distributed, nonparametrics statistical analyses were used. Repeated measures ANOVA was used to compare hidden platform Morris water maze performance between groups. Student's t tests and Mann-Whitney U-tests were used to compare all other variables. P values less than 0.05 were considered significant. Error bars represent SEM.

2.3 RESULTS

2.3.1 Repetitive Closed Skull Injury Impairs Morris Water Maze Performance

Similar to Laurer et al. 2001, an impactor tip was fitted with rubber and used to deliver consistent, concussive insults directly to the skull of the mouse (**Figure 2.1 A, B**). Overall, this resulted in <5 % mortality rate and <3 % skull fractures. Mice with skull fractures were not included in the study. All mice experienced a brief period of apnea lasting no longer than 20 seconds immediately following impact and exhibited tonic clonic convulsions for up to 30 seconds following injury.

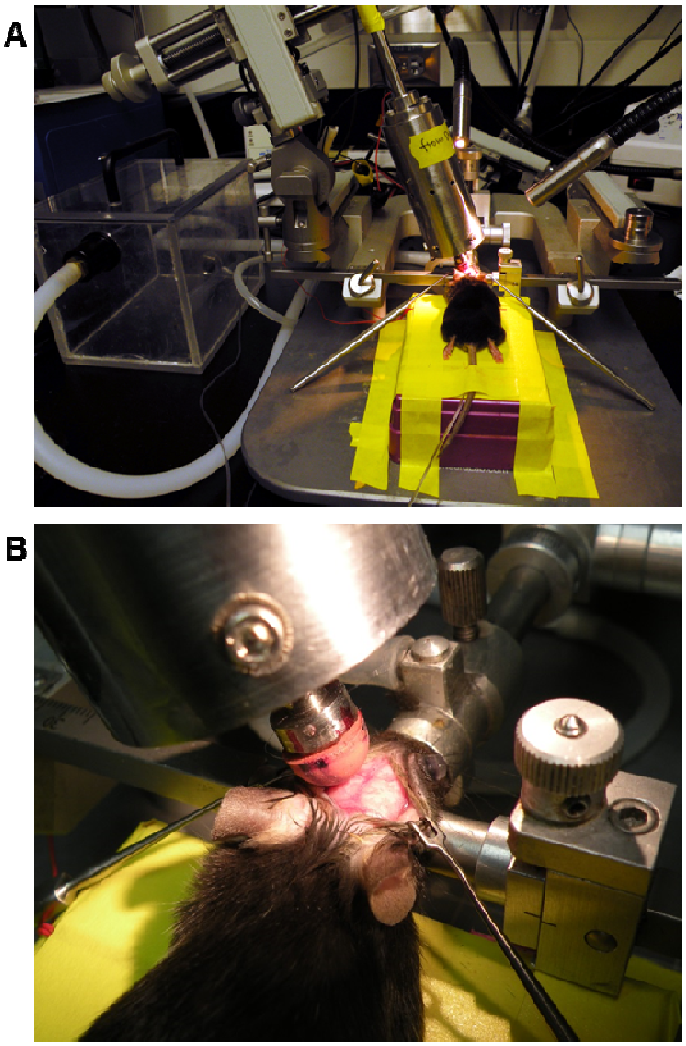

Figure 2.1 Electromagnetic repetitive closed-skull injury. (A) Mice are anesthetized and placed in a stereotaxic frame. (B) Head bars are used to hold the head in place while an electromagnetic device fitted with a rubber tip impacts the skull over the left somatosensory cortex.

Mice subjected to two concussive impacts demonstrated impaired performance in Morris Water Maze (MWM) during the week following injury (rcTBI n=10, sham n=11; **Figure 2.2 A-H**). Mice were tested in the MWM on days 3-6, where day 0 indicates the first day of injury. Under these conditions, repeated measures ANOVA of hidden platform testing revealed a statistically significant effect of day ($p<0.0000$), injury ($p<0.0000$), and a day x injury interaction ($p=0.0101$). Overall, injured mice spent more time than shams searching for the hidden platform (42.92 ± 3.49 s versus 18.70 ± 2.68 s; $p<0.0001$, student's t test) and traveled farther to find the platform ($p<0.0001$, student's t test). However, they also had reduced velocity compared to shams ($p=0.0002$, student's t test), which may be indicative of slight motor deficits. Both shams and injured mice were able to find the visible platform, confirming impaired eyesight was not a factor contributing to worse performance. Sham mice also completed the probe trial successfully, a test of spatial memory, but injured mice did not perform better than chance.

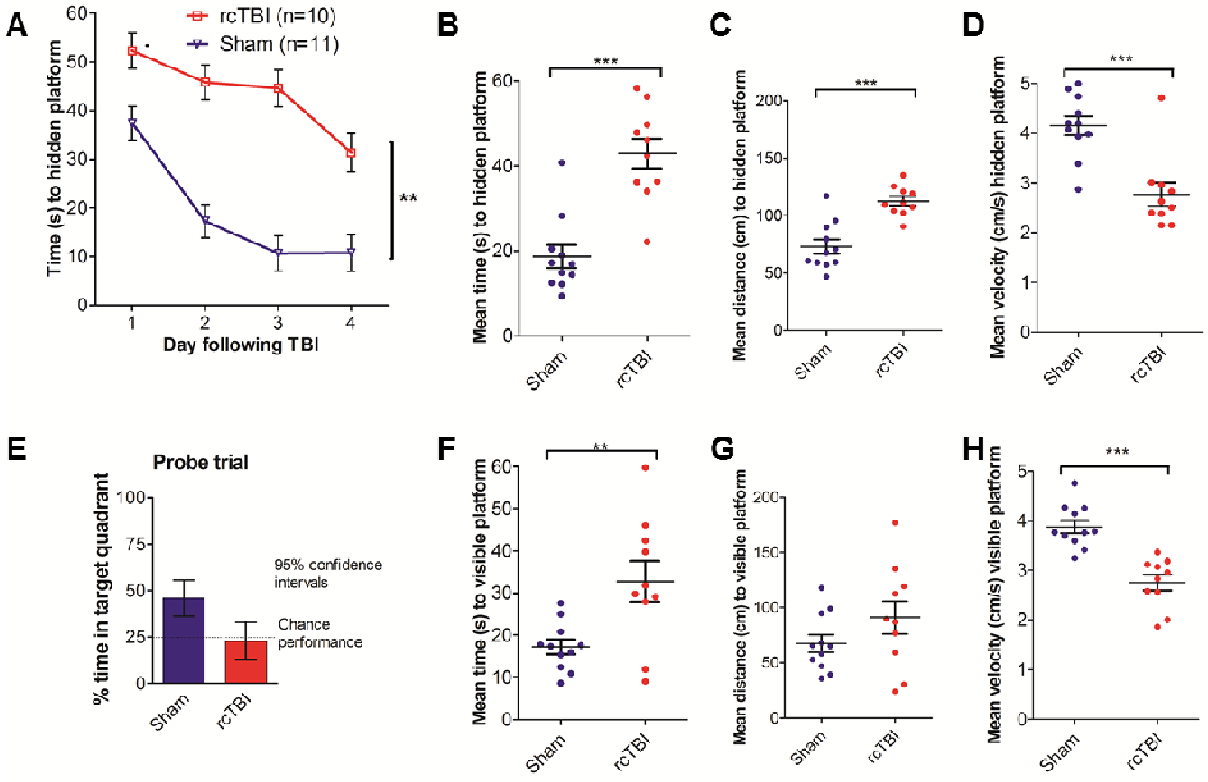

Figure 2.2 Morris Water Maze performance is impaired acutely (7 days) in rcTBI mice. Mice received 2 closed skull impacts (rcTBI) or no impacts (sham) and were tested 3 days after the first injury. (A) Sham injured mice but not rcTBI mice learned over the 4 day testing period

to find the hidden platform. Mean (B) time (C) distance and (D) velocity to the hidden platform were also impaired in rcTBI mice compared to sham controls. (E) Sham mice performed better than chance on the probe trial, but rcTBI mice did not. Mean (F) time (g) distance and (h) velocity to the visible platform. (** $p<0.005$, ***$p<0.0005$).

A second cohort of mice was then randomized to either rcTBI (n=9) or sham (n=9) groups. Morris Water Maze testing beginning 44 days after first injury did not reveal any day x injury interaction (Repeated measures ANOVA p=0.1705, **Figure 2.3 A**). However, analysis of the mean time for injured mice to find the hidden platform revealed a significant difference from shams (student's t test p=0.0051, **Figure 2.3 B**). No differences in distance traveled (p=0.0845, **Figure 2.3 C**) or velocity (p=0.1663, **Figure 2.3 D**) was observed. All mice found the visible platform and too the same amount of time (p=0.4266, **Figure 2.3 F**), traveled the same distance (p=0.4329, **Figure 2.3 G**), and swam at the same speed (p=0.6107, **Figure 2.3 H**) to find it. However, neither group performed better than chance on the probe trial, which may indicate a problem with the MWM experimental setup (**Figure 2.3 E**). Overall, these results indicate that while mice appear to be relatively normal, they may still exhibit signs of cognitive impairment at 7 weeks post-injury. Further testing will be required to definitively characterize behavioral changes at this time point.

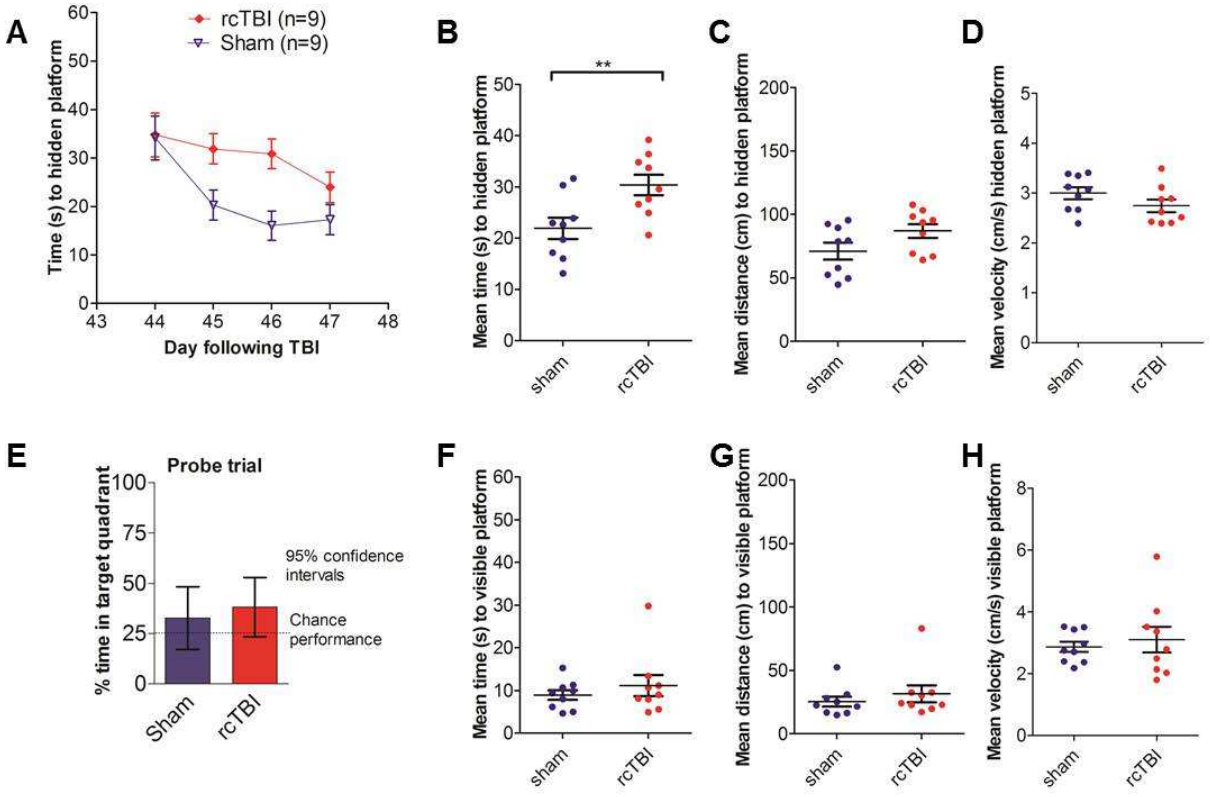

Figure 2.3 Morris Water Maze impairments are mostly recovered by 7 weeks post-injury. Mice that received rcTBI or sham treatment were tested in water maze beginning 44 days after the first injury. (A) Sham injured mice and rcTBI mice learned to find the hidden platform over a 4 day testing period. Mean time (B) to the hidden platform but not distance traveled (C) or velocity (D) was impaired in injured mice compared to shams. Mice did not perform better than chance on a probe trial (E). All mice found the visible platform quickly (F) and injury did not affect distance (G) or velocity (H) measurements.

2.3.2 No Evidence of Histological Abnormalities or Cell Loss

Sections from sham mice and rcTBI mice were assessed for histological abnormalities by cresyl violet staining 7 days post-injury (**Figure 2.4 A-H**). No areas of ischemic injury, hemorrhage, or contusion were present in any region in any of the samples. The hippocampal CA3 and polymorphic layer of the dentate gyrus are susceptible regions to brain injury but did not show any cell loss at 7 days post-injury (**Figure 2.4 E, F**). A stereological comparison of the number of cells in this area confirms this observation; these data can be found elsewhere (Shitaka, et al. 2011). Subtle increases in the cellularity of the corpus callosum were observed

in rcTBI mice compared to shams (**Figure 2.4 H**). Adjacent sections were also stained for cleaved caspase 3, an indicator of cellular apoptosis (**Figure 2.5 A, B**). No labeling was observed in rcTBI mice at 7 days post-injury. Tissue from a mouse subject to middle cerebral artery occlusion (MCAo), a model of cerebral ischemia, confirm the sensitivity of this antibody to apoptotic cells (**Figure 2.5 C**).

2.3.3 Gliosis after Repetitive Closed Skull Injury

At 7 days post rcTBI or sham injury, sections from mice that performed water maze (n=10 and n=11, respectively) were labeled for iba-1, a marker of microglia and macrophage (**Figure 2.6 A, B, E**). The number of iba-1-positive cells present in the corpus callosum and external capsule was quantified by stereology. A significant difference between shams versus rcTBI mice was observed at 7 days post-injury (one-tailed student's t test $p<0.0001$; **Figure 2.6 E**). For a detailed timecourse of iba-1 in the corpus callosum and other regions, see Shitaka et al (2011). In a separate cohort of mice, GFAP-positive astrocytes were quantified by optical density in shams (n=6) and rcTBI (n=6) mice 7 days after injury (**Figure 2.6 B, D, F**). In these mice, the amount of GFAP labeling was significantly increased after injury ($p=0.0077$, **Figure 2.6 F**).

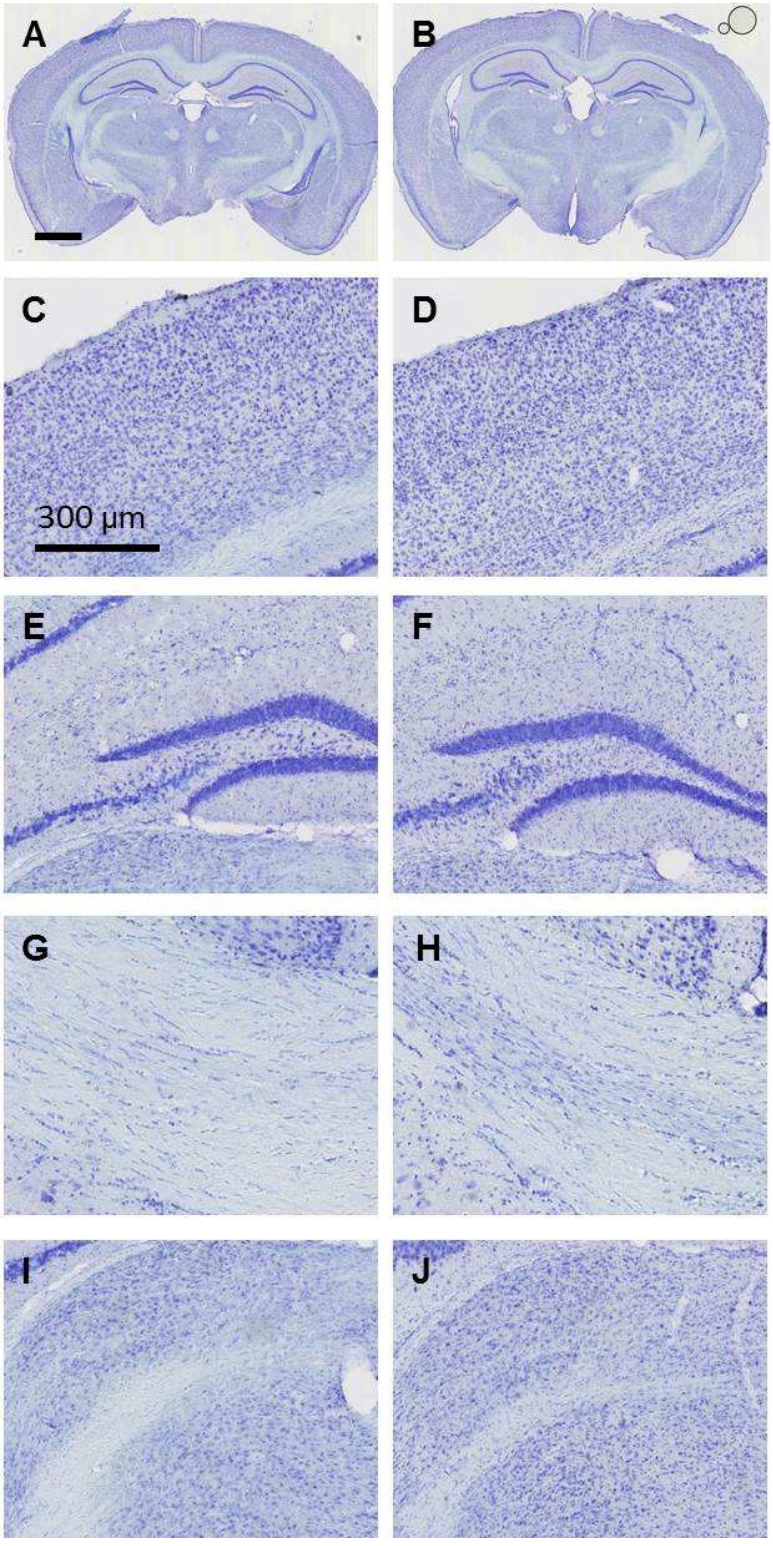

Figure 2.4 Cresyl violet staining in sham and injured mice does not reveal any gross histological abnormalities. Sections from sham mice (A, C, E, G, I) and rcTBI mice (B, D, F, H, J) were stained with cresyl violet 7 days post injury. No cell loss was seen in sections (A), cortex (B), hippocampal dentate gyrus/CA3 (E, F), corpus callosum (G, H), or thalamus (I, J).

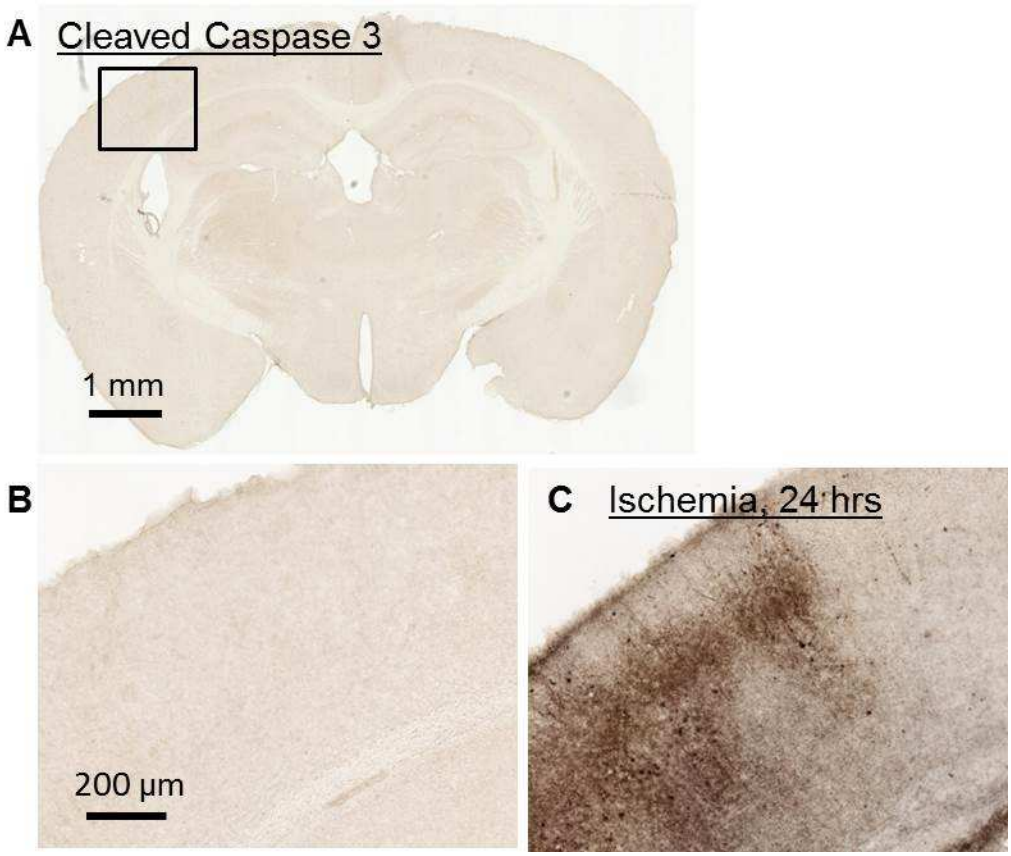

Figure 2.5 Apoptosis is not evident by cleaved caspase 3 labeling in injured mice. Sections from rcTBI mice were stained for cleaved caspase 3, a key protein involved in apoptosis. No labeling was seen in any sections from mice at 7 days (A, B). Inset in (B) is higher magnification view of box in (A), a region of injured external capsule. By contrast, labeling was prominent in a mouse sacrificed 24 hours after MCAo, a model of cerebral ischemia (C).

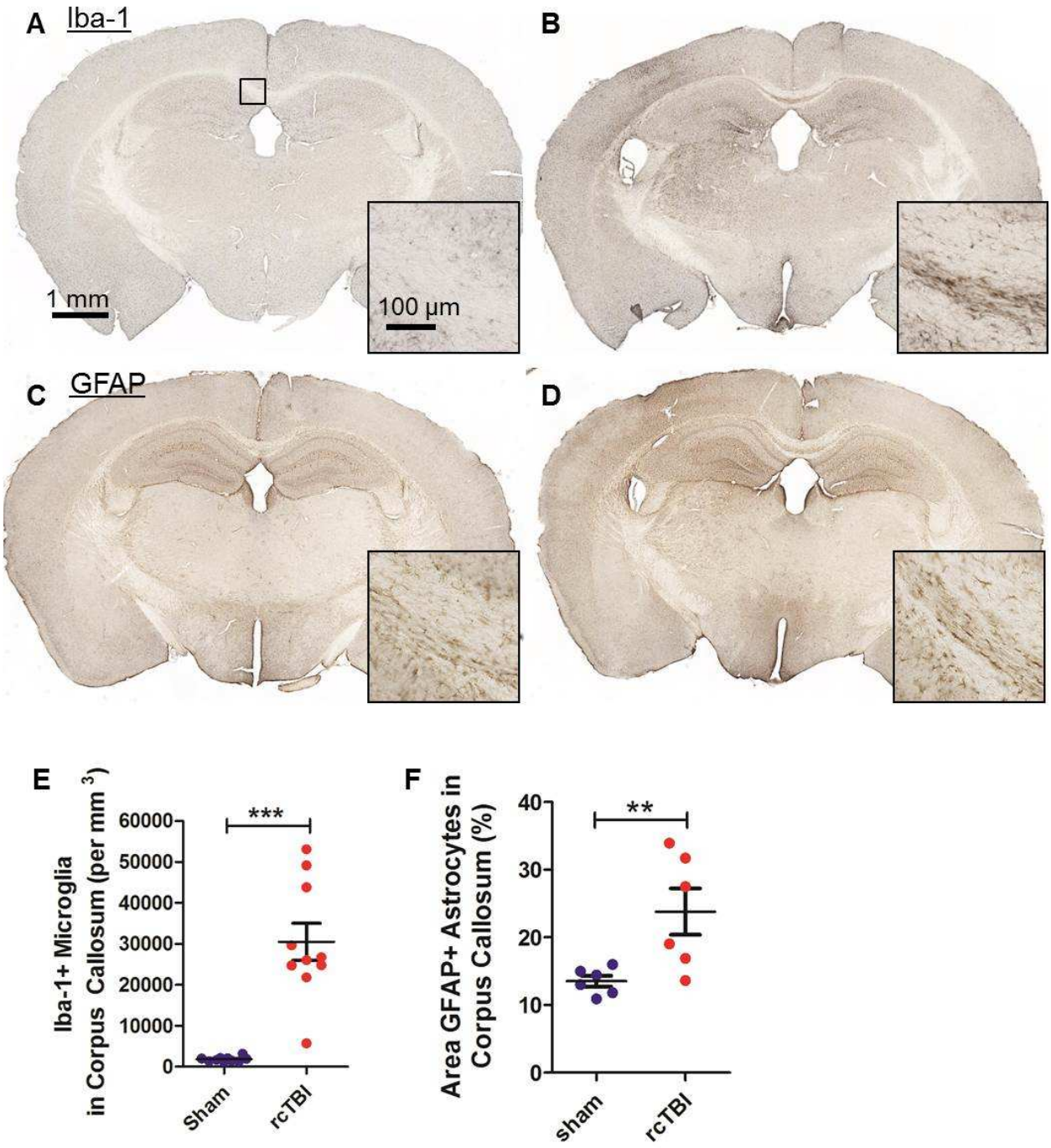

Figure 2.6 Microglia and astrocytes increase 7 days post-injury. Sections from sham (A, C) or rcTBI (C, D) mice were labeled for iba-1 (A, B) or gfap (C, D). Insets are from region boxed in (A). Iba-1 was quantified by stereology (E) to determine the total number of iba-1 positive cells in the corpus callosum and external capsule ipsilateral to injury. Gfap was quantified by optical density (F) which measures the total area fraction containing gfap-positive astrocyte processes. (***p<0.0001, **p<0.01)

2.3.4 Axonal Injury after Repetitive Closed Skull Injury

Silver staining was also performed on mice used in behavioral experiments and sacrificed 7 days post-injury (**Figure 2.7 A, B, C**). Silver staining was increased in shams versus controls at this timepoint (two-tailed student's t test $p<0.0001$, **Figure 2.7 C**). Silver staining is thought to label protein aggregates and has been shown to reflect ultrastructural abnormalities visible by electron microscopy (Shitaka et al. 2011). An additional timecourse of silver staining changes can be found in Shitaka et al. (2011).

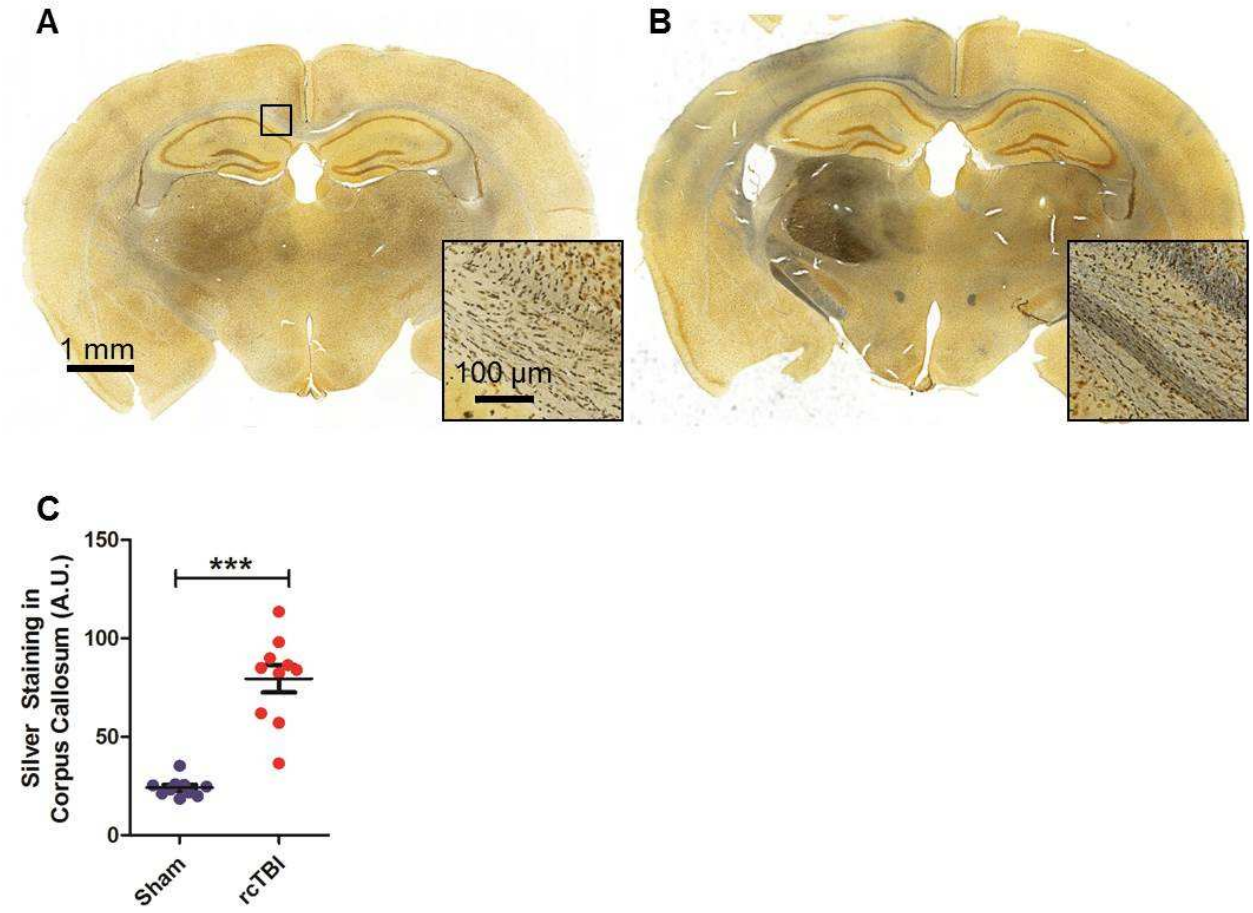

Figure 2.7 Silver staining reveals increased axonal injury in rcTBI mice 7 days post-injury. Silver staining was performed on sham (A) and rcTBI (B) mice. Insets are from region of corpus callosum boxed in (A). Optical density of silver staining (black precipitate) was preformed after subtracting background (gold granules) from each image (C). (***$p<0.0001$)

Mice were sacrificed at 2 days (n=5) or 7 days (n=10, from behavioral experiments) after the first injury and a qualitative survey was carried out for axonal injury markers including amyloid precursor protein (APP), NF200, RM014, and SMI-32 **(Figure 2.8 A-P**). APP is normally transported along the axon and accumulates in swellings after axonal injury. NF200, RM014 and SMI-32 are antibodies to neurofilament. NF200 labels 200 kDa heavy-chain neurofilaments. RM014 has been used to detect areas of neurofilament compaction in traumatic brain injury (Stone, et al. 2001). SMI-32 detects non-phosphorylated neurofilament heavy chain, which has been reported to indicate areas of axonal injury (Budde, et al. 2008; McKee et al. 2009). All antibodies labeled prominent axonal varicosities in pericontusional corpus callosum in a controlled cortical impact (CCI) mouse model of moderate-severe brain injury (**Figure 2.8 A, E, I, M**). No axonal swellings were detectable in sham injured mice sacrificed at 7 days (**Figure 2.8 B, F, J, N**), though diffuse background labeling was evident in SMI-32 labeled sections (**Figure 2.8 N**). Additionally, in all mice including shams, NF200 labeled fibers of the cingulum bundle, which displayed normal axonal morphology distinct from injury (not shown). Clearly abnormal axons were evident in external capsule at 2 days after rcTBI using antibodies to APP, NF200, and SMI-32 (**Figure 2.8 C, G, O**). However by 7 days post-injury, only sparse axonal swellings could be found using these same markers (**Figure 2.8 D, H, P**). No RM014 labeling was found at 2 days or 7 days in these sections (**Figure 2.8 K, L**). At both injury timepoints, changes to axons were only apparent in external capsule overlying the lateral ventricle ipsilateral to impact (shown) which may represent a particularly vulnerable region in this injury model.

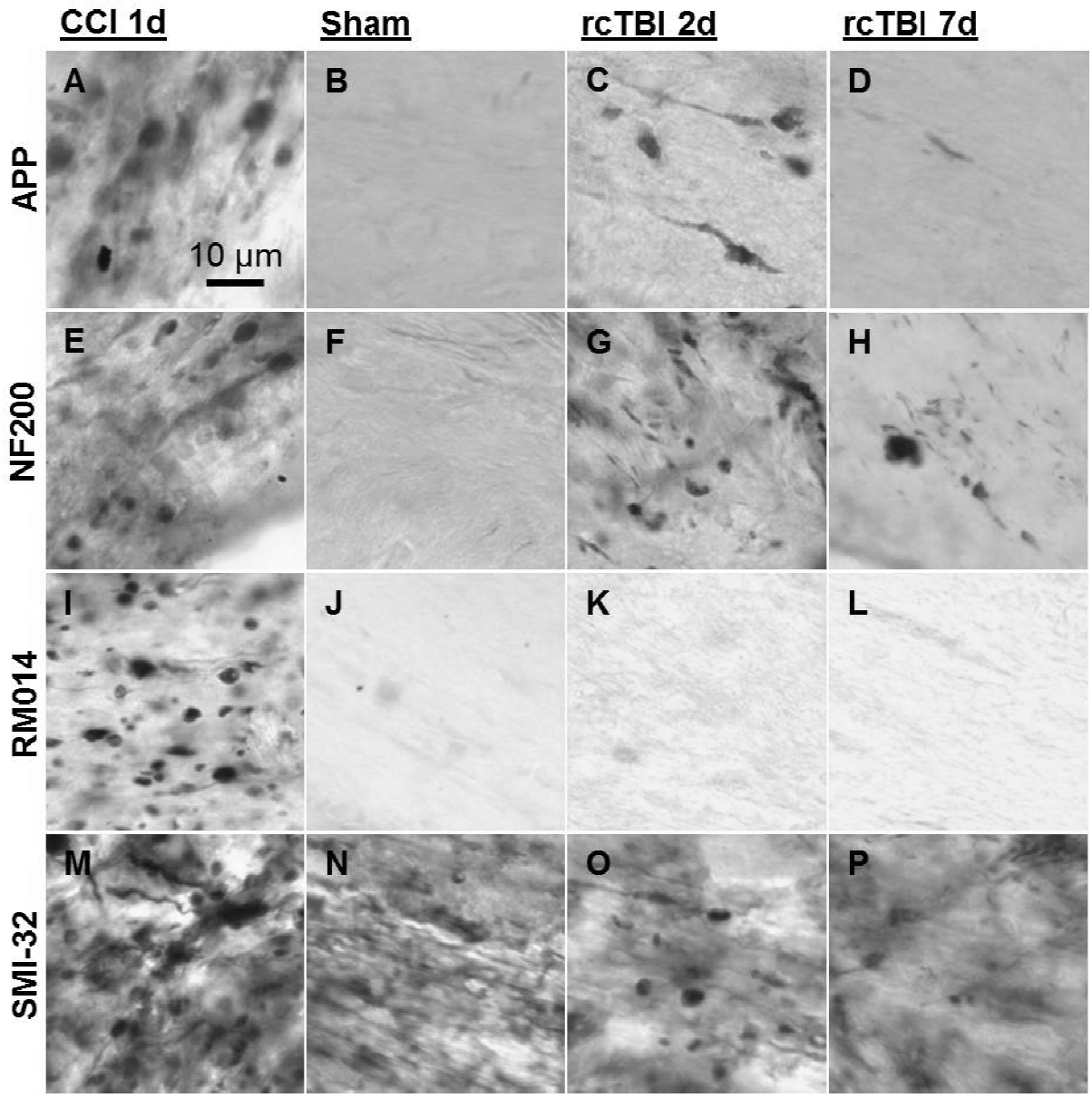

Figure 2.8 Additional markers of axonal injury. Representative images of axonal injury from 1 day CCI (A, E, I, M), 7 day sham (B, F, J, N), 2 day rcTBI (C, G, K, O) or 7 day rcTBI (D, H, L, P) mice. Sections were labeled for amyloid precursor protein (A, B, C, D) or with antibodies to neurofilament NF200 (E, F, G, H), RM014 (I, J, K, L), and SMI-32 (M, N, O, P). Images in CCI mice were captured from pericontusional corpus callosum. All other images were taken from external capsule underlying the site of impact (or sham injury) near the lateral ventricle.

2.3.5 Electrophysiological Integrity of Corpus Callosum Axons 7 days after Injury

Axonal conduction was measured by slice electrophysiology. Compound action potentials (CAPs) were evoked by placing a stimulating electrode in the center of the corpus

callosum in the injured hemisphere and were recorded in the corpus callosum opposite of midline (**Figure 2.9 A**). Peaks corresponding to both myelinated (N1) and unmyelinated (N2) axonal populations were detectable and could be abolished with application of the sodium channel blocker tetrodotoxin (TTX; **Figure 2.9 B, C**).

The height of the CAP response was measured for quantitative analysis in sham (n=7) and rcTBI (n=8) mice (**Figure 2.10 A-E**). This revealed no significant differences between sham and injured mice in both myelinated (one-tailed student's t test p=0.0508, **Figure 2.10 B**) or unmyelinated fibers (one-tailed student's t test p=0.4296, **Figure 2.10 C**). Varying the stimulus intensity from 0 to 4 mA generated input-output curves for each population of axons (**Figure 2.10 D, E**).

Velocity was also determined by varying the distance between stimulating and recording electrodes and measuring the latency to the peak of each CAP (**Figure 2.11 A-E**). A significant difference in the velocity of both myelinated (one-tailed student's t test p=0.0331, **Figure 2.11 D**) and unmyelinated (one-tailed student's t test p=0.0072; **Figure 2.11 E**) axons was observed.

Refractoriness, the ability of an axon to fire action potentials in quick succession, was also measured by varying the interpulse interval from 8 ms to 1.5 ms (**Figure 2.12 A-C**). As the interpulse interval became shorter, fewer axons were able to fire action potentials and the amplitude of the second CAP became smaller (**Figure 2.12 B, C**). This property did not appear to be altered by injury in either axon population.

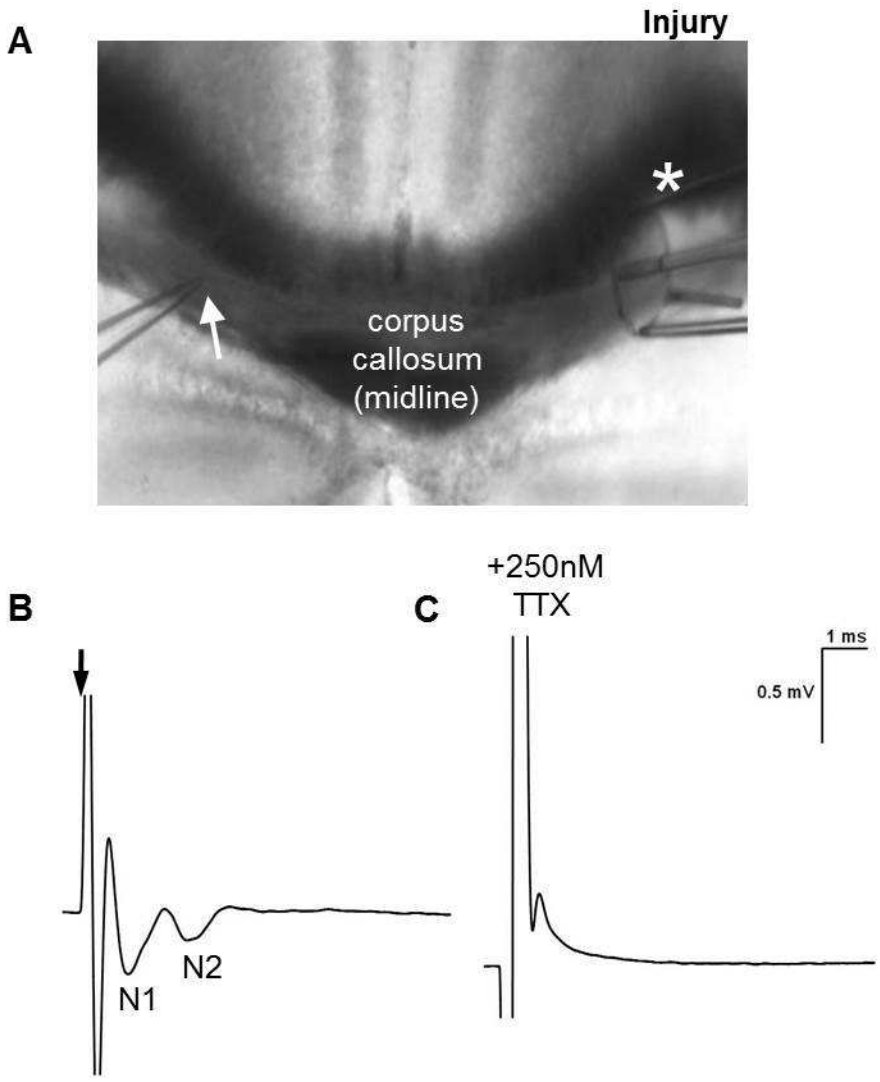

Figure 2.9. Electrophysiological recording of compound action potentials in mouse corpus callosum. (A) A stimulating electrode (asterisk) was placed in the corpus callosum underlying the site of injury and a recording electrode was placed 1 mm away in corpus callosum opposite midline. (B) 100 µs stimulation (arrow) resulted in a brief stimulus artifact followed by an early peak corresponding to myelinated axons (N1) and a later peak corresponding to unmyelinated axons (N2). (C) Both peaks could be eliminated through application of 250 nm TTX to block sodium channels.

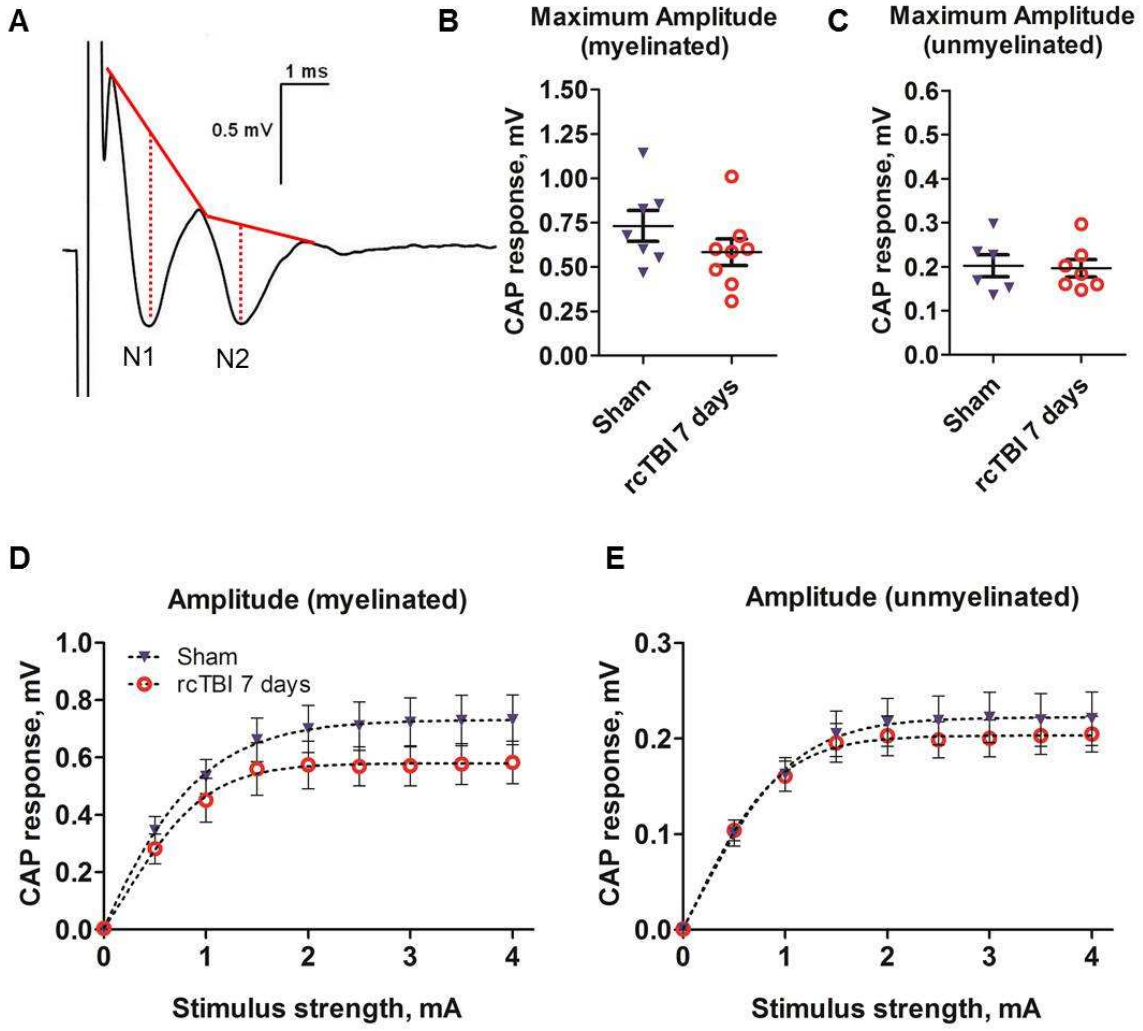

Figure 2.10 No change in compound action potential amplitude 7 days post-injury. (A) Representative trace (average of 8 sweeps) showing myelinated (N1) and unmyelinated (N2) axon response. Amplitude was measured by drawing a line between peaks (solid red line) and measuring from this line to the trough of the CAP (dashed line). The maximum amplitude of the CAP was determined for both myelinated (B) and unmyelinated (C) axons. A range of stimulus currents from 0-4 mA was used to generated input-output curves for myelinated (D) and unmyelinated (E) axons (Dotted line is non-linear fit). (Error bars are standard error of the mean)

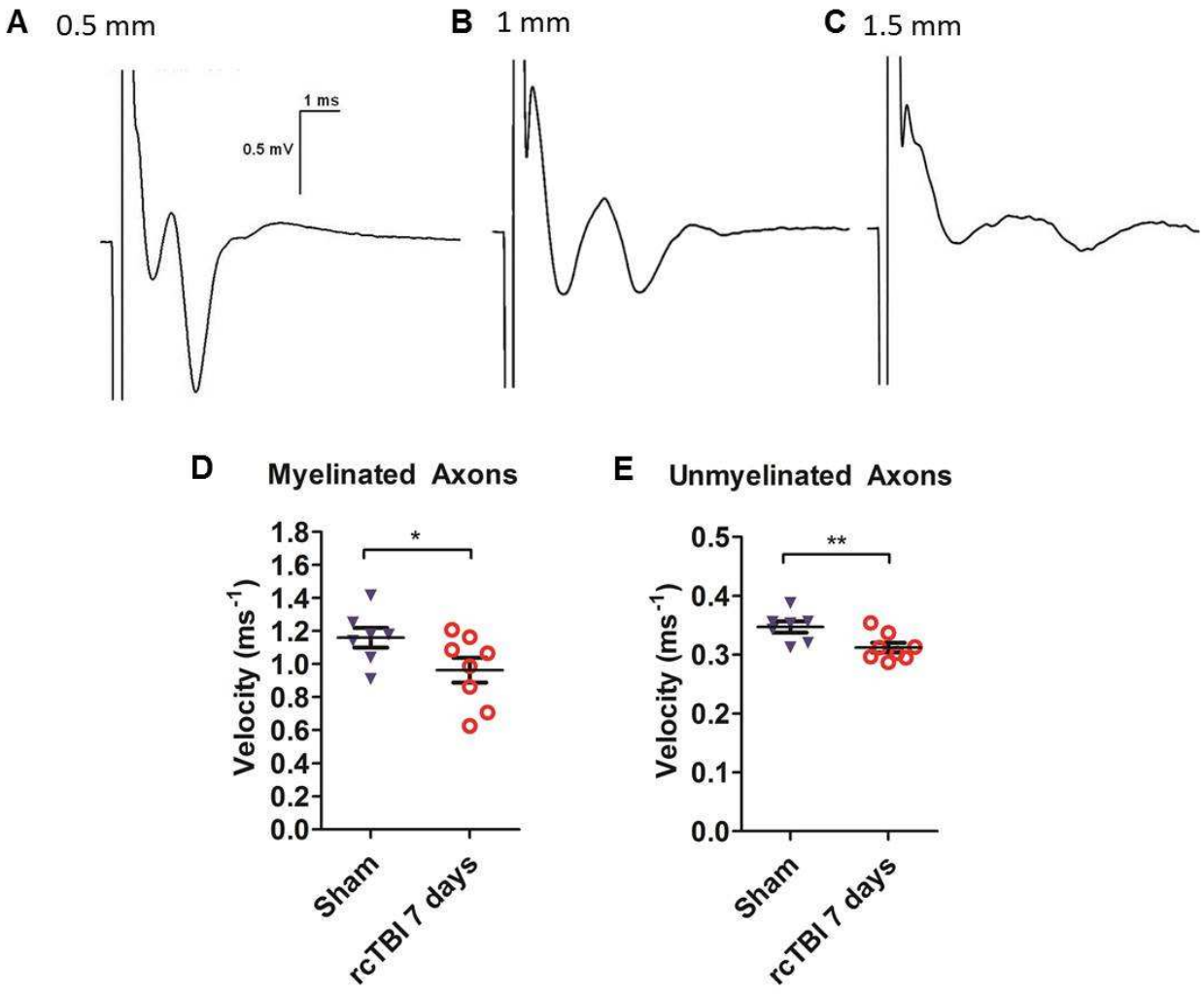

Figure 2.11 Velocity is reduced in both myelinated and unmyelinated axons 7 days post-injury. Moving the recording electrode to 0.5 (A), 1 (B), or 1.5 mm (C) from the stimulating electrode altered the latency to the peak of the CAPs. Velocity was determined by measuring the time from stimulus to CAP peak in the myelinated (D) and unmyelinated (E) fibers. (Error bars are standard error of the mean, *p<0.05, **p<0.01)

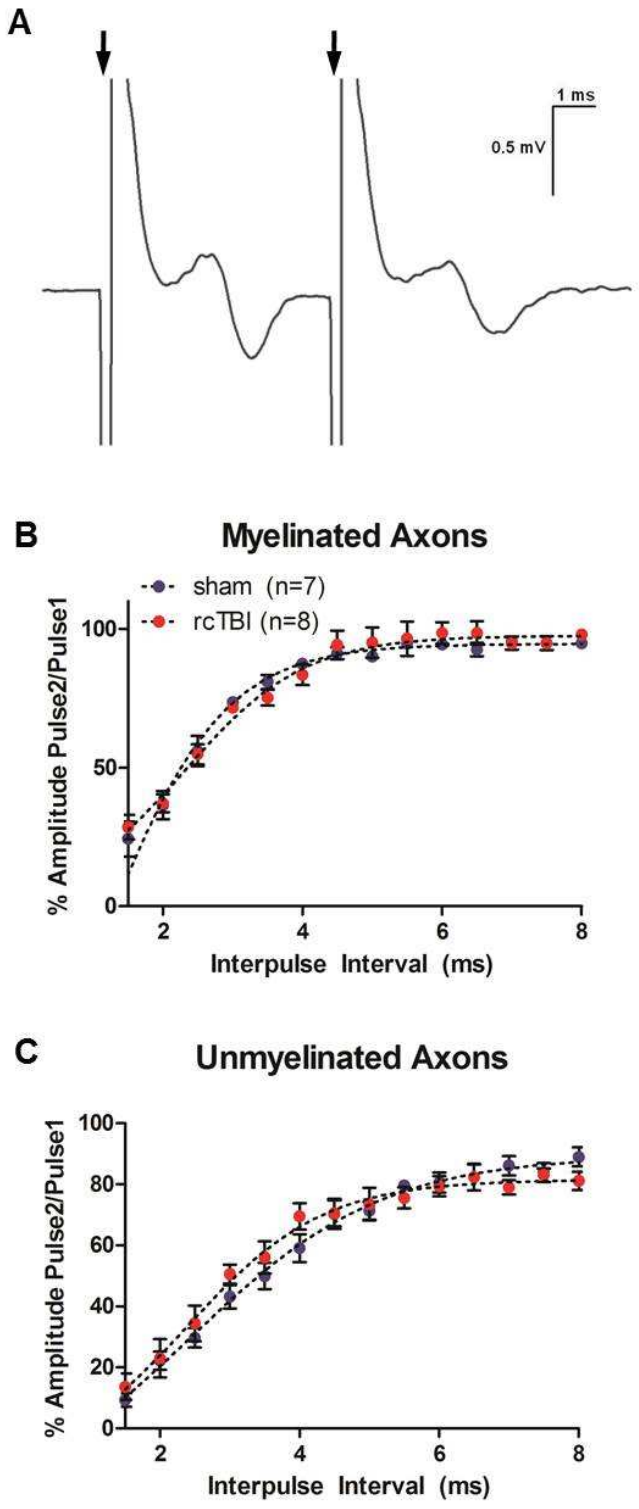

Figure 2.12 Axonal refractoriness was not altered by injury. (A) Altering the interval between two stimuli (arrows) at half maximum generated two CAP responses. The height of the second CAP response is plotted as the percentage of the initial CAP height for both myelinated (B) and unmyelinated (B) axons. (Dotted line represents non-linear fit, error bars are standard error of the mean)

2.3.6 Electrophysiological Integrity of Corpus Callosum Axons 1 day after Injury

Compound action potential measurements were repeated in a second cohort of mice that was sacrificed immediately following the second sham (n=3) or rcTBI (n=5) injury (1 day after the initial impact). Input-output curves were generated for each axon population (**Figure 2.13 A, B**) and the maximum CAP amplitude was measured. The amplitude of myelinated axons was unchanged (one-tailed Mann-Whitney test p=0.3929, **Figure 2.13 C**) but the amplitude of the unmyelinated response appeared to be significantly reduced (one-tailed student's t test p= 0.0283, **Figure 2.13 D**). Velocity measurements were not significantly altered in myelinated (one-tailed student's t test p=0.0883) or unmyelinated (one-tailed student's t test 0.3414) axons at this early timepoint (**Figure 2.13 E, F**).

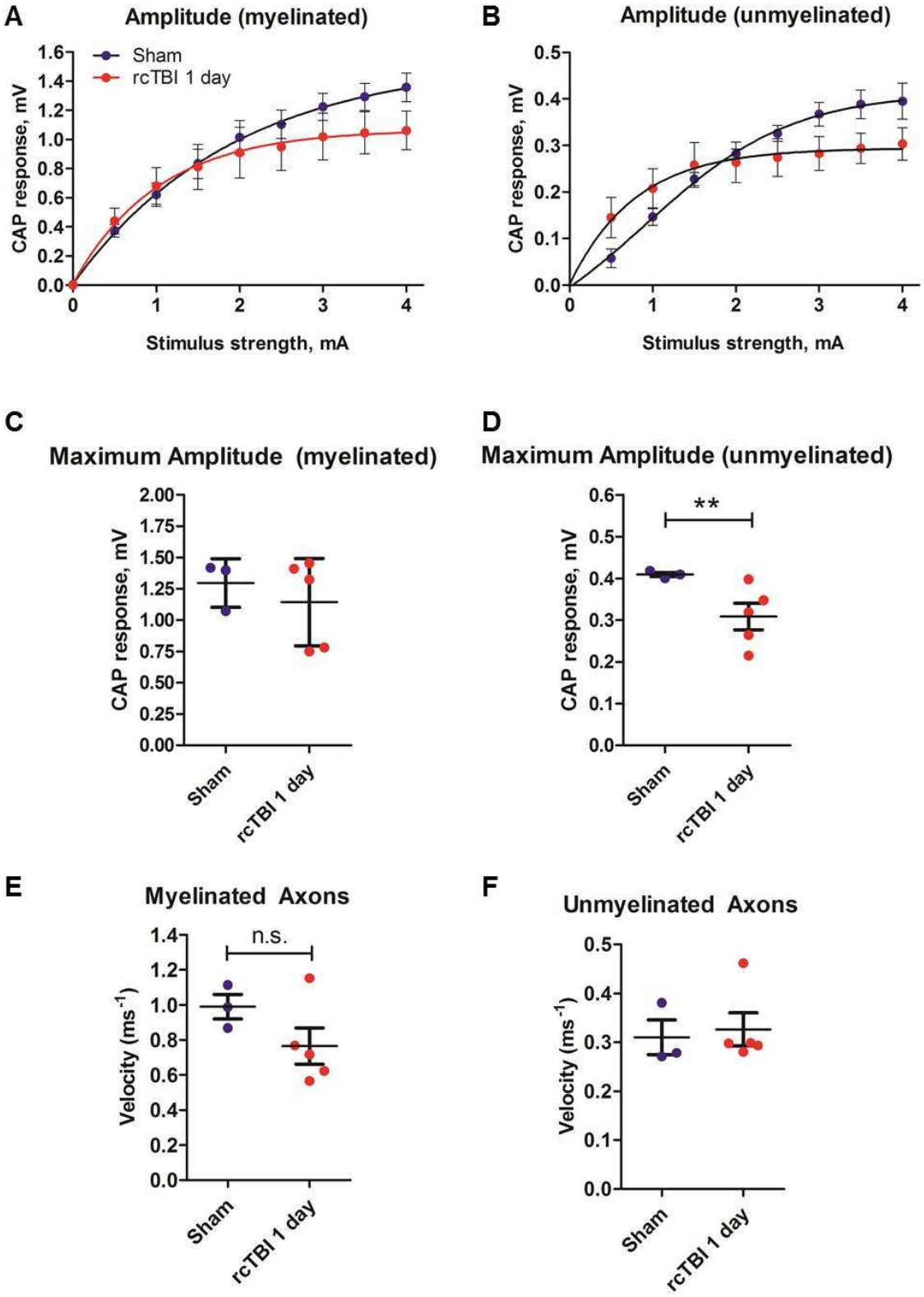
A
Amplitude (myelinated)
Sham
rcTBI 1 day
CAP response, mV
Stimulus strength, mA
B
Amplitude (unmyelinated)
CAP response, mV
Stimulus strength, mA
C
Maximum Amplitude (myelinated)
CAP response, mV
Sham
rcTBI 1 day
D
Maximum Amplitude (unmyelinated)
**
CAP response, mV
Sham
rcTBI 1 day
E
Myelinated Axons
n.s.
Velocity (ms-1)
Sham
rcTBI 1 day
F
Unmyelinated Axons
Velocity (ms-1)
Sham
rcTBI 1 day

Figure 2.13 Compound action potential amplitude and velocity measurements at 1 day post-injury. Input-output curved in sham and injured myelinated (A) and unmyelinated (B) axons. Solid line represents non-linear fit. Maximum CAP amplitude is not altered in myelinated (C) but is altered in unmyelinated (D) axons in injured mice. No differences were observed in velocity measurements (E, F). (Error bars represent standard error of the mean, **p<0.01, n.s. = not significant).

2.4 DISCUSSION

Here, we characterize the consequences of repetitive closed-skull injury in mouse and the resulting behavioral, histological and physiological white matter abnormalities. After two concussive impacts, mice were observed to have impaired spatial learning and memory immediately following injury which was mostly recovered by 7 weeks. Acutely after injury, prominent gliosis was observed by iba-1 and gfap labeling in addition to axonal injury evident by silver staining, APP, NF200, and SMI-32. Further, unmyelinated axons had reduced CAP amplitude at 1 day and both myelinated and unmyelinated axons had impaired velocities at 7 days post-injury compared to shams. Altogether, this confirms that repetitive closed-skull injuries produce subtle but measurable pathologies and suggests this is a useful model for investigating concussion.

This data are scientifically relevant because few studies to date have investigated models of concussive-type injuries and the relationship between concussion and axonal injury. Strengths of this study include the development of a reliable concussion model that does not produce contusions, gross histological abnormalities, or overt cell loss. This model also reproduces axonal injury and gliosis, two key characteristics that have been observed across the spectrum of traumatic brain injury severity (Oppenheimer 1968; Blumbergs et al. 1994; Oehmichen, et al. 1999; Johnson et al. 2013a; Johnson et al. 2013b). As demonstrated in Morris Water Maze, this is also a useful model to study the evolution of behavioral changes long-term. Altogether, the injury model reported here appears to represent several aspects of

uncomplicated concussive traumatic brain injury which accounts for the majority of all traumatic brain injuries that occur each year in the United States.

These results are consistent with those reported by other groups using similar injury models. Other models of concussive brain injury have demonstrated similar behavioral impairments in Morris Water Maze, in addition to other tasks not reported here such passive avoidance and depression behaviors (DeFord et al. 2002; Zohar et al. 2003; Creeley et al. 2004; Longhi et al. 2005; Milman et al. 2005). Histologically, few studies have examined axonal pathology after concussive injury. However, APP immunohistochemistry has been performed in other mouse models, and similar to results here, only small areas of APP-positive axons were seen acutely after injury (Laurer et al. 2001; Creed et al. 2011). Here, we expand upon these observations using multiple injury markers. We observed that the greatest amount of injury was evident immediately following impacts (2 days after the first injury). While areas of dense labeling could be found in white matter immediately below the impact site, injury appeared relatively focal compared to the widespread changes visible by silver staining. Thus, in this model, silver staining appears to be a particularly sensitive technique for visualizing axonal injury after concussion. Electron microscopy has been performed in this injury model to confirm that silver staining does in fact reflect ultrastructural changes in axons and is reported in Shitaka et al. as well as in Chapter V (2011).

Electrophysiological findings presented here contrast with those reported in Creed et al, which used a similar impact device fitted with a large metal impact tip to strike the skull at midline, between lambda and bregma (2011). In their report, single concussive injury resulted in reduced amplitude of the myelinated CAP at both 1 day and 14 days post-injury and increased refractoriness of unmyelinated axons at 14 days. Velocity measurements were not reported. Here, the main electrophysiological finding in this repetitive concussive model was reduced velocity of both populations of axons 7 days post-injury. That we did not detect a reduction in the amplitude of myelinated fibers (though a small, non-significant decrease may be

present) likely reflects different injury severity as similar numbers of mice and electrophysiology methods were used in both studies. Indeed in Creed et al., apoptosis in neurons was visible by fluorojade b in the cortex and hippocampal dentate gyrus, which may indicate that the single concussive impact produced more damage than the repetitive injuries reported here (2011).

This study does have limitations. First, and most concerning, is that sham mice failed the probe trial in the 7 week experiment. While differences in mean time to the hidden platform were observed between rcTBI and sham groups we cannot rule out that that this result did not occur by chance. However, if both groups failed to learn across the four days of the trial due to experimental design, the results would be biased towards not finding any differences between groups. Thus, slight impairments in spatial learning and memory seem to persist out to 7 weeks post-injury, but this experiment will need to be repeated again in the future to confirm these findings. Second, additional electrophysiology experiments should be performed to confirm these findings. Including groups of mice subject to 3 or more concussive impacts or moderate-severe traumatic brain injury would aid in our understanding of the ability of electrophysiology to resolve alterations in axonal conductance due to injury. Also, given the small n of the 1 day electrophysiology experiment, it should be repeated to confirm that velocity is not impaired at early this early timepoint. Third, analysis of injury was limited to corpus callosum and external capsule. Over relevant changes may be occurring in grey matter regions and at synapses in particular. However, assaying injury processes taking place in these areas was outside the scope of the present study.

Finally, like other rodent injury models, not all aspects of human concussion are modeled. In mouse repetitive closed-skull injury, compression forces are exerted upon the brain rather than rotational acceleration/deceleration forces. At present it is unknown how aspects of axonal injury may be altered by these different types of biomechanical forces. Recently a ballistic model of concussion in rat was reported that results in rapid rotational acceleration/deceleration of the head—comparisons between injury modalities may provide

future insights (Davidsson, et al. 2011). Another aspect of human concussion not modeled here is the effect of multiple subconcussive impacts of the resulting pathology. In a study of high school football players wearing a Head Injury Telemetry system, an average of 652 impacts were recorded per player over a 14-week season (Broglio, et al. 2011). Though only a small subset of impacts resulted in concussion, how a large number of blows to the head may "prime" the brain is unknown.

The finding that microglia are increased dramatically after injury has important therapeutic implications. Activated microglia have been observed in human traumatic brain injury several years after the initial insult (Ramlackhansingh, et al. 2011; Johnson et al. 2013a). In other injury models and *in vitro* systems they appear to play an important role in phagocytosis of axonal debris acutely following injury and in secretion of neurotrophic factors (Batchelor, et al. 2002; Hosmane, et al. 2012). Ultimately, however, it is unknown whether these cells are helpful, harmful, or neutral in regards to concussive injury and axonal degeneration process in particular. Determining their role is one clear direction of these studies, as concussion therapies may be designed to augment or inhibit microglial activation.

Another intriguing finding is that axonal velocity was reduced 7 days following repetitive concussion. One possible implication is that such functional alterations after concussive injury may contribute to post-concussion symptoms experienced by patients. In particular, complaints related to cognitive function are common, and information processing speed has been reported to be reduced in individuals who suffer mild TBI or multiple concussions (Gronwall, et al. 1975; O'Jile, et al. 2006; Johansson, et al. 2009; Dean, et al. 2013). While other factors including inflammatory processes and mechanical damage to synapses are likely to contribute to these deficits in processing speed, changes in white matter including axonal conductance velocity may be important considerations (Fjell, et al. 2011; Mazerolle, et al. 2013). Given these results, future studies should be performed to determine how long alterations in axonal conductance velocity persist following injury. In other injury models, functional deficits appear to resolve by

14 days post-injury (Reeves, et al. 2005). Determining how physiological changes contribute to behavioral alterations in this model is an important future direction of these studies.

Likewise, silver staining, iba-1, and gfap are dramatically increased after injury and these markers may indicate an underlying histological basis for behavioral and functional changes that occur after concussive TBI. A full characterization of the size, location, timecourse, and nature of injured axons may provide insight into the susceptibility of specific axonal populations to injury. For example, in other studies it has been reported that antibodies that label APP or neurofilament accumulations reveal different subsets of injured axons (Stone et al. 2001; DiLeonardi, et al. 2009). Further analysis will be required to determine if this is a feature of repetitive closed-skull injury. Additionally, mice time sacrificed between 2 and 7 days post-injury may also provide more clues to the temporal vulnerability of axons. For example, single concussive impacts in this model do not produce significant silver stain-positive axonal injury compared to shams, but two injuries separated by 1 day produce argyrophillic accumulation (Shitaka et al. 2011). Determining the window of vulnerability of axons to a second impact is an on-going subject of research in the lab and repeating APP and neurofilament immunohistochemistry at finer temporal resolution may aid our understanding of this process. Such studies have real clinical implications as currently there is evidence that suffering multiple back-to-back concussions can contribute to worse long-term outcome from injury, but the vulnerability of the brain to second injury is not well understood (Guskiewicz et al. 2003).

In sum, the rcTBI model is a useful tool for investing the pathophysiology of concussion, particularly as it relates to axonal injury. We propose to use this model to screen therapeutic compounds that may reduce behavioral and functional alterations and that reduce the vulnerability of the brain to second impact (Scheff, et al. 1999; Okonkwo, et al. 2003; Zhang, et al. 2012) . This model may also be useful for radiological-pathological correlation studies to determine the significance of changes evident by advanced *in vivo* imaging methods (Bennett, et al. 2012). Additionally, we will use transgenic mice and pharmacological compounds to

determine the interaction between iba-1 positive microglia/macrophage and axonal degeneration. Other studies may uncover unique factors that contribute to axon injury following concussion and provide novel therapeutic targets.

CHAPTER 3

In Vivo Diffusion Tensor Imaging Detects Axonal Injury in a Mouse Model of Repetitive Closed-Skull Traumatic Brain Injury

3.1 INTRODUCTION

Traumatic axonal injury (TAI) is a hallmark of traumatic brain injury (TBI), and may be a leading cause of cognitive impairment and disability following head injury (Smith, et al. 2003b). Few methods exist for detecting TAI, with a positive diagnosis usually taking place post-mortem following histological analysis for accumulated amyloid precursor protein (APP), an integral membrane protein that is normally transported along the length of the axon (Blumbergs et al. 1994; Sherriff et al. 1994; Geddes, et al. 2000).

Increasingly, diffusion tensor imaging (DTI) has been used as a non-invasive method for detecting TAI in vivo (Niogi, et al. 2010). DTI measures the directional diffusion of water. In white matter, this diffusion is restricted by the orientation of axon bundles. In regions such as the corpus callosum, water preferentially diffuses along a single axis and has high anisotropy (Le Bihan 2007). When white matter is injured, as in traumatic brain injury, the characteristic diffusion of water is altered.

We have previously validated DTI signal changes after TBI with histology for APP-positive injured axons. In these studies, which used a mouse model of moderate-severe TBI, areas with reduced relative anisotropy and axial diffusivity were shown to contain greater numbers of APP-positive swellings (Mac Donald et al. 2007a; Mac Donald et al. 2007b). However, from these studies and others, it is not clear whether DTI is sensitive to mild injuries without contusion where the mechanisms of axonal injury may be different.

Recently, our group developed a model of mild repetitive closed-skull TBI (rcTBI) in mouse to study the pathological changes underlying concussion. In this model, young male mice are subject to two concussive impacts within a 24-hour period. Interestingly, only sparse APP-positive axons were visible following injury, though axonal degeneration was evident by both silver staining and electron microscopy and coincided with a prominent microglial response and clear deficits in spatial learning and memory (Shitaka et al. 2011).

As DTI is a quantitative method for assessing the integrity of white matter regions, we sought to apply this technique to this mild repetitive closed-skull TBI model to determine if APP-negative axonal injury results in detectable DTI changes 24 hours and 7 days after impact. Results from these experiments have important implications for the use and interpretation of DTI following mild TBI.

3.2 METHODS

Animals

Six- to eight-week C57BL/6j mice were purchased from Jackson Laboratories and housed in standard cages under a 12-hour light/dark cycle with approval from the Animal Studies Committee at Washington University in Saint Louis. Mice were divided into 3 groups: 7 day sham injury with sacrifice 7 days later, rcTBI with sacrifice 24 hours later, and rcTBI with sacrifice 7 days later Each group initially consisted of six mice. The final n for the rcTBI 24 hour group was 4; a scan of one mouse in this group failed for technical reasons and a second was excluded due to a small hemorrhage within white matter. Repetitive closed-skull injury was performed as described previously (Shitaka et al. 2011). Briefly, mice were anesthetized with inhaled isofluorane and placed in a stereotaxic frame. A midline incision was made to expose the skull and the 9 mm rubber impactor tip was aligned with Bregma. The tip was then moved to the location of the impact (A/P: -1.8 mm, M/L: -3.0 mm) and an electromagnetic impactor (My NeuroLabs) was used to drive an impact to a depth of 3.3 mm. Body temperature was closely

monitored and maintained throughout the procedure. Following the impact, the incision was sutured closed, antibiotic ointment was applied, and mice were allowed to recover on a heat pad before returning to their cage. Sham-operated mice received the same treatment but an impact was not delivered. This procedure was repeated at 24 hours for a total of two impacts per mouse. Mice in the 24 hour scan group were immediately taken for DTI after the second impact.

Diffusion Tensor Magnetic Resonance Imaging

All scans were performed using a previously published method (Mac Donald et al. 2007b). Mice were anesthetized with isofluorane maintained at 1% throughout the duration of the scan while circulating warm water preserved a constant body temperature. Images were acquired with a 4.7T scanner (Oxford Instruments 330) and actively shielded gradient coil (180 mT/m, 400 ms rise time) interfaced with a Varian Unity-INOVA console controlled by Sun Microsystems Ultra-60 Sparc workstation. The following acquisition parameters were used: TR= 3s, TE= 40ms, and FOV/Resolution 20 x 20 mm / 192 x 192. Voxel size during acquisition was 104 µm X 104 µm X 0.5 mm (zero padded to 256 x 256). A multislice spin-echo sequence was modified to include a Stejskal-Tanner gradient-sensitizing pair in order to acquire coronal diffusion weighted images. Diffusion gradients were applied in six directions. B-values used were 0 and 764. Each scan required approximately 3 hours. Software written in Matlab (Mathworks, Natick, MA) was used to calculate the six elements of the diffusion tensor and to determine relative anisotropy (RA; overall measure of the asymmetry of diffusion), axial diffusivity (AD, λ_1; diffusion along a primary direction), radial diffusivity (RD, $\lambda_\perp$; diffusion perpendicular to the primary direction), and mean diffusivity (MD).

Diffusion Tensor Imaging Analysis

Imaging analysis was performed using Image J. The sync windows plugin was used to trace the regions of interest (ROI) on RA, AD, RD, and MD images simultaneously. The ROIs were carefully defined by anatomical boundaries with the anterior-most boundary being the first section containing hippocampus and the posterior boundary being the last section where the corpus callosum crosses at midline. This resulted in a total of 3 slices per mouse. Corpus callosum and external capsule ipsilateral to midline were included in the white matter ROI with the ventral boundary being drawn at the interface between the hippocampus and thalamus (**Figure 3.1 A** red outline). Dorsal cortex ipsilateral to midline was selected as a second ROI using the same boundaries (**Figure 3.1 A**, yellow outline) Signal intensity within each ROI was measured across slices and weighted by the number of voxels in each sketched region to obtain RA, AD, RD, and MD measures.

Histology

Immediately following each scan, mice were sacrificed by isofluorane overdose, perfused with 0.3% heparin phosphate-buffered saline (PBS), and brains were removed and placed in 4% paraformaldehyde (PFA) for 24 hours. After fixation, brains were equilibrated in 30% sucrose PBS and cut into 50 µm-thick sections using a freezing microtome. Sections were then either rinsed in PBS and stored in 4% PFA for 5 days for silver staining or underwent processing for Iba-1 immunohistochemistry. Evaluation was conducted on sections taken at 400 µm intervals along the anterior-posterior axis of the brain. For silver staining, a Neurosilver Kit (FD Neurotech) was used according to the manufacturer's instructions with the exception of a single two-minute incubation with solution C as previously described (Shitaka et al. 2011). For APP and Iba-1 staining, endogenous peroxidases were quenched with 0.03% H_2O_2, blocked in 3% normal goat serum in 0.25% Triton-X tris-buffered saline (TBS-X), and incubated overnight in 1:1000 rabbit anti-Iba-1 (Wako) or 1:1000 rabbit anti-APP (Invitrogen) in 3% normal goat

serum (NGS) TBS-X. Antibody binding was visualized using 1:1000 goat anti-rabbit (Vector Laboratories) in TBS-X, followed by 1:400 AB complex (Vector Laboratories), and DAB substrate enhanced with nickel chloride (Sigma). All sections were mounted onto slides and digitally scanned using an Olympus Nanozoomer Whole-Slide Imaging System to generate photomicrographs.

Iba-1 stereology and silver stain quantification in corpus callosum was performed as published in Shitaka et al (2011). In short, ROI parameters were the same as used for DTI analysis. Image J was used to measure silver staining by densitometry. The optical fractionator probe in StereoInvestigator (Microbrightfield) was employed to count the number of Iba-1-positive cells. A grid size of 180 x 180 µm and counting frame of 80 x 80 µm ensured that the Gunderson's coefficient of error was <0.1 for all counts.

Statistical Methods

Prism 5.0 (GraphPad) was used for statistical analysis. All DTI data were analyzed by one-way ANOVA followed by Bonferroni's multiple comparisons test. For histology, a one-tailed t test was performed as it was expected that silver staining and Iba-1 positive cells would increase following injury as previously published (Shitaka et al. 2011). Linear regression and Pearson's product moment correlation was performed to determine the relationship between DTI and histological measures. In all cases, only p-values less than 0.05 were considered significant.

3.3 RESULTS

3.3.1 DTI of white matter

Separate cohorts of mice were scanned using DTI 7 days after sham treatment or 24 hours or 7 days after the first closed-skull traumatic brain injury (**Figure 3.1 A-F**). Analysis of corpus callosum and external capsule 24 hours after injury revealed no significant changes in DTI measurements compared to shams (**Figure 3.1 C-F**). At 7 days, relative anisotropy and radial diffusivity remained unchanged (**Figure 3.1 C. D**), but a statistically significant decrease in axial diffusivity was apparent compared to shams ($p<0.01$) and injured mice at 24 hours ($p<0.01$; **Figure 3.1 E**). Decreased mean diffusivity was also evident compared to sham ($p<0.05$) and injured mice at 24 hours ($p<0.01$; **Figure 3.1 F**).

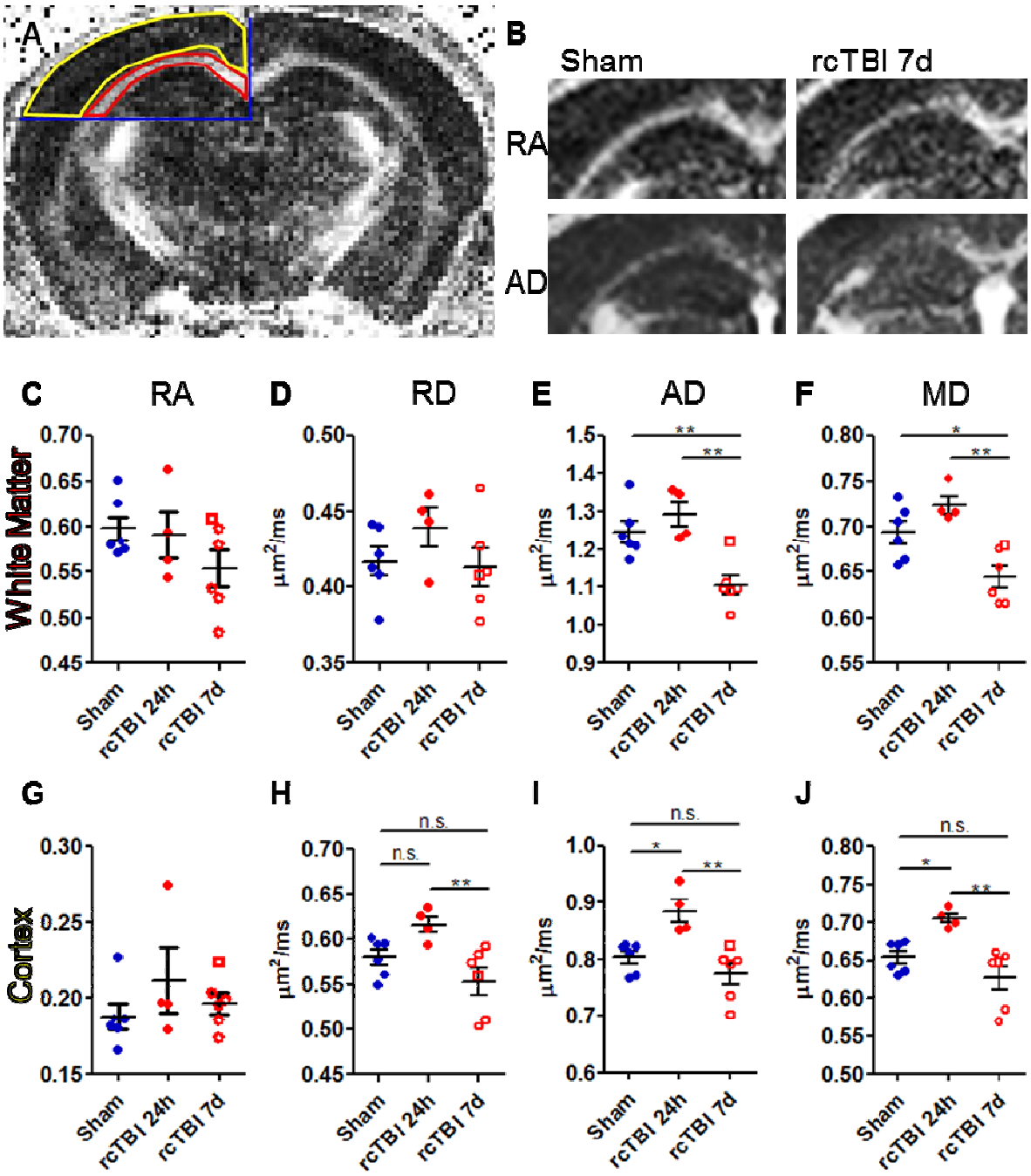

Figure 3.1 Diffusion tensor imaging in rcTBI mice. (A) The regions of interest (red, yellow) were defined by anatomical boundaries (blue) and were used for quantitative analysis of diffusion tensor images. (B) Representative images of ipsilateral relative anisotropy (RA) and axial diffusivity (AD) in both a sham and an rcTBI mouse at 7 days. White indicates higher signal intensity and greater RA or AD. (C, G) Relative anisotropy (D, H) Axial diffusivity. (E, I) Radial diffusivity. (F, J) Mean diffusivity. (C-F) White matter. (G-J) Cortex (*p<0.05, **p<0.01, ***p<0.001, one-way ANOVA with Bonferroni post-test, error bars represent ±SEM. Square symbol in 7 day group indicates a mouse with histologically mild injury, a possible outlier.)

3.3.2 DTI of cortex

Considering injury results in significant histological abnormalities in cortex in addition to the white matter, analysis of DTI signal within cortex ipsilateral to injury was also performed. As cortex is an isotropic structure, little RA was observed within cortex in any injury group (**Figure 3.1 G**). No change between sham and injured mice at 7 days was apparent in AD, RD, or MD (**Figure 3.1 H-J**). However, AD, RD, and MD were significantly increased in injured mice at 24 hours compared to both shams ($p<0.05$) and injured mice at 7 days ($p<0.01$; **Figure 3.1 H-J**).

Given the changes in white matter AD and cortical MD, it was possible to separate the three injury groups based on these parameters (**Figure 3.2**). One potential outlier in the 7 day injury group overlapped with sham mice and has been marked with a unique symbol in all figures as this mouse appeared to have minimal injury when analyzed by both DTI and histology.

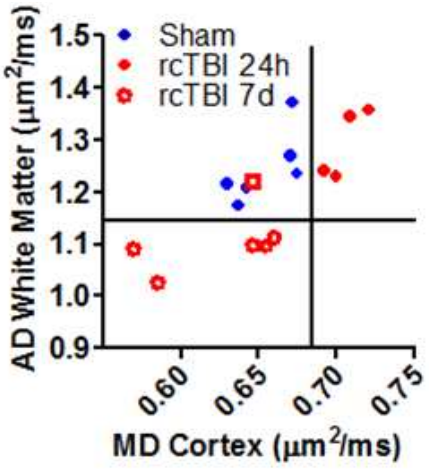

Figure 3.2 Mean diffusivity in cortex versus axial diffusivity in white matter separates mice into distinct injury groups. (Open Square symbol in 7 day group indicates a mouse with histologically mild injury, a possible outlier.)

3.3.3 Histological findings

Immediately following DTI scans, mice in the sham and injured cohorts were sacrificed and tissue was processed for APP, Iba-1, and silver staining. As previously reported (Shitaka et al. 2011), only occasional APP-positive swellings were detectable in injured mice and were virtually indistinguishable from shams with this marker (**Figure 3.3 A-D**). Quantification of Iba-1 and silver staining within corpus callosum and external capsule revealed levels similar to those observed in Shitaka et al (Shitaka et al. 2011) in both sham and 7 day injured mice (**Figure 3.4 A-D**). This indicates that the additional 3 hours of anesthesia during the MRI scan does not appear to substantially affect these histological markers. Mice sacrificed at the 24 hour timepoint did not have Iba-1 or silver stain abnormalities, as previously reported (Shitaka et al. 2011), and were not included in the stereological analysis.

Interestingly, the density of silver staining in the corpus callosum and external capsule correlated strongly with RA (r=-0.8639, p=0.0265; **Figure 3.4 E**). Silver staining did not statistically significantly correlate with AD (r=-0.6293, p=0.1806), RD (r= 0.5920, p=0.2157), or MD (r=-0.0402, p=0.9397). Iba-1 immunoreactive microglial cell counts were also not

significantly correlated with any of the DTI measures: RA (r=-0.7506, p=0.0856), AD (r=-0.3865, p=0.4491), RD (r=0.6238, p=0.1856), MD (r=0.1574, p=0.7658).

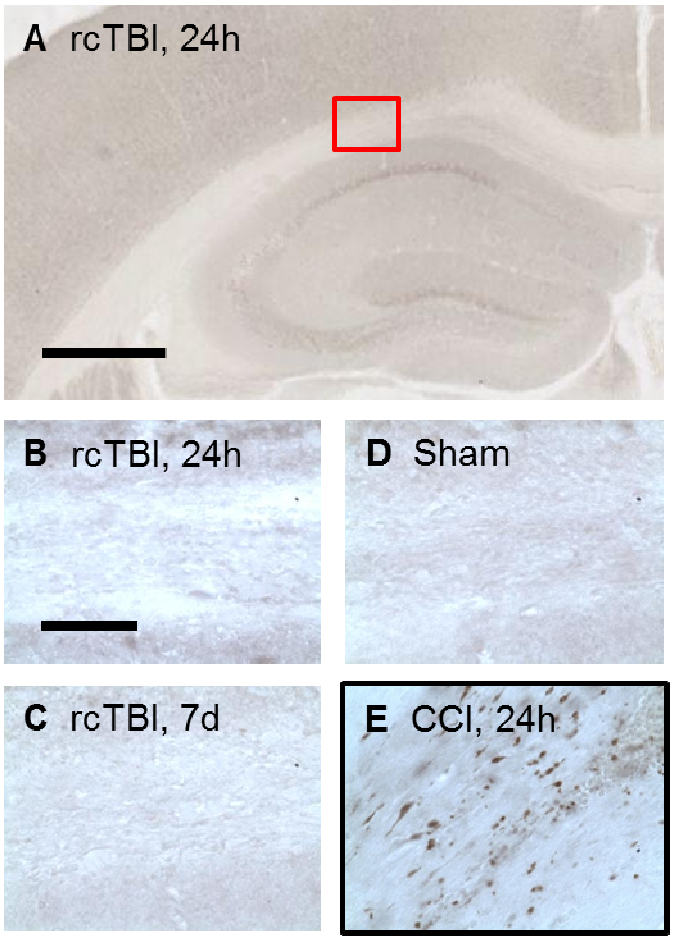

Figure 3.3 APP immunohistochemistry. (A, B) Injury did not result in APP positive axons in the corpus callosum of mice analyzed at 24 hours or (C) 7 days following impacts and were similar to (D) sham mice. (E) A mouse subject to moderate controlled cortical impact (CCI) brain injury and sacrificed at 24 hours served as a positive control for APP staining (red box indicates location of B-E, scale bar in A=500 µm, scale bar in B=50 µm).

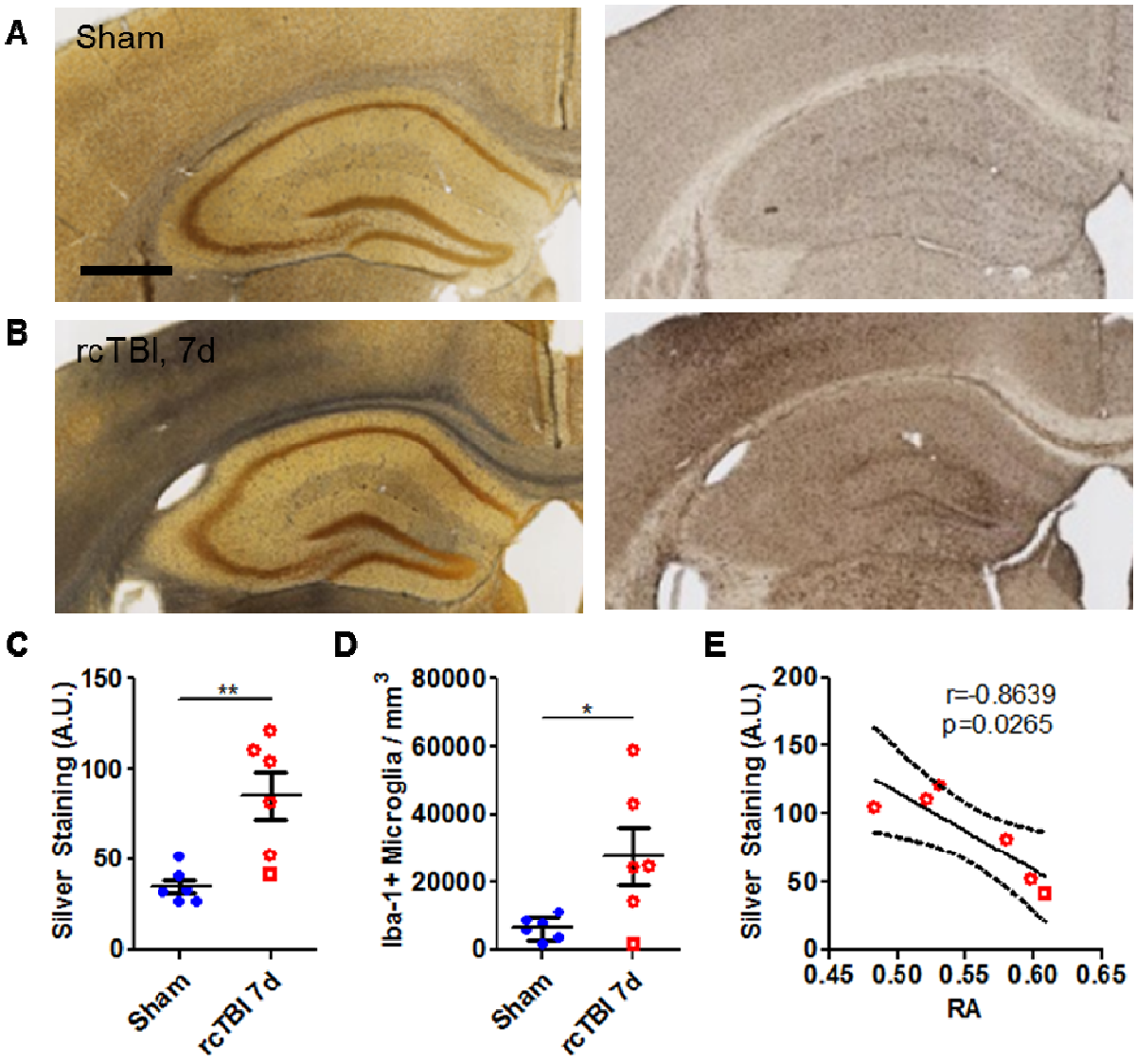

Figure 3.4 Axonal injury and microglial activation in 7 day rcTBI. (A) Sham operated mice had little silver stain (black precipitate, left panel) and few Iba-1-positive cells (right panel) in the corpus callosum (scale bar=500 µm). (B) Silver staining (left panel) and increased numbers of Iba-1-positive cells (right panel) were evident in the corpus callosum of mice 7 days post-injury. Quantification of silver by densitometry (C, arbitrary units A.U.) and of Iba-1 by stereology (D) confirmed observed changes (*p<0.05, **p<0.01, Student's one-tailed t test). (E) Silver staining strongly correlated with changes in relative anisotropy at 7 days post-injury (Pearson's correlation, two-tailed, solid line represents linear regression, dotted lines represent 95% confidence interval. Square symbol in 7 day group indicates a mouse with a histologically mild injury, a possible outlier).

3.4 DISCUSSION

Here we present findings that mild repetitive closed-skull injuries in mice result in detectable changes by DTI. Importantly, these DTI abnormalities are present despite of a lack of APP-positive histology, which has been considered a “gold standard” for identifying traumatic axonal injury. Previous studies from our group have shown that the numbers of APP-positive axonal varicosities correlate strongly with RA in a model of moderate-severe traumatic brain injury (Mac Donald et al. 2007b). In this work, we show RA correlates just as strongly with the degree of silver staining in the corpus callosum of mildly injured mice.

Both axial diffusivity and mean diffusivity have been widely used to assess axonal degeneration in the central nervous system (Pierpaoli, et al. 2001). In our model, both of these parameters were reduced within white matter in the injured 7 day group compared to shams. Notably, neither silver stain, a marker of protein aggregates, nor Iba-1-positive microglial cells correlated well with AD and MD changes. While both protein aggregation and microglial pathology may have contributed to some of the reduced diffusivity, weak correlations between these measures indicate other histological markers are needed that better reflect AD and MD changes. In addition, because Iba-1 did not correlate with any DTI parameter, it is important to note that this method may not be suitable to resolving microgliosis. Other imaging modalities may therefore be required to detect this prominent microglial response in vivo (Ramlackhansingh et al. 2011; Wang, et al. 2011).

Given the coincident decrease in axial diffusivity and mean diffusivity, it is interesting that no significant changes in relative anisotropy were seen. This is different from TBI with contusion, where AD is reduced, overall diffusivity is unchanged or increased, and subsequently, RA is reduced (Mac Donald et al. 2007b). In this model, it is possible that a larger sample size may resolve the non-significant reduction in RA. Alternately this could indicate that in mild injuries, analysis of single components of the diffusion tensor may be more sensitive than RA.

Increased radial diffusivity is another common feature of DTI in TBI and in other models with prominent demyelination or edema (Song, et al. 2003; Mac Donald et al. 2007a; Klawiter, et al. 2011). We observed no significant change in this parameter in our model, which is in line with previous observations by electron microscopy that revealed myelin degradation is not characteristic of this mild injury (Shitaka et al. 2011).

Unlike white matter, imaging of cortex revealed an acute, transient increase in AD, RD, and MD, likely reflecting edema. While these changes were significant at 24 hours, they were resolved by 7 days post-injury. This is potentially useful for determining time since injury. Here, increased mean diffusivity in cortex and unaltered AD in white matter characterized mice imaged 24 hours following initial injury, whereas normalized MD in cortex and decreased AD in white matter characterized mice imaged 7 days post-injury.

These results highlight the evolving nature of traumatic brain injuries, as the DTI changes within white matter were not immediately apparent at 24 hours but were distinct 7 days following injury. Similarly, earlier characterization of this model has shown that Iba-1 and silver stain abnormalities also develop 3-7 days after injury (Shitaka et al. 2011). Thus, it is likely that DTI measurements are reflective of a progressive degenerative process taking place within the corpus callosum and external capsule of these injured mice. Clinically, this may also mean that DTI days or weeks after mild head injury may be more informative for detecting and diagnosing axonal injury. However, given our observed alterations in AD and MD were approximately 10%, it is unclear whether these changes would be significant within a human population where normal white matter diffusion may vary greatly between subjects. This may be one explanation why DTI in human mild TBI patients has resulted in conflicting reports of the observed changes in DTI signal (Zhang, et al. 2010; Cubon, et al. 2011; Henry, et al. 2011).

There are several limitations of this work. First, sample sizes are small and to fully validate this model, larger groups will be required. However, given the small sample and the relatively mild injuries studied, it is encouraging that these DTI changes are evident and

correlate with histological abnormalities. Second, this research is limited by the histological markers chosen for analysis. To fully characterize this model, markers for neurofilament, myelin, and activated astrocytes might further inform the nature of these DTI alterations. Quantitative electron microscopy may be the ultimate "gold standard" but is beyond the scope of the current work. Third, mice that received a single injury were not assessed here, and so we did not determine whether single injury alone results in DTI signal change. We have previously demonstrated that mice subject to single injuries do not have significantly more silver staining or microglial activation compared to shams at 7 days post-injury thus it is unlikely that a single impact would be detectable by DTI (Shitaka et al. 2011). Fourth, the interval between injuries was kept fixed at 24 hours; further studies will be required to determine the effect of different intervals between injuries. As a final note, the imaging protocol used was not optimized for measuring MD changes.

Despite these limitations, this study shows that DTI is capable of detecting populations of degenerating axons in the absence of APP pathology. Future studies will be required to determine the distinct DTI signatures of axonal degeneration following repeated mild injuries in order to differentiate injury phenotypes that may or may not include disrupted APP transport. Full validation of detection methods and interpretation of DTI signal changes will be important to providing meaningful evaluation and targeted therapeutics for patients with multiple concussive injuries.

CHAPTER 4

Array Tomography for the Detection of Axonal Injury

4.1 INTRODUCTION

A barrier to analysis of axonal injury in repetitive concussive traumatic brain injury (rcTBI) is the ability to resolve small injured axons by light microscopy. This is due in large part, to the low signal to noise of very small structures that are at or below the resolution of light microscopy. In humans and macaques, axon diameters within the corpus callosum range between 0.2 to >6 μm (Lamantia, et al. 1990; Aboitiz, et al. 1992). In rodents, axonal diameter is smaller, typically in the 0.1 to 1 μm range (Kim, et al. 1996; Olivares, et al. 2001). Following traumatic brain injury in mice, swollen axons in corpus callosum can become very large (5 μm or more), and are clearly visible with standard immunohistochemistry using antibodies to amyloid precursor protein (APP) and neurofilaments. However, several observations have led us to hypothesize that immunohistochemistry and light microscopy may not reflect the true amount of axonal injury present after TBI in mouse, particularly after mild concussive injuries.

First, standard immunohistochemistry techniques for APP and neurofilaments reveal only small areas of axonal injury at 2 days after the first injury that appear to resolve by 7 days (Chapter 2, **Figure 2.8**). However, axonal injury is evident by silver staining and has been confirmed by electron microscopy timepoints later than 2 days (Shitaka et al. 2011). Electron microscopic analysis of repetitive concussive TBI (rcTBI) has confirmed that injured axons are present throughout the ipsilateral corpus callosum and external capsule at 7 days post-injury (Shitaka et al. 2011, Chapter 5 **Figure 5.8**). These axons display compaction of cytoskeletal elements, organelle accumulation, and axolemma collapse. A key observation is that few of these injured axons appear to have diameters greater than 1 micron, and most are less than

500 nanometers—at or below the resolution of standard light microscopy techniques. Indeed other investigators have documented cases of axonal injury without axonal swelling, and it may be possible for axon degeneration to proceed without the classic “beads-on-a-string” morphology (Stone et al. 2001). Additionally, in this mild injury model, white matter abnormalities are apparent by diffusion tensor imaging, where mean (MD) and axial diffusivity (AD) are both significantly reduced at 7 days post-injury. Neither MD nor AD correlate with the amount of silver staining or iba-1 labeling for microglia (Bennett et al. 2012). The inability to explain DTI measures by standard histological techniques further supports the idea that we are underestimating the amount of axonal injury in rcTBI by these methods.

To test this hypothesis, we adapted array tomography for measuring axonal injury. Array tomography was developed in the lab of Stephen Smith to quantitatively measure synapses in the cortex (Micheva, et al. 2007). In array tomography, improved spatial resolution is achieved along the z-axis through physical sectioning on an ultramicrotome, which greatly improves the signal to noise ratio and allows identification of individual synapses (Micheva et al. 2007; Kay, et al. 2013). While this technique has not been rigorously validated by quantitative EM, the use of several antibodies to label pre- and post-synaptic densities and the careful co-registration of fluorescent labels with scanning electron micrographs has confirmed the spatial correlation of immunofluorescence with ultrastructural details (Micheva et al. 2007). Further, the advantages of this technique over traditional electron microscopy are the ability to assay large volumes of tissue in a relatively high-throughput fashion, to label multiple proteins of interest, and to perform these experiments with a standard epifluorescent microscope.

Here, we outline a method for using array tomography to examine axon injury. We show preliminary data using this technique to resolve injured and uninjured axons at a level of resolution not previously possible except with electron microscopy. Altogether, this is a promising new method for quantitative analysis of axons that could be applied to many fields beyond traumatic brain injury.

4.2 METHODS

Animals

Male C57Bl/6j mice were purchased from Jackson Laboratory between 6-8 weeks of age (stock#000664). Two male APP knockout mice were obtained from Jackson Laboratory at 2 months of age (stock# 004133). Two 12-month-old male TauP301S mice and two 3-month-old tau knockout mice were also used for these experiments and were bred in house. All animals were housed in accordance with the Animal Studies Committee at Washington University in Saint Louis. Mice were provided with food and water ad libitum and were maintained under a 12 hour light/dark cycle.

Surgical procedures

Mice were subject to closed-skull sham injury or rcTBI injury as previously described (n=5 per group, Chapter 2). A second group of mice underwent controlled cortical impact injuries at a depth of 1.0 mm (n=2) or 1.5 mm (n=4), which has been described elsewhere (Brody, et al. 2007). Briefly, mice are anesthetized, placed in a stereotaxic frame, and a midline incision is made. A 5 mm craniotomy is performed over the left parietal cortex. An electromagnetic impactor fitted with a 3 mm metal tip is positioned M/L -1.2 mm relative to midline and +1.5 mm lambda. Impacts are delivered at 5 m/s with a dwell time or 100ms. After irrigation with phosphate buffered saline (PBS) a plastic skull cap is glued in place, the midline incision is sutured closed, and the mice are allowed to recover on a heat pad before being returned to their cage.

Tissue embedding and sectioning for array tomography and electron microscopy

Tissue embedding and sectioning was performed as described by others with minor modifications (Kay et al. 2013). Briefly, animals were sacrificed by deep anesthesia with

isofluorane followed by cardiac perfusion with 10 milliliters room temperature 0.3% heparin in 0.01 M PBS. This was immediately followed by perfusion with 10 milliliters 4% paraformaldehyde (cat# 15710 E.M.S), 0.025% sucrose in 0.01 M PBS. Brains were removed and placed in fixative for 20-30 minutes and then were sectioned into 1 mm thick coronal slabs using a razor blade and a brain slicing matrix. Corpus callosum and external capsule ipsilateral to injury was then dissected into 5 x 2 x 1 mm blocks which were further post-fixed for 1-2 hours. Following fixation, blocks were dehydrated in an ascending ethanol series (50%, 70%, 95%, 100%, 100%). Each dehydration step was performed for 5 minutes with gently shaking using chilled solutions. Blocks were then placed in one wash with equal parts 100% ethanol and LR White (cat# 14381 E.M.S) followed by two washes in 100% LR White. Blocks were allowed to equilibrate overnight at 4℃ in LR White and were then placed in gelatin capsules (cat#70100, E.M.S.) and cured overnight in a 53℃ oven. Gelatin could be removed by gentle heating in a 60℃ water bath.

Arrays were produced using a histo Jumbo diamond knife (Diatome). To collect ribbons, the top and bottom edges of each tissue block was painted with a thin layer of Weldwood contact cement (DAP products) mixed with equal parts xylene. Ribbons were collected on gelatin subbed coverslips, air-dried, and stored at room temperature prior to immunofluorescent labeling.

For parallel electron microscopy studies, after perfusion, 1 mm thick coronal slabs of the contralateral, uninjured hemisphere was placed in 1% PFA, 1% glutaraldehyde in 0.01 M phosphate buffer overnight. Three slabs were prepared per mouse, beginning at the anterior-most end of the hippocampus. Sections were then incubated in 1% osmium tetroxide, dehydrated in ethanol, and embedded in Polybed 812 (cat# 08792, Polysciences, Inc.) as previously described. Semithin sections were cut with glass knives and stained with toluidine blue to identify the region of interest and ultrathin sections 70-90 nm were cut and stained with Reynold's lead citrate and 4% uranyl acetate.

Immunofluorescence

For immunofluorescent labeling, a PAP pen was used to draw a hydrophobic barrier around the tissue ribbon. Sections were then incubated in 50 mM glycine in Tris buffered saline (TBS) for 5 minutes. TBS-glycine was aspirated off and a blocking solution containing 0.05% Tween, 0.1% bovine serum albumin (BSA) in TBS was applied for 20 minutes. Following blocking, primary antibodies were applied and coverslips were placed in a humidified chamber at 4℃ overnight. The following day, tissue was wa shed in TBS and incubated in secondary antibody in blocking solution for 1 hour at room temperature protected from light. Tissue was then washed again in TBS and 5 µg/ml 4',6-Diamidino-2-Phenylindole, Dihydrochloride (DAPI; cat #D1306, Invitrogen) in TBS was applied for 5 minutes followed by a final wash in TBS. Coverslips were mounted on glass slides in Vectashield fluorescent mounting medium (cat# H-1000, Vector Laboratories). See **tables 4.1** and **4.2** for a complete listing of primary and secondary antibodies and dilutions that have been tested in array tomography sections and optimized for immunofluorescent labeling. All immunofluorescence was imaged using a Zeiss Axiovert 200 laser scanning confocal microscope with a 40x 1.2 NA water immersion lens or a Zeiss Axioskop 2 MOT Plus wide-field fluorescence microscope with a 63x 1.4 NA oil immersion lens.

Electron microscopy in uninjured sham mice

All electron micrographs were captured using a Joel 100C electron microscope. Three grids were prepared and analyzed per mouse (n=5 mice). Images of axonal cross-sections were captured at a direct magnification of 6,000x beginning at the base of the cingulum and continuing to the lateral edge of the tissue section. Tissue sections were placed on grids with 125 µm holes. To avoid user bias, one field of axons was sampled from each grid square. The axonal field closest to grid bar nearest to midline was chosen. Areas of sectioning artifacts,

folds, and transversely or longitudinally cut axons were avoided. This resulted in 5-8 images per section and 80 images total.

Quantitative measurement of axonal diameters

Image J (NIH) was used for all image analysis. In each electron micrograph, a 5 x 5 µm area was selected in the center of the image for measuring axon diameters. A scaled line was drawn across the narrowest portion of the axon, excluding the myelin sheath, and this measurement was recorded. All cross-sectional axons with distinct borders were measured from each image, excluding those touching the edge of the image. In total, this analysis included an area of 400 μm^2 (16 fields each 5 x 5 µm) out of an estimated total area of 0.5 mm^2 (from measurement of toluidine blue stained semithin sections) per mouse. This includes ipsilateral corpus callosum and external capsule immediately below the injury site ±1.5 mm anterior-posterior.

Approximately the same volume of tissue was analyzed by capturing 4 images from a single 70-90 nm section per animal (n=5 uninjured sham mice) corresponding to the area of corpus callosum beneath the cingulum and extending to the lateral edge of the external capsule. Within each image, four 5 x 5 µm areas of cross-sectional axons were randomly selected for. This resulted in a total of 16 areas for analysis from each mouse. Rabbit anti-tubulin immunofluorescence was performed using a goat anti-rabbit Alexa 488 secondary antibody. In image J, a line was drawn across the middle of the narrowest portion of each fluorescent point and the full width at half max (FWHM) was determined from the intensity profile. These measures were rapidly collected from several axons per field using a publically available Image J macro (courtesy John Lim, v.3 available at http://imagej.1557.x6.nabble.com/FWHM-on-line-selection-td5004777.html).

Creating projection images of axons

Images of immunofluorescent arrays were captured and processed in Image J as previously described for synapses in Kay et al. 2013 and the macros that have been developed for simplifying this process can be found in the supplementary information of their publication. In short, images of serial sections are first compiled in a stack (see Macro 1, supplemental material Kay et al. 2013) and then the multistackreg Image J plugin is used to align each section (courtesy Brad Busse, available at http://bradbusse.net/downloads.html). For axons, tubulin-labeled images were used for all alignments and the transformation file was applied to all subsequent channels. Following alignment, max z-projection images were created from each stack, channels were merged and converted to color, and the resulting image was cropped to the area of interest.

Table 4.1 Primary antibodies for imaging axons by array tomography.

Primary Antibody	Short Name	Company	Cat. No.	Size	Dilution	Notes
Mouse anti-neurofilament H phosphorylated	SMI-31	Calbiochem (Millipore)	NE1022	100 µl	1:100	Labels many axons, not injury specific
Mouse anti-neurofilament H non-phosphorylated	SMI-32	Calbiochem (Millipore)	NE1023	100 µl	1:20 or 1:100	Preferentially labels injured axons
Mouse anti-neurofilament 200 kDa + 160 kDa	SMI-34	Abcam	ab24571	250 µl	1:200	Labels many axons, not injury specific
Rat monoclonal to myelin basic protein	MBP	Abcam	ab7349	1 ml	1:100	Good myelin labeling
Rabbit polyclonal anti-β-APP	APP	Invitrogen	51-2700	200 µl	1:50	Seems to label injured axons and many vesicle structures. Some punctate background labeling was apparent in APP-/- tissue
Rabbit polyclonal to α-tubulin	alpha-tubulin	Abcam	ab18251	50 µg	1:200	Labels all axons
Rabbit polyclonal anti-200 kDa neurofilament	NF200	Sigma-Aldrich	n4142	200 µl	1:200	Labels many axons, not injury specific
Phospho-tau (pS202)	AT8	Pierce	MN-1020	100 µg	1:50	Labels tau aggregates, no labeling in Tau-/-
Phospho-tau (pS202)	CP13	Courtesy P.Davies		ascites fluid, 5 ml	1:50	Labels tau aggregates, no labeling in Tau-/-
Paired helical filaments	PHF1	Courtesy P.Davies		ascites fluid, 5 ml	1:50	Labels tau aggregates, no labeling in Tau-/-
Mouse monoclonal to stathmin 3	STMN3, SCLIP	calbiochem (millipore)	ab76678	ascites	1:50	Punctate labeling in neurites

Table 4.2 Secondary antibodies used for array tomography.

Secondary Antibody	Company	Cat. No.	Size	Dilution
Donkey anti-rabbit Alexa 488	Invitrogen	A21206	0.5 ml	1:200
Goat anti-rat Alexa 488	Invitrogen	A11006	0.5 ml	1:200
Goat anti-mouse 488	Jackson Immunoresearch	115-546-146	0.75 mg	1:200
Goat anti-mouse Alexa 594	Invitrogen	A11032	0.5 ml	1:200
Donkey anti-rabbit Cy3	Jackson Immunoresearch	711-165-152	0.5 mg	1:200

4.3 RESULTS

4.3.1 Adapting array tomography for the detection of injured axons

Overall the workflow is similar to that reported for analysis of synapses (**Figure 4.1**) though there are additional considerations to take into account for the preparation of arrays for analysis of axons. Most importantly, orienting tissue blocks in the gelatin capsules for embedding needs be done with care so that the maximum amount of white matter can be sectioned later. Second, because axons have clear orientations, it is important to consider this in downstream analysis. For example, axons cut crosswise will appear punctate while axons cut longitudinally will appear as short segments that have different X-Y locations in each section. Assaying axons so that isotropic volumes are measured in each array or sampling from a sufficient number of randomly selected areas throughout the tissue may be the best approach to avoiding orientation-dependent sampling bias.

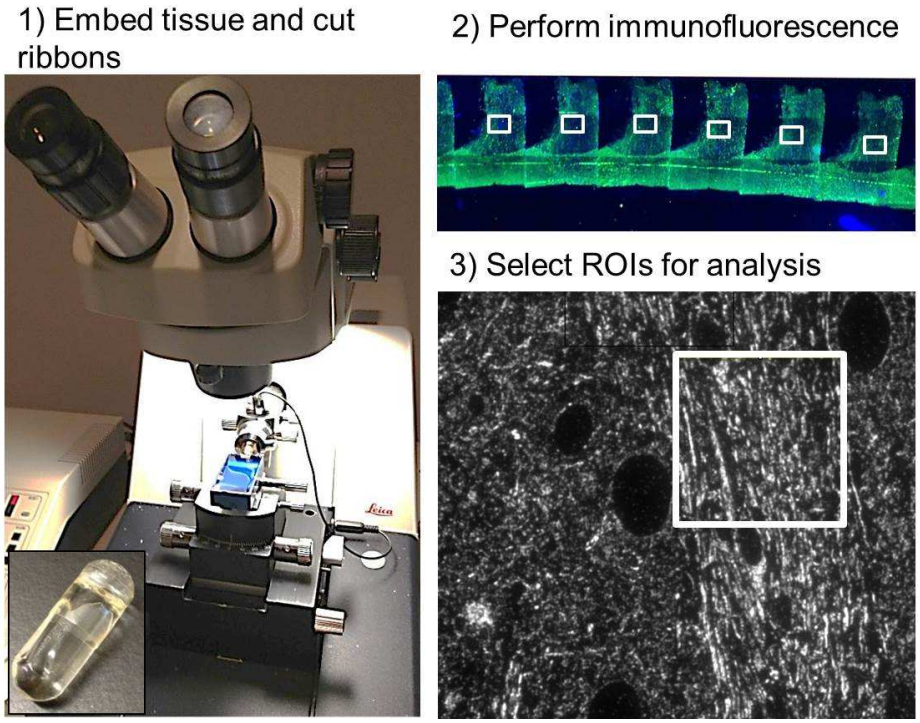

Figure 4.1 Array tomography workflow. (1) Sections are embedded in LR white media in gelatin capsules (inset) and an ultramicrotome is used to produce 70-90 nm section ribbons using a histojumbo diamond knife. (2) Standard immunofluorescent techniques are used to label each ribbon and images from sections are captured using a 63x lens on an epifluorescent microscope. (3) Each image can then be further subdivided into smaller regions for analysis, excluding cell bodies and tissue processing artifacts.

Several antibodies were tested and their sensitivity to the detection of axons and axonal injury was determined (**Tables 4.1** and **4.2**). We found an antibody to tubulin that appears to robustly detect axons in the mouse corpus callosum and external capsule. Using this antibody we were able to resolve individual axons by array tomography (**Figure 4.2 A-L** and **4.3 B**). By comparison, we were not able to resolve single axons by conventional laser scanning confocal microscopy of tubulin immunofluorescence in thick sections (**Figure 4.3 A**).

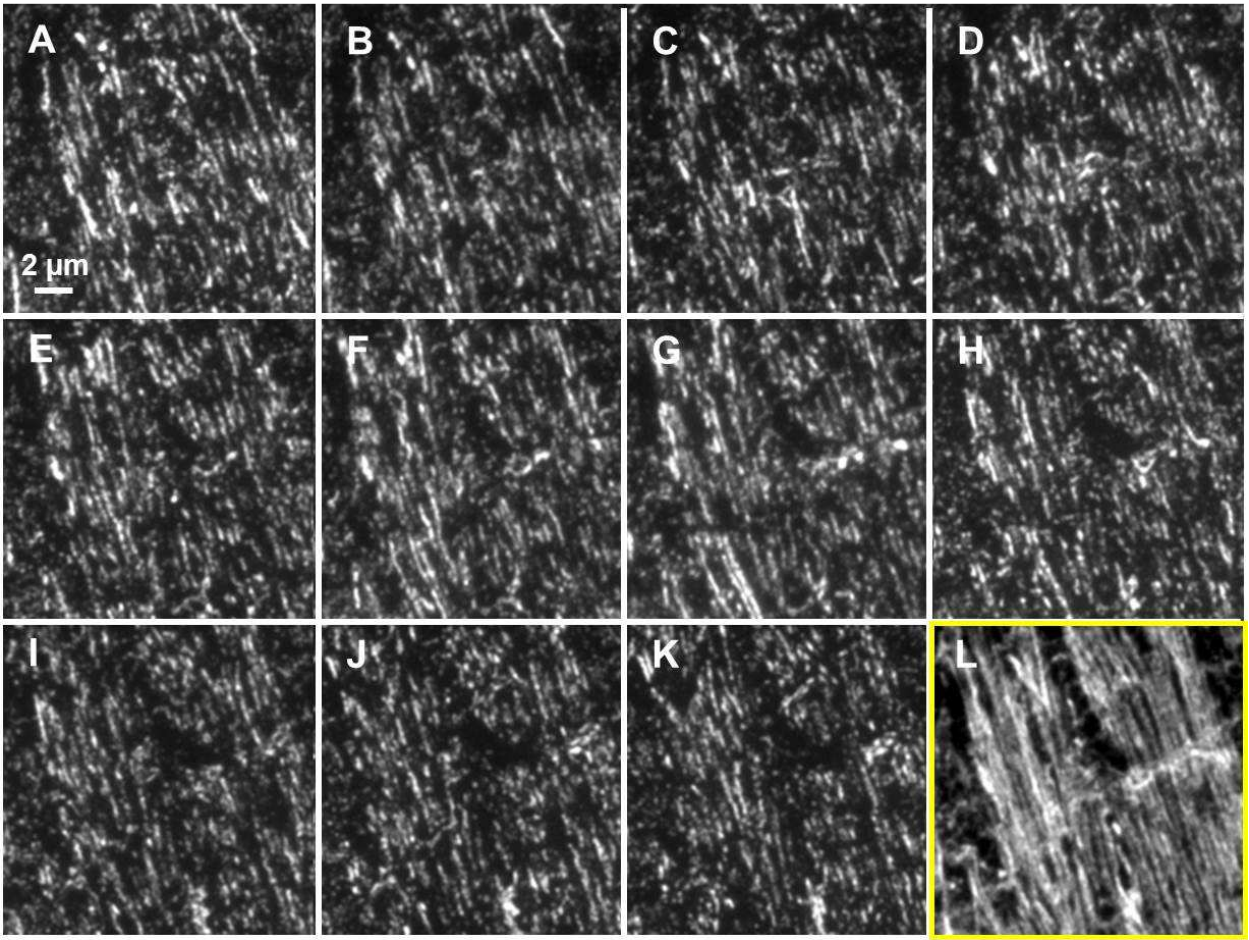

Figure 4.2 Example of a short array containing uninjured mouse external capsule labeled with anti-tubulin and Alexa 488. (A-K) Images of eleven 70 nm thick ultrathin sections labeled with anti-tubulin and Alexa 488. Images have been co-registered so that each represents the same 19.5 x 19.5 µm area. (L) A projection of the 11 image stack shows a reconstruction of individual, longitudinally/transversely cut axons within this stack.

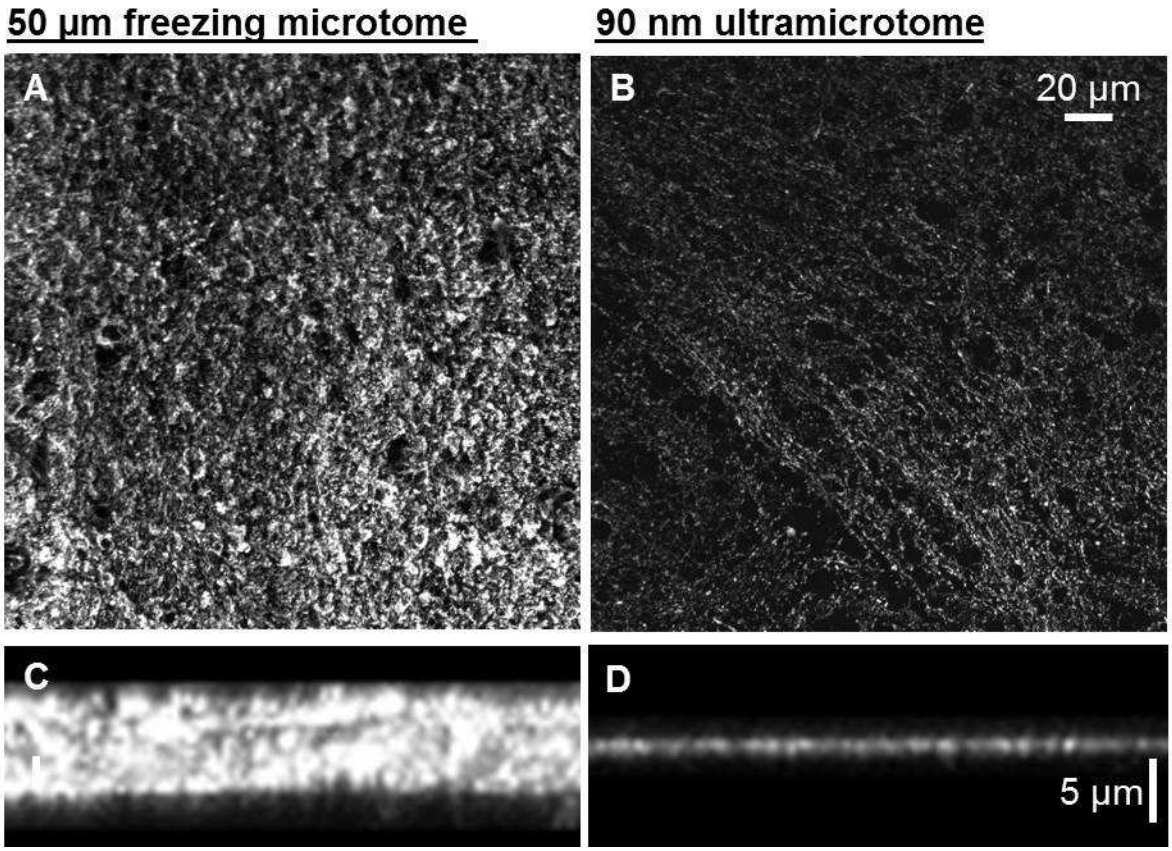

Figure 4.3 Side by side comparison of tubulin labeling in thick sections and ultrathin sections. (A) A confocal X-Y projection image of a section of uninjured mouse corpus callosum mouse cut at a 50 µm thickness on a freezing microtome and labeled with anti-tubulin and Alexa 488. (B) A confocal X-Y projection image of an ultrathin section from a similar region of corpus callosum cut at 90 nm on ultramicrotome and labeled with anti-tubulin and Alexa 488. (C and D) are X-Z images showing the improved spatial resolution along this axis.

4.3.2 Comparison of tubulin-labeled ultrathin sections with electron microscopy

To determine how tubulin labeling in ultrathin sections reflects axonal ultrastructure, corpus callosum and external capsule in one hemisphere from sham injured mice (n=5) was prepared for array tomography and the opposite hemisphere was prepared for electron microscopy (**Figure 4.4 A-F**). Axon diameters were measured in both electron micrographs and fluorescent images. A total area of 0.002 mm^2 was analyzed in each case. By electron microscopy, we were able to measure the diameters of 2612 axons and in ultrathin sections, 1178 axons. A frequency distribution of these measures shows that the 25 % percentile for

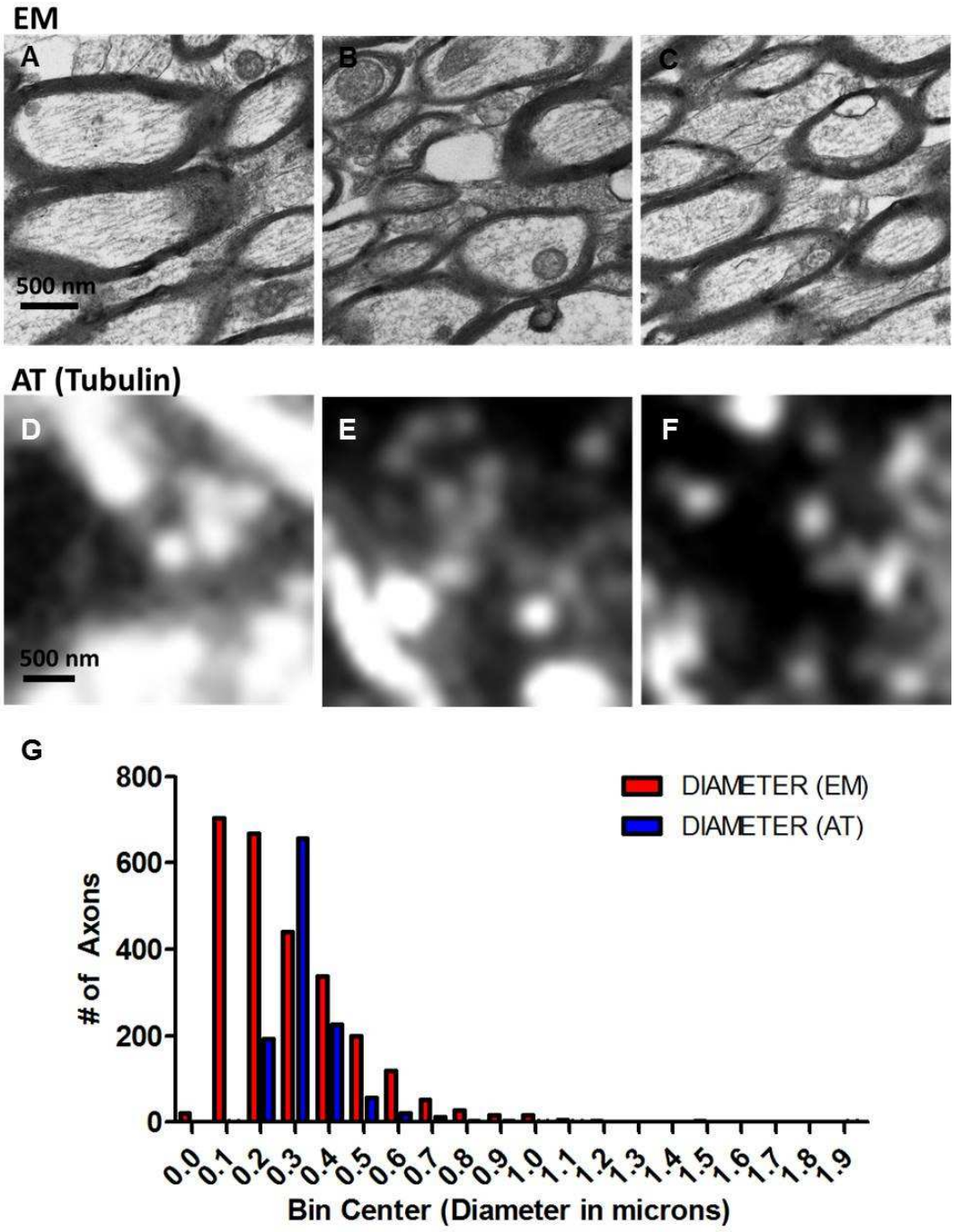

Figure 4.4 Electron microscopy versus tubulin-labeled ultrathin sections in uninjured wild-type mouse corpus callosum and external capsule. (A-C) Electron micrographs or (D-F) tubulin-Alexa 488 fluorescence images were obtained of axonal cross-sections and were used for axon diameter measurements. (G) Frequency distribution of axon diameter measurements from electron micrographs (EM) and ultrathin sections used in array tomography (AT). An equal tissue area was examined by each technique. A total of 5 mice were included in this analysis, with the right hemisphere being prepared for EM and the left for AT.

axon diameters was 0.14 μm, the median was 0.23 μm, and the 75% percentile was 0.39 (**Figure 4.4 F**). In tubulin-Alexa 488-labeled ultrathin sections, the 25% percentile was 0.26 μm, the median was 0.30 μm, the 75% percentile was 0.36 μm. In all, this indicates that tubulin labeling does not identify all axons and, in particular, very small diameter fibers are not imaged. Specifically, some smaller diameter axons may appear larger due to spatial low-pass filtering.

4.3.3 Axonal Injury Markers in Ultrathin Sections

Axonal injury markers were tested in sections containing corpus callosum and external capsule from mice subject to a moderate controlled cortical impact (CCI) traumatic brain injury and sacrificed at 24 hours (n=2). Markers to phosphorylated or non-phosphorylated heavy chain neurofilaments and amyloid precursor protein (APP) resolved structures resembling classic axonal varicosities (**Figure 4.5** and **4.6**). However, labeling in APP knockout mice subject to controlled cortical impact (n=2) indicates that the antibody used is not specific to APP (**Figure 4.5 C inset**).

Further, when tested in an uninjured sham mouse, SMI-31 appeared to label uninjured axonal segments (**Figure 4.7 A**). This injury nonspecific labeling was also seen using other neurofilament antibodies such as NF200 and SMI-34 (data not shown). SMI-32 alone appeared to not be present in uninjured sham mice (**Figure 4.7 B**). Thus, SMI-32 was used in subsequent studies as an axon injury specific marker. Other investigators have reported similar results using SMI-31 and SMI-32 (Budde et al. 2008).

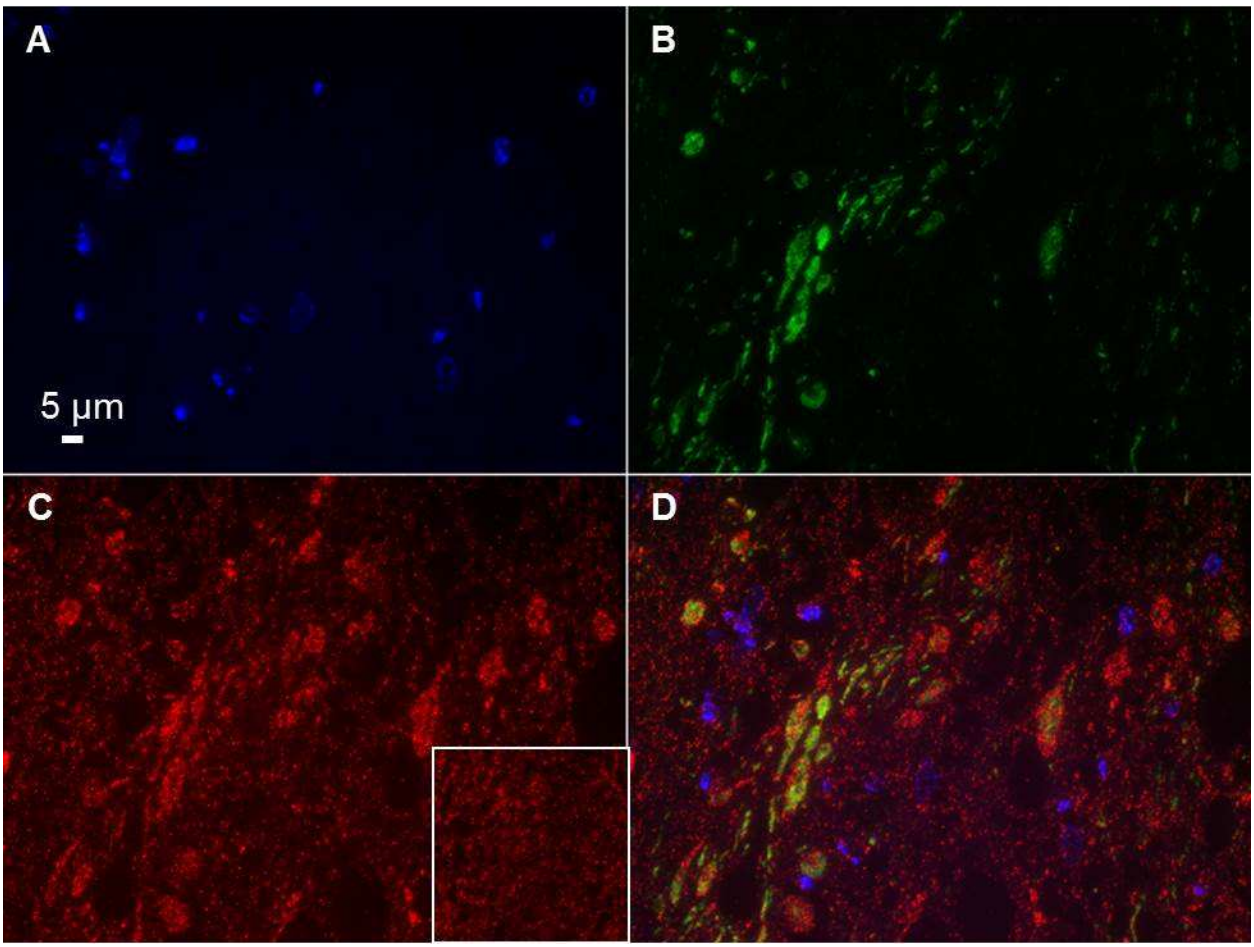

Figure 4.5 Axonal injury markers SMI-31 and APP in 24 hour 1.0 mm CCI external capsule. (A) DAPI labeling indicates cell nuclei. (B) SMI-31 Alexa 488 labeled axons. (C) APP Cy3 labeled axons (inset is from CCI injured APP knockout mouse). (D) Composite image of DAPI, SMI-31, and APP.

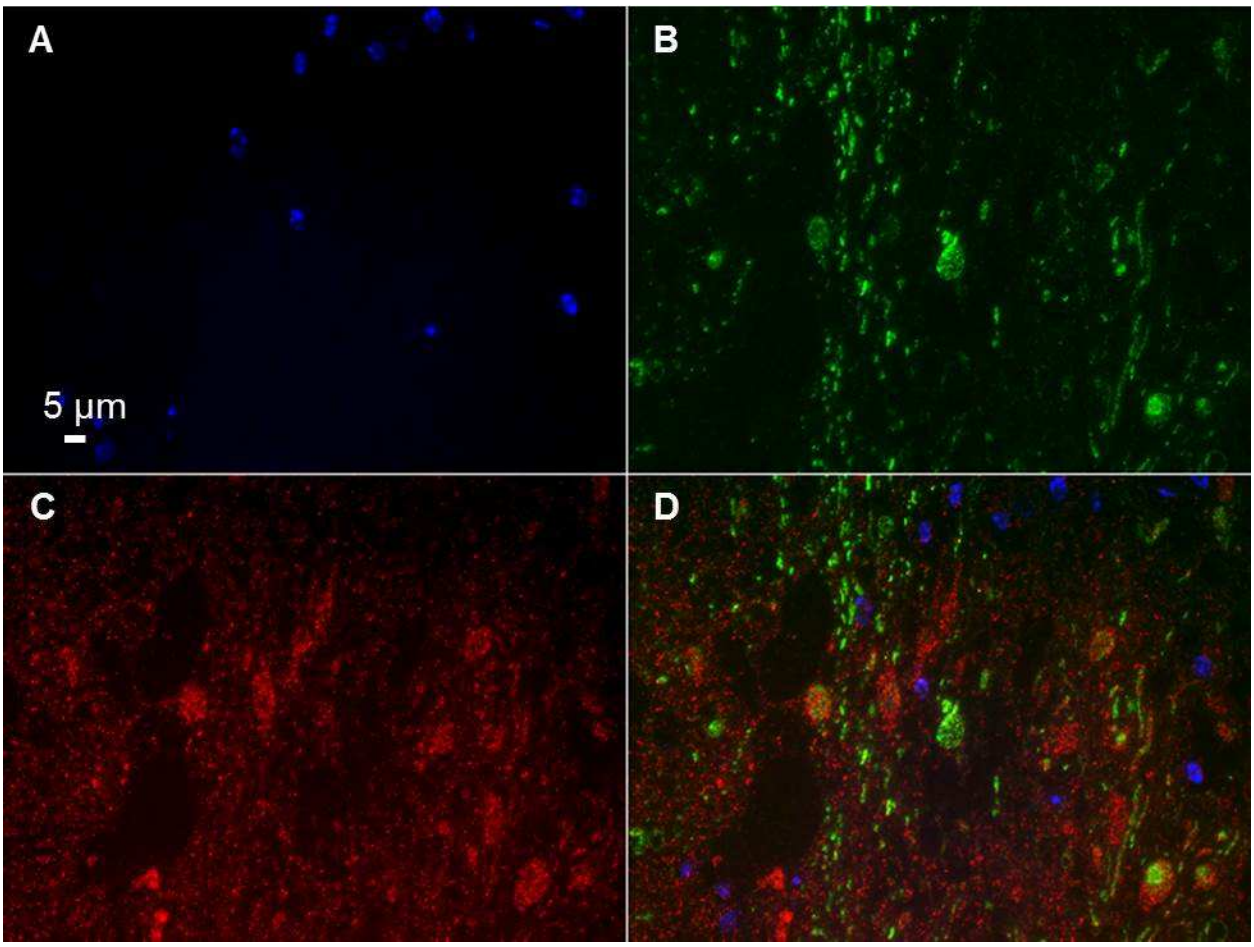

Figure 4.6 Axonal injury markers SMI-32 and APP in 24 hour 1.0 mm CCI external capsule. (A) DAPI labeling indicates cell nuclei. (B) SMI-32 Alexa 488 labeled axons. (C) APP Cy3 labeled axons. (D) Composite image of DAPI, SMI-31, and APP.

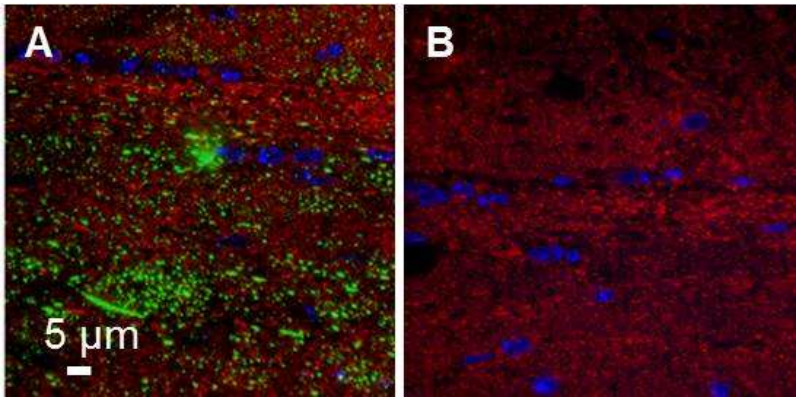

Figure 4.7 Axonal injury markers SMI-31 and SMI-32 in uninjured sham external capsule. (A) SMI-31 labels axons in an uninjured mouse while (B) SMI-32 does not. Green is SMI-31 or SMI-32, red is tubulin Cy3, and blue is DAPI.

4.3.4 Preliminary data using SMI-32/Tubulin to measure axonal injury after TBI

To measure axonal injury in TBI, tissue blocks containing corpus callosum and external capsule from uninjured sham (n=5), repetitive concussive TBI (n=5), and 1.5 mm CCI (n=4) mice were prepared 7 days post-injury. Sections from each were stained for anti-SMI-32 to label areas of injury and anti-tubulin to label all axons (**Figure 4.8**). In sham mice, little to no SMI-32 was detected and tubulin-labeled axons did not appear to be swollen or distorted (**Figure 4.8 A, B**). Mice subjected to rcTBI had areas of small punctate SMI-32 labeling as well as regions of SMI-32/tubulin co-localization (**Figure 4.8 C, D**). In moderate TBI, clear disruption of axons was evident with large SMI-32 swellings appearing with or without tubulin co-localization. Further, the overall amount of tubulin appeared to be greatly reduced. This indicates that quantitative measurement of total axonal injury may be represented by positive SMI32 staining, tubulin staining loss, or a ratio between SMI-32 and tubulin labeling.

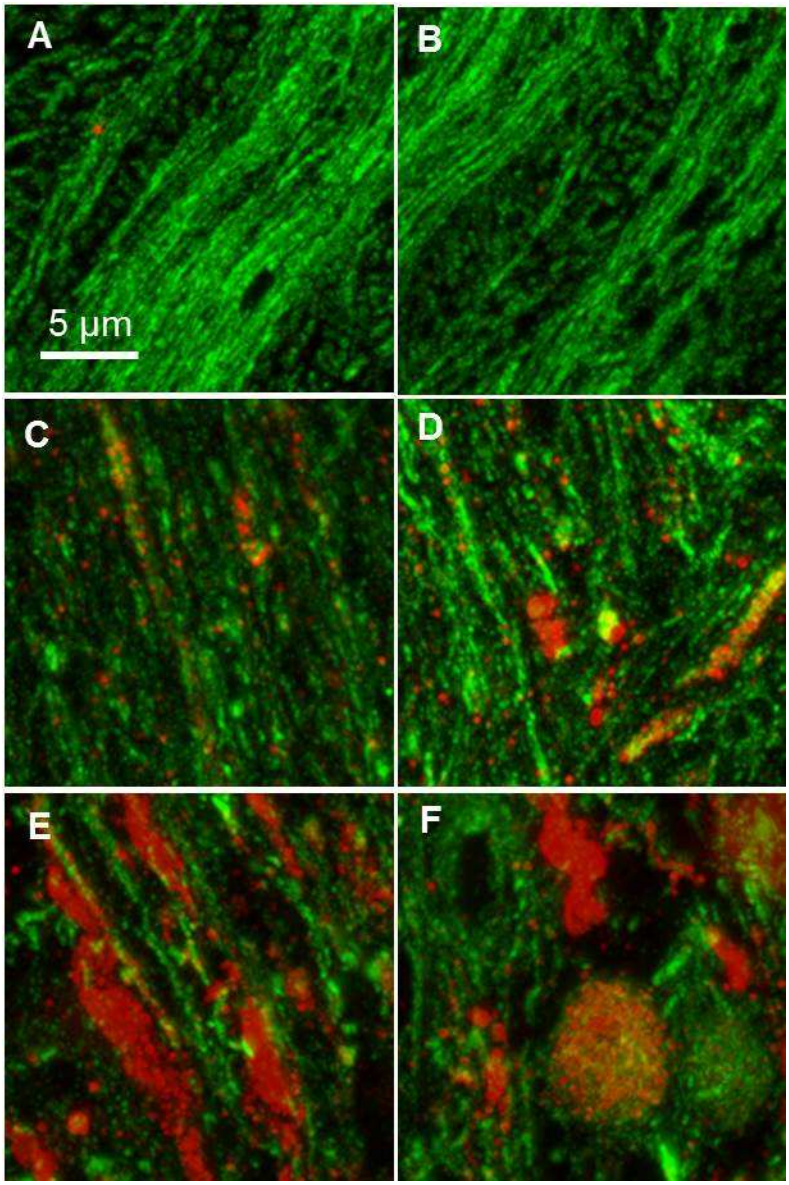

Figure 4.8 Projection images of arrays (20-30 sections each) from external capsule labeled with the axonal injury marker SMI-32 (red) and tubulin (green). (A, B) Axons from uninjured wild-type mice displayed little SMI-32 labeling. (C,D) Mice subjected to mild repetitive concussive traumatic brain injury had punctate areas of SMI-32 labeling and occasional co-localization of SMI-32 and tubulin in swollen axons at 7 days. (E,F) Larger axonal varicosities >3 µm in diameter were apparent in a model of 1.5 mm CCI moderate traumatic brain injury at 7 days. Tubulin loss was also evident.

4.3.5 Other markers for array tomography

In addition to assaying classic markers of axonal injury in white matter, we also tested antibodies to myelin basic protein (MBP) and to the microtubule associated protein tau. Anti-MBP prominently labeled myelinated axons in white matter tracts (**Figure 4.9**). The tau antibodies PHF1, AT8, and CP13 were all tested in tissue from aged mice carrying a familial frontotemporal dementia mutation (TauP301S). These phospho-tau antibodies all detected perinuclear aggregates in entorhinal cortex (PHF1 shown, **Figure 4.10**). No tau labeling was seen in the cortex of tau knockout mice (PHF1 shown, **Figure 4.10 C inset**).

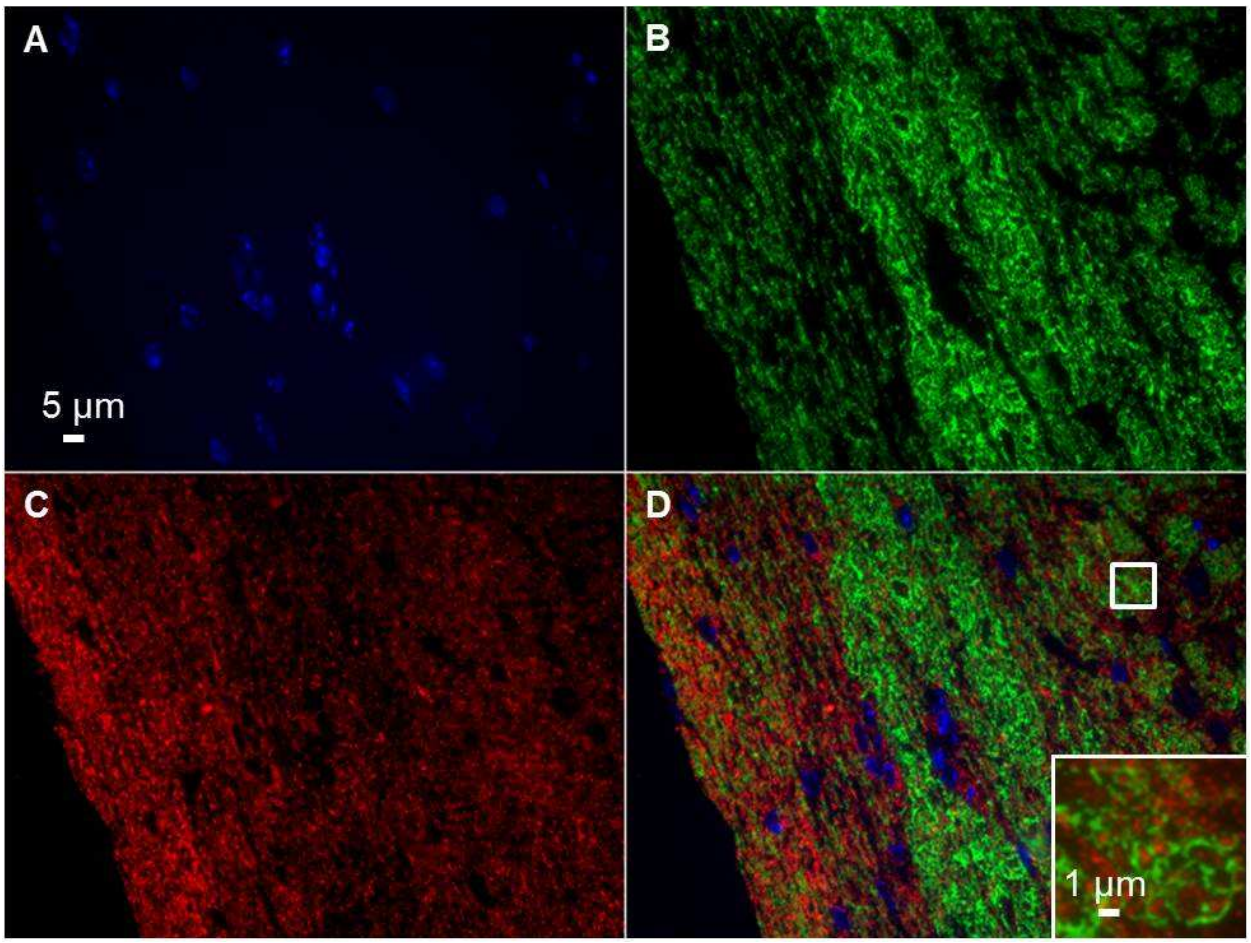

Figure 4.9 Myelin basic protein and tubulin labeling in the external capsule of an uninjured wild-type mouse. (A) DAPI labeling indicates cell nuclei. (B) Myelin basic protein-Alexa 488 labeled axons. (C) Tubulin-Alexa 594 labeled axons. (D) Composite image of DAPI, myelin basic protein, and tubulin. Inset shows an enlarged view of the box in (D), where individual myelinated axonal cross-sections are clearly visible.

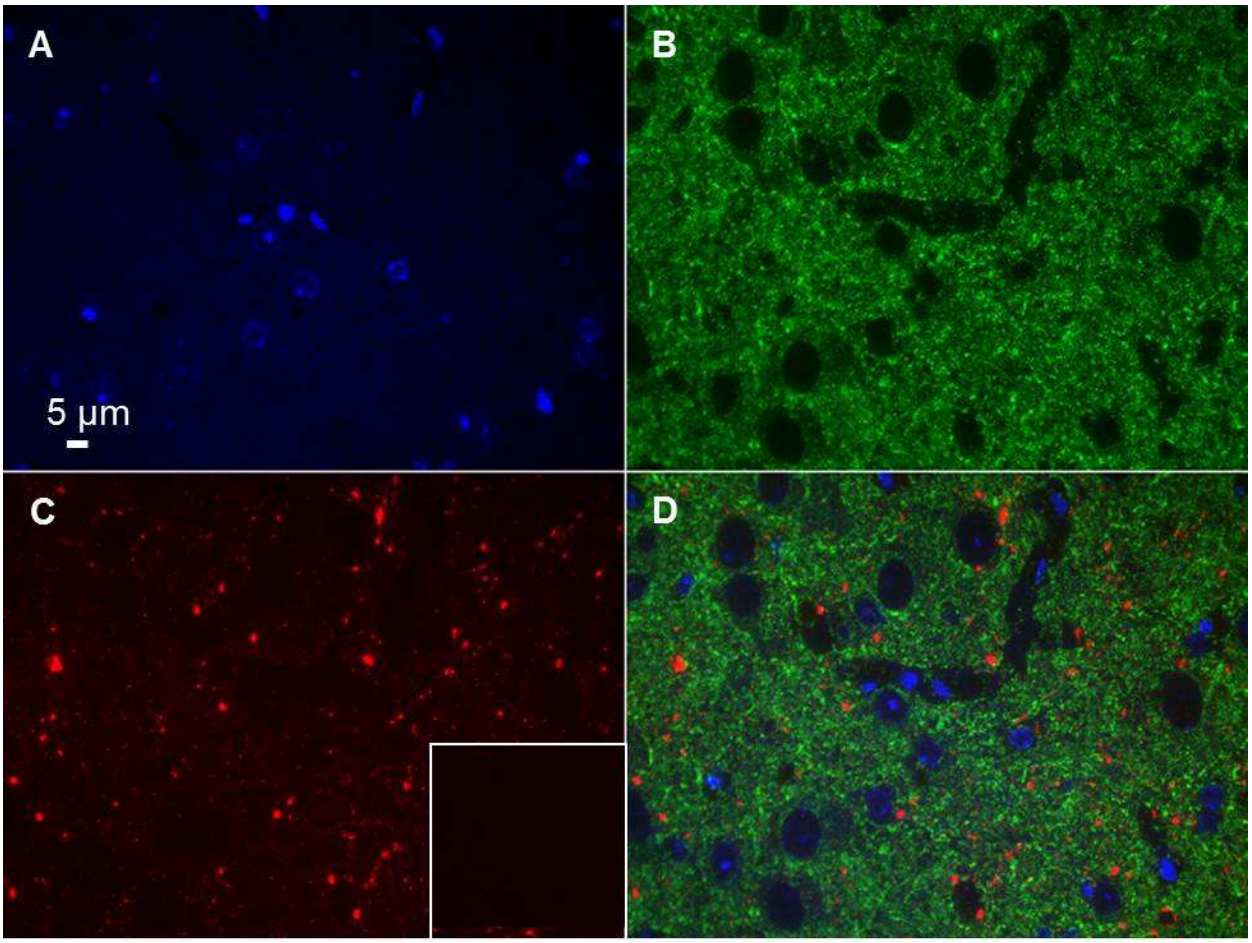

Figure 4.10 PHF-1 tau and tubulin labeling in the entorhinal cortex of a 12-month-old Tau P301S mouse. (A) DAPI labeling indicates cell nuclei. (B) Tubulin Alexa 488 labeled axons. (C) PHF1 Cy3 labeled axons. Inset shows the absence of PHF1 labeling in cortec from a tau knockout mouse (D) Composite image of DAPI, tubulin, and PHF1.

4.4 DISCUSSION

Here we apply the powerful technique of array tomography to the detection of injured axons. This promising method appears to distinguish injury in axons with diameters greater than ~200 µm in the repetitive concussive and moderate-severe TBI models compared to uninjured shams. Further, a wide range of antibodies were tested that can be used in several downstream applications beyond the field of traumatic brain injury.

Previously, array tomography has been used to quantify synaptic density near amyloid plaques in mice, to quantifying synapses in human AD patients with or without the *APOE4* allele, to investigate mitochondria distribution in the soma and neurites of mutant tau mice, to reconstruct tau-containing axons and synapses in a reversible tauopathy model, and to examine morphological changes in mouse blood vessels and aortic aneurysms (Koffie, et al. 2009; Kopeikina, et al. 2011; Koffie, et al. 2012; Saatchi, et al. 2012; Kopeikina, et al. 2013; Polydoro, et al. 2013; Pooler, et al. 2013). To date, this is the only investigation of which we are aware using this technique to study axonal injury specifically. The ability to qualitatively and quantitatively examine axonal pathology is broadly relevant to several injury and neurodegenerative disease studies which currently rely on traditional histological measures and *in vivo* MRI techniques to investigate axonal injury. However, use of standard techniques only reflects axonal injury if it results in large scale changes. Here, we show by electron microscopy that most mouse axons in corpus callosum and external capsule are smaller than 500 nanometers, which is well below the typical resolution of these techniques. Using array tomography we were able to resolve individual axons with diameters near 200 nm or greater.

Further, in these small axons we were able to detect axonal injury in mice that were subjected to repetitive concussive TBI and were sacrificed at 7 days. These results are in accordance with silver staining abnormalities and electron microscopy data in this injury models which indicates widespread axonal damage in spite of the lack of traditional immunohistochemistry findings (Shitaka et al. 2011). Thus, it would appear that array tomography may be useful for future studies investigating axonal injury in this model. This technique has the advantage of being more quantitative than silver staining, which is measured semi-quantitatively by optical density. Also, array tomography is less costly than electron microscopy as it can be performed with a standard epifluorescent microscopy. Further, compared to electron microscopy, this technique has higher throughput and allows for a greater

volume of tissue to be processed at a time. It also has the advantage that many antibodies are available which to aid in the study of specific proteins in axonal injury.

However, there are several limitations that should be addressed. First, while arrays can provide high spatial resolution data that conventional histology cannot, electron microscopy remains the gold standard. In these studies, we were not able to resolve small axons <200 nm in diameter and based on data from parallel electron microscopy studies, this appears to be nearly half of the total population of axons in the corpus callosum and external capsule as determined in this study and by others (Olivares et al. 2001). Further, considering that we were also not able to resolve all large diameter axons, it may be that the rabbit polyclonal anti-tubulin antibody chosen for these studies does not label all axonal populations. Testing additional tubulin antibodies may shed light on this issue. On the other hand, we were not able to determine how the differential preparation and handling of tissue for EM versus AT may have contributed, in part, to this discrepancy. Thus direct quantitative comparison between EM and AT may not be entirely appropriate. Ideally, such a study would be performed in the same tissue sections—prior to embedding in LR White, tissue would be incubated in osmium tetroxide. After immunofluorescence, lead citrate and uranyl acetate would be applied to the tissue sections and scanning electron would be performed. This correlative electron microscopy approach has been reported by Micheva and colleagues and may be a future direction for validation of axonal injury measures in array tomography (2007).

Additional studies to be performed include further validating this method and developing a protocol to apply stereological approach to the quantification of injury. For future validation, not only should injured axons be measured in corpus callosum and external capsule of mice subjected to varied levels of injury (**Figure 4.10**), but early and late timepoints should be examined. Qualitatively, injury appears to result in reduced tubulin-positive axons. If this is truly the result of axon injury and not an artifact of tissue preparation, then at an early timepoint <24 hours post-injury there should be more tubulin labeling than at a later timepoint >1 month post-

injury. Moreover, current efforts are aimed at applying stereological principles to the collection and analysis of data from array tomography sections. In the future, 3-4 sections will be collected along the anterior-posterior axis of each tissue block. From each section, 6-8 images will be collected and 8-10 20 x 20 μm crop boxes from each image will examined so that a minimum of 100-200 areas will be analyzed per mouse. All areas chosen for analysis will be randomly selected using a grid. This approach will ensure a rigorous and unbiased measurement of axonal injury throughout the volume of the injured corpus callosum and external capsule.

Finally, future studies may also use this method to study other aspects of axonal injury in both traumatic brain injury and other conditions. Labeling myelin basic protein, for example could be used not only to determine if myelinated axons are preferentially injured in rcTBI, but could also be used to investigate demyelinating disorders such as multiple sclerosis. Given the ability to discriminate individual axons in large areas of tissue, it may be possible to detect early signs of demyelination, and discern the effects of therapeutic or genetic manipulations on disease progression. Also, given our ability to detect abnormally phosphorylated tau species using multiple antibodies, a clear direction of this work is to apply this method to the detection of tau alterations after traumatic brain injury. Previously, our lab has observed abnormal accumulations of phosphorylated intra-axonal tau following moderate-severe injury (Tran, et al. 2011a; Tran, et al. 2011b). Considering the sensitivity of this technique, it will be interesting to use arrays to measure intra-axonal tau in less severe injury models such as rcTBI. Last, an exciting direction is to use this method to detect axon degeneration in tissue from human patients where it may be possible to answer key questions about Chronic Traumatic Encephalopathy or Alzheimer's disease through quantitation of axon injury or loss and correlative analysis with clinical measures.

To summarize, we have adapted array tomography to identify injured axons in tissue from two different experimental TBI mouse models. Several markers are available for

examining different aspects of axonal integrity including tubulin, neurofilaments, APP, myelin basic protein, and phospho-tau species. Future studies will be aimed at using this method quantitatively in both mouse models and in human tissue.

CHAPTER 5

Acute Reduction of Microglia does not Alter Axonal Injury in a Mouse Model of Repetitive Concussive Traumatic Brain Injury

5.1 INTRODUCTION

While 91% of athletes will recover from symptoms of concussion within a week, there is increasing awareness of the long-term consequences of suffering one or more concussions, particularly among retired professional football players and boxers. (Corsellis et al. 1973; Mortimer 1985; Roberts et al. 1990; Geddes, et al. 1999; Guo, et al. 2000; Guskiewicz et al. 2003; McCrea et al. 2003; Guskiewicz, et al. 2005; McKee et al. 2009) While the origins of these long-term effects are unknown, studies in post-mortem samples from human TBI and from individuals known to have received multiple concussive injuries have consistently revealed the presence of degenerating axons and inflammation months to years after the initial insult.(Oppenheimer 1968; Adams, et al. 1982; Blumbergs, et al. 1989; Gultekin, et al. 1994; Chen et al. 2009; Goldstein et al. 2012; Johnson et al. 2013a; McKee, et al. 2013a) These processes have also been viewed *in vivo* using diffusion tensor imaging to visualize white matter injury in concussed individuals and using PET ligands to the peripheral benzodiazepine receptor to confirm the presence of microglia and macrophage in TBI patients.(Chappell, et al. 2006; Zhang, et al. 2006; Zhang et al. 2010; Cubon et al. 2011; Henry et al. 2011; Ramlackhansingh et al. 2011; Bazarian, et al. 2012) Our group and others have developed mouse models of mild repetitive concussion and have also observed the presence of injured axons within white matter and the accumulation of glial cells.(Laurer et al. 2001; Uryu et al. 2002; Creeley et al. 2004; Creed et al. 2011; Shitaka et al. 2011; Mouzon, et al. 2012)

Interestingly, in our repetitive closed-skull injury model we have observed that the accumulation and activation of microglia within white matter regions precedes the degeneration of axons as visualized by silver staining.(Shitaka et al. 2011) Altogether, these data have led us to hypothesize that microglia and macrophage may contribute to secondary axon injury processes following concussion.

To address this hypothesis we used a CD11b-TK transgenic mouse model to reduce the numbers of microglia within the corpus callosum and external capsule. CD11b-TK mice express a mutated form of thymidine kinase (TK) from herpes simplex virus under the CD11b promoter.(Gowing, et al. 2006) When mice are treated with the nucleotide analog ganciclovir or its more soluble prologue, valganciclovir, the drug is metabolized by cells expressing thymidine kinase into a toxic product that leads to cell death. Valganciclovir will only become toxic to CD11b+ cells expressing herpes simplex virus thymidine kinase and is not toxic to genetically wild-type mice such as the CD11b-TK -/- littermate controls. Research from other groups has shown that daily intraperitoneal (IP) injection of ganciclovir into these mice effectively depletes circulating macrophages and prevents proliferation of microglia in the brain.(Heppner, et al. 2005; Gowing et al. 2006) Here we show that intracerebroventricular (ICV) delivery of different doses of valganciclovir resulted in a dose-dependent reduction of microglial cells in mice subjected to repetitive closed-skull injury. The effects of reducing the microglial population on both acute and sub-acute axon degeneration after injury were assessed by silver staining. We found that reducing the number of microglial/macrophage cells had little effect on the amount of axon degeneration at either 7 days or 21 days post-injury.

5.2 METHODS

Animals

CD11b-TK mice were acquired from Jean-Pierre Julien at Laval University (Quebec, CA). CD11b-TK mice express herpes simplex virus thymidine kinase under the CD11b promoter expressed in microglia and macrophage. Male CD11b-TK +/- founder mice were crossed to C57bl/6j female mice (cat# 000664, JAX). The resulting offspring were genotyped using previously published methods.(Gowing et al. 2006) Mice carrying the CD11b-TK transgene were termed CD11b-TK+/- mice, and littermates not carrying the transgene were termed CD11b-TK -/- mice and are genetically wildtype. All mice were housed under a 12 hour light-dark cycle and given food and water ad libitum in accordance with the protocols of the Animal Studies Committee at Washington University in Saint Louis.

Osmotic pumps

Alzet osmotic pumps (cat#1002, #2004) with flow rates of 0.25 µl/hour were used for these experiments. A complete description of pump assembly can be found elsewhere.(DeVos, et al. 2013) Briefly, cannula tubing (cat#312VT) and osmotic pump connector cannula (cat#3280PM/SP, cut 2.5 mm below pedestal) were purchased from Plastics One. Pump reservoirs were filled with either valganciclovir (cat#SML0191, Sigma) in 0.9% sterile saline (NaCl) or with 0.9% NaCl. Osmotic pump flow tubes were stripped of their plastic caps and the flow tubes were connected to one-inch lengths of cannula tubing. The other end of the cannula tubing was attached to the osmotic pump connector cannula. The entire assembly was primed by placing the reservoir in conical tubes containing 0.9% NaCl and tubes were stored at 37℃ for 36-48 hours prior to implantation. This longer priming step was deemed necessary because cannula tubing was not filled with drug—preliminary experiments with 1.5% Evan's blue solution in saline showed that it takes ~36 hours for solution to travel from the reservoir of 14 day 0.25 µl/hour pumps to the end of the cannula under these conditions.

Surgical procedures

Six to eight-week-old CD11b-TK +/- and wild-type littermate controls were used in all experiments. Mice were randomly assigned to either NaCl or valganciclovir treatment groups. For implantation of osmotic pumps, mice received inhaled isofluorane anesthesia and the head was fixed in a stereotaxic frame. Temperature was regulated using a heat pad (Sun microsystems II). A midline incision was made to expose the skull and a small (0.9mm) burr hole was drilled contralateral to the rcTBI impact site at A/P -0.84 mm relative to bregma, ML +1.5 mm relative to midline at bregma. Pumps were implanted subcutaneously and a drop of cyanoacrylate glue was applied to the bottom of the plastic portion of the cannula. A cannula guide was used to drive the metal osmotic pump connector cannula through the burr hole into the lateral ventricle (D/V -2.5 mm) and to hold it firmly in place for 1-2 minutes while the glue set. The top of the cannula was trimmed and the incision was sutured closed. Mice received antibacterial ointment and were placed on a heat pad for recovery. Once animals were ambulatory they were housed individually to prevent cagemates from tampering with pumps.

Seven days after pump implantation, pumps were removed, fitted with new cannulas, placed in individual conical tubes containing 0.9% NaCl and 0.01% sodium azide (NaN_3) and stored at 37℃. Mice then received two repetitive closed skull injuries 24 hours apart as described previously.(Shitaka et al. 2011) Briefly, a rubber tip was fitted on an electromagnetic impact device which was used to impact the skull with the tip centered at A/P -1.8, M/L -1.5 bregma to a depth of -3.3 mm . Sham injured mice underwent the same surgical procedures but did not receive impacts. Immediately following the second impact, pumps were rinsed in filtered phosphate buffered saline (PBS) and re-implanted as described above to resume drug delivery.

Histology

Mice were sacrificed by isofluorane overdose and decapitation either 7 days or 21 days after the first repetitive closed-skull injury. All mice were perfused with 10 milliliters cold 0.03% heparin in PBS. Brains were then removed and placed in 4% paraformaldehyde (PFA) for 24-48 hours at 4℃ and then in 30% sucrose in PBS for 24-48 hours at 4℃. Once equilibrated in sucrose, they were frozen on dry ice and sliced into 50 µm sections on a freezing microtome. Serial sections were collected in cryoprotectant (30% ethylene glycol, 15% sucrose, 0.03 M phosphate buffer) and stored at 4℃ until use.

For floating immunohistochemistry was performed on sections to visualize rabbit polyclonal anti-Iba-1 (cat# 019-19741, Wako), chicken polyclonal anti-GFAP (cat#ab4674, Abcam), rabbit polyclonal anti-β-APP (cat# 512700, Invitrogen), or mouse monoclonal RM014 (cat# 34-1000, Novex). For this, sections were washed 3 times for 5 minutes in TBS, incubated in 0.03% hydrogen peroxide (H_2O_2) for 10 minutes, washed 3 times for in TBS, then blocked for 30 minutes in either 3% normal goat serum (NGS, cat#S-1000, Vector Labs) or 3% normal donkey serum (NDS, cat#017-000-121, Jackson ImmunoResearch) in 0.25% Triton-X tris buffered saline (TBS-X). Following blocking, primary antibodies were applied at a 1:1000 dilution in blocking solution and incubated overnight at 4℃ with gentle shaking. The following day, sections were again washed, incubated one hour at room temperature in either biotinylated goat anti-rabbit IgG (cat#BA-1000, Vector Labs), biotinylated donkey anti-chicken IgG (cat#703-065-155, Jackson ImmunoResearch) secondary antibodies were diluted 1:1000 in TBS-X, washed again, then incubated in 1:400 ABC reagent (cat#PK-6100, Vector Labs) in TBS for another hour. Finally, sections were washed and placed in 3-3'-diaminodebzidine tetrahydrochloride (DAB; cat# D5905) for 5-6 minutes. After development in DAB the sections were washed, placed on slides and allowed to air dry, and coverslipped with cytoseal (cat# 8312-4, Richard-Allan Scientific). For RM014 staining specifically, the following modifications to

the above protocol were made 1) sections were blocked in 1:10 mouse serum, 2) the primary antibody was incubated 1:2 with biotinylated goat anti-mouse Fab IgG (cat#115-007-003, Jackson ImmunoResearch) for 20 minutes prior to application to the sections overnight and 3) the secondary antibody was unnecessary, sections were immediately incubated in ABC on day 2.

Adjacent sets of floating sections were subjected to silver staining (cat#PK301, NeuroSilver Kit II, FD Neurotech) following the manufacturer's instructions with minor modifications, as previously reported(Shitaka et al. 2011). Sections were incubated for 5 days in paraformaldehyde prior to silver staining and were only incubated in solution C once for 2 minutes.

For cresyl violet staining, sections were rinsed in TBS twice for 5 minutes then mounted on glass slides. Once air-dried, they were placed in cresyl violet solution (cat#PS102-1, FD Neurotech) for 5 minutes then rinsed and coverslipped following manufacturer's protocol.

For TUNEL-NeuN double-immunofluorescence (IF) 50 µm free floating sections washed with TBS and incubated for 15 minutes with 0.02 mg/ml proteinase K in TBS. A positive control for TUNEL labeling was generated by incubating a tissue section in 1 µg/ml DNAse I for 20 minutes at room temperature. Sections were then washed and blocked in 3% NGS in TBS-X for 30 minutes and incubated overnight in 1:1000 rabbit polyclonal anti-NeuN (cat# ABN78, Millipore) in blocking solution. The following day, sections were washed and incubated in donkey anti-rabbit IgG Cy3 (cat# 711-165-152, Jackson ImmunoResearch) for 1 hour at room temperature in the dark. Sections were then washed, mounted on glass slides, and allowed to air dry for 1 hour. A hydrophobic barrier was drawn with a PAP pen around each section and TUNEL staining was performed according to FragEL DNA Fragmentation Detection Kit (cat# QIA39, Calbiochem) manufacturer's instructions. Double IF images were captured using a Zeiss Axiovert 200 laser scanning confocal microscope.

Electron Microscopy

For electron microscopy, mice were perfused with 10 mls of PBS-Heparin followed immediately by 10 mls of 1% PFA, 1% Glutaraldehyde in 0.1 M sodium cacodylate buffer. Brains were fixed using the same solution for 1 hour, then sliced into 2-3 1 mm coronal slabs per mouse. Slabs were fixed for 5 days before being incubated in 1% osmium tetroxide in sodium cacodylate buffer overnight, followed by dehydration in ascending ethanol series, and embedding Polybed 812 (cat# 08792, Polysciences, Inc.). Embedding media was cured for 24 hours in a dessicator and then in a 60℃ oven for 4 8 hours. Semithin sections stained with toluidine blue were prepared using glass knives to identify the region of corpus callosum and external capsule ipsilateral to injury in each coronal slab. Tissue was then thin sectioned (70-90 nm) on a Leica Ultracut E Microtome, stained with 4% uranyl acetate and Reynolds lead citrate, and viewed on a Jeol 100C Electron Microscope. Three-five grids were prepared from each block of tissue and two blocks (1 mm separation) were prepared from each animal. At least one grid from each block was qualitatively assessed blinded to injury status or genotype for evidence of axonal injury.

Stereological quantification and optical density measurements

For all histological analysis, the region of interest (ROI) was defined to include corpus callosum and external capsule underlying the impact site. For each mouse, the ROI began with the most anterior section containing hippocampal dentate gyrus and ended with the most posterior section containing corpus callosum fibers that cross midline. This yielded 3-4 sections for analysis per animal. The midline served as the medial boundary for the ROI, while the lateral boundary was formed by drawing a horizontal line between the ventral hippocampus and dorsal thalamus in each coronal section.

Iba-1 stereological methods have been previously published.(Shitaka et al. 2011) In brief, stereological quantification was performed blinded to genotype or drug treatment status using StereoInvestigator's (MicroBrightfield) optical fractionator technique. The ROI was traced in each section and a 180 x 180 µm grid size and 80 x 80 µm counting frame was applied determine the number of Iba-1 positive cells in the corpus callosum and external capsule. This ensured Gunderson's coefficient of error was <0.1.

For quantification of silver staining, 20x images were captured of all sections using the Olympus Nanozoomer Whole Slide Imaging System as previously reported.(Shitaka et al. 2011) From the Nanozoomer file, 1.25x .tiff images of sections containing the dentate gyrus of the hippocampus and corpus callosum were exported and opened in Image J (NIH). Background (gold color) was subtracted from each image using the color splitter and image calculator functions so that only the grey-black silver deposits were visible. ROIs were traced as described for Iba-1 analysis on 32-bit images and measurements were taken to acquire mean grey values corresponding to the intensity of silver staining (0-255) within each ROI. Three serial sections were averaged from each animal to produce a final silver staining value. Optical density measurements were also taken blinded to genotype and drug treatment status.

For GFAP optical density measurements, 5x images of corpus callosum and external capsule were captured using the Nanozoomer. The .tiff files were converted to 32-bit images in Image J and positive signal on each image was selected using Li's Minimum Cross Entropy thresholding method, a function of the Auto Threshold plugin. ROIs were selected and drawn as described for Iba-1 stereology and silver staining. The summarize function under analyze particles was used to acquire the area fraction occupied by positive GFAP signal. These values were averaged from three serial sections and the resulting value is reported.

qPCR

Quantitative polymerase chain reaction (qPCR) was performed to determine gene expression levels of interleukin 1β (IL1-β), interleukin 6 (IL6), inducible nitric oxide synthetase (iNOS), chemokine (C-C motif) ligand 2 (CCL2), and tumor necrosis factor α (TNFα). Immediately following sacrifice, brains were harvested and a 2 mm coronal slice was collected. The anterior-most portion of the slice corresponded to the anterior end of the hippocampus. The section was further dissected by making a cut parallel to the interface between hippocampus and thalamus, and only the dorsal section (approximately 30 mg) was reserved for qPCR. The sections were frozen on crushed dry ice and stored at -80℃. Tissue was later lysed in Qiazol (Qiagen) and disrupted using a rotor-stator homogenizer following the manufacturer's protocol for homogenization of fatty tissues. The final RNA pellet was resuspended in 100 µl RNAse-free water and further purified using an RNeasy Kit (Qiagen). DNAse was applied to the column to remove genomic DNA contamination. For cDNA preparation, 1 µg RNA was used in each RNA-cDNA reaction (High Capacity RNA-to-cDNA Kit, Applied Biosystems). For each qPCR reaction, 1 µl of undiluted cDNA was added to 15 µl Syber Green PCR Master Mix (Applied Biosystems), 13 ul ddH20, and 1 µl 10 mM forward and reverse primers (Table 1). Samples were loaded on a MicroAmp Fast Optical 96-Well Reaction Plate (Applied Biosystems) and qPCR was carried out on a 7500 fast real-time PCR system (Applied Biosystems). The following conditions were used: 95℃ for 10 min followed by 40 cycles of 95℃ for 15 sec and 60℃ for 1 min.

ΔΔCt values were calculated by normalizing the expression of each gene to the geometric mean of three reference genes (*hprt, pgk1, gapdh*). Subsequently, these target gene values were normalized to the arithmetic mean values in untreated naïve mice (n=4). Exponential transform was performed to achieve fold change measures of each gene where 1 is equal to naïve mice.

Table 5.1 Primer sequences used for qPCR.

Encoded Protein	Accession Number	Direction	5'-3'	Amplicon Size (bp)
PGK1	NM_008828.2	Forward Reverse	ctccgctttcatgtagaggaag gacatctcctagtttggacagtg	117
GAPDH	NM_008084	Forward Reverse	catggacttccgtgttccta gcggcacgtcagatcca	55
HPRT1	NM_013556.2	Forward Reverse	cctaagatgagcgcaagttgaa ccacaggactagaacacctgctaa	86
IL1-β	NM_008361.3	Forward Reverse	acggaccccaaaagatgaag ttctccacagccacaatgag	139
IL6	NM_031168.1	Forward Reverse	caaagccagagtccttcagag gtccttagccactccttctg	150
iNOS	NM_010927	Forward Reverse	tggtccgcaagagagtgct cctcattggccagctgctt	108
CCL2	NM_011333	Forward Reverse	aggtgtcccaaagaagctgta atgtctggacccattccttct	85
TNFα	NM_013693	Forward Reverse	cttctgtctactgaacttaggg caggcttgtcactcgaattttg	134

Data analysis and statistics

All data were analyzed and graphed using GraphPad (Prism). Shapiro-Wilks normality tests were applied to determine if data were normally distributed. Rank transformations were applied to data that failed normality tests. In experiments with two test groups, student's t-tests were used. Two-way ANOVAs were used in all other cases except analysis of sham mice with or without cannulation, in which case a one-way ANOVA was performed. Post-hoc comparisons between CD11b-TK +/- and -/- mice were pre-specified. Statistical significance was defined as $p<0.05$ for t-tests and ANOVAs and $p<0.0167$ for post-hoc tests.

5.3 RESULTS

5.3.1 Acute effects of microglia on axonal injury in mice receiving low-dose valganciclovir (7d)

Previous reports indicate that daily systemic administration of valganciclovir causes hematopoetic toxicity and is fatal to CD11b-TK +/- mice within 10 days (Gowing et al. 2006). On the other hand, delivery of the drug directly into the brain can result in microglial reduction without the toxicity seen after IP injection (Simard, et al. 2006). Continuous administration is required as macrophages will rapidly repopulate areas of microglial depletion in the absence of the drug (Varvel, et al. 2012). As our goal was to test the effects of microglial depletion on axonal injury at timepoints between one week and one month following injury, we chose to administer valganciclovir continuously by intracerebroventricular (ICV) osmotic pump. However, since there is deformation of the brain during the brain injury, we chose to remove the pumps during the 24 hours required for the rcTBI procedure to prevent additional injury of the brain caused by the cannula (**Figure 5.1**). For initial experiments a valganciclovir concentration of 1 mg/ml was chosen as it has been shown by other groups to be effective in reducing microglial cells(Simard et al. 2006; Grathwohl, et al. 2009).

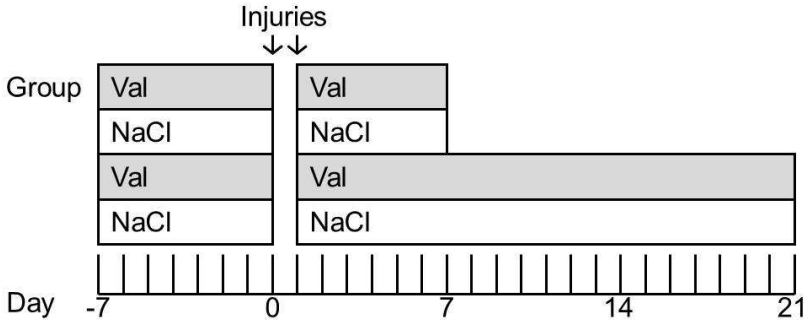

Figure 5.1 Experimental design. CD11b-TK +/- or -/- controls were treated with either valganciclovir or saline by intracerebroventricular (ICV) osmotic pump for 7 days prior to injury. Pumps were then removed and a closed-skull or sham injury was performed (day 0). Twenty-four hours later a second injury was delivered. Pumps were immediately reimplanted and drug or saline treatment was resumed for another 7 days (acute time point) or 21 days (sub-acute time point).

Within the ipsilateral corpus callosum and external capsule, treated CD11b-TK +/- mice (n=13) had a 35% reduction in the number of microglial cells compared to littermate controls (n=11) at the 7 day time point after injury (one-tailed student's t-test, p=0.008; **Figure 5.2 A-D**, **G**). To control for the effects of injection of vehicle alone, the experiment was repeated with additional groups that received 0.9% NaCl (**Figure 5.3 A**; CD11b+/- valganciclovir n=9, NaCl n=7; CD11b-TK -/- valganciclovir n=6, NaCl n=8). An effect of genotype (p=0.0359) and treatment (p=0.0226) was seen, but not an effect of genotype x treatment (two-way ANOVA, p=0.1039; **Figure 5.3 A**). Planned comparisons revealed a significant difference between valganciclovir treated CD11b-TK +/- versus littermate controls (p=0.0110; **Figure 5.3 A**), no difference between the two genotypes receiving vehicle alone (p=0.7096), and a significant difference between CD11b-TK +/- valganciclovir treated and vehicle treated mice (p=0.0057).

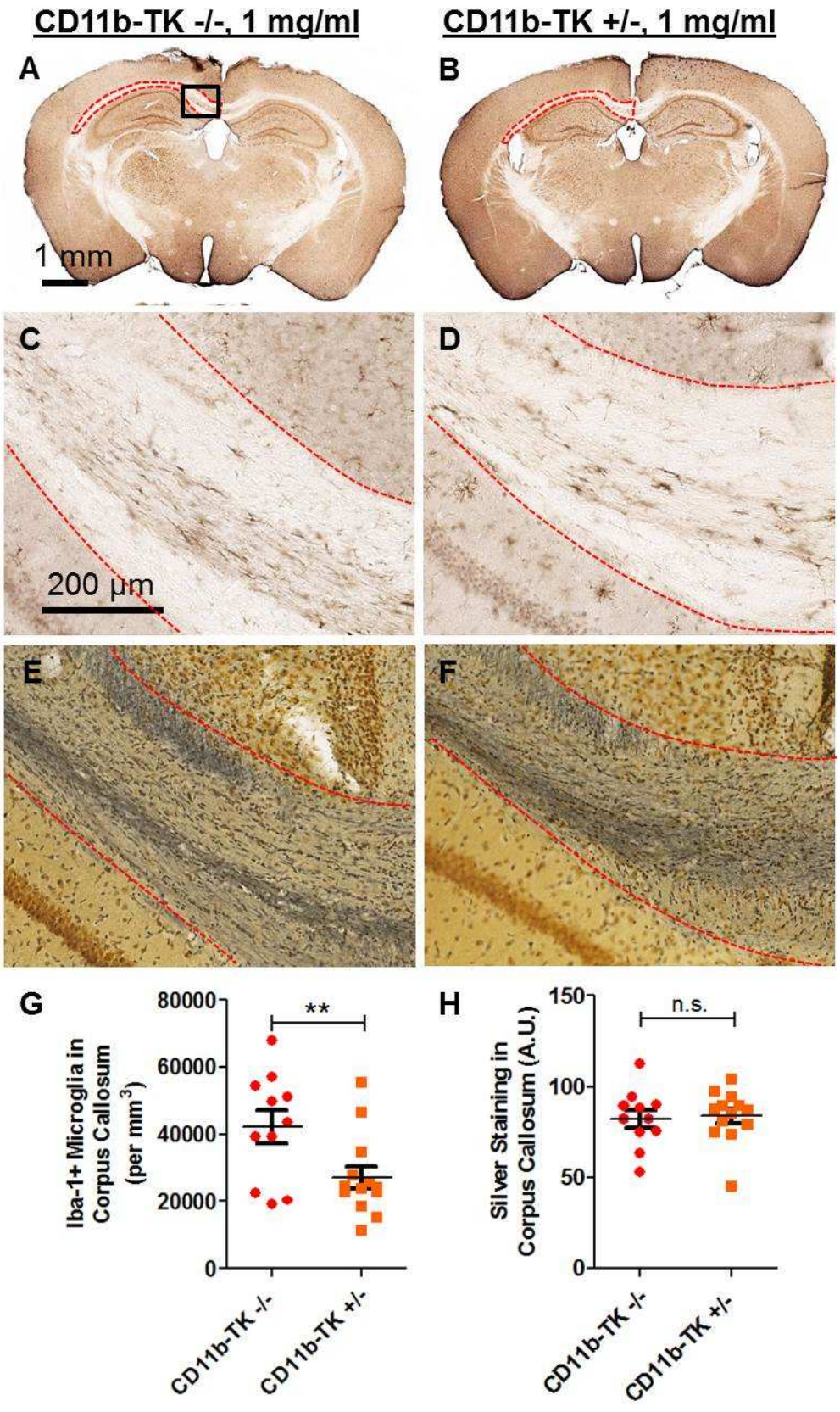
CD11b-TK -/-, 1 mg/ml
CD11b-TK +/-, 1 mg/ml
A
B
1 mm
C
D
200 µm
E
F
G
Iba-1+ Microglia in Corpus Callosum (per mm3)
80000
60000
40000
20000
0
**
CD11b-TK -/-
CD11b-TK +/-
H
Silver Staining in Corpus Callosum (A.U.)
150
100
50
0
n.s.
CD11b-TK -/-
CD11b-TK +/-

Figure 5.2 Treatment of CD11b-TK +/- mice with ICV low-dose valganciclovir (1 mg/ml) reduces microglia but does not affect silver staining 7 days following rcTBI. Iba-1 staining in treated CD11b-TK -/- (A, C) and +/- (B, D) mice. (C, D) Higher magnification views of Iba-1 staining in corpus callosum ipsilateral to injury (region boxed in A, outlined with red dashed line). Silver staining in valganciclovir treated CD11b-TK -/- (E) and +/- (F) mice. (G) Stereological quantification of Iba-1-positive microglia in CD11b-TK +/- mice shows a ~35% reduction compared to controls (one-tailed student's t-test, **p<0.01. Dashed line indicates sham levels). (H) Silver staining in white matter was unchanged (A.U.= arbitrary units). (Error bars represent standard error of the mean).

We then used silver staining to assess injured axons in mice with reduced numbers of microglia. No difference in the intensity or distribution of silver staining was observed in either the first (two-tailed student's t-test, p=0.8292; **Figure 5.2 E-F, H**) or the second groups of mice (two-way ANOVA, genotype p=0.8478, treatment p= 0.6147, genotype x treatment p = 0.2769; **Figure 5.3 B**). We have previously shown that silver staining is a sensitive method to assess axonal injury in this repetitive concussive injury model.(Shitaka et al. 2011)

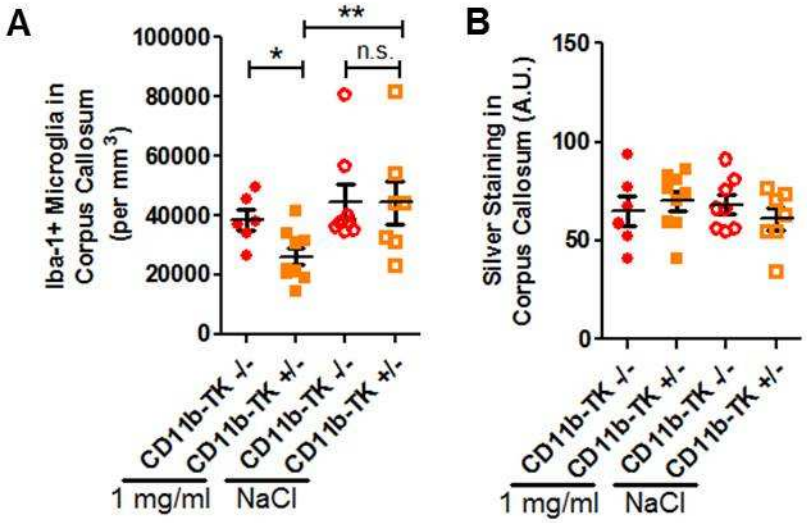

Figure 5.3 Low-dose valganciclovir (1 mg/ml) but not saline reduces microglia and has no effect on silver staining 7 days after injury in an independent cohort of mice. (A) Iba-1 staining (B) silver staining in corpus callosum and external capsule of CD11b+/- and -/- mice receiving either drug or vehicle treatment (A.U.= arbitrary units, *p<0.05, **p<0.01, n.s. = not significant). (Error bars represent standard error of the mean).

5.3.2 Dose-response of microglia to valganciclovir treatment in CD11b-TK mice

We reasoned that a modest reduction in the number of microglial cells within the white matter may not be adequate to produce an effect on the extent of axonal injury. We therefore next tested higher doses of valganciclovir in mice that received rcTBI to increase the amount of microglial depletion. Using the same injection paradigm as before, mice were treated with either 2 (n=3), 5 (n=3), 10 (n=5), or 50 mg/ml (n=8) of valganciclovir (**Figures 5.4 and 5.5**). At 5-7 days post-injury (14 days after initial pump implantation), CD11b-TK +/- mice in the 50 mg/ml group became lethargic, had difficulty walking, and a 50% mortality rate. Wild-type littermate controls treated identically with 50 mg/ml valganciclovir (n=6) appeared normal. Upon histological examination, intraparenchymal hemmorhages and extensive tissue loss within the hippocampus and thalamus were apparent in the treated CD11b-TK +/- mice (**Figure 5.4 A-B**). Mice that received intermediate doses of 2, 5, or 10 mg/ml appeared normal physically and histologically (**Figure 5.5 A-F**). Therefore, 10 mg/ml was selected for future experiments as this dose consistently resulted in microglial depletion in the hemisphere opposite injection near the corpus callosum and external capsule (**Figure 5.5 E, F**).

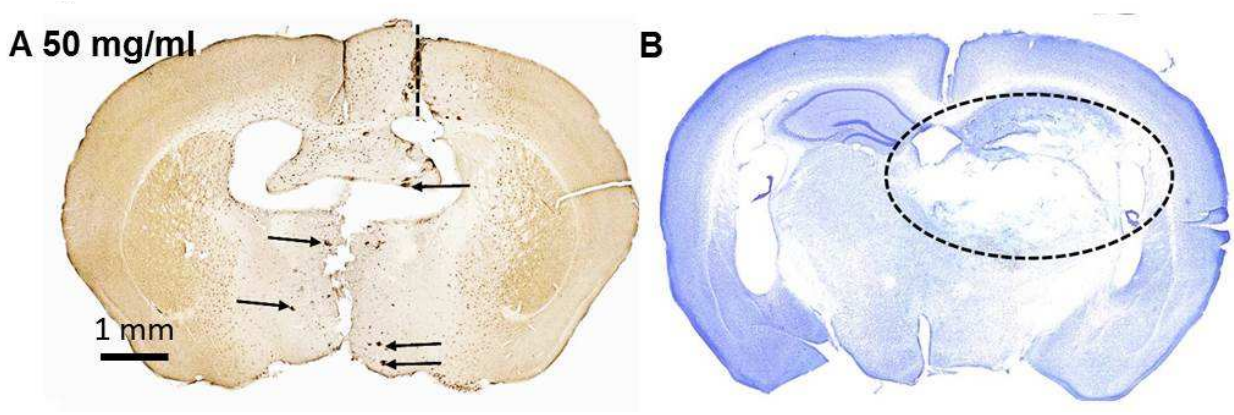

Figure 5.4 High-dose (50 mg/ml) valganciclovir treatment was toxic in CD11b-TK +/- mice 7 days post-injury. (A) An Iba-1 stained section near the cannula site (dashed line) shows depletion of microglia but also numerous microhemorrhages (arrows). (B) Cresyl violet staining in a section posterior to valganciclovir injection shows extensive tissue loss in the hippocampus and thalamus (dashed oval).

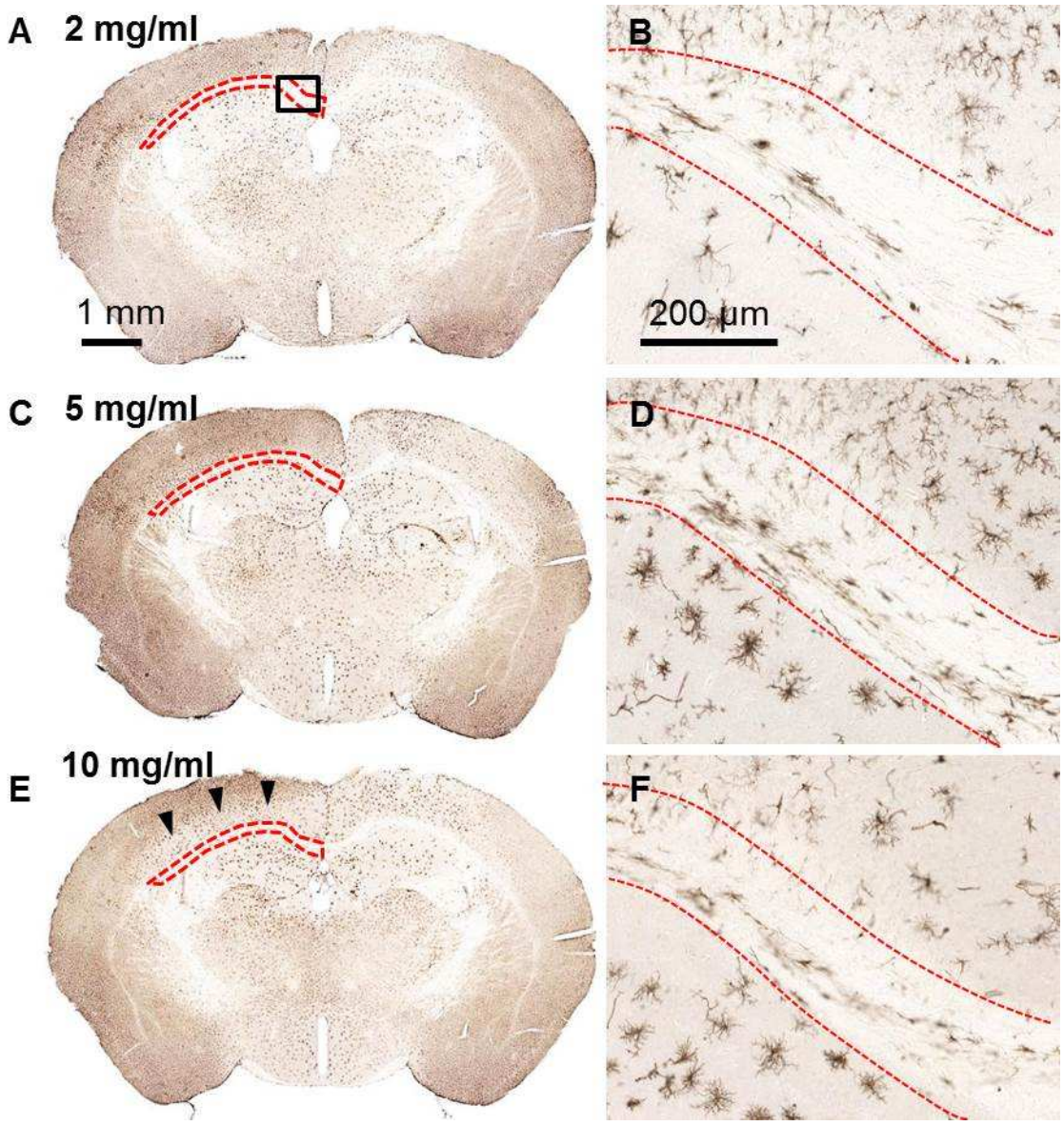

Figure 5.5 Valganciclovir dose-response in CD11b-TK mice 7 days post-injury. Iba-1 stained whole sections (A, C, E) and higher-magnification images (box A) corresponding to the region of interest assessed for iba-1 depletion by stereology (outlined with red dashed line, B, D, F). CD11b-TK +/- mice treated with 2 (A, B), 5 (C, D), or 10 (E, F) mg/ml valganciclovir. Microglial depletion is most prominent ipsilateral to cannulation and drug delivery (right). Arrowheads indicate region of microglial reduction in cortex of hemisphere opposite drug infusion.

5.3.3 Acute effects of intermediate dose valganciclovir on axonal injury (7d)

A separate cohort of mice was treated with 10 mg/ml valganciclovir and examined 7 days after rcTBI (**Figure 5.6 A-F**). At 7 days post-injury, the number of Iba-1 positive cells within the corpus callosum and external capsule ipsilateral to injury was 56% reduced in CD11b-TK +/- (n=7) compared to littermate controls (n=7; one-tailed student's t-test, p=0.0004; **Figure 5.6 A, B, E**). Again, no significant reduction in the amount of silver staining was observed (two-tailed student's t-test, p=0.6045; **Figure 5.6 C, D, F**).

To determine if other aspects of axonal injury were affected by microglial depletion, other injury markers were assayed in adjacent tissue sections for APP and neurofilament compaction (**Figure 5.7 A-D**). APP is a marker of fast axonal transport that accumulates in axonal swellings within hours of axonal injury (Gentleman et al. 1993; Sherriff et al. 1994). The neurofilament antibody RM014 has been used to detect neurofilament compaction, an indicator of cytoskeletal disruption in degenerating axons (Stone et al. 2001). Both of these markers were present near the site of cannulation in all mice (**Figure 5.7 A, B**), but were sparse and detected infrequently in more posterior regions ipsilateral to injury (**Figure 5.7 C, D**). Most commonly they occurred in white matter tracts overlying the lateral ventricle, which may be a particularly vulnerable region in this model. However, no qualitative difference was observed between genotypes, indicating that these markers of axonal injury were not affected by microglial depletion..

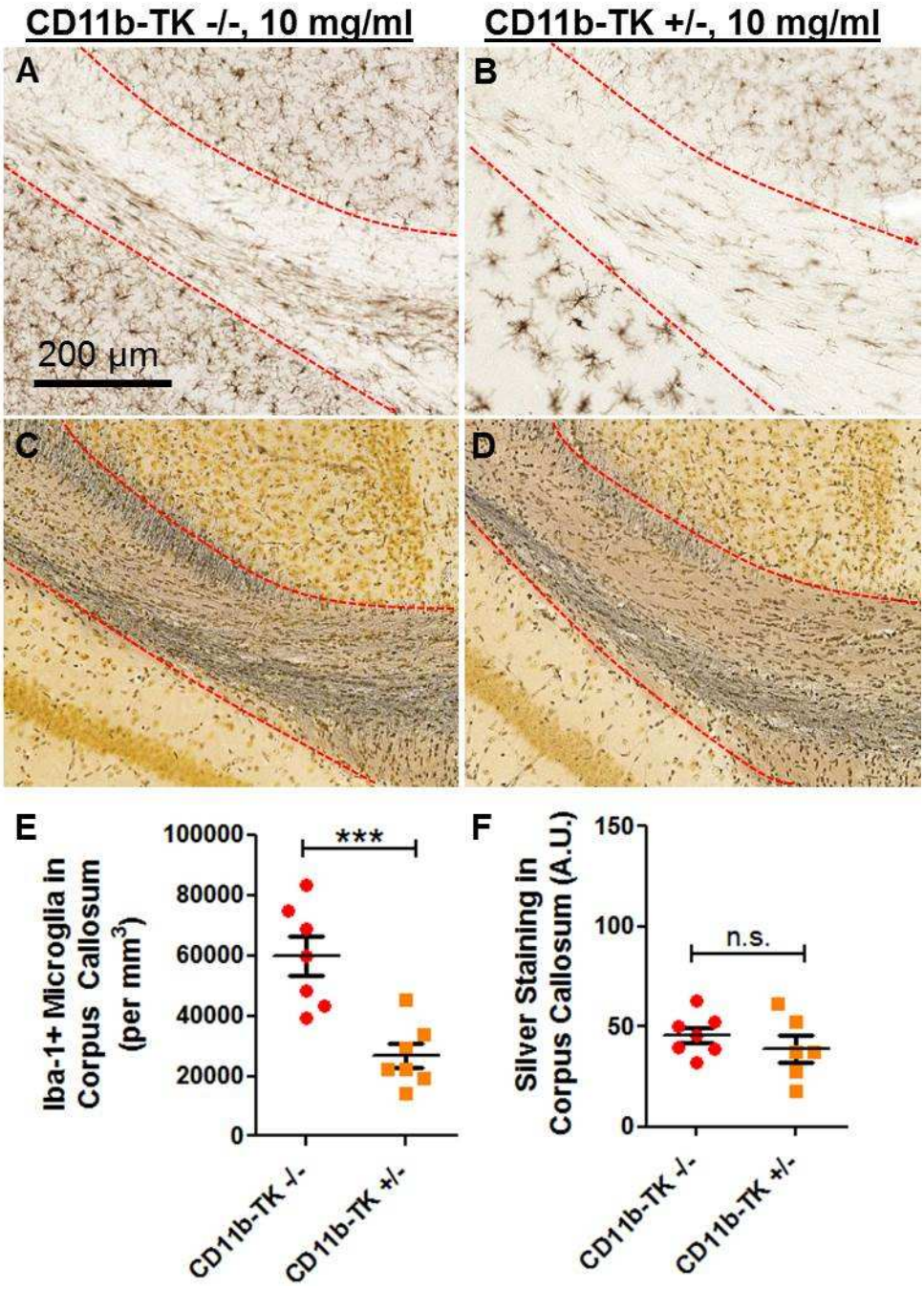

Figure 5.6 Acute intermediate dose valganciclovir (10 mg/ml) reduces Iba-1 but not silver staining in CD11b-TK mice 7 days after rcTBI. Iba-1 staining in corpus callosum (outlined with red dashed line) in treated CD11b-TK -/- (A) and +/- (B) mice. Silver staining in adjacent sections from CD11b-TK -/- (C) and +/- (D) mice. (E) Iba-1 was reduced by 56% in CD11b-TK +/- mice compared to controls (one-tailed student's t-test, ***$p<0.001$). (F) No change in silver staining was observed (A.U.= arbitrary units, n.s. = not significant). (Error bars represent standard error of the mean).

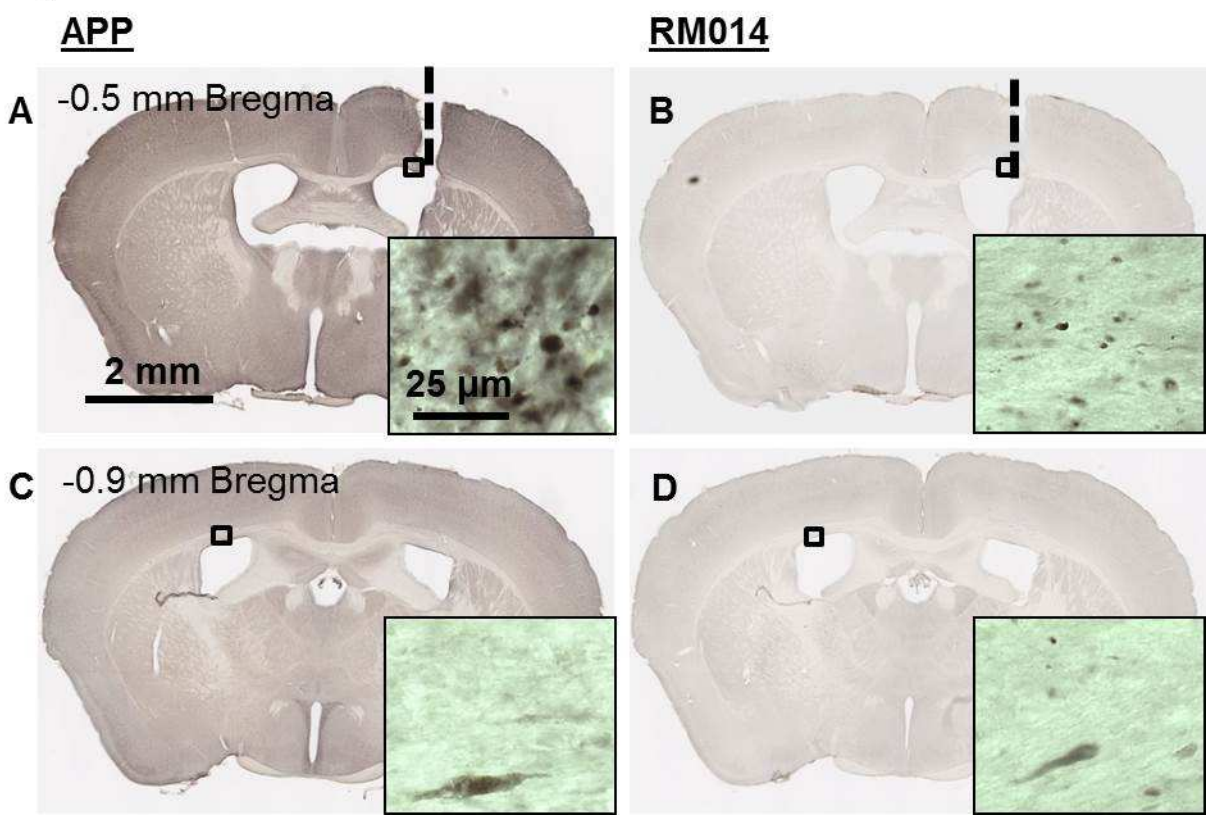

Figure 5.7 Amyloid precursor protein (APP) and neurofilament (RM014) labeling in an injured CD11b-TK -/- mouse treated with 10 mg/ml valganciclovir and sacrificed 7 days post-injury. APP and labeling was prominent at the site of cannulation (dashed line) -0.5 mm relative to bregma (A, B). Only sparse axonal swellings were detectable in the contralateral hemisphere (injured side) in the corpus callosum and external capsule corresponding to the region of interest assessed for axonal injury in these experiments (C, D). Insets show higher magnification of labeling in boxed regions in A and C.

To further confirm that no subtle alterations in axonal injury severity are occurring after microglial depletion, qualitative electron microscopy was carried out in a sham littermate control treated with 10 mg/ml valganciclovir (n=1; **Figure 5.8 A-C**), injured littermate controls treated with 10 mg/ml valganciclovir (n=2; **Figure 5.9 A-C**), or CD11b-TK +/- mice treated with 10 mg/ml valganciclovir (n=2; **Figure 5.10 A-C**). The frequency and characteristics of axonal injury 7 days post-injury were assessed. Corpus callosum and external capsule ipsilateral to injury directly beneath the impact site were analyzed. In sham injury with 10 mg/ml

valganciclovir treatment, most axons displayed a normal appearance, with intact myelin sheaths and regularly spaced microtubules and neurofilaments (**Figure 5.8 A, B**). However, occasional swollen axons displayed organelle accumulation consistent with injury and were likely artifacts of cannulation (**Figure 5.8 C**).In contrast, the effects of repetitive concussive TBI were more dramatic. In both CD11b-TK +/- and -/- mice injured and treated with valganciclovir axonal injury was a prominent feature within the corpus callosum and external capsule. Notably, small myelinated axons displayed abnormal morphology with organelle accumulation, cytoskeletal disorganization, and axolemma collapse (**Figures 5.9-10**). These features are all consistent with Wallerian degeneration. Overall, injury levels were approximately the same as reported previously in this model.(Shitaka et al. 2011) No overt differences were detected between CD11b-TK +/- and -/- mice. These observations were confirmed by a second, blinded observer (Dr. Krikor Dikranian). These observations further confirm that axonal injury was not affected by microglial depletion.

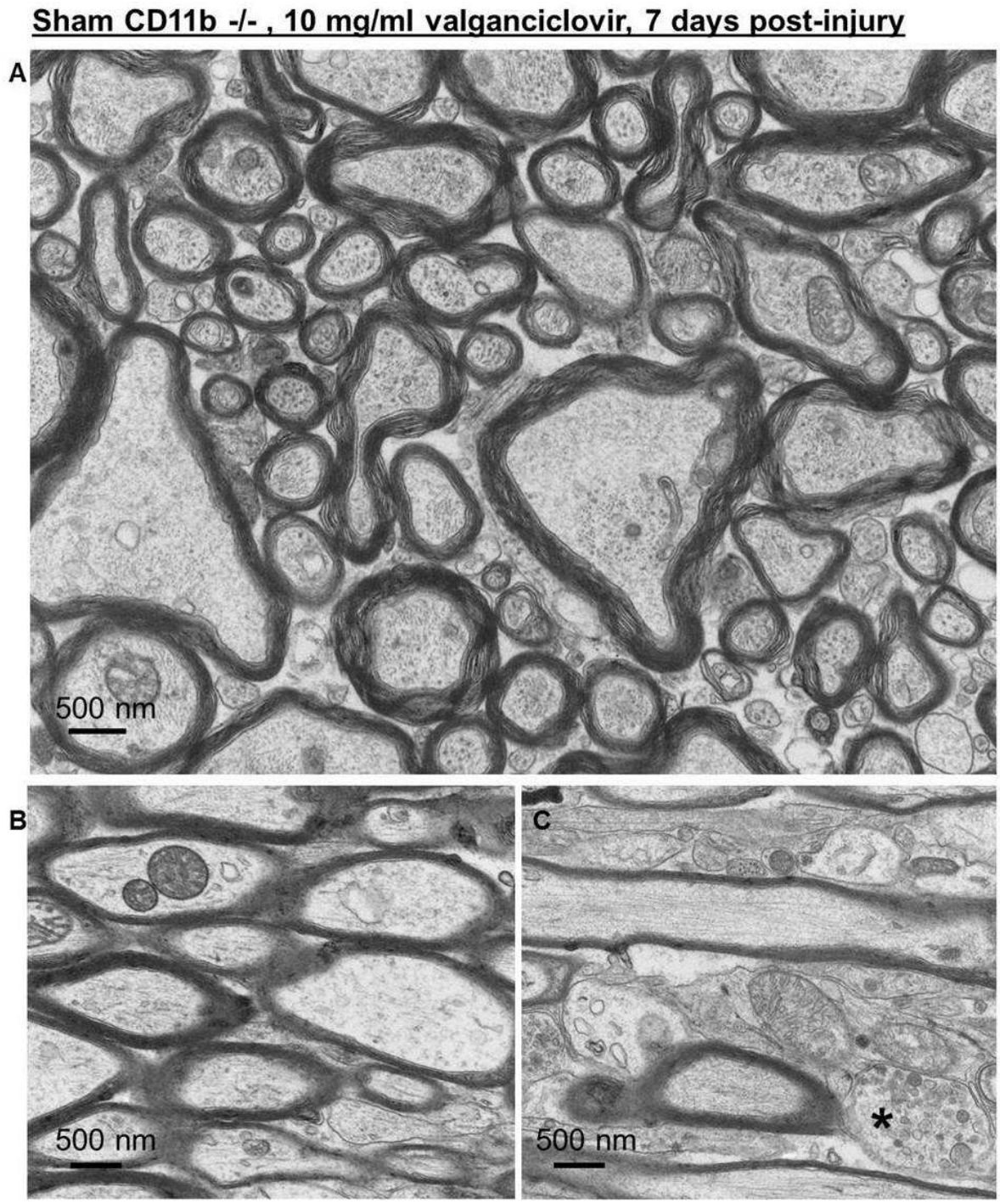

Figure 5.8 Normal axonal ultrastructure in a cannulated sham CD11b-TK -/- mouse treated with10 mg/ml valganciclovir and sacrificed 7 days post sham injury. (A, B) Axons in the corpus callosum near the cingulum display organized cytoskeletal elements and intact myelin sheaths. (C) In a region containing axons cut parallel to the predominant direction of the corpus callosum. an asterisk indicates a swollen unmyelinated axon with abnormal organelle accumulation. Note nearby axons appear relatively intact, however.

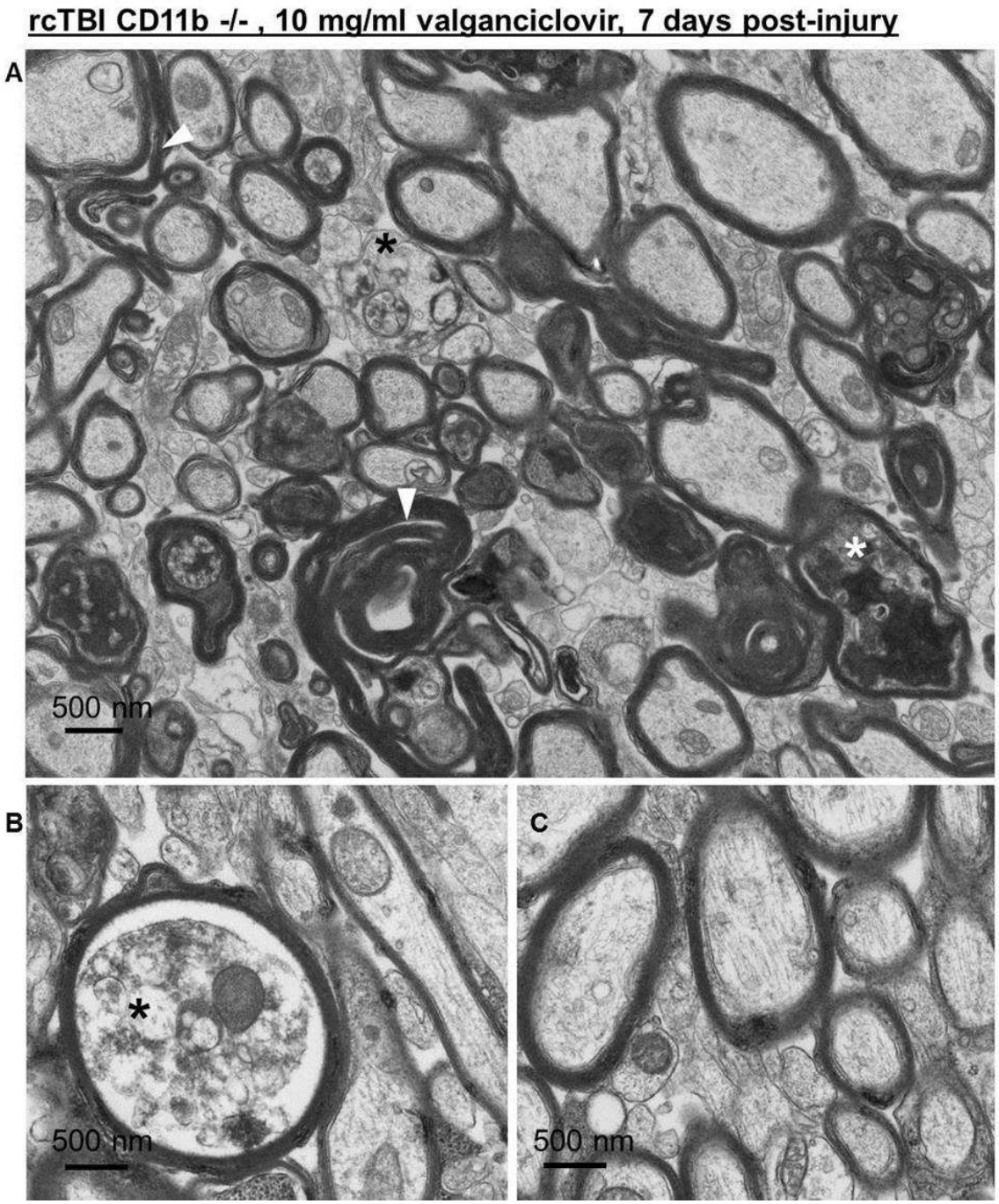

Figure 5.9 Ultrastructural abnormalities in an injured CD11b-TK -/- littermate control mouse treated with 10 mg/ml valganciclovir and sacrificed 7 days post-injury. (A) Arrowheads indicate regions of end stage axonal degeneration in corpus callosum near the cingulum where the axolemma has completely collapse. Asterisks denote examples of myelinated and unmyelinated axons with organelle accumulation. (B) A myelinated axon undergoing Wallerian degeneration (asterisk). (C) A region of relatively healthy appearing axons in corpus callosum.

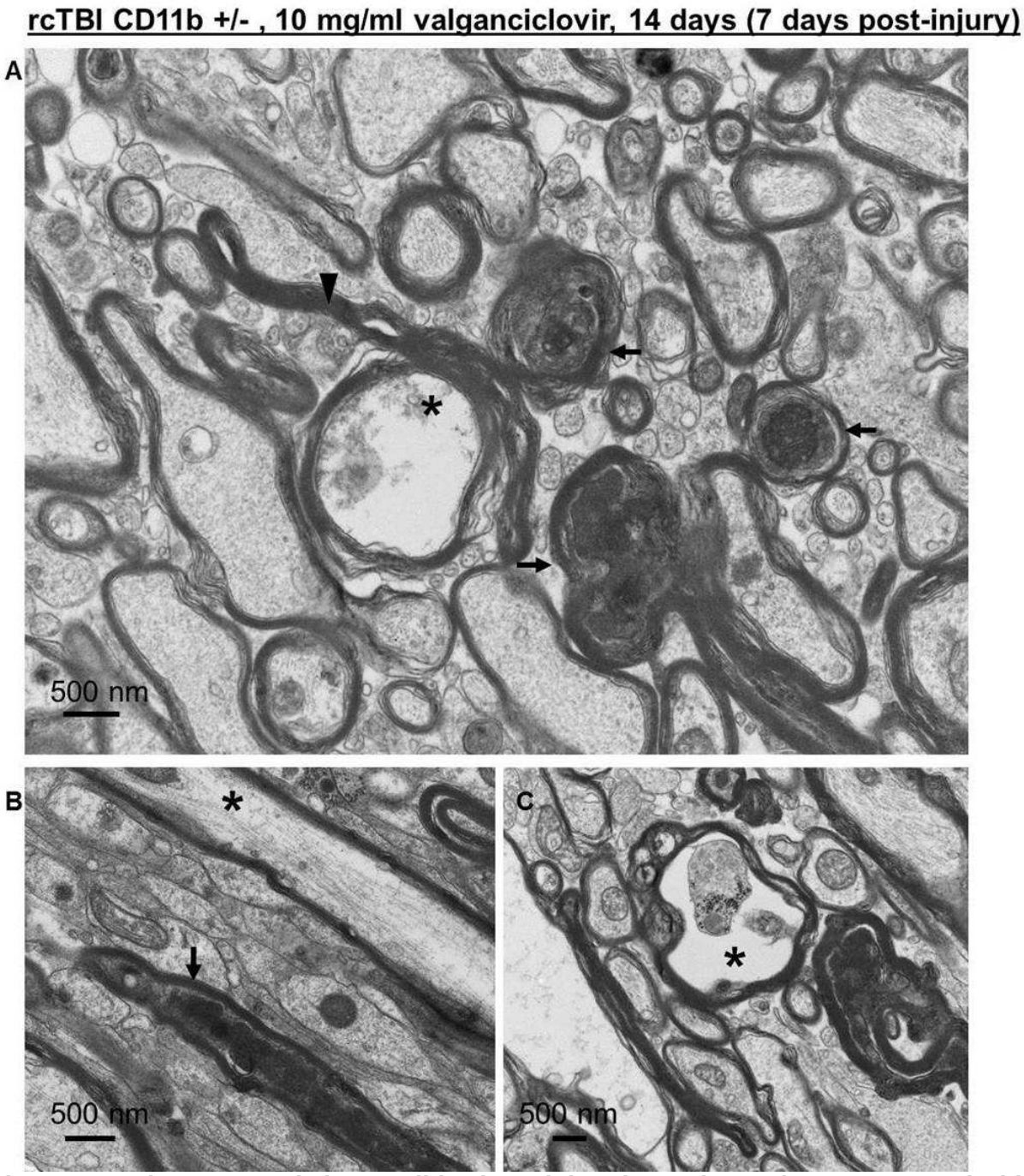

Figure 5.10 Ultrastructural abnormalities in an injured CD11b-TK +/- mouse treated with 10 mg/ml valganciclovir and sacrificed 7 days post-injury. (A) Arrowheads indicate regions of end stage axonal degeneration in corpus callosum near the cingulum where the axolemma has completely collapsed. The asterisk denotes a swollen axon undergoing late stage degeneration and arrows indicate examples of axons containing densely packed intracellular aggregates. (B) Arrow indicates an axon cut parallel to the predominant direction of the corpus callosum with abnormal accumulation of electron-dense intra-axoplasmic material in a region of relatively normal axons (asterisk). (C) Asterisk indicates an axon undergoing axolemma collapse.

5.3.4 Sub-acute effects of low and intermediate dose valganciclovir on axonal injury (21d)

Next we sought to determine if longer-term reduction of microglia alters the evolution of axonal injury over time (**Figures 5.11 and 5.12**). We have previously reported that silver staining abnormalities persist out past 49 days (Shitaka et al. 2011). We chose to analyze mice at 21 days post-injury because this would allow us to treat mice with valganciclovir for one month (28 days) and would not require that the osmotic pumps be replaced—a procedure requiring additional surgery. In the low dose experiment, mice were treated with 1 mg/ml valganciclovir (CD11b+/- n=7, -/- n=6) or 0.9% NaCl (CD11b+/- n=5, -/- n=5; **Figure 5.11**). Overall, analysis of microglial activation by two-way ANOVA revealed no effect of genotype ($p=0.3307$) or treatment ($p=0.9511$), but a significant genotype x treatment interaction ($p=0.0118$). Additionally, a significant reduction of microglial cells in the corpus callosum and external capsule of about 35% in valganciclovir treated CD11b-TK +/- mice compared to valganciclovir treated littermate controls was observed ($p =0.0099$, **Figure 5.11 A, B, E**). No difference was seen in NaCl treated mice between genotypes ($p=0.2488$). The difference between microglial cells in valganciclovir treated vs NaCl treated CD11b-TK +/- mice was not quite statistically significant ($p=0.0547$; **Figure 5.11 E**). Again, as in the acute experiments, no difference was seen across groups in the amount of silver staining (**Figure 5.11 C, D, F**).

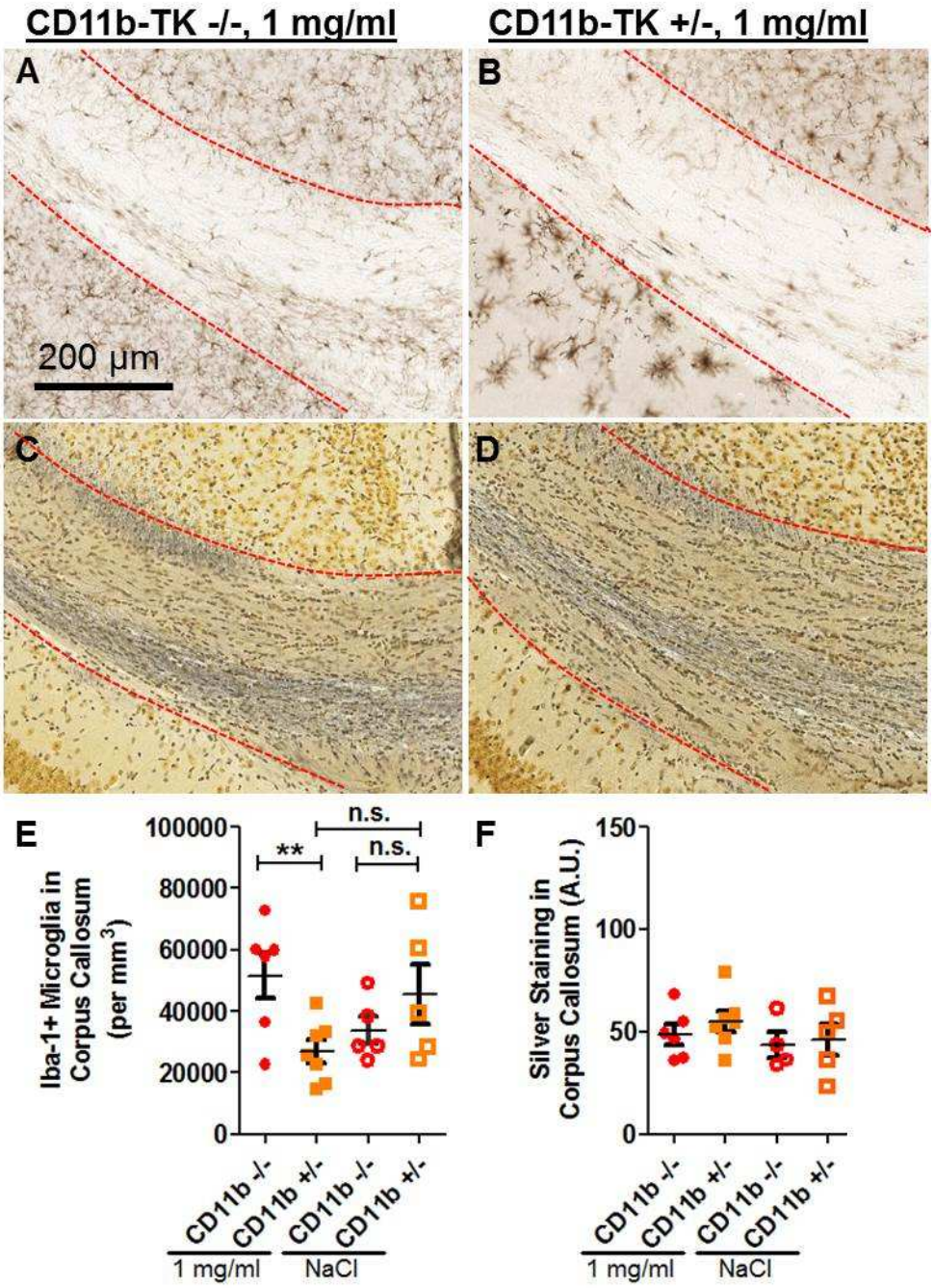

Figure 5.11 Treatment with low dose valganciclovir (1 mg/ml) but not saline reduces Iba-1 but not silver staining in corpus callosum 21 days after rcTBI. Iba-1 staining in valganciclovir treated CD11b-TK -/- (A) and +/- (B) mice. Silver staining in valganciclovir treated CD11b-TK -/- (C) and +/- (D) mice. (E) Iba-1 was reduced by 35% in CD11b-TK +/- mice compared to -/- controls (one-tailed student's t-test, **p<0.01). (F) No change in silver staining was observed (A.U.= arbitrary units, n.s. = not significant). (Error bars represent standard error of the mean).

An additional group of either CD11b-TK +/- mice (n=6) or littermate controls (n=8) received the intermediate 10 mg/ml valganciclovir and was sacrificed 21 days post-injury (Figure 12A-D). Though the mice did not display an overtly abnormal behavioral phenotype, histological examination revealed tissue loss similar to that seen with the 50 mg/ml dose. Thus, the duration of drug administration at intermediate doses can also produce a toxic effect in CD11b-TK mice. Due to the clear toxicity of the drug, Iba-1 and silver staining were not quantified in these animals.

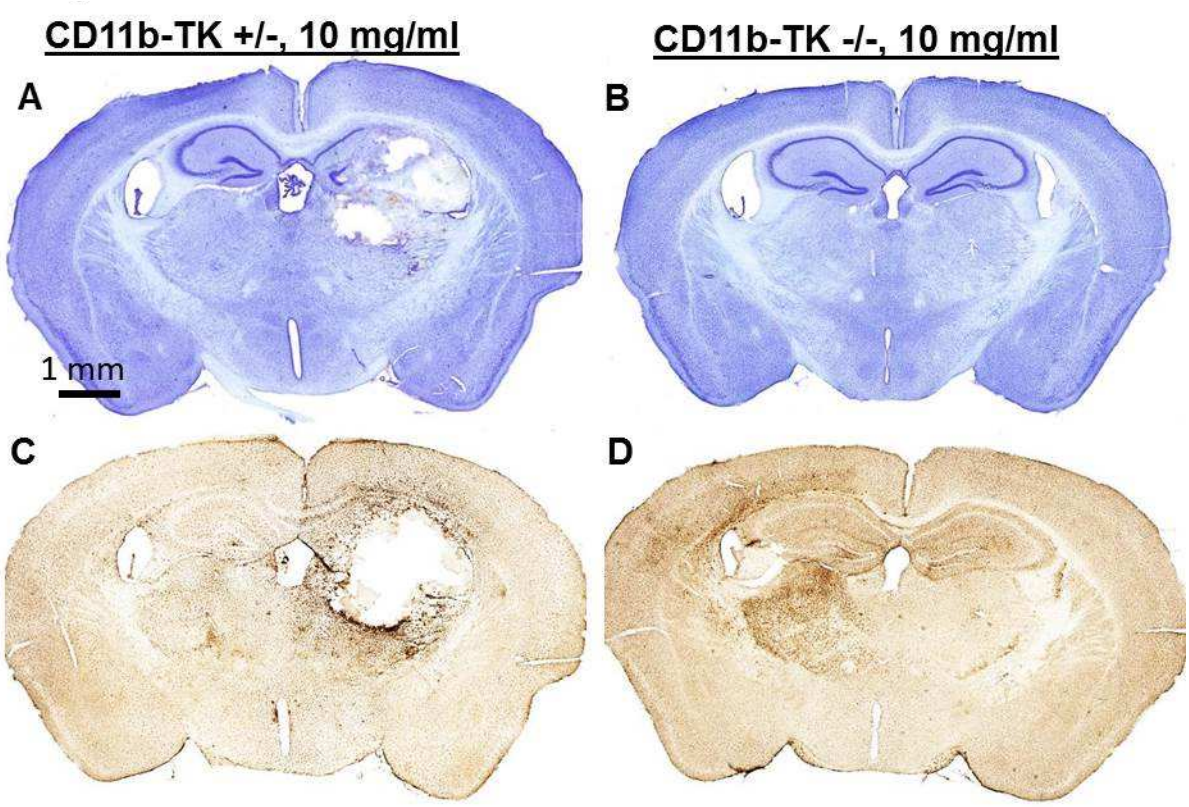

Figure 5.12 Sub-acute treatment with intermediate dose valganciclovir is toxic in injured CD11b-TK mice. 28 days total treatment resulted in tissue loss as visualized by cresyl violet in the hippocampus and thalamus of injured CD11b-TK +/- (A) but not -/- (B) mice. Iba-1 staining shows the extent of microglial depletion in CD11b-TK+/- (C) and not in a CD11b-TK -/- (D) littermate control mouse subjected to rcTBI.

5.3.5 TUNEL-labeling in mice treated with intermediate dose valganciclovir

Given the apparent toxicity of intermediate dose valganciclovir (10 mg/ml) in CD11b-TK mice treated for 21 days post-injury, we performed TUNEL-labeling to determine if this intermediate dose induces apoptosis in neurons 7 days post-injury (**Figure 5.13 A-B**). Sections from CD11b-TK +/- (n=7) and -/- (n=7) mice treated with valganciclovir were double-labeled for TUNEL and NeuN, a neuron-specific marker. The hippocampal CA3 ipsilateral to cannulation and drug infusion was the focus of these investigations as this is a region significantly affected by toxicity by 21 days post-injury. However, no apoptotic neurons were detected here (or in any other area) at 7 days post-injury. This would indicate that neurodegeneration begins later than day 7 post-injury. As a positive control to assess the sensitivity of our TUNEL labeling, we treated adjacent sections with DNAase-I to induce DNA nicks. This caused prominent TUNEL staining (**Figure 5.13C**). Thus, the lack of TUNEL staining in the valganciclovir treated mice is likely to accurately indicate a lack of apoptotic injury.

5.3.6 Effect of cannulation on silver staining

To determine whether cannulation produces axonal injury that may be masking the potentially beneficial effects of microglial depletion, we next determined the level of silver staining in CD11b-TK -/- sham mice alone (n=5; **Figure 5.14 A, C**), CD11b-TK -/- sham mice receiving ICV saline by osmotic pump (n=5; **Figure 5.14 B, D**), and CD11b-TK +/- sham mice receiving intermediate dose valganciclovir by osmotic pump (n=5; **Figure 5.14 E, G**). No difference was observed between groups (one-way ANOVA, p=0.7006; **Figure 5.14 F).** This result indicated that contralateral cerebroventricular cannulation did not produce detectible axonal injury in the ipsilateral corpus callosum region of interest.

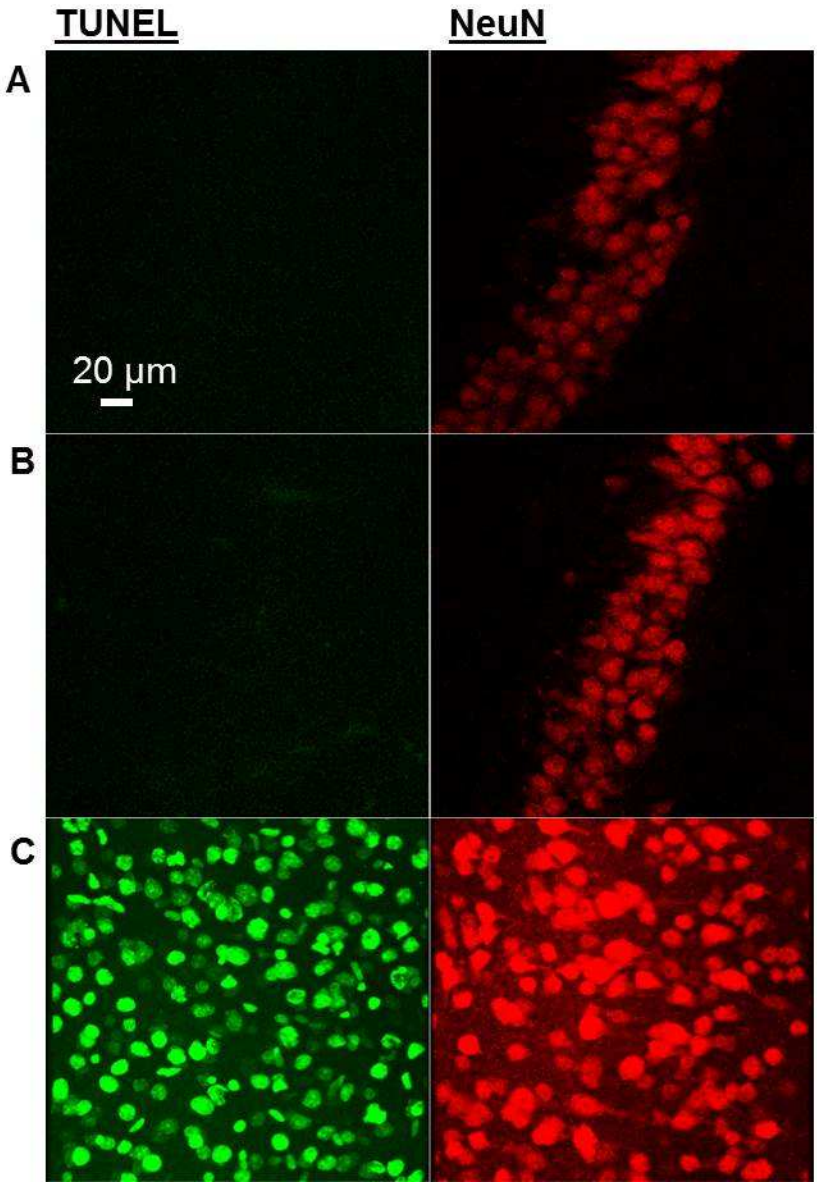

Figure 5.13 Double immunofluorescence for TUNEL (green) or NeuN (red) in CA3 does not indicate neuronal apoptosis in injured mice treated with 10 mg/ml valganciclovir and sacrificed 7 days post-injury. TUNEL labeling was not observed in NeuN+ cells in the hippocampal CA3 of CD11b -/- (A) or +/- (B) mice. A positive control for TUNEL labeling was generated by incubating adjacent sections in DNAse I to induce double-stranded DNA breaks (C). All images were acquired using the same settings on a laser scanning confocal microscope.

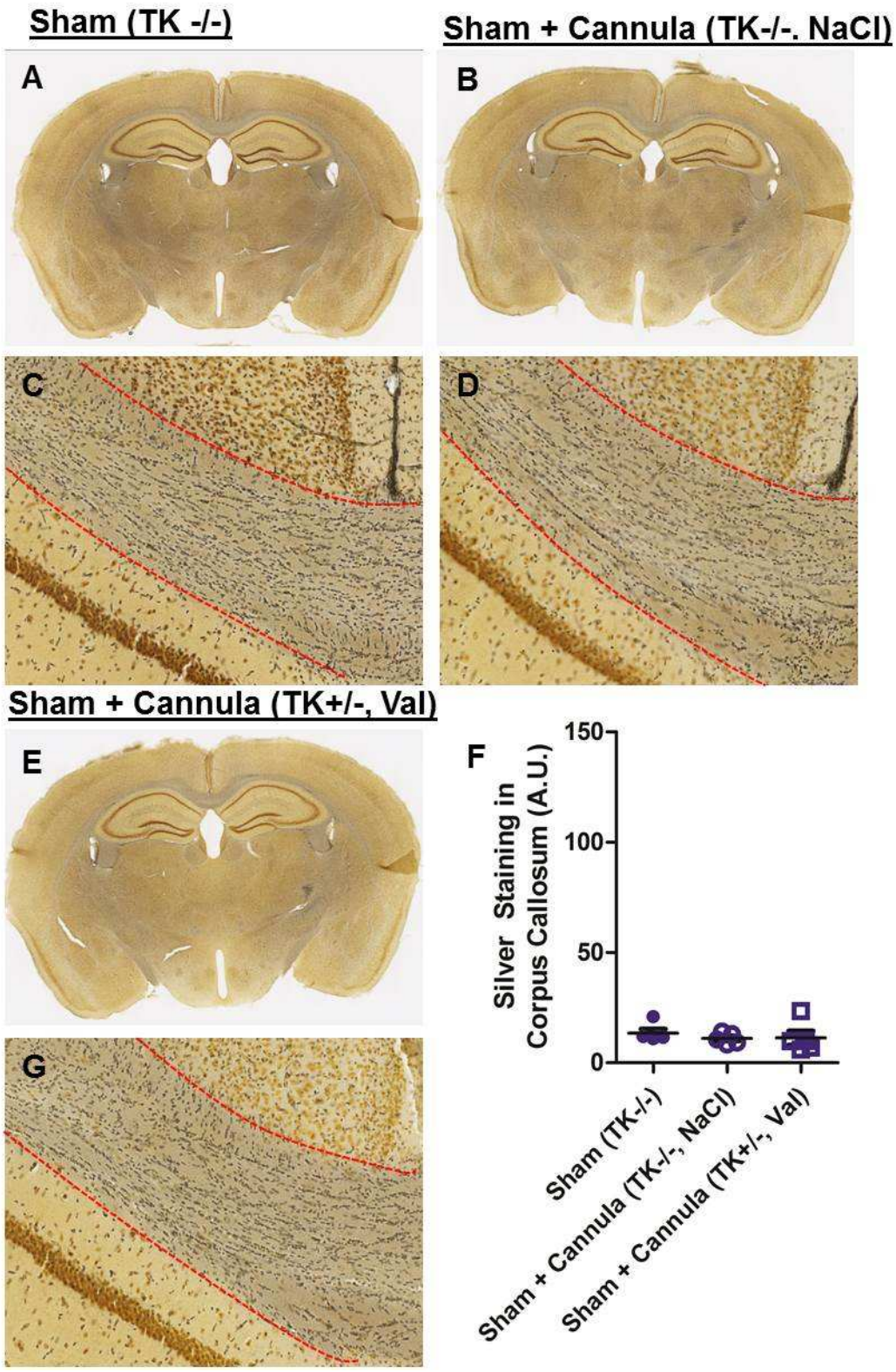

Figure 5.14 Cannulation does not contribute to silver staining in the region of interest assessed for axonal injury. Silver staining was performed in sections from CD11b-TK -/- mice that underwent the sham procedure alone (A, C) or the sham procedure plus cannulation and

treatment with saline (NaCl, B, D). Silver staining was also performed in sections from CD11b-TK +/- mice that underwent the sham procedure plus cannulation and treatment with 10 mg/ml valganciclovir (E, G). All mice were sacrificed 7 days post sham injury. (F) No difference in silver staining was observed between groups. (A.U. arbitrary units).

5.3.7 Astrocyte response in valganciclovir treated mice

To confirm that only microglial numbers are being altered in this model, we analyzed the numbers of GFAP-positive astrocytes in regions of microglial depletion. We did not see any change in the numbers of GFAP-positive astrocytes in the corpus callosum and external capsule of mice treated with 1 mg/ml valganciclovir or 0.9% NaCl for 14 days (two-way ANOVA, genotype p= 0.6028, treatment p=0.9339, genotype x treatment p=0.7852; **Figure 5.15 A-C**). Similarly, there were no apparent changes in astrocytes due to valganciclovir treatment within grey matter areas.

5.3.8 Inflammatory response in valganciclovir treated mice

To determine how the inflammatory response was affected by microglial depletion in the setting of traumatic brain injury, RNA was purified from injured and uninjured mice acutely treated (14 days total) with 10 mg/ml valganciclovir and the amount of TNFα, IL-1β, IL6, iNOS, and CCL2 mRNA was determined by qPCR (**Figure 5.16 A-E**). Injury alone appeared to result in at most modest (<5-fold) increases in expression of these genes (rcTBI vs. sham CD11b -/- mice; **Figure 5.16 A-E**). Surprisingly, treatment of CD11b +/- mice with valganciclovir produced substantially greater changes in inflammatory gene expression in both injured and uninjured mice. Qualitatively, only TNFα appear to be increased to a greater extent in in CD11b-TK +/- injured vs. uninjured mice (**Figure 5.16 E**). Thus, while valganciclovir treatment of CD11b-TK mice reduces microglial cells, it may also drastically alter the inflammatory environment in this model.

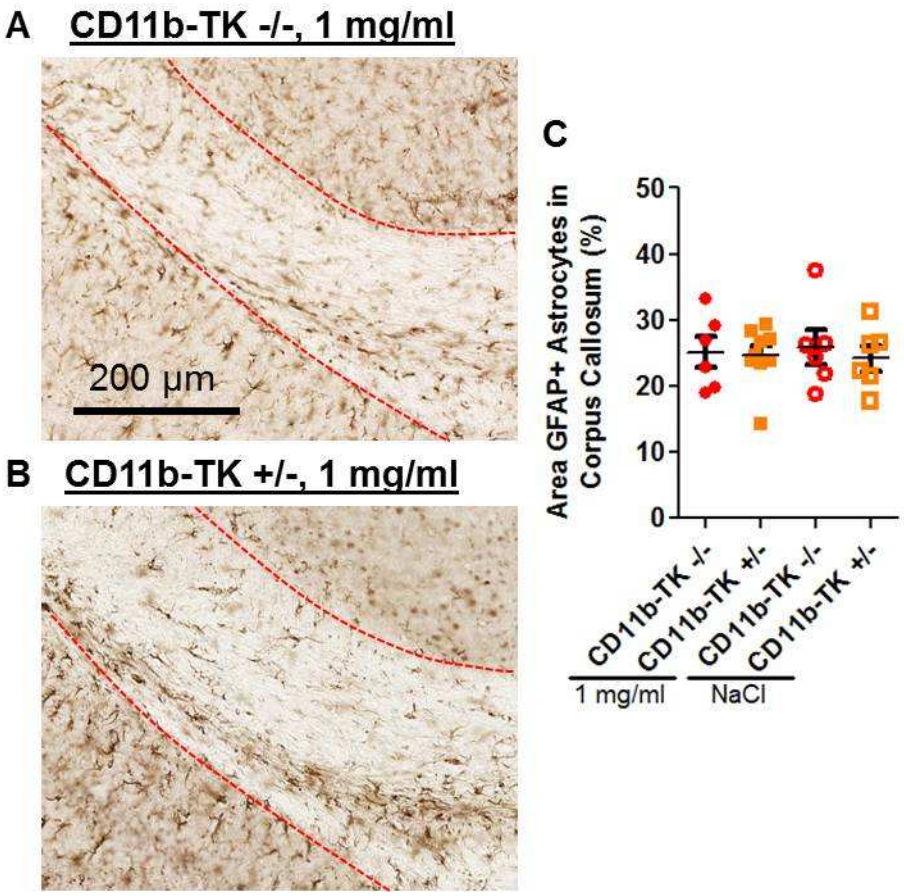

Figure 5.15 Astrocytes 7 days after rcTBI in mice treated with 1 mg/ml valganciclovir or NaCl. GFAP staining in treated CD11b-TK -/- (A) and +/- (B) mice. (C) No differences in GFAP optical density was observed between groups.

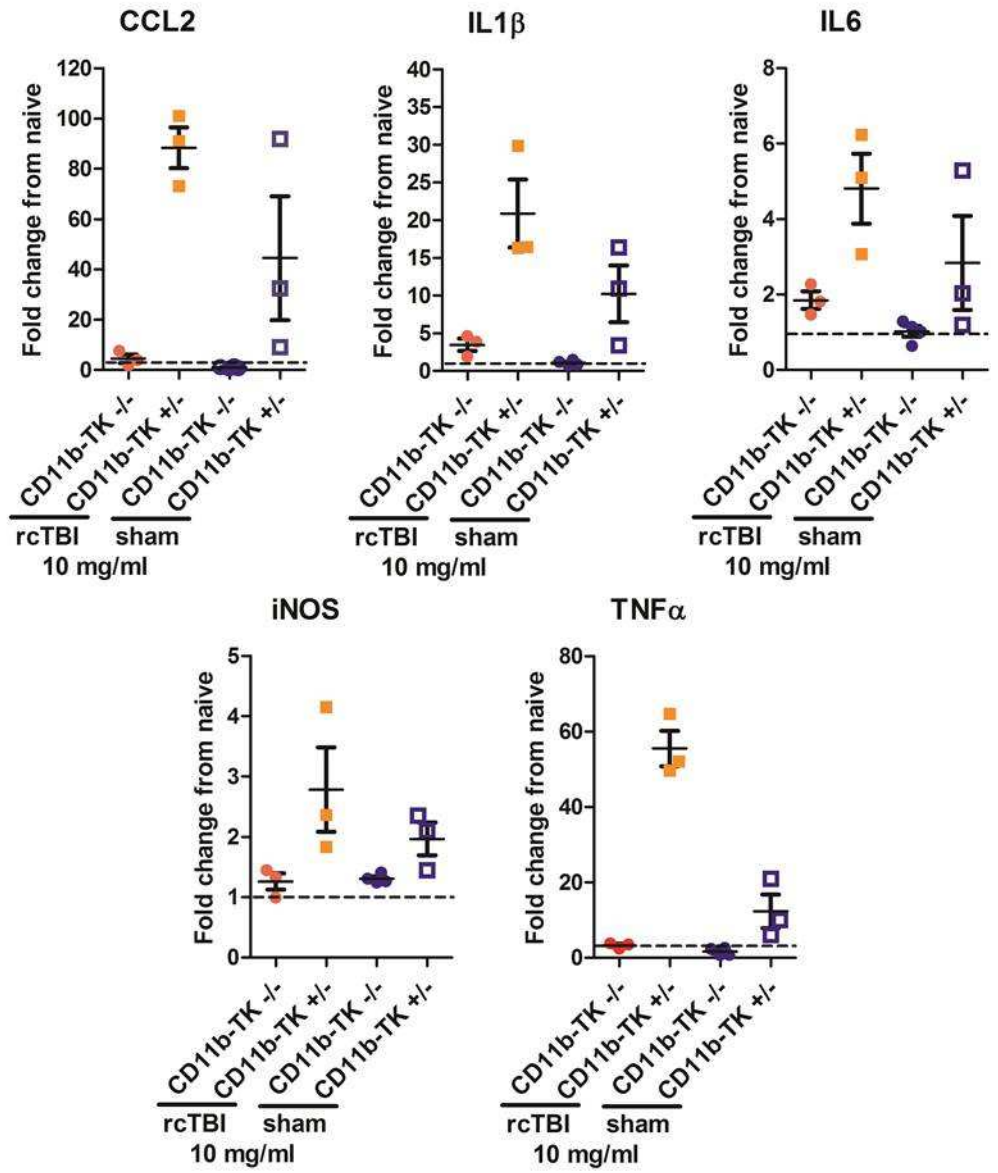

Figure 5.16 qPCR measurement of inflammatory gene expression. Relative expression of (A) *Ccl2*, (B) *Il1β*, (C) *Il6*, (D) *iNOS*, and (E) *Tnfα* in each mouse was normalized first to the geometric mean of 3 reference genes (*Hprt, Pgk1, Gapdh*) and then to arithmetic mean of the uninjured, naïve mice (n=4; dashed line).

5.4 DISCUSSION

In summary, we found that a reduction of the microglial population within the corpus callosum and external capsule by 35-56% neither increases nor decreases the extent of silver staining abnormalities. The most likely interpretation is that while microglia migrate to and proliferate around areas of axonal injury, overall they remain neutral in regards to the early processes of axon degeneration. We also provide further evidence that the CD11b-TK mouse line is a powerful tool for manipulating the microglial and macrophage response, but show that the dose of valganciclovir must be carefully determined to prevent unintended, non-specific toxicity and altered inflammatory gene expression in the central nervous system.

These studies are important because to our knowledge, there are no previous reports directly addressing the relationship between microglia and axon injury following *in vivo* mild repetitive traumatic brain injury. The contribution of microglia to other aspects of injury has been explored in more severe, brain injury models. Other researchers have used minocycline to reduce microglial activation, where it was reported to reduce brain lesion volume, caspase 1 activation, and cerebral edema after closed-skull TBI in mouse(Sanchez Mejia, et al. 2001; Bye, et al. 2007; Homsi, et al. 2009; Homsi, et al. 2010). However, only one of these studies measured axonal injury (by APP immunohistochemistry), and similar to results reported here, no difference was observed between minocycline treated and vehicle treated mice despite a 59% reduction in microglial activation(Homsi et al. 2010). In another study in rats, administration of anti-inflammatory drug ibuprofen for four months after TBI worsened performance on Morris Water Maze, a test of spatial learning and memory, compared to vehicle-treated rats.(Browne, et al. 2006) . The effect of treatment on microglial activation and axonal injury was not assessed.

In the present study, we reduced the number of microglia present in white matter tracts and assayed axonal injury using multiple injury markers and electron microscopy. This study is limited, however, in that we cannot rule out the possibility of functional consequences to the

depletion of microglia, independent of histological abnormalities.(Reeves et al. 2005) In addition, this study is also limited in that it is possible that the maximum reduction of the microglial population by 56% was not enough to produce an effect on white matter integrity. The remaining microglia may be able to compensate for the loss by ramping up production of secreted factors. Indeed, qPCR analysis revealed considerably more TNF-α, IL1-β, IL6, iNOS, and CCL2 mRNA following valganciclovir treatment. These factors may directly impair axons or modulate the inflammatory response in a complex fashion.(Ashki, et al. 2006; Davies, et al. 2006; Morganti-Kossmann, et al. 2007) Given this increase, it is remarkable that more severe silver staining abnormalities were not detected. This could indicate that axons are resilient to many aspects of the inflammatory response. An important line of future investigation will involve elucidating the full time course of the changes in cytokine expression in response to injury and in response to valganciclovir administration. Whether microglia and macrophages were directly responsible for the increases in secreted cytokine mRNA or whether the reduction in microglia induced expression by other cell types was not examined. Another alternative explanation for our results is that there could be both beneficial and harmful subtypes of microglia that are approximately evenly reduced by the experimental manipulations resulting in a net neutral effect on white matter.(Kigerl, et al. 2009) A final alternative explanation could be that any beneficial effects of microglial reduction were offset by the upregulation of inflammatory gene expression in response to the valganciclovir treatment.

This study was also limited in that it did not assess the specific contribution of the resident microglial population versus peripheral macrophages to injury. In this injury model, however, we have not observed IgG accumulation or a large population of CD45+^{hi}, CD11b+ cells (unpublished observations) that would be indicative of infiltration of peripheral macrophages. Thus, while peripheral macrophages may be present in rcTBI brains, most Iba-1 positive cells are likely resident microglia.

While these data indicate microglial cells are likely neutral overall in regards to axon injury following repetitive concussion in the acute and subacute phase, it remains mysterious why microglial cells migrate to the corpus callosum and external capsule and remain activated long-term. Activated microglia and macrophage have been observed in corpus callosum and other brain regions in human TBI patients several months or years after injury, indicating this is not a mouse-specific phenomenon.(Oppenheimer 1968; Ramlackhansingh et al. 2011; Johnson et al. 2013a) As these are phagocytic cells, it may be that ongoing axon degeneration results in debris that stimulates the microglial response. Microglial clearance of this debris may be neither beneficial nor harmful in the relatively short time scale assessed in these experiments, but could play an important role in long-term chronic sequelae of injury including axonal sprouting and regeneration not assessed here.(Hosmane et al. 2012) Indeed, microglia are important sources of brain derived neurotrophic factor (BDNF) and other neurotrophins that stimulate axonal sprouting and may be central to recovery from injury.(Batchelor et al. 2002; Venkatesan, et al. 2010) Future work may help to address these questions and provide deeper insight into the biological function of microglia after injury. Other studies may also address the effect of microglial reduction in more severe brain injury, where the role of microglial cells may be distinct.(Jiang, et al. 2012; Loane, et al. 2014)

A technical note regarding the toxicity of valganciclovir in CD11b-TK mice warrants discussion. It was surprising that valganciclovir administration at intermediate and high doses produced such widespread tissue loss in CD11b-TK mice. Work from Grathwohl and colleagues has previously reported that administration of 50 mg/ml valganciclovir can produce microhemorrhages following one month of treatment.(Grathwohl et al. 2009) Their group was using an independently derived line of CD11b-TK mice. Mice used in our experiments were generated in the lab of Jean-Pierre Julien and the thymidine kinase gene contains a mutation resulting in increased sensitivity to drug treatment. This increased sensitivity could explain why 10 mg/ml was sufficient to produce toxicity after 28 days and 50 mg/ml increased mortality by

50% after 14 days of treatment in our experiments. The underlying cause of this toxicity is unknown; the profoundly upregulated cytokine mRNA levels detected by qPCR may indicate either a cause or an effect of the toxicity. Repeating experiments in other transgenic mouse models of microglial depletion/manipulation (Table A2 in the Appendix) may aid in determining whether this phenomenon is specific to the CD11b-TK model or is a consequence of microglial depletion after rcTBI. Use of some of these other mouse lines, such as the MAFIA or CX3CR1^{CreER} line may also be more amenable to the study of the long-term effects of microglia in traumatic brain injury (Burnett, et al. 2004; Parkhurst, et al. 2013).

Altogether, the finding that microglia appear to be neutral in regards to injury is an important consideration for the design of future therapeutics. This could indicate that drugs specifically targeting axonal injury may be more useful following concussive-type injuries than those targeting microglial cells. Alternatively, methods to more completely prevent the activation and/or proliferation of microglial cells without toxicity should be sought for further studies.

CHAPTER 6

Use of Pharmacological Compounds to Manipulate the Microglial Response after Repetitive Concussive Injury

6.1 INTRODUCTION

The pathological processes that lead to long-term consequences of multiple concussions are unclear. Primary mechanical damage to axons during concussion is likely to contribute to dysfunction. Secondary damage has been hypothesized to be induced or exacerbated by inflammation. The main inflammatory cells in the brain are microglia, a type of macrophage. Between 4 and 7 days after repetitive concussive traumatic brain injury (rcTBI) in mouse, microglial cells increase more than three-fold in the corpus callosum and external capsule and persist for at least 7 weeks post-injury (Shitaka et al. 2011). Concomitantly, axonal injury in these regions is evident by silver staining and electron microscopy 7 days post-injury and similarly persists for at least 7 weeks (Shitaka et al. 2011). This brings to question what the role of microglia is in relation to axonal injury after concussion. Here, we sought to use a pharmacological approach to reduce the microglial response in white matter following injury and determine if this cell type contributes to axonal injury.

Numerous compounds have been used in experimental models to manipulate microglia, and many of these have been summarized in Table A3 of the appendix. Based on previous literature, 5 different compounds were chosen to test: mac-1-saporin, minocycline, (RS)-2-chloro-5-hydroxyphenylglycine (CHPG), brilliant blue g (BBG), and microRNA-124 (miRNA-124). Mac-1-saporin is an antibody to CD11b (Mac-1), a receptor found on all microglia and macrophage, bound to the toxin saporin. Binding of the antibody to CD11b-positive cells is

reported to lead to internalization of the toxin and subsequent microglial/macrophage cell death (Dommergues, et al. 2003; Garcia-Alloza, et al. 2007; Zhao, et al. 2007). Minocycline, an antibiotic used for acne and other bacterial infections, has been reported to be an inhibitor of microglial activation in several disease and injury models including traumatic brain injury. Minocycline has also been used in clinical trials for amyotrophic lateral sclerosis (ALS), Huntington's disease, and multiple sclerosis (Kim, et al. 2009). The mechanism of minocycline's action on microglial cells is not well characterized, though it has been reported that it interferes with p38 kinase, interrupting signaling cascades that stimulate microglial proliferation and cytokine synthesis, and that it inhibits caspase-1, caspase-3, inducible nitric oxide synthetase and matrix metalloproteinases (Greenwald, et al. 1992; Amin, et al. 1996; Chen, et al. 2000; Hua, et al. 2005). CHPG, on the other hand, is an antagonist of metabotropic glutamate receptor 5 (mGluR5) which is constitutively expressed on microglia and macrophage. Stimulation of mGluR5 with CHPG has been reported to prevent proliferation, nitric oxide and TNFα synthesis in microglial cultures activated with bacterial lipopolysaccharide (Byrnes, et al. 2009a). These effects were also observed when CHPG was delivered intrathecally following spinal cord injury (Byrnes, et al. 2009b). The fourth compound tested, brilliant blue g, is a selective antagonist of the ATP-gated ionotropic purinoreceptor $P2X_7R$. $P2X_7R$ is primarily expressed on microglia and macrophage and ATP activation results in proliferation and increased synthesis of TNFα, IL1β, and reactive oxygen species via the p38/NFκB pathway (North 2002; Monif, et al. 2009). Like CHPG, BBG was administered intrathecally in rats after spinal cord injury and microglial number was reported to reduce the number of OX42-positive microglia in spinal cord by nearly 50% at 14 days post-injury. Finally, miRNA-124 was chosen because it has been observed to be dramatically reduced in activated microglia (Ponomarev, et al. 2011). Increasing miRNA-124 expression suppressed inflammation-induced injury in a model of multiple sclerosis.

In the present studies, each compound or its vehicle was administered to mice that received repetitive closed skull injuries (rcTBI) and the number of iba-1-positive cells was quantified by stereology at acute timepoints. Silver staining was used to assess axonal injury. Altogether, it was determined that despite experimental evidence suggesting these pharmacological approaches effect microglia in other experimental models, none reduced iba-1-positive cells in white matter tracts after rcTBI. This may reflect the complex nature of the inflammatory response to axonal injury and provide insight into the basic biology of microglia.

6.2 METHODS

Animals

In all experiments, 6-8 week old C57/bl6j mice were purchased from Jackson and used for experiments. All mice were housed under a 12-hour light/dark cycle and given food and water ad libitum in accordance with the Animal Studies Committee at Washington University in Saint Louis.

Surgical procedures

Repetitive closed-skull injury was performed as previously described using an electromagnetic impactor fitted with a rubber tip. Two impacts were delivered 24 hours apart. In mice receiving continuous intracerebroventricular (ICV) drug infusion, osmotic pumps were implanted immediately following the second injury. For this, a 0.9 mm burr hole was drilled at A/P -0.84 mm relative to bregma M/L +1.5 mm right of midline at bregma. A plastic cannula was secured with cyanoacrylate glue to the skull at a depth of 2.5 mm. This cannula was attached to an osmotic pump via vinyl tubing. The 7 day osmotic pumps used in this experiment had flow rates of 0.5 µl/hour (Model 1007D, DuRect) and were implanted subcutaneously. Bolus injections of mac-1-saporin or vehicle were delivered by bolus injection using a 10 µl syringe (701RN, Hamilton) fitted with a 1.5” 33 ga needle (Hamilton). A nanoinjector pump was

used to deliver drug at a rate of 0.3 µl/min. After injection, the needle was left in place for 5 minutes before being slowly retracted. The burr hole was then sealed with dental wax. After the end of surgical procedures, the incision was sutured closed, antibiotic ointment was applied, and mice were allowed to recover from anesthesia on a heat pad before returning to their cages. All mice with osmotic pumps were singly housed. All drug treatments were administered in the lateral ventricle ipsilateral to injury to minimize the contribution of cannulation or bolus injection to axonal injury in the region of interest within the opposite hemisphere.

Drug preparation and administration

Mac-1-saporin (Mac-1-SAP) was purchased from Advanced Targeting Systems (cat# IT-06). The stock solution of 1.7 µg/µl in phosphate buffered saline (PBS) was injected ICV without dilution so that mice received either 2, 4, or 9 µg of Mac-1-SAP or an equal volume of 0.01 M PBS.

For minocycline experiments, minocycline hydrochloride (cat# M9511, Sigma-Aldrich) was dissolved in 0.01 M PBS and heated at 37℃ for 30 minutes to dissolve. To determine the dose-response of microglia to minocycline, intraperitoneal (IP) injections of 5, 20, 45 or 90 mg/kg or PBS were performed immediately following injury and again daily until mice sacrifice. In a follow-up experiment, mice were pretreated with 45 mg/kg minocycline 1 hour prior to injury and received IP injections every 12 hours until sacrifice.

For CHPG experiments, (RS)-2-Chloro-5-hydroxyphenylglycine sodium salt (cat# 3695, Tocris Bioscience) was dissolved in 1% dimethylsulfoxide, 0.9% saline and 5, 10, or 20 mM CHPG or vehicle was loaded into osmotic pumps. For BBG (cat# B-0770, Sigma-Aldrich) was dissolved in 0.9% saline and osmotic pumps were filled with 1, 10, or 100 µM or saline. In miRNA-124 experiments, hsa-miR-124 was purchased from Ambion (cat# 4464066, mirVana). 5 nmol of miRNA124 was dissolved in 0.9% saline, encapsulated in 14% Lipofectamine 2000,

and loaded into osmotic pumps. Pumps were primed overnight at 37℃ in saline prior to implantation after injury.

Histology

All mice were sacrificed 4 or 7 days after the first closed-skull injury by deep isofluorane anesthesia followed by cardiac perfusion with ice cold 0.03% heparin in PBS. Brains were removed and immersion fixed for 24 hours in 4% paraformaldehyde, then equilibrated in 30% sucrose in PBS for 24 hours prior to sectioning on a freezing microtome. Eight sets of 50 μm thick sections, corresponding to a sampling interval of 400 μm throughout the brain were collected as previously described. Rabbit anti-iba-1 (Wako) was used to label microglia and macrophage following immunohistochemical methods described in Chapter 5 and in Shitaka et al (2001). Likewise, silver staining was performed on adjacent sections as described previously.

Quantitative analysis of histology

The number of iba-1-positive cells in the corpus callosum were quantified by stereology. 3-4 sections per mouse were analyzed, beginning with the anterior-most section containing corpus callosum overlying the hippocampus. The optical fractionator method was used, with a grid size of 180 x 180 and a counting frame of 80 x 80. All iba-1-positive cell bodies in corpus callosum and external capsule ipsilateral to injury were counted.

For optical density quatification of silver staining, digital images of all slides were captured using the Nanozoomer whole slide imaging system (Hamamatsu). Background was reduced from each image and the amount of silver deposits in the region of interest (ROI) was determined by mean grey value for each of 3-4 sections per mouse. ROI parameters for silver staining were the same as for iba-1 stereology. Detailed methods can be found in Chapter 5.

6.3 RESULTS

6.3.1 Mac-1-saporin reduces iba-1 and silver staining but displays off-target toxicity

Administration of 9 µg of Mac-1-SAP was initially tested as this was a similar dose to one used by Garcia-Allonza and colleagues to eliminate microglia in an Alzheimer's disease mouse model. Mice received either Mac-1-SAP (n=7) or vehicle (n=8) and were sacrificed 4 days post-injury (**Figure 6.1 A-F**). At this timepoint, the number of iba-1-positive cells in the corpus callosum and external capsule was reduced by 49% (one-tailed student's t test p=0.0145, Figure 6.1 A, B, E). Silver staining in this region was reduced by 68% (two-tailed student's t test p=0.0003, **Figure 6.1 C, D, F**). Cresyl violet staining was performed in these mice and in additional mice that were treated with Mac-1-SAP and sacrificed 7 days post-injury (n=3, **Figure 6.2 A-C**). This revealed cell loss Mac-1-SAP treated mice in the hippocampal CA3 that was apparent at 4 days (Figure 6.2 B) and severe at 7 days (**Figure 6.2 C**). Thus, it appears that treatment with Mac-1-SAP results in non-specific neurotoxicity. Such widespread cell loss likely contributes to the reduction in silver staining seen in mice 4 days post-injury.

In a second experiment, mice were treated with lower doses (2 and 4 µg; n=3 per group), sacrificed at 7 days, and iba-1 immunohistochemistry was performed (**Figure 6.3 A, B**). At both of these lower doses, tissue integrity was evidently compromised. Additionally, these doses did not appear to reduce iba-1-positive cells in the injured hemisphere.

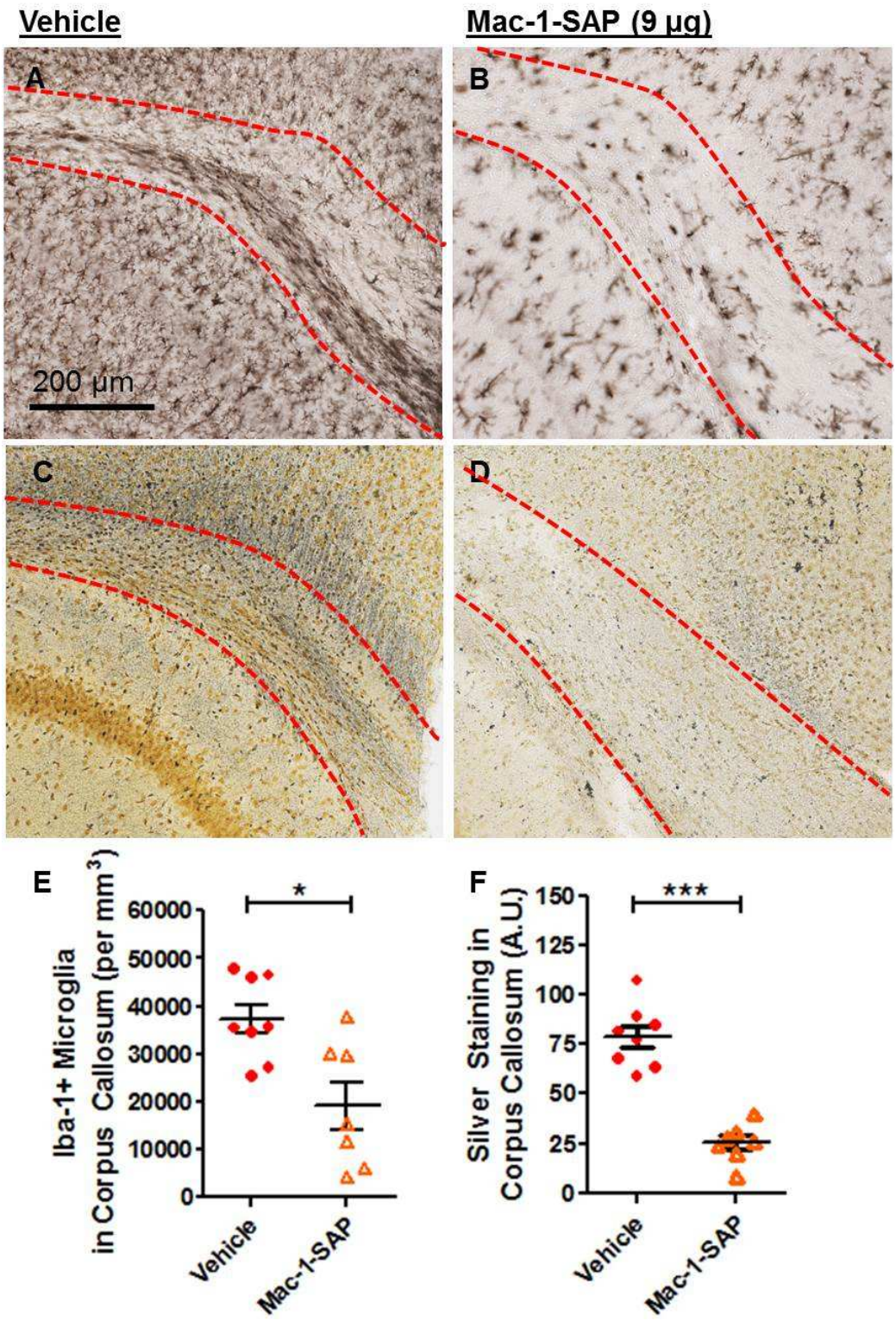

Figure 6.1 Mac-1-SAP treatment reduced iba-1 and silver staining at 4 days post-injury. Mice were treated with vehicle (A, C) or 9 µg (B, D). (E) Quantification of iba-1 by stereology revealed a significant decrease in the number of cells present in the corpus callosum and external capsule. (F) Silver stainined was also reduced as measured by optical density. (*p<0.05, ***p<0.001, a.u. = arbitrary units, error bars represent standard error of the mean)

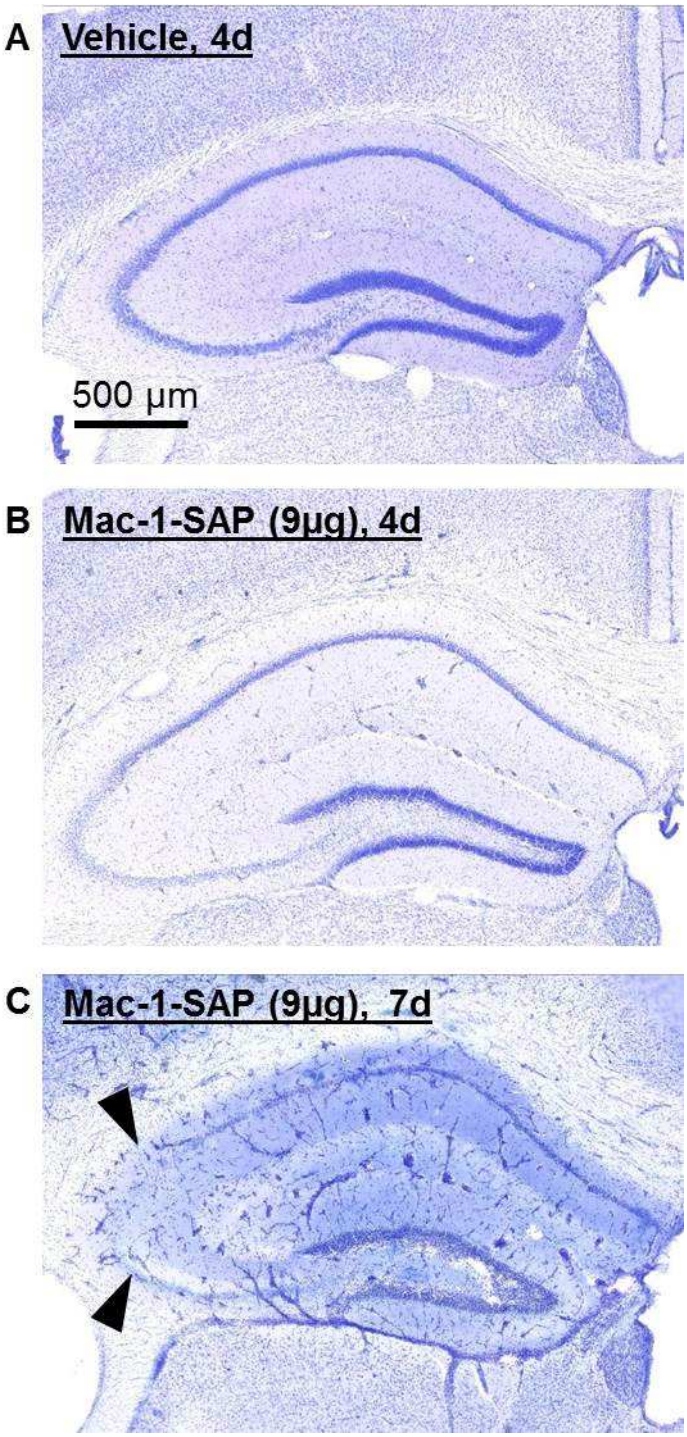

Figure 6.2 Mac-1-Saporin treatment leads to neuron loss in the hippocampal CA3. Cresyl violet stained sections from mice sacrificed 4 days post-injury treated with vehicle (A) appear normal while mice treated with 9 µg Mac-1-SAP (B) have reduced cellularity in the CA3. Cell loss in the CA3 (arrowheads denote region of greatest loss) and blood brain barrier compromise was marked at 7 days (C).

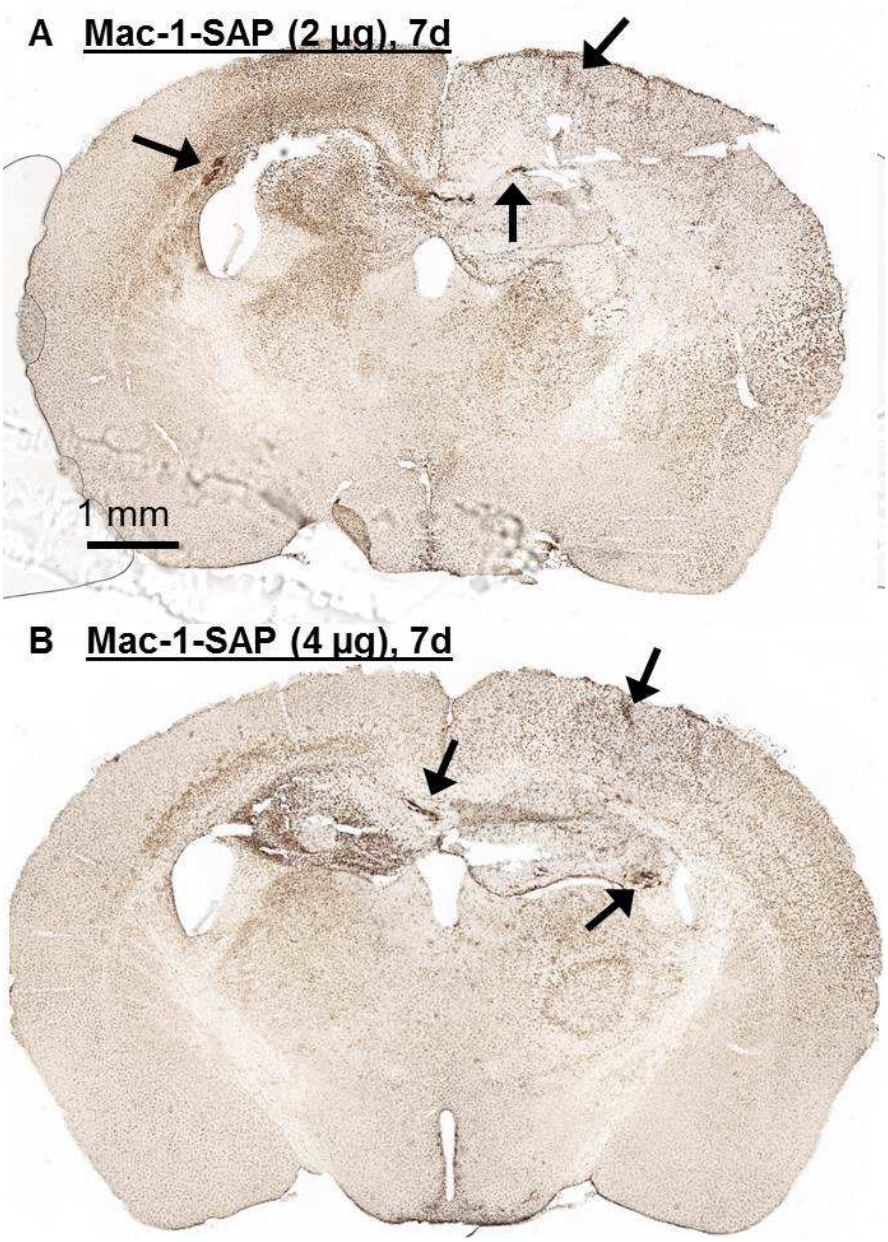

Figure 6.3 Lower doses of Mac-1-SAP were also toxic at 7 days post-injury. Iba-1 labeling was reduced in the injected hemisphere (right side) of mice treated with both 2 µg (A) and 4 µg (B). Tissue was evidently compromised and diaminobenzidine labeled intraparenchymal hemorrhages (arrows).

6.3.2 Minocycline treatment does not reduce the number of microglia or the amount of silver staining in the corpus callosum and external capsule after injury

A separate cohort of mice received 5, 20, 45, or 90 mg/kg minocycline (n=5 per group) daily by intraperitoneal injection immediately following the second injury. Compared to mice injected with vehicle alone, treatment with minocycline had no effect on the number of iba-1-positive cells at any dose 7 days post-injury (one way ANOVA p=0.0540, **Figure 6.4 A-F**). Two individuals from each group were randomly selected for silver staining which also indicated no difference between groups (**Figure 6.5 A-F**).

In rodents, the half-life of minocycline has been reported to be as short as 3 hours and reaches peak concentrations in the brain at 1 hour post-IP injection. A second group of mice (n=3 per group, **Figure 6.6 A-C**) was subject to a more aggressive treatment paradigm and received IP injections of 45 mg/kg minocycline 1 hour before the first injury and again every 12 hours for 7 days. Quantification of iba-1 in corpus callosum and external capsule did not reveal any differences between minocycline and vehicle treated mice (one-tailed student's t test p=0.2902, **Figure 6.6 C**).

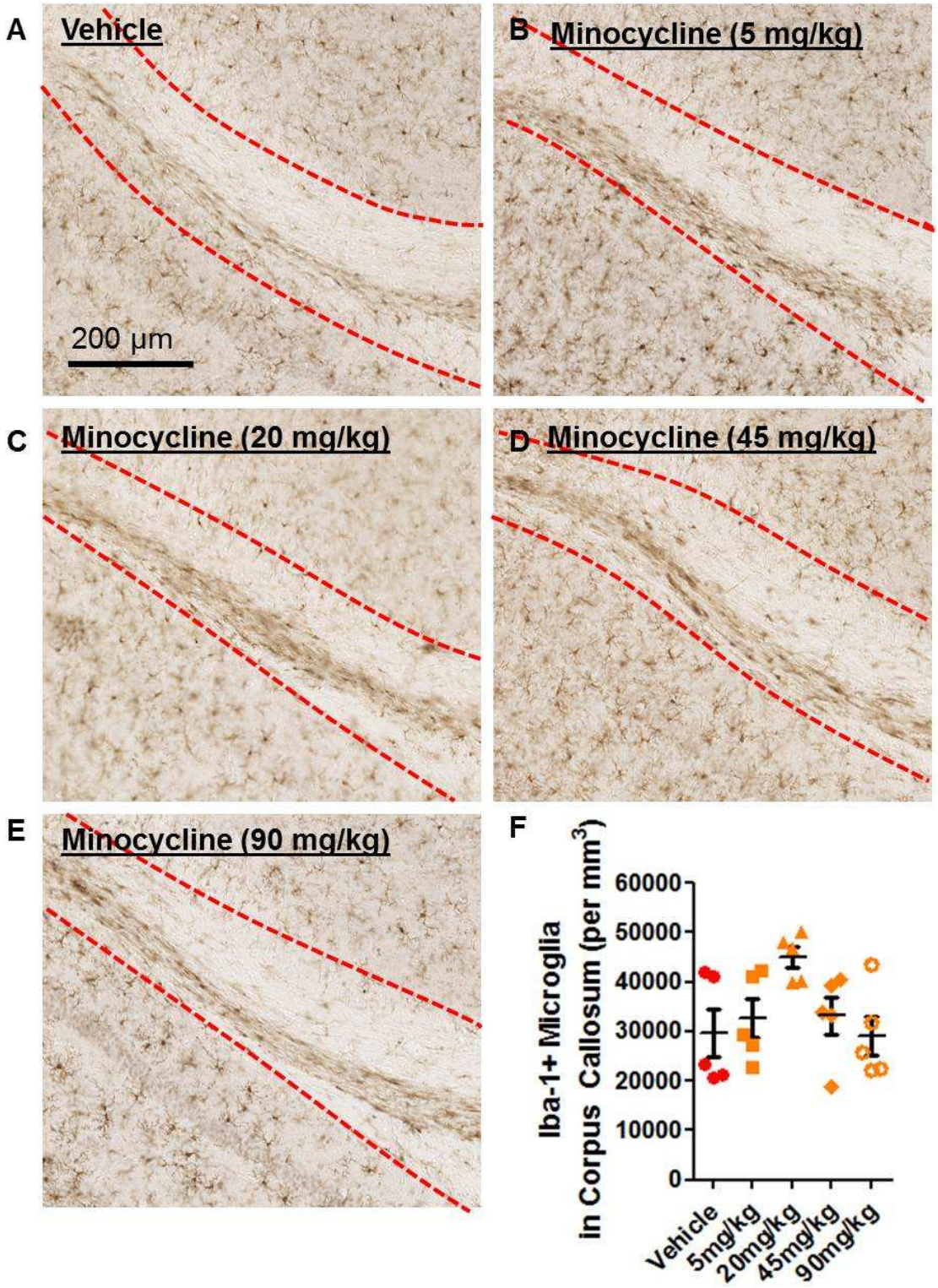

Figure 6.4 Minocycline administration does not alter iba-1 labeling at any dose. Mice that received vehicle (A), 5 (B), 20 (C), 45 (D), or 90 (E) mg/kg all had similar numbers of iba-1-positive cells in the corpus callosum and external capsule. No differences were observed by stereological analysis. (Dashed red line indicates corpus callosum, error bars are ± SEM)

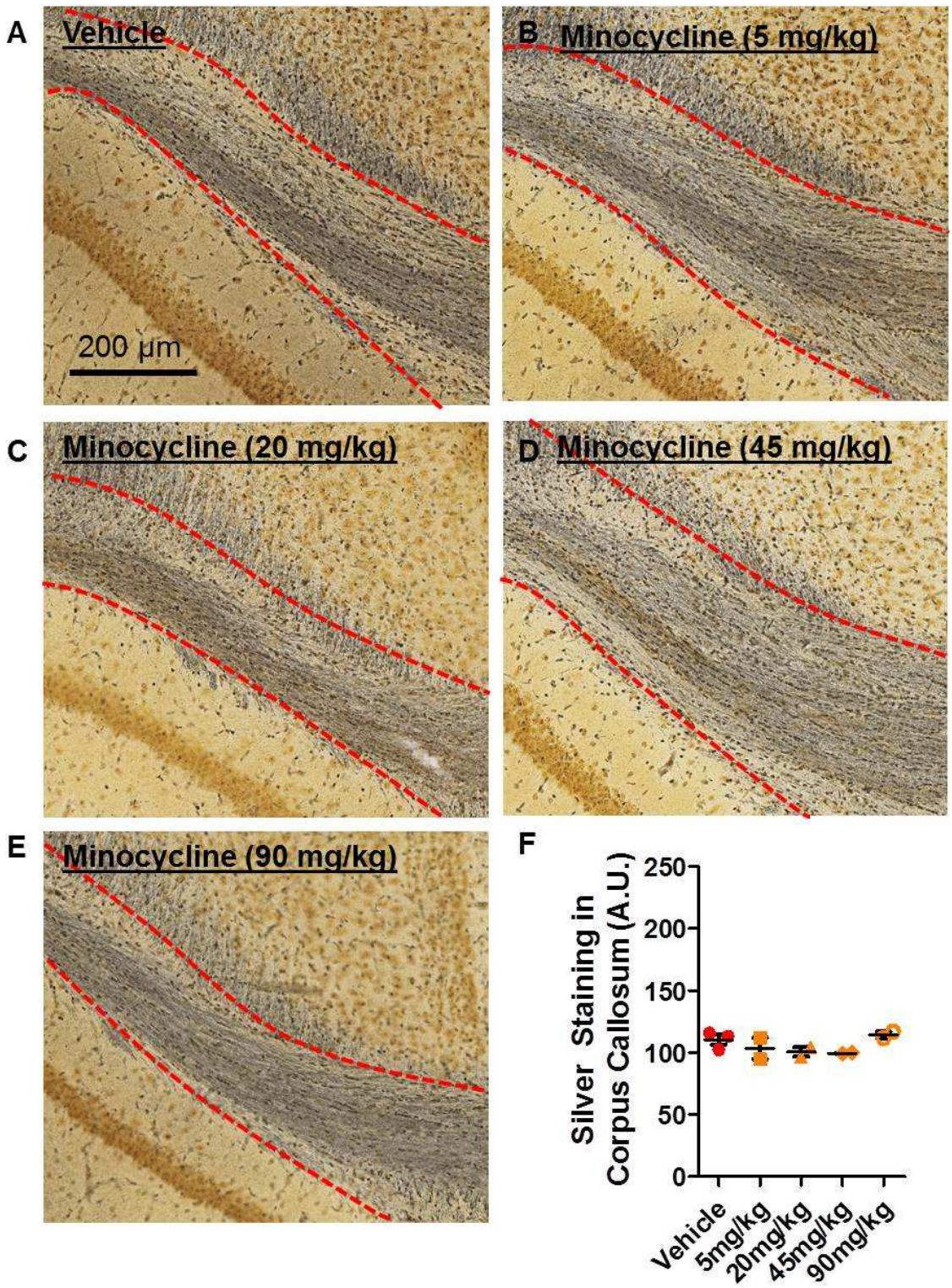

Figure 6.5 Silver staining does not reveal any differences in mice treated with minocycline. Mice that received vehicle (A), 5 (B), 20 (C), 45 (D), or 90 (E) mg/kg all had similar silver staining in the corpus callosum and external capsule. No differences were observed by optical density measurement. (Dashed red line indicates corpus callosum, error bars are ± SEM)

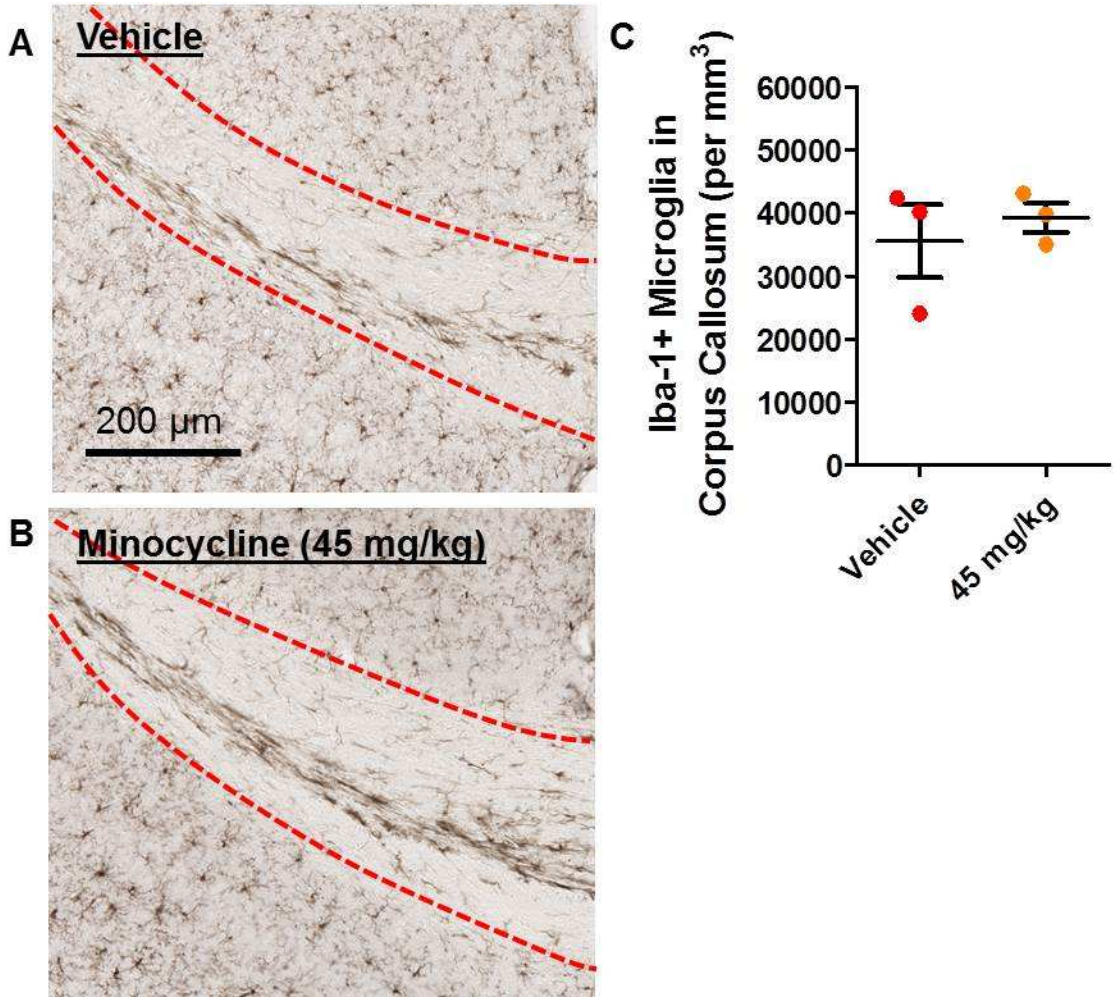

Figure 6.6 Treatment with minocycline every 12 hours beginning 1 hour prior to injury did not alter the number of iba-1-positive cells. Mice treated with vehicle (A) or 45 mg/kg minocycline (B) had similar numbers of iba-1-positive cells in the corpus callosum and external capsule 7 days post-injury. No difference was evident by iba-1 sterology (C). (Dashed red line indicates corpus callosum, error bars are ± SEM).

6.3.3 CHPG does not suppress microglial numbers or silver stain abnormalities in white matter.

Another cohort of mice was then treated with 5 (n=3), 10 (n=4), or 20 (n=3) mM CHPG by ICV osmotic pump implanted immediately following the second injury. Mice were sacrificed 7 days after injury and the number of iba-1 positive cells in the corpus callosum and external capsule were quantified by stereology (**Figure 6.7 A-E**). Though a slight trend was observed, compared to controls treated it did not reach significance (one way ANOVA p=0.3546, Figure **6.7 E**). Similarly, silver staining was not altered by treatment (one way ANOVA p=0.5389,

Figure 6.8 A-E). Another cohort of mice (n=3 per group, data not shown) was treated with 50 mM CHPG or vehicle and did not have reduced iba-1 (one-tailed student's t test, p=0.4351) or silver staining (two-tailed student's t test p=0.9563) 7 days post-injury.

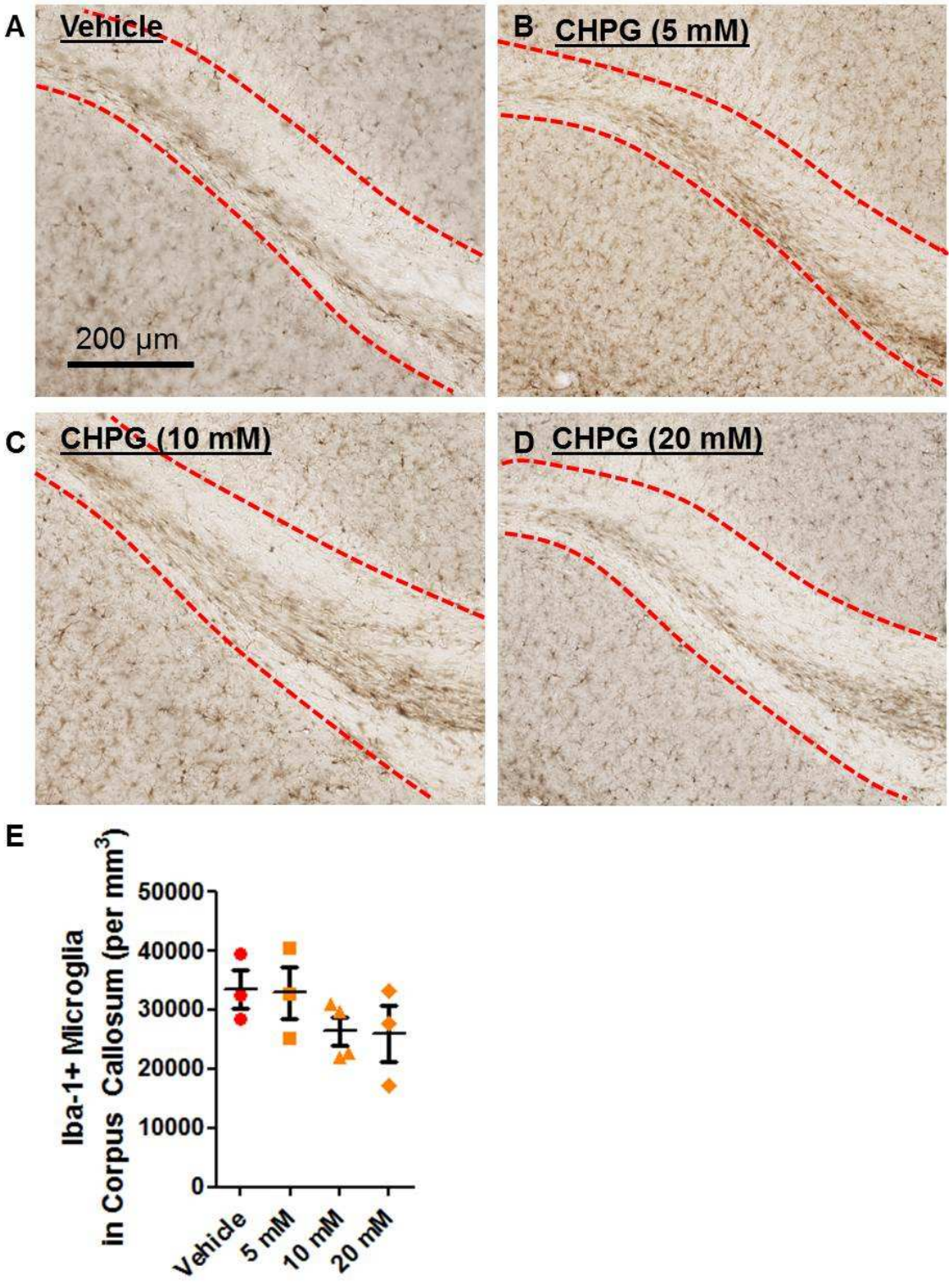

Figure 6.7 The number of iba-1-positive microglia is unchanged by CHPG in injured mice. Mice treated with vehicle (A) or 5 (B), 10 (C), or 20 (D) mM CHPG had similar numbers of iba-1-positive cells in the corpus callosum and external capsule 7 days post-injury. No difference was evident by iba-1 sterology (E). (Dashed red line indicates corpus callosum, error bars are ± SEM).

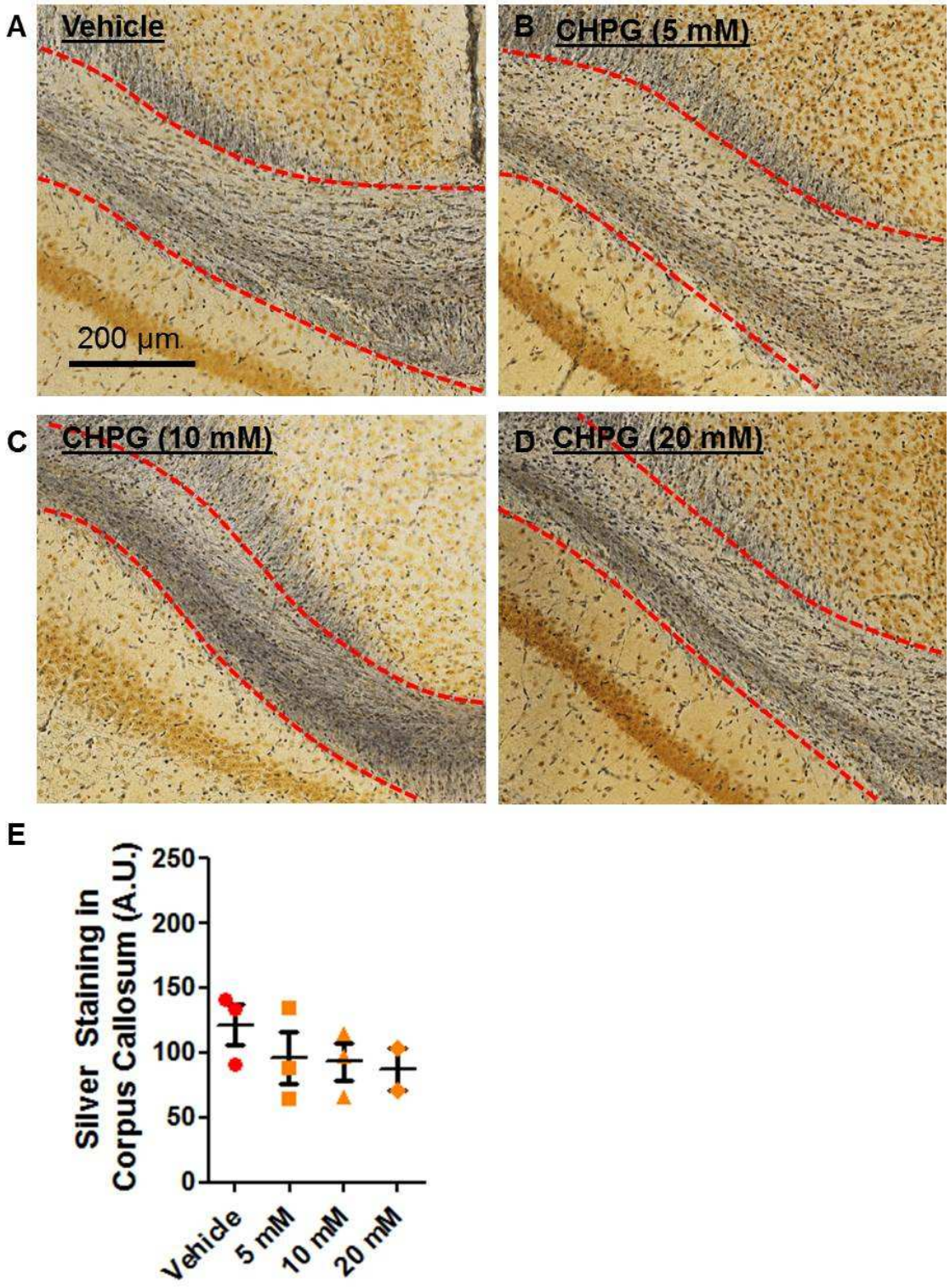

Figure 6.8 Silver staining was not altered by CHPG at any dose. Mice treated with vehicle (A) or 5 (B), 10 (C), or 20 (D) mM CHPG had similar levels of silver staining in the corpus callosum and external capsule 7 days post-injury. No difference was evident by optical density measurement (E). (Dashed red line indicates corpus callosum, error bars are ± SEM).

6.3.4 Brilliant Blue G does not reduce microglia or alter silver staining after injury.

In the fourth set of experiments, vehicle (n=4), 1 (n=4), 10 (n=4), or 100 (n=5) μM brilliant blue g (BBG) was administered continuously by osmotic pump immediately following injury. The number of microglial cells in the corpus callosum and external capsule did not appear to be altered 7 days after injury (**Figure 6.9 A-D**). One-way ANOVA of iba-1 stereology did not reveal any change (p=0.7493 **Figure 6.9 E**). Silver staining was similarly unaffected by BBG treatment (p=0.2960, **Figure 6.10 A-E**).

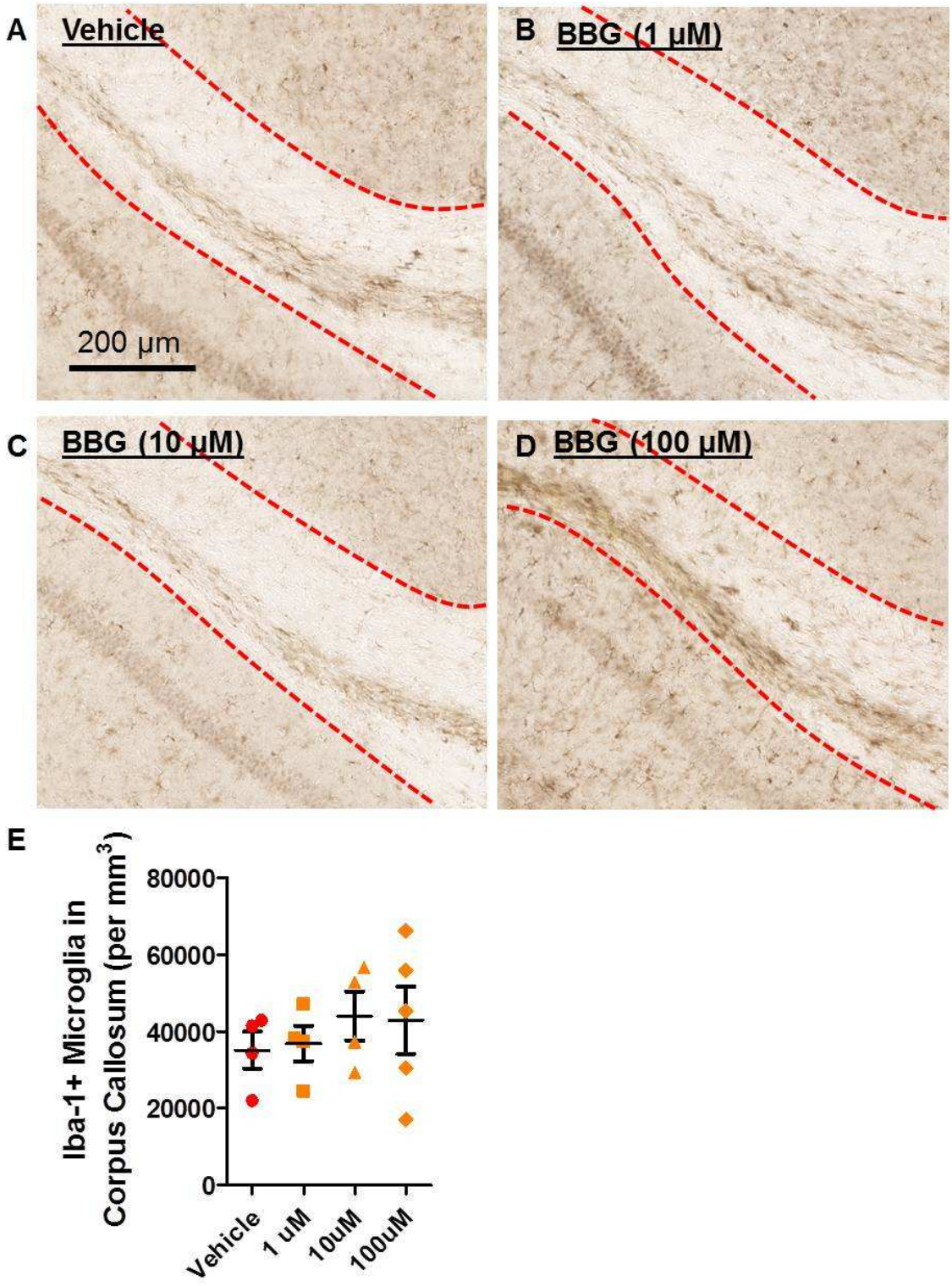

Figure 6.9 Brilliant Blue G does not reduce iba-1-positive cells in injured mice. Mice treated with vehicle (A) or 1 (B), 10 (C), or 100 (D) µM CHPG had similar numbers of iba-1-positive cells in the corpus callosum and external capsule 7 days post-injury. No difference was evident by iba-1 sterology (E). (Dashed red line indicates corpus callosum, error bars are ± SEM).

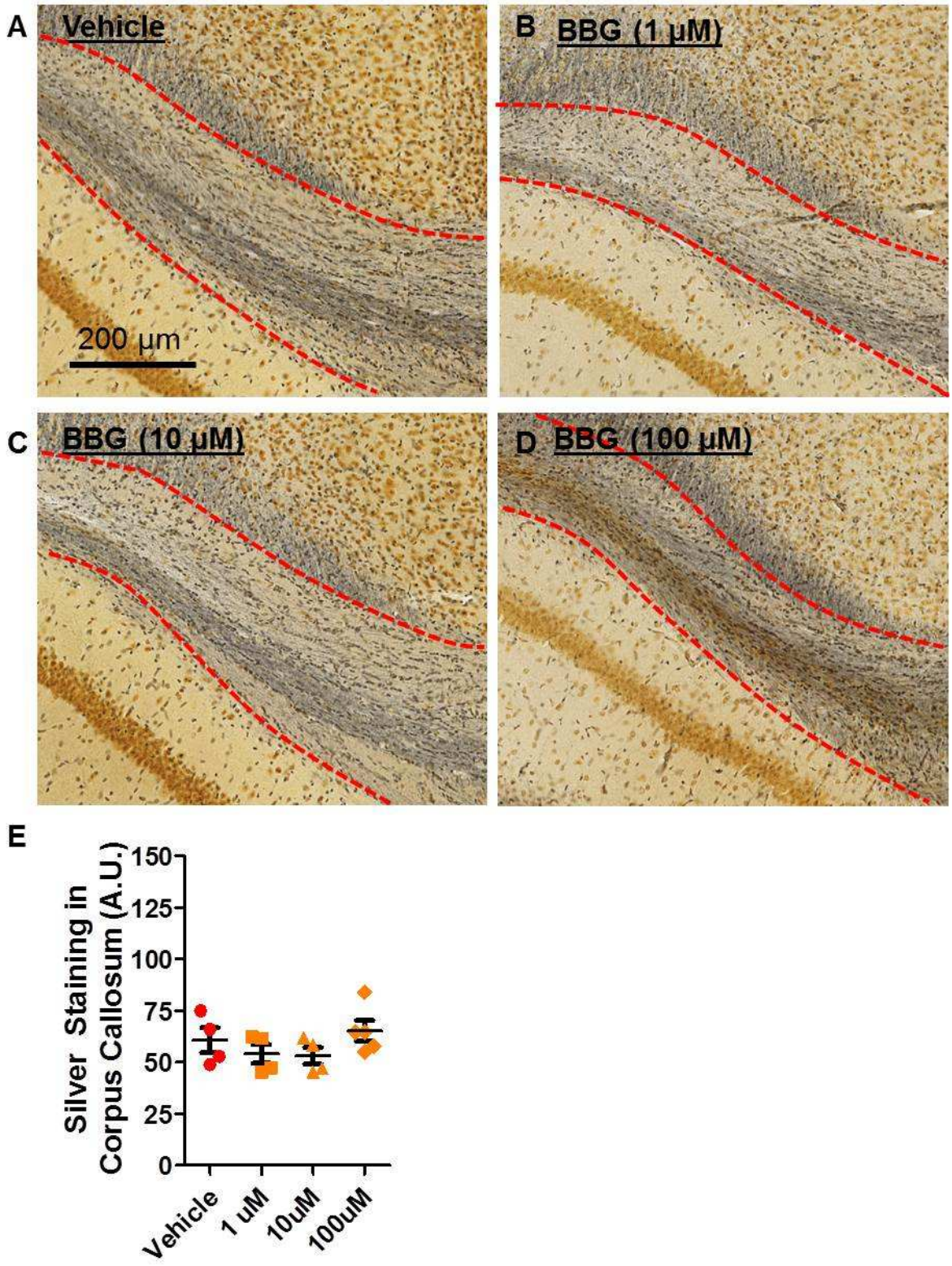

Figure 6.10 Silver staining was not altered by Brilliant Blue G. Mice treated with vehicle (A) or 1 (B), 10 (C), or 100 (D) µM CHPG had similar silver staining in the corpus callosum and external capsule 7 days post-injury. No difference was evident by optical density measurement (E). (Dashed red line indicates corpus callosum, error bars are ± SEM).

6.3.5 Exogenous miRNA-124 does not suppress microglia numbers in white matter.

miRNA-124 liposomes were prepared and injected ICV by osmotic pump immediately following injury. Each mouse received a total of 11 µg miRNA or vehicle and was sacrificed 7 days post-injury (**Figure 6.11 A-C**). Though there was a trend towards reduced microglia in the corpus callosum and external capsule, it did not reach significance at 7 days post-injury (one-tailed student's t test p=0.1035). Silver staining was not assessed. To determine whether lipofectamine containing vehicle alone effects the number of iba-1-positive cells, the experiment was repeated in injured mice treated with vehicle containing lipofectamine (n=5) or saline only (n=4, **Figure 6.11 D**). This revealed no significant difference in the number of iba-1-positive cells between groups (two-tailed student's t test, p=0.1045).

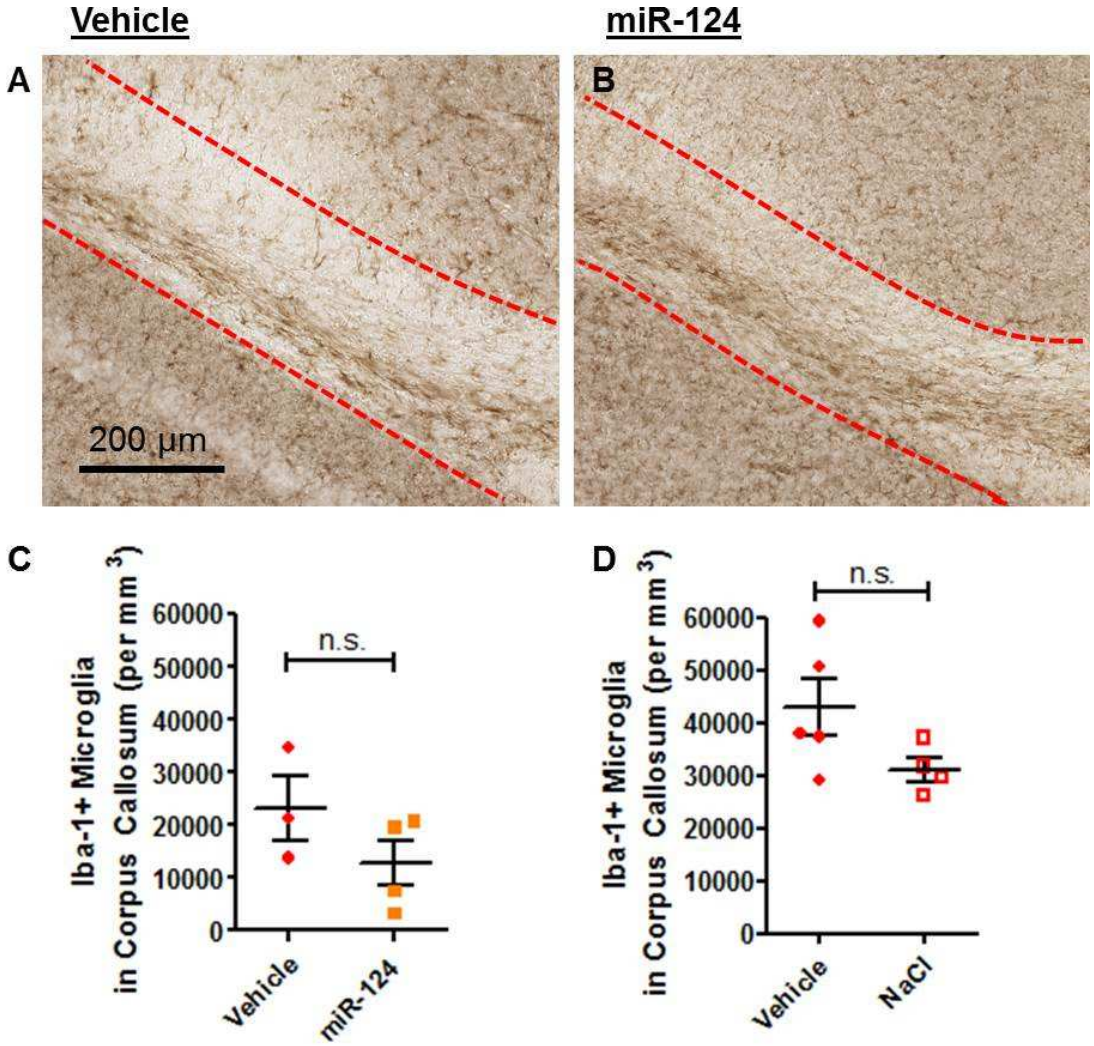

Figure 6.11 miR-124 does not reduce iba-1-positive cells in injured mice. Mice treated with vehicle (A) or miR-124 (B had similar numbers of iba-1-positive cells in the corpus callosum and external capsule 7 days post-injury (C). No change in the number of iba-1 cells was seen due to lipofectamine containing vehicle alone (D). (Dashed red line indicates corpus callosum, error bars are ± SEM).

6.4 DISCUSSION

Here, we tested several different compounds in the repetitive closed-skull injury (rcTBI) model to determine their ability to reduce the microglial response in the corpus callosum and external capsule. Treatment with a range of doses of minocycline, CHPG, or BBG failed to reduce the number of iba-1-positive cells at 7 days post-injury. Further, silver staining was not altered by these drugs, indicating that unmeasured changes to the inflammatory response outside of microglial number alone do not significantly alter silver stain-positive axonal injury. Similarly miR-124 treatment did not produce a significant alteration to microglial number. Mac-1-SAP, on the other hand, did reduce the number of microglia, but also exhibited non-specific neurotoxicity which has not been previously reported.

There are both strengths and limitations in these studies that should be addressed. One strength is the use of stereological approach to quantify microglia and macrophage in white matter. Previous reports using these compounds rely on optical density or non-stereological counts of microglia and macrophage per area of tissue. Stereology has several advantages over these methods including 1) removing user bias in selection of counting fields 2) allowing specific identification and quantification cell bodies and 3) avoiding confounds due to variability in staining intensity from sample to sample. A second strength is the use of a range of compounds that should affect inflammation through a variety of mechanisms. Thus, the failure to alter iba-1-positive cells in white matter is unlikely to be due to the targeting of a single pathway. Likewise different routes of drug administration—intracerebral bolus injection, continuous infusion, or intraperitoneal injection—and different experimental timelines were tried to increase the likelihood of altering the microglial response.

However, there are also several limitations. First, the sample sizes in these experiments were small. As such, we cannot rule out the possibility that small effects on the number of microglial cells were missed. However, as the overall goal of the experiment was to find a compound that would reduce the microglial response by 50% or more, it is reasonable to conclude that none of the compounds produced a large effect. Similarly, because iba-1 stereology was the only method used to measure the microglial response, the overall effect of these drugs on other aspects of inflammation, including cytokine production, phagocytosis, and expression of other markers was not determined. Consequentially, compounds may have modified other more subtle characteristics of the microglial response. If these changes did occur, however, they appear to be neutral in regards to axonal injury in this model as assessed by silver staining. Of note, no morphological changes were observed in microglia in mice treated with minocycline, CHPG, BBG, or miR-124.

Last, only the effect of these drugs on microglia within the white matter was measured. Assessing changes in microglial cells within grey matter is outside the current scope of this study, but may be an important consideration in the future. In particular, if drugs did reduce microglial number in grey matter regions, it would be interesting to determine why white matter was not affected. Differences in the diffusion of different compounds into white matter versus grey matter have been observed (Lieberman, et al. 1995; Prabhu, et al. 1998). Here, the ability of these drugs to penetrate throughout brain regions was not determined and may be one possible explanation of the results. In experiments where drug was delivered by ICV injection, preliminary experiments from our lab using fluorescent dextrans and Evan's blue (data not shown), and from others indicate that compounds can diffuse from ventricles into the neighboring parenchyma and white matter tracts (Konsman, et al. 2000). Additionally, differences between gene and protein expression differences in microglia in white matter versus grey matter have not been characterized though the morphology of cells in different regions is distinct. It is possible that white matter residing cells have inherently different sensitivity to drug

treatment. Pursuing these topics may increase our understanding of the basic biology of microglial cells.

Overall, the inability to reproduce previously published results and alter the microglial response in this model has several implications. Foremost, it points to the need for more rigorous statistical methods and experimental testing, including the use of multiple cohorts of mice to verify that the effects of drug treatment have not arisen by chance. Unbiased quantification methods, such as stereology, should be used in all cases. Second, others have reported that microglial phenotype is heavily determined by the sequence of signaling received by microglia (Perry, et al. 2014). In these studies, treatments that occurred following injury (CHPG, BBG, miR-124) may have failed because microglial cell activation was already "primed". Thus, it may be necessary to pretreat microglia to prevent their activation post-injury. This warrants further investigation as it has clear implications for clinical therapeutic design. Finally, how biomechanical forces alone may alter the microglial phenotype is unknown, though in one *in vitro* study it was determined that mechanical stretch induces chloride channel currents that can alter microglial morphology (Eder, et al. 1998). Future studies may address this effect in the context of traumatic brain injury.

Altogether, the development of new compounds that can minimize microglial activation in a variety of disease and injury settings is needed. Better understanding of microglial biology will be required and importantly, understanding how concussive injury activates the inflammatory response will be central to these future investigations.

CHAPTER 7

Human Apolipoprotein E4 Worsens Acute Axonal Pathology but not Amyloid-beta Immunoreactivity following Traumatic Brain Injury in 3xTG-AD Mice

7.1 INTRODUCTION

Clinical studies have revealed an increased risk of poor outcome following TBI in patients with one or more *APOE4* alleles (Mayeux, et al. 1995; Jordan, et al. 1997; Teasdale, et al. 1997; Friedman, et al. 1999; Kutner, et al. 2000; Teasdale, et al. 2005). The largest of these studies demonstrated that the effect of *APOE* genotype was significant only in younger patients (Teasdale et al. 2005). ApoE is a major lipid carrier in the brain (Mahley 1988), and there have been multiple mechanisms proposed to account for the effect in TBI and other brain injuries (Verghese, et al. 2011). One hypothesis is that *APOE* genotype affects secondary neurodegenerative processes following TBI. This hypothesis is based on the ideas that 1) *APOE4* is a major genetic risk factor for Alzheimer's disease (Corder, et al. 1993; Strittmatter, et al. 1993), 2) TBI is a major environmental risk factor for dementia of the Alzheimer's type (Plassman et al. 2000; Jellinger 2004), and 3) ApoE has been shown to interact with two key Alzheimer's disease proteins, Aβ and tau (Bu 2009). Supporting this hypothesis, human mutant APP transgenic mice with the *APOE4* allele show greater accumulation of Aβ chronically following TBI (Hartman, et al. 2002). However, *APOE* genotype can affect acute outcomes following TBI (Nicoll, et al. 1995; Friedman et al. 1999; Liaquat, et al. 2002; Smith, et al. 2006) and Aβ and tau pathologies can accumulate rapidly following TBI (Roberts, et al. 1991; Roberts, et al. 1994; Smith, et al. 2003a; Ikonomovic, et al. 2004; Uryu, et al. 2007). While ApoE isoform

specific differences have been studied in mouse models of TBI, few studies have addressed interactions between ApoE genotype on acute Aβ deposition following injury (Sabo, et al. 2000; Laskowitz, et al. 2010; Mannix, et al. 2011). Furthermore, the interaction between *APOE* genotype and tau pathology has not been investigated to our knowledge.

Recently, we showed that 3xTG-AD mice carrying three human familial AD mutations ($PS1_{M146V}$, tau_{P301L}, and APP_{SWE}) develop both acute amyloid beta and tau pathology following injury (Tran et al. 2011a; Tran et al. 2011b). We hypothesized that in the presence of the *APOE4* allele, both acute Aβ and tau pathology after injury would be exacerbated. To test this, we crossed 3xTG-AD transgenic mice to mice that have the human *APOE2*, *-E3*, and *-E4* alleles knocked-in (Sullivan, et al. 1997a; Oddo, et al. 2003). The results of stereological analysis suggest that *APOE* genotype may not affect acute Aβ or tau pathology after injury. Instead, *APOE* genotype appears to result in increased numbers of injured axons as evident by APP-positive white matter varicosities. Considering this surprising finding, we confirmed that the *APOE4* genotype worsens post-traumatic axonal injury in non-3xTG-AD mice expressing human *APOE* alleles. Altogether, this indicates a primary role for ApoE in acute post-traumatic axonal injury that appears to be unrelated to its interactions with Aβ or tau.

7.2 METHODS

Animals

Female 3xTG-AD mice were initially acquired from Frank LaFerla and were bred to male ApoE targeted replacement mice (ApoE-TR) of all 3 isoforms (Fig. 1). Heterozygotes from two separate crosses were mated to avoid sibling matings. The resulting litters were screened for quadruple homozygotes by PCR using previously published methods (Sullivan et al. 1997a; Oddo et al. 2003). Since the tau and APP alleles co-segregate in the 3xTG-AD line whereas the PS1 and ApoE alleles segregate independently, 1 out of 64 mice born were expected to be

homozygous for all four transgenes (**Figure 7.1**). We produced at least 4 of these quadruple homozygotes for each genotype to establish the 3xTG-ApoE2, -ApoE3, and –ApoE4 lines. Non-sibling quadruple homozygotes were then mated to yield the experimental mice used for the current study. All mice were housed on a 12 hour light-dark cycle with food and water ad libitum in accordance with the Animal Studies Committee at Washington University in St. Louis.

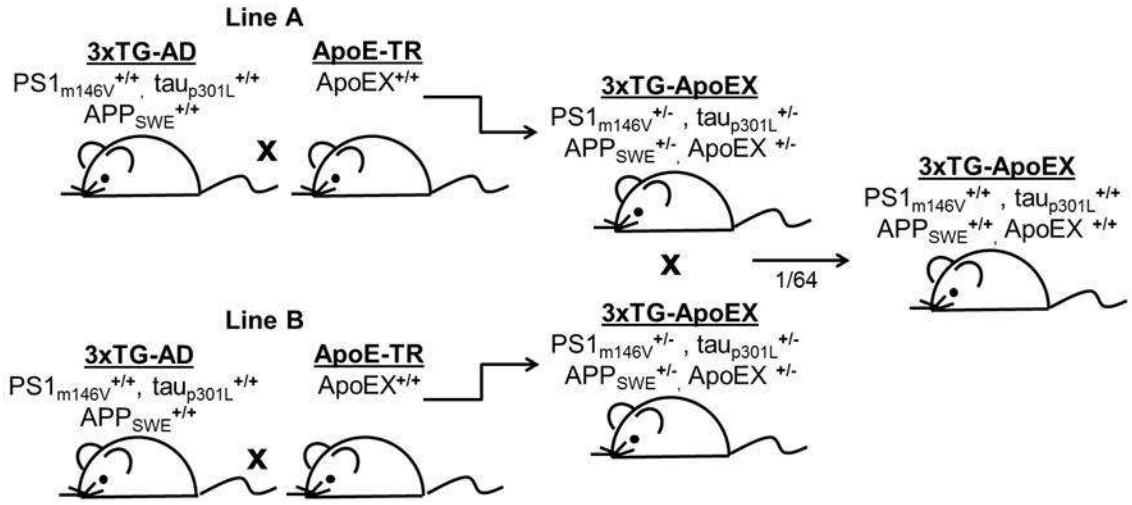

Figure 7.1 Generation of 3xTG-ApoE mice. For each of the three human ApoE alleles, two independent lines of 3xTg-ApoE heterozygotes were initially produced from 3xTg-AD and ApoE targeted replacement homozygotes (ApoE-TR: ApoEX+/+ represents either ApoE2, ApoE3, or ApoE4 homozygote mice). Non-sibling heterozygotes were mated, and 1 out of 64 mice was expected to be homozygous at all 4 alleles. Quadruple homozygotes were selected by PCR and used as the initial founders of each 3xTG-ApoE line.

Controlled Cortical Impact (CCI)

Two to three-month-old male and female ApoE-TR mice (Sullivan, et al. 1997b) and six to eight-month-old male and female 3xTG-ApoE mice were used in the following experiments. 17 3xTG-ApoE2, 13 3xTG-ApoE3, and 11 3xTG-ApoE4 mice were randomly assigned to either injury or sham groups and a 2 mm controlled cortical impact was performed as described previously (Brody et al. 2007). Additional injury groups included 5 ApoE2, 5 ApoE3, and 5 ApoE4 mice. Briefly, mice were anesthetized with isofluorane and placed in a stereotaxic

frame. A rectal probe and heat pad was used to maintain constant body temperature. A midline incision was made to expose the skull and a 5 mm circular burr was used to perform a craniotomy over the left somatosensory cortex. A 3 mm steel impactor tip was then aligned to +1.5 mm (A/P), relative to lambda and -1.2 mm (M/L) relative to midline. An electromagnetic device delivered an impact to the brain to a depth of 2 mm (5 m/s, 100 ms dwell time). The contusion was irrigated with saline and plastic skull cap was affixed with suture glue to cover the craniotomy. Sham mice underwent the same surgical procedure but did not receive an impact. Mice were allowed to recover on a heat pad before being returned to their cage.

Immunohistochemistry.

24 hours following CCI, mice were deeply anesthetized with isofluorane and perfused with 0.3% heparin in phosphate buffered saline (PBS). Brains were dissected and fixed in 4% paraformaldehyde (PFA) for 24 hours and then equilibrated in 30% sucrose PBS. All sections were sliced 50 µm thick on a freezing microtome. Every 6th section (300 microns), was then stained for APP (Zymed, 0.25 µg/ml), Aβ40 (Invitrogen, 0.5 µg/ml), Aβ42 (Invitrogen, 0.5 µg/ml), total human tau (Thermo Scientific, 1 µg/ml), or pS199 tau (Invitrogen, 1:1000). Three minutes of 70% formic acid retrieval was used to unmask epitopes for Aβ40 and Aβ42 and ten minutes of formic acid for pS199 tau. All other staining methods were followed as published (Tran et al. 2011a).

Stereology

Stereology was performed blinded to genotype using a Nikon Eclipse 80i microscope with a motorized stage. Both the optical fractionator and space balls probes in StereoInvestigator version 8.2 were used for analysis. Regions of interest were drawn under a 4x objective as previously described for fimbria, pericontusional corpus callosum and external capsule, and hippocampal CA1 beginning with most anterior section containing both blades of

the dentate gyrus and including the following 3-4 sections per mouse (Mac Donald et al. 2007b; Tran et al. 2011a). All counts were performed using a 60x lens. For APP and tau, a grid size of 200 x 200 and counting frame of 40 x 40 were used. For Aβ40 and Aβ42, a 200 x 200 grid and 80 x 80 counting frame were used. For pS199 tau, a 200 x 200 grid and 50 x 50 counting frame were used. For the space balls hemispherical probe, a radius of 17 µm was used. In all cases, a guard depth of 5 µm and a probe height of 17 µm was used. These parameters ensured that the Gunderson's coefficient of error was below 0.15 in all cases.

Statistics

Scatter plots were constructed and Shapiro-Wilk tests were performed to assess for evidence of non-normally distributed data. All data was normally distributed except for APP stereology in ApoE4 mice (p-value <0.05). In this case, a Kruskal-Wallis one-way ANOVA was performed followed by Mann-Whitney U tests. All other data was analyzed by two-way ANOVAs (injury and genotype) with Bonferroni's corrections for multiple comparisons. Significance was determined as $p<0.05$ for two-way ANOVAs and $p<0.01$ for all post-hoc comparisons. Planned comparisons included injured versus sham mice for each genotype and comparisons of injured 3xTG-ApoE4 mice to injured 3xTG-ApoE2 and -ApoE3 mice. This resulted in a total of 5 planned comparisons for each analysis.

7.3 RESULTS

7.3.1 APOE genotype alters the extent of axonal injury

Amyloid precursor protein (APP) is a marker of fast axonal transport failure that accumulates in injured axons at the location of disrupted microtubules (Koo, et al. 1990; Gentleman et al. 1993; Tang-Schomer et al. 2012). For these experiments, APP was used to assay axonal injury (**Figure 7.2, A, D, E, J, K, P, Q, V, Fig. 3, A-C**). 3xTG-ApoE sham operated mice did not have axons containing APP, in contrast with CCI injured mice at 24

hours. At 24 hours post-injury, APP positive axons were visible in corpus callosum, external capsule, and ipsilateral fimbria (Fig. 2 A). Stereological quantification of APP+ axons in fimbria revealed main effects of genotype (p=0.001), injury (p<0.000001), and a genotype x injury interaction (**Figure 7.2 V;** p=0.0006). Planned post-hoc comparisons indicated that injured 3xTG-ApoE4 mice have significantly greater numbers of APP-positive axonal varicosities in ipsilateral fimbria compared to injured 3xTG-ApoE2 (p=0.00016), and injured 3xTG-ApoE3 mice (p=0.00002).

Considering this unexpected result, this experiment was repeated using ApoE-TR mice. Stereological quantification of APP+ axons (**Figure 7.3 A-C**) in pericontusional corpus callosum and external capsule revealed an effect of genotype (p =0.005) where ApoE4 mice have more APP-positive axons that ApoE3 (p=0.008) mice but not ApoE2 mice (p=0.056). Thus, we confirmed the finding that ApoE4 expressing mice have greater APP-positive axonal injury in two separate mouse models.

7.3.2 Injury results in increased intra-axonal amyloid-β in all genotypes

Since APP is cleaved by secretases to produce amyloid beta in injured axons (Smith et al. 2003a; Tran et al. 2011a), adjacent sets of serial sections were stained for Aβ40 (**Figure 7.2, B, F, G, L, M, R, S, W**) and Aβ42 (**Figure 7.2, C, H, I, N, O, T, U, X**). Similar to APP, Aβ40 and Aβ42 were seen in injured mice but not in shams. Analysis of Aβ40 revealed a main effect of injury (**Figure 7.2**, W; p<0.000001), but no effect of genotype (p=0.26) or genotype x injury interaction (p=.094). There appeared to be a trend towards increased Aβ40 in 3xTg-ApoE4 mice, but this did not reach statistical significance. Similarly, analysis of Aβ42 also revealed a main effect of injury (**Figure 7.2, X**; p=0.000001), but no effect of genotype (p=0.4192) or genotype x injury interaction (p=0.5639).

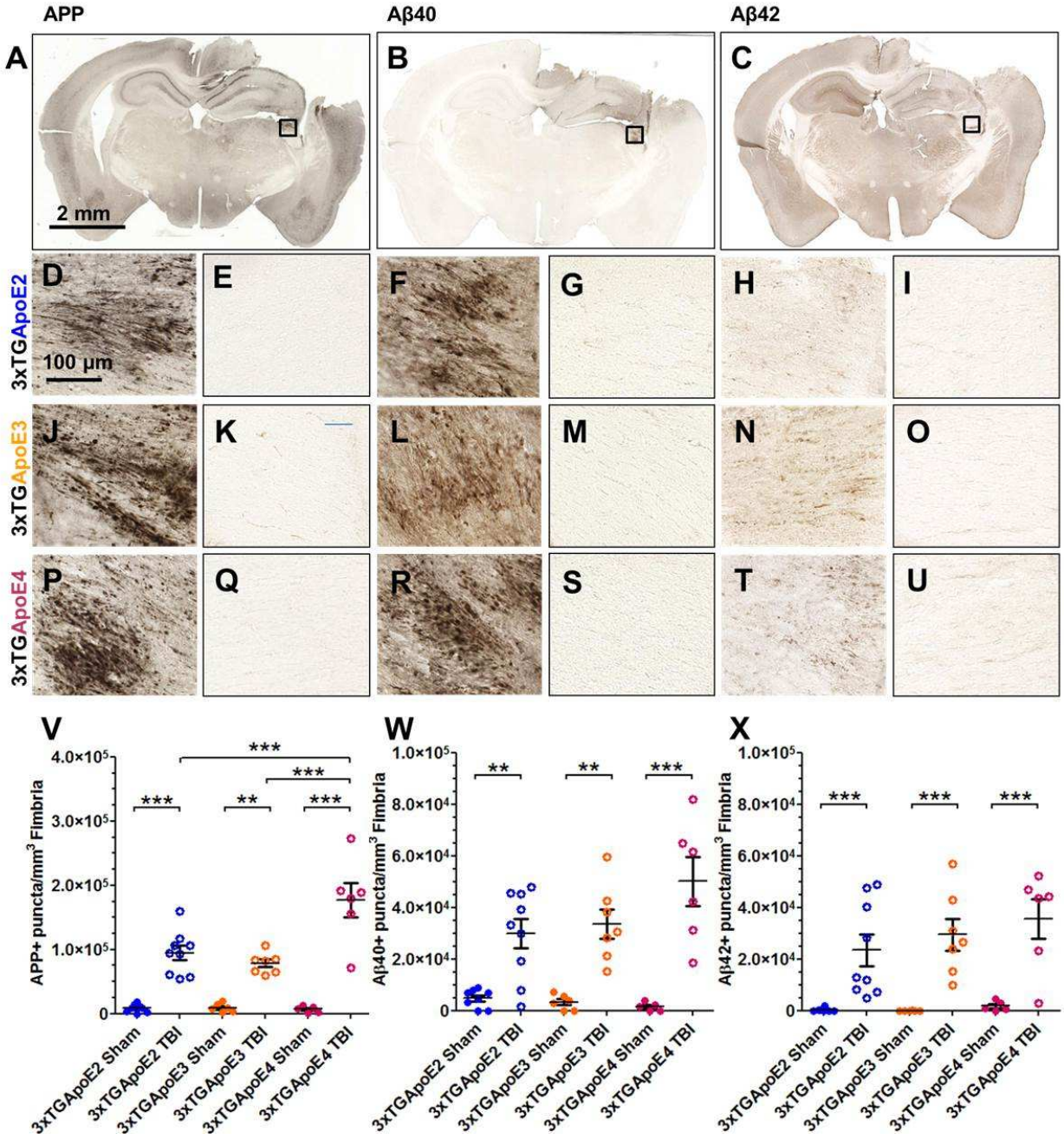

Figure 7.2 APP and Aβ immunohistochemistry in 3xTG-ApoE mice. Representative coronal slice images of APP (A), Aβ40 (B), and Aβ42(C) staining from an injured 3xTG-ApoE2 mouse. Higher magnification images of fimbria (box) from injured (D, F, H) and sham (E, G, I) 3xTG-ApoE2 stained for APP (D, E), Aβ40 (F, G), and Aβ42 (H, I). 3xTG-ApoE3 injured (J, L, N) and sham (K, M, O) stained for APP (J,K), Aβ40 (L, M), and Aβ42 (N,O). 3xTG-ApoE4 injured (P, R, T) and sham (Q, S, U) stained for APP (P, Q), Aβ40 (R, S), and Aβ42 (T, U). Stereological quantification of axonal varicosities containing APP (V), Aβ40 (W), or Aβ42 (X). Error bars represent standard error. (**p<0.01, ***p<0.001).

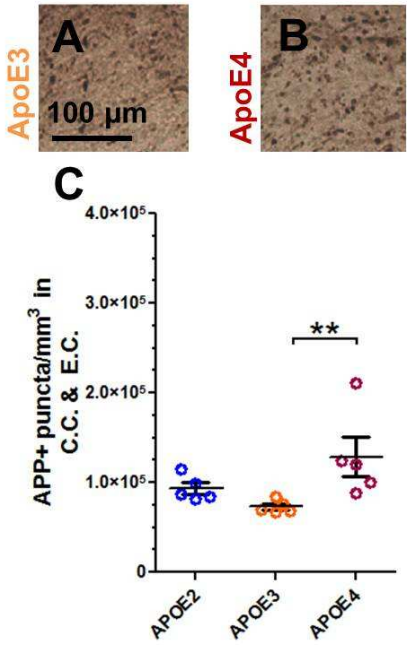

Figure 7.3 APP immunohistochemistry in ApoE-TR mice. Representative images from pericontusional corpus callosum (C.C) and external capsule (E.C.) of ApoE3 (A) and ApoE4 (B) mice stained for APP. Stereological quantification of axonal varicosities containing APP (C). Error bars represent standard error. (**p<0.01).

7.3.3 APOE genotype alters somatodendritic and intra-axonal tau in 3xTG-AD mice

The microtubule stabilizing protein tau also accumulates in the hippocampal CA1 and in the fimbria following injury in 3xTG-AD mice (Tran et al. 2011a). To image accumulation of tau in 3xTG-ApoE mice, an antibody that recognizes total human tau was used to label a 4th set of serial sections (**Figure 7.4, A-B, D-G, J-M, P-S**). Similar to 3xTg-AD mice, tau was observed in the somatodendritic compartment of hippocampal CA1 neurons. Length of these tau-positive neurites was measured using stereological methods. This revealed a main effect of genotype (**Figure 7.4, V**; p=0.006), but no effect of injury (p=0.52) or genotype x injury (p=0.96). 3xTG-ApoE4 sham and injured mice had significantly more accumulated tau than 3xTG-ApoE3 mice (p=0.009), but the difference with 3xTG-ApoE2 mice was not statistically significant after correction for multiple comparisons (p=0.013).

Total human tau was also assessed in the fimbria (**Figure 7.4, B, F, G, L, M, R, S, W**). Stereological analysis again revealed a main effect of genotype (Fig. 4, W; p=0.000003), but no effect of injury (p=0.94) or genotype x injury (p=0.31). Notably, both injured and sham 3xTG-ApoE4 mice had greater tau accumulation in axons than either 3xTG-ApoE2 (p=0.0002) or 3xTG-ApoE3 mice (p=0.000005).

To test whether *APOE* genotype effects phosphorylation of tau, a 5th set of adjacent sections was also stained for phospho-serine199 (pS199) tau (**Figure 7.4, C, H, I, N, O, T, U**). Similar to total human tau, pS199 tau was observed in the hippocampal CA1 and fimbria at 24 hours post injury (**Figure 7.4, C**). Main effects of genotype (**Figure 7.4, X**; p=0.0069) and injury (p=0.0092) were observed, but no there was no genotype x injury interaction effect (p=0.3097). Only the difference between injured and sham levels of pS199 tau in 3xTG-ApoE3 mice reached statistical significance, however. No difference was seen between injured and sham 3xTG-ApoE2 and 3xTG-ApoE4 mice or between injured 3xTG-ApoE4 mice and the other genotypes.

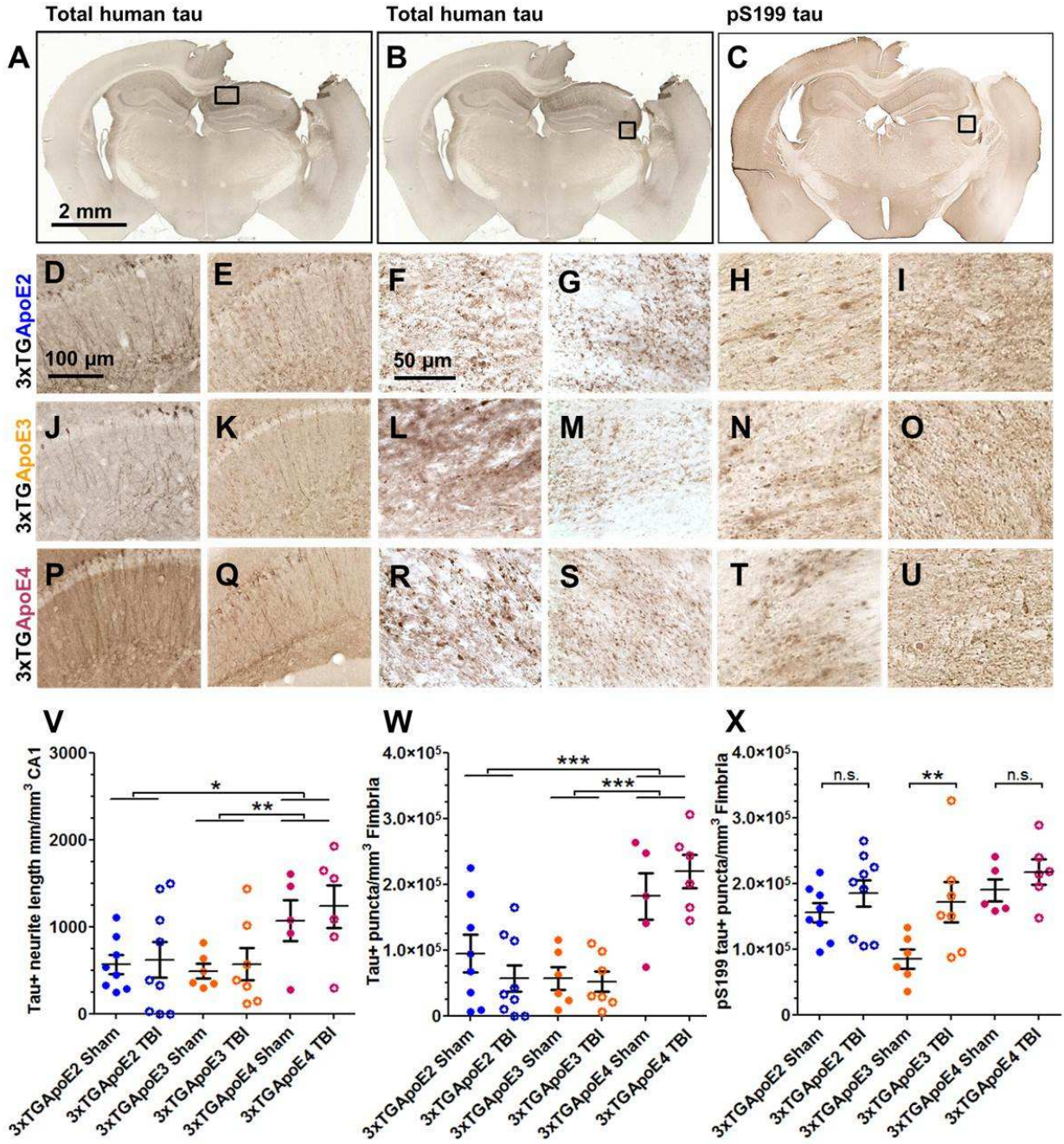

Figure 7.4 Tau immunohistochemistry. Representative coronal slice images of total human tau (A, B) and pS199 tau (C) staining from a 3xTG-ApoE2 mouse. Higher magnification images of boxed region from injured (D, F, H) and sham (E, G, I) 3xTG-ApoE2 stained for total tau in CA1 (D, E), or total tau in fimbria (F, G), and pS199 tau (H, I) in fimbria. 3xTG-ApoE3 injured (J, L, N) and sham (K, M, O) stained for total tau in CA1 (J, K), or in fimbria (L, M), and pS199 tau in fimbria (N,O). 3xTG-ApoE4 injured (P, R, T) and sham (Q, S, U) stained for total tau in CA1 (P, Q), or in fimbria (R, S), and pS199 tau in fimbria (T, U). Stereological quantification of the length of neurites containing tau in the CA1 (V), and axonal varicosities in fimbria containing either tau (W) or pS199 tau (X). Error bars represent standard error. (n.s.= not significant, **p<0.01, ***p<0.001).

7.4 DISCUSSION

To summarize, 24 hours following moderate controlled cortical impact, 3xTG-AD mice with the *APOE4* allele have greater APP accumulation within axons than mice with the *APOE2* or *APOE3* alleles. ApoE4 targeted replacement mice without other human transgenes were also found to have greater APP accumulation compared to ApoE3 targeted replacement mice. This suggests that modulation of the severity of axonal injury may be a primary contributor to the *APOE* genotype effect on outcomes following TBI. However, contrary to our hypothesis regarding neurodegenerative pathology following TBI, *APOE* genotype had no effect on the intra-axonal accumulation of Aβ40 or Aβ42; there was a similar increase in Aβ in all 3 genotypes. Also surprisingly, there was no interaction between injury and *APOE* genotype on tau pathology; indeed, more total human tau was found in the somatodendritic and axonal compartments of 3xTG-ApoE4 mice regardless of injury status.

Altogether, the 3xTG-ApoE mouse TBI model has similarities with and differences from the 3xTG-AD TBI model reported previously (Tran et al. 2011a; Tran et al. 2011b). Both recapitulate key aspects of acute human TBI pathology, displaying axonal varicosities containing APP, Aβ, and tau (Uryu et al. 2007). Mice expressing only ApoE or PDAPP-ApoE mice have also been studied in the setting of traumatic brain injury (Hartman et al. 2002; Crawford, et al. 2009b; Mannix et al. 2011). However, neither of these models produced these three types of pathology. Notably, in the 3xTG-AD mice both Aβ and tau pathologies increased acutely following TBI, but in 3xTg-ApoE mice, only amyloid beta but not tau was affected by acute TBI. The absence of a TBI-related exacerbation of tau pathology may be due to a protective effect of all 3 human ApoE isoforms compared with endogenous mouse ApoE, as has been reported for Abeta pathology in another AD mouse model (Holtzman, et al. 1999).

One possible explanation for these results is that the axons of 3xTG-ApoE4 mice are more susceptible to injury. This may represent a loss of function of ApoE4 in the setting of traumatic brain injury, similar to that seen in ApoE deficient mice (Chen, et al. 1997; Lynch, et

al. 2002; Namjoshi, et al. 2013). Alternately, it may represent a toxic gain of function of ApoE4. Others have proposed that ApoE4 may undergo a cleavage step to produce a toxic fragment that induces mitochondrial dysfunction and neuronal death (Chang, et al. 2005). Studies comparing axonal injury in hemizygous ApoE4+/- mice may help differentiate between a loss or gain of function. Interestingly, our group recently showed that wild-type mice treated with COG1410, an ApoE-mimetic, following controlled cortical impact have fewer APP-positive axons in pericontusional white matter 3-7 days after injury compared to saline treated mice (Jiang et al. 2012). As COG1410 is a modified peptide sequence from human ApoE3, this could indicate that ApoE4 lacks an axon-protective effect found in the other two isoforms.

Another possible interpretation of these results is that ApoE affects the production, processing, or trafficking of APP specifically. For example, ApoE4 has been shown to be more efficient at recycling APP from the cell surface back into the endocytic pathway (Ye, et al. 2005). Additional markers of axonal injury and complementary injury models will be required to determine whether there is a specific APP effect or a general effect on axonal injury. Thus, interpretation of the main finding from this study, that ApoE4 mice displayed more APP accumulations following injury than the other genotypes, is limited by our current understanding of the role of ApoE in axon biology.

It is also notable that both sham and injured 3xTG-ApoE4 mice have more total human tau staining but not pS199 tau than mice expressing either ApoE2 or ApoE3. Further characterization of phospho-tau epitopes may contribute to a clearer picture of tau pathology in this model. Increased total human tau in 3xTG-ApoE4 is not unexpected given several previous lines of research. First, ApoE4 fragments have been shown to induce tau accumulation (Huang, et al. 2001; Brecht, et al. 2004). Impaired ApoE4 binding to ApoE receptors in mice may cause dysregulation of tau kinases such as GSK3β and greater accumulation of the protein at baseline (Ohkubo, et al. 2003). Other researchers have reported that ApoE is produced in neurons following injury and neuronal production of apoE4 contributes to tau hyperphosphorylation and

microtubule instability (Horsburgh, et al. 1996; Tesseur, et al. 2000a; Tesseur, et al. 2000b). We have not addressed the question of neuronal apoE production following traumatic brain injury. Last, apoE2 and apoE3 have been shown in vitro to bind tau and prevent hyperphosphorylation, while apoE4 lacks this ability (Strittmatter, et al. 1994). As the current study did not address the production of apoE in neurons following injury, it is unknown whether neuronal apoE production is the mechanism of tau accumulation occurring in this model. However, it is unlikely to be a major contributor since no significant difference was detected between sham and injured 3xTG-ApoE4 tau or pS199 tau levels; sham mice are not expected to have neuronal apoE expression.

This study was limited in that APP immunohistochemistry was the only method employed to assess axonal injury. Additional markers of axonal injury including neurofilament immunohistochemistry, silver staining, electron microscopy, electrophysiology, and diffusion tensor imaging will be of interest to determine whether there is a global effect of *APOE* genotype on axonal injury or whether the effects are limited to the processing underlying abnormal APP accumulation (i.e. failed fast axonal transport). Functional tests such as Morris Water Maze will also be useful to understand the implications of increased APP accumulation within the fimbria. Further, biochemical studies will be necessary to determine the effects of *APOE* genotype on specific assembly forms of amyloid beta and tau following TBI. Last, a full characterization of the time course for both amyloid beta and tau pathology will be helpful for interpreting these results and assessing the utility of these mouse lines. Such analysis may also uncover chronic effects of *APOE* genotype on amyloid beta and tau deposition that were not apparent in this initial acute injury analysis. Clearly, this will be the first of many studies required to address all of the issues in the field, and a complete characterization is beyond the scope of this paper.

Another potential limitation is the choice of the 3xTG-AD line of mice. While these mice have been informative in studying amyloid beta and tau dynamics following moderate TBI,

overexpression of these transgenes may mask some of the effects of ApoE genotype in injury. Mice expressing both human amyloid precursor protein and tau under endogenous promoters may be an alternative to the 3xTG-AD model for future studies (Andorfer, et al. 2003; Guo, et al. 2012).

Altogether, these results demonstrate that it is feasible to produce mouse models for studying interactions between *APOE* genotype and important aspects of human acute neurodegenerative pathology following traumatic brain injury. Considering the finding that *APOE4* genotype contributes to increased axonal injury, this research has important implications for targeted therapeutics to benefit susceptible *APOE4* carrying populations following TBI. Future research will seek to use this model for pharmacogenetic studies and to further understand how *APOE* genotype modifies axonal injury in both moderate TBI and less severe repetitive closed skull injury models (Shitaka et al. 2011).

CHAPTER 8

Conclusions and Future Directions

8.1 SUMMARY

To characterize the repetitive closed-skull traumatic brain injury (rcTBI) mouse model, histological, electrophysiological, and advanced magnetic resonance imaging (MRI) methods were used. Two key observations were made 1) rcTBI results increased activation and proliferation of microglia and 2) there is histological evidence of axonal injury from APP, NF200, SMI-32, and silver staining in the absence of overt cell loss or damage. Interestingly, silver staining appears to have the greatest sensitivity to axonal injury at 7 days, while other immunohistochemical markers labeled the greatest amount of injury at 2 days. Further, electrophysiological compromise of axons was evident at 7 days, where compound action potential amplitude in both myelinated and unmyelinated axons was reduced. Diffusion tensor imaging in this mouse model revealed acute abnormalities in injured white matter. Decreases in mean diffusivity and axial diffusivity at 7 days suggest that analysis of individual components of the diffusion tensor may be the most sensitive to mild traumatic axonal injury. Altogether, these features are in line with what is known about characteristics of human traumatic brain injury and both *in vivo* and *ex vivo* human concussion studies (Oppenheimer 1968; Blumbergs et al. 1994; Niogi et al. 2010; Ramlackhansingh et al. 2011; Johnson et al. 2013a; Johnson et al. 2013b).

Factors that might influence the extent of axonal injury after concussion were also explored. To determine how the robust upregulation of microglial activity may contribute to on-going processes of axonal injury, rcTBI was performed in the valganciclovir-inducible CD11b-TK mouse model of microglial depletion. At 7 day and 21 days, a 35% reduction in microglia had no effect on the amount of silver staining in white matter tracts. A 56% reduction also failed to alter silver staining or axonal injury evident by electron microscopy 7 days post-injury.

Unexpectedly, this model resulted in intraparenchymal hemorrhages with long-term or high-dose valganciclovir treatment. Altogether, based on these data, it does not appear that microglia contribute to acute and sub-acute axonal injury.

In a separate set of experiments, I attempted to manipulate the microglial response using Mac-1-SAP, minocycline, CHPG, BBG, or miR-124. With the exception of Mac-1-SAP, the number of microglia was unaffected by drug treatment after injury. In the case of Mac-1-SAP, a CD11b targeted toxin, cell loss and intraparenchymal hemorrhages were pronounced at 7 days. Whether or not this toxicity is due to a similar mechanism seen in CD11b-TK mice or related to the metabolization of Mac-1-SAP is unknown. Overall, this indicates a need for better microglial-targeting compounds.

Last, data was presented from a more severe controlled cortical impact (CCI) injury model where presence of the human apolipoprotein E4 allele worsened axonal injury acutely after impact. Surprisingly, *APOE4* expression did not affect acute accumulation of Aβ or tau in axons. This suggests that *APOE* may be one contributing factor to axonal injury and poor outcome following traumatic brain injury.

8.2 FUTURE DIRECTIONS

One clear direction of this research is to explore the connection between functional axonal injury and behavioral outcomes. In this work, I show that injured mice have Morris Water Maze deficits and reduced compound action potential velocities. Other work in the lab has found that mice also have impairments in tasks such as the tail suspension and social recognition tests (Klemenhagen, et al. 2013). An intriguing possibility is that axonal injury may be the substrate for behavioral deficits and it would be informative to directly test this hypothesis. This could be done by making use of the inherent variability in the injury model. Individuals would be prescreened into “high” injury and “low” injury groups using behavioral tests performed within the first 2-3 days post-injury. Pairs of sham and injured mice could be

tested in a single day of hidden platform Morris Water Maze, tail suspension, social recognition, and/or rotarod testing. Low injury mice would be defined as having behavior test scores within 1 standard deviation of a group of sham control mice. High injury mice would have test scores of more than 1 standard deviation. I would expect that the high injury mice would have reduced compound action potential velocities at 7 days post-injury and that low injury mice would be similar to shams. Further, following electrophysiology, slices could be embedded in gelatin and re-sectioned on a freezing microtome (see protocol in appendix) so that correlations between behavioral, electrophysiological, and histological parameters like silver staining could be examined.

If mice with the greatest behavioral deficits also have functional and histological changes, then follow up experiments could examine manipulating axonal injury severity and the effect this has on behavioral tests. For example, in Chapter 7, I observed that mice with the *ApoE4* allele have increased axonal injury after moderate-severe TBI compared to mice with *ApoE2* or *3*. I would expect that after repetitive concussive injury, *ApoE4* mice would have increased silver staining compared to *E2* and *E3* mice and that *ApoE4* they would also have the greatest behavioral deficits. Administration of an ApoE mimetic drug, such as COG1410, may alleviate these deficits in *ApoE4* mice (Laskowitz, et al. 2007; Jiang et al. 2012). In addition, such a study would shed light on whether or not *ApoE4* affects axons through a toxic gain of function or a loss of function mechanism. If COG1410 can prevent increased axonal injury in *ApoE4* mice, then it would appear that *ApoE4* is a loss of function mutation. If COG1410 has no effect, then it is likely *ApoE4* works through a toxic gain of function, such as the release of a toxic cleavage product (Chang et al. 2005).

Alternately, if electrophysiology and histology do not correlate with any behavioral measures, it would suggest that future experiments and therapeutic design should target aspects of repetitive concussion other than axons. Other areas of investigation should include looking at changes to synapses. To date, no comprehensive study has examined the effects of

concussive brain injury on synaptic structure, due in large part to the availability of high-throughput quantitative methods for investigation. More recently, however, array tomography has been used to address these questions (Micheva et al. 2007; Kay et al. 2013). In this method, tissue is embedded in plastic resin similar to preparation for electron microscopy. Serial 70-100 nm sections are cut in ribbons, “arrays”, on an ultramicrotome using a large diamond knife. These arrays can then be immunofluorescently labeled with antibodies to synaptic proteins and individual structures can be counted. Unlike using traditional 10 micron thick or larger tissue sections, physically sectioning allows considerably improved z-axis resolution. The tools and methods are currently in place in the lab to perform these studies.

Specifically it would be informative to investigate how activated microglia may alter synaptic structure and behavior. Microglia are important mediators of synaptic pruning during development, and it is becoming increasingly apparent that they play an active role at the synapse in the adult brain (Paolicelli, et al. 2011; Schafer, et al. 2012; Parkhurst et al. 2013; Zhan, et al. 2014). Recently, it was reported that release of microglial BDNF at the synapse is an important event in the learning response, as it helps regulate synapse formation and elimination (Parkhurst et al. 2013). How might this process be affected by concussions—or multiple concussions? Synaptic alterations though to be the underlying basis for schizophrenia and autism and it is intriguing to consider that trauma-induced synaptic changes might contribute to behavioral alterations or cognitive impairments after concussion. Interestingly, in the larger TBI population, individuals with a history of TBI are at increased risk for developing psychiatric disorders (Orlovska et al. 2013). How milder injuries might contribute to synaptic alterations and subtle behavioral change (or the more striking behavioral and personality changes seen in Chronic Traumatic Encephalopathy) is an exciting direction for future investigations.

In sum, these experiments will all test the underlying assumption (of this research and of the TBI field in general) that axonal injury is the central pathological process taking place in mild

or concussive TBI. While axonal injury may prove to be a key aspect of these mild injuries, this assumption may be an artifact of our ability to detect pathology. Designing experiments to directly test this assumption will be important for therapeutic development to reduce the long-term consequences of these injuries.

8.3 CONCLUDING REMARKS

With the increasing public awareness of the risks associated with concussion, more talented scientists will be attracted to this area of research and it is my hope that this work be used as a starting point for future investigations into the nature of repetitive concussive traumatic brain injury. Here, I found that microglia do not play a role early on in the process of axon degeneration, but it remains to be answered why microglial cells remain present in white matter tracts for several weeks (or in humans, years) post-injury or how they might modulate long-term outcomes, contribute to synaptic alterations, and initiate behavioral changes. I have also reported that apolipoprotein E genotype influences the severity of axonal injury immediately following TBI, and it will be necessary to repeat these studies in the repetitive closed-skull injury model and to determine by what mechanism *APOE* exerts its effects on axonal injury. Altogether, have detailed how this rcTBI mouse model can be used in future investigations to explore the effects of genetic or environmental factors on concussive injury and I have presented an experimental approach for assessing injury including immunohistochemistry, electrophysiology, behavior, and diffusion tensor MRI.

REFERENCES

Abdel Baki, S. G., et al. (2009). A hierarchy of neurobehavioral tasks discriminates between mild and moderate brain injury in rats. Brain Res **1280**: 98-106.

Aboitiz, F., et al. (1992). Fiber composition of the human corpus callosum. Brain Res **598**(1-2): 143-153.

Adams, J. H., et al. (1982). Diffuse axonal injury due to nonmissile head injury in humans: an analysis of 45 cases. Ann Neurol **12**(6): 557-563.

Amin, A. R., et al. (1996). A novel mechanism of action of tetracyclines: effects on nitric oxide synthases. Proc Natl Acad Sci U S A **93**(24): 14014-14019.

Andorfer, C., et al. (2003). Hyperphosphorylation and aggregation of tau in mice expressing normal human tau isoforms. J Neurochem **86**(3): 582-590.

Ashki, N., et al. (2006). Nitric oxide reversibly impairs axonal conduction in Guinea pig spinal cord. J Neurotrauma **23**(12): 1779-1793.

Bachstetter, A. D., et al. (2013). Clinically relevant intronic splicing enhancer mutation in myelin proteolipid protein leads to progressive microglia and astrocyte activation in white and gray matter regions of the brain. J Neuroinflammation **10**: 146.

Batchelor, P. E., et al. (2002). Macrophages and Microglia Produce Local Trophic Gradients That Stimulate Axonal Sprouting Toward but Not beyond the Wound Edge. Mol Cell Neurosci **21**(3): 436-453.

Bazarian, J. J., et al. (2006). Bench to bedside: evidence for brain injury after concussion--looking beyond the computed tomography scan. Acad Emerg Med **13**(2): 199-214.

Bazarian, J. J., et al. (2012). Subject-specific changes in brain white matter on diffusion tensor imaging after sports-related concussion. Magn Reson Imaging **30**(2): 171-180.

Benakis, C., et al. (2010). JNK inhibition and inflammation after cerebral ischemia. Brain Behav Immun **24**(5): 800-811.

Bennett, R. E., et al. (2012). Diffusion tensor imaging detects axonal injury in a mouse model of repetitive closed-skull traumatic brain injury. Neurosci Lett **513**(2): 160-165.

Blumbergs, P. C., et al. (1989). Diffuse axonal injury in head trauma. J Neurol Neurosurg Psychiatry **52**(7): 838-841.

Blumbergs, P. C., et al. (1994). Staining of amyloid precursor protein to study axonal damage in mild head injury. Lancet **344**(8929): 1055-1056.

Brecht, W. J., et al. (2004). Neuron-specific apolipoprotein e4 proteolysis is associated with increased tau phosphorylation in brains of transgenic mice. J Neurosci **24**(10): 2527-2534.

Brody, D. L., et al. (2007). Electromagnetic controlled cortical impact device for precise, graded experimental traumatic brain injury. J Neurotrauma **24**(4): 657-673.

Broglio, S. P., et al. (2011). Cumulative head impact burden in high school football. J Neurotrauma **28**(10): 2069-2078.

Browne, K. D., et al. (2006). Chronic ibuprofen administration worsens cognitive outcome following traumatic brain injury in rats. Exp Neurol **201**(2): 301-307.

Bu, G. (2009). Apolipoprotein E and its receptors in Alzheimer's disease: pathways, pathogenesis and therapy. Nat Rev Neurosci **10**(5): 333-344.

Budde, M. D., et al. (2008). Axonal injury detected by in vivo diffusion tensor imaging correlates with neurological disability in a mouse model of multiple sclerosis. NMR Biomed **21**(6): 589-597.

Burnett, S. H., et al. (2004). Conditional macrophage ablation in transgenic mice expressing a Fas-based suicide gene. J Leukoc Biol **75**(4): 612-623.

Bye, N., et al. (2007). Transient neuroprotection by minocycline following traumatic brain injury is associated with attenuated microglial activation but no changes in cell apoptosis or neutrophil infiltration. Exp Neurol **204**(1): 220-233.
Byrnes, K. R., et al. (2009a). Metabotropic glutamate receptor 5 activation inhibits microglial associated inflammation and neurotoxicity. Glia **57**(5): 550-560.
Byrnes, K. R., et al. (2009b). Activation of metabotropic glutamate receptor 5 improves recovery after spinal cord injury in rodents. Ann Neurol **66**(1): 63-74.
Cantu, R. C. (1998). Second-impact syndrome. Clin Sports Med **17**(1): 37-44.
Cao, T., et al. (2012). Morphological and genetic activation of microglia after diffuse traumatic brain injury in the rat. Neuroscience **225**: 65-75.
Centers for Disease Control and Prevention, N. C. f. I. P. a. C. (2003). Report to Congress on mild traumatic brain injury in the United Sates: steps to prevent a serious public health problem. Atlanta (GA), Centers for Disease Control and Prevention.
Chang, S., et al. (2005). Lipid- and receptor-binding regions of apolipoprotein E4 fragments act in concert to cause mitochondrial dysfunction and neurotoxicity. Proc Natl Acad Sci U S A **102**(51): 18694-18699.
Chappell, M. H., et al. (2006). Distribution of microstructural damage in the brains of professional boxers: a diffusion MRI study. J Magn Reson Imaging **24**(3): 537-542.
Chen, M., et al. (2000). Minocycline inhibits caspase-1 and caspase-3 expression and delays mortality in a transgenic mouse model of Huntington disease. Nat Med **6**(7): 797-801.
Chen, X. H., et al. (2009). A lack of amyloid beta plaques despite persistent accumulation of amyloid beta in axons of long-term survivors of traumatic brain injury. Brain Pathol **19**(2): 214-223.
Chen, Y., et al. (1997). Motor and cognitive deficits in apolipoprotein E-deficient mice after closed head injury. Neuroscience **80**(4): 1255-1262.
Collins, M. W., et al. (2002). Cumulative effects of concussion in high school athletes. Neurosurgery **51**(5): 1175-1179; discussion 1180-1171.
Conte, V., et al. (2004). Vitamin E reduces amyloidosis and improves cognitive function in Tg2576 mice following repetitive concussive brain injury. J Neurochem **90**(3): 758-764.
Corder, E. H., et al. (1993). Gene dose of apolipoprotein E type 4 allele and the risk of Alzheimer's disease in late onset families. Science **261**(5123): 921-923.
Coronado, V. G., et al. (2012). Trends in Traumatic Brain Injury in the U.S. and the public health response: 1995-2009. J Safety Res **43**(4): 299-307.
Coronado, V. G., et al. (2011). Surveillance for traumatic brain injury-related deaths--United States, 1997-2007. MMWR Surveill Summ **60**(5): 1-32.
Corsellis, J. A., et al. (1973). The aftermath of boxing. Psychol Med **3**(3): 270-303.
Crawford, D. K., et al. (2009a). Assaying the functional effects of demyelination and remyelination: revisiting field potential recordings. J Neurosci Methods **182**(1): 25-33.
Crawford, F., et al. (2009b). Apolipoprotein E-genotype dependent hippocampal and cortical responses to traumatic brain injury. Neuroscience **159**(4): 1349-1362.
Creed, J. A., et al. (2011). Concussive brain trauma in the mouse results in acute cognitive deficits and sustained impairment of axonal function. J Neurotrauma **28**(4): 547-563.
Creeley, C. E., et al. (2004). Multiple episodes of mild traumatic brain injury result in impaired cognitive performance in mice. Acad Emerg Med **11**(8): 809-819.
Cubon, V. A., et al. (2011). A diffusion tensor imaging study on the white matter skeleton in individuals with sports-related concussion. J Neurotrauma **28**(2): 189-201.
Daneshvar, D. H., et al. (2011). Long-term consequences: effects on normal development profile after concussion. Phys Med Rehabil Clin N Am **22**(4): 683-700, ix.
Davidsson, J. and M. Risling (2011). A new model to produce sagittal plane rotational induced diffuse axonal injuries. Front Neurol **2**: 41.

Davies, A. L., et al. (2006). Recombinant human TNFalpha induces concentration-dependent and reversible alterations in the electrophysiological properties of axons in mammalian spinal cord. J Neurotrauma **23**(8): 1261-1273.
Dean, P. J. and A. Sterr (2013). Long-term effects of mild traumatic brain injury on cognitive performance. Front Hum Neurosci **7**: 30.
DeFord, S. M., et al. (2002). Repeated mild brain injuries result in cognitive impairment in B6C3F1 mice. J Neurotrauma **19**(4): 427-438.
DeVos, S. L. and T. M. Miller (2013). Direct intraventricular delivery of drugs to the rodent central nervous system. J Vis Exp(75): e50326.
DiLeonardi, A. M., et al. (2009). Impaired axonal transport and neurofilament compaction occur in separate populations of injured axons following diffuse brain injury in the immature rat. Brain Res **1263**: 174-182.
Dixon, C. E., et al. (1987). A fluid percussion model of experimental brain injury in the rat. J Neurosurg **67**(1): 110-119.
Dommergues, M. A., et al. (2003). Early microglial activation following neonatal excitotoxic brain damage in mice: a potential target for neuroprotection. Neuroscience **121**(3): 619-628.
Eder, C., et al. (1998). Involvement of stretch-activated Cl- channels in ramification of murine microglia. J Neurosci **18**(18): 7127-7137.
Fjell, A. M., et al. (2011). Reduced white matter integrity is related to cognitive instability. J Neurosci **31**(49): 18060-18072.
Fleminger, S., et al. (2003). Head injury as a risk factor for Alzheimer's disease: the evidence 10 years on; a partial replication. J Neurol Neurosurg Psychiatry **74**(7): 857-862.
Friedman, G., et al. (1999). Apolipoprotein E-epsilon4 genotype predicts a poor outcome in survivors of traumatic brain injury. Neurology **52**(2): 244-248.
Friess, S. H., et al. (2007). Neurobehavioral functional deficits following closed head injury in the neonatal pig. Exp Neurol **204**(1): 234-243.
Garcia-Alloza, M., et al. (2007). A limited role for microglia in antibody mediated plaque clearance in APP mice. Neurobiol Dis **28**(3): 286-292.
Geddes, J. F., et al. (1999). Neuronal cytoskeletal changes are an early consequence of repetitive head injury. Acta Neuropathol **98**(2): 171-178.
Geddes, J. F., et al. (2000). Traumatic axonal injury: practical issues for diagnosis in medicolegal cases. Neuropathol Appl Neurobiol **26**(2): 105-116.
Gennarelli, T. A., et al. (1982). Diffuse axonal injury and traumatic coma in the primate. Ann Neurol **12**(6): 564-574.
Gentleman, S. M., et al. (1993). Beta-amyloid precursor protein (beta APP) as a marker for axonal injury after head injury. Neurosci Lett **160**(2): 139-144.
Gessel, L. M., et al. (2007). Concussions among United States high school and collegiate athletes. J Athl Train **42**(4): 495-503.
Gilchrist, J., et al. (2011). Nonfatal traumatic brain injuries related to sports and recreation activities among persons aged </=19 years--United States, 2001-2009. MMWR Morb Mortal Wkly Rep **60**(39): 1337-1342.
Ginhoux, F., et al. (2010). Fate mapping analysis reveals that adult microglia derive from primitive macrophages. Science **330**(6005): 841-845.
Giza, C. C. and D. A. Hovda (2001). The Neurometabolic Cascade of Concussion. J Athl Train **36**(3): 228-235.
Goldstein, L. E., et al. (2012). Chronic traumatic encephalopathy in blast-exposed military veterans and a blast neurotrauma mouse model. Sci Transl Med **4**(134): 134ra160.
Gowing, G., et al. (2006). Mouse model for ablation of proliferating microglia in acute CNS injuries. Glia **53**(3): 331-337.

Grady, M. S., et al. (1993). The use of antibodies targeted against the neurofilament subunits for the detection of diffuse axonal injury in humans. J Neuropathol Exp Neurol **52**(2): 143-152.
Graham, D. I., et al. (1995). Distribution of beta-amyloid protein in the brain following severe head injury. Neuropathol Appl Neurobiol **21**(1): 27-34.
Grathwohl, S. A., et al. (2009). Formation and maintenance of Alzheimer's disease beta-amyloid plaques in the absence of microglia. Nat Neurosci **12**(11): 1361-1363.
Greenwald, R. A., et al. (1992). Tetracyclines suppress matrix metalloproteinase activity in adjuvant arthritis and in combination with flurbiprofen, ameliorate bone damage. J Rheumatol **19**(6): 927-938.
Gronwall, D. and P. Wrightson (1975). Cumulative effect of concussion. Lancet **2**(7943): 995-997.
Gultekin, S. H. and T. W. Smith (1994). Diffuse axonal injury in craniocerebral trauma. A comparative histologic and immunohistochemical study. Arch Pathol Lab Med **118**(2): 168-171.
Guo, Q., et al. (2012). APP physiological and pathophysiological functions: insights from animal models. Cell Res **22**(1): 78-89.
Guo, Z., et al. (2000). Head injury and the risk of AD in the MIRAGE study. Neurology **54**(6): 1316-1323.
Guskiewicz, K. M., et al. (2005). Association between recurrent concussion and late-life cognitive impairment in retired professional football players. Neurosurgery **57**(4): 719-726; discussion 719-726.
Guskiewicz, K. M., et al. (2003). Cumulative effects associated with recurrent concussion in collegiate football players: the NCAA Concussion Study. JAMA **290**(19): 2549-2555.
Hamberger, A., et al. (2009). Concussion in professional football: morphology of brain injuries in the NFL concussion model--part 16. Neurosurgery **64**(6): 1174-1182; discussion 1182.
Han, S. H. and S. Y. Chung (2000). Marked hippocampal neuronal damage without motor deficits after mild concussive-like brain injury in apolipoprotein E-deficient mice. Ann N Y Acad Sci **903**: 357-365.
Hartman, R. E., et al. (2002). Apolipoprotein E4 influences amyloid deposition but not cell loss after traumatic brain injury in a mouse model of Alzheimer's disease. J Neurosci **22**(23): 10083-10087.
Hassel, B., et al. (1992). Selective inhibition of glial cell metabolism in vivo by fluorocitrate. Brain Res **576**(1): 120-124.
Hawkes, C. A. and J. McLaurin (2009). Selective targeting of perivascular macrophages for clearance of beta-amyloid in cerebral amyloid angiopathy. Proc Natl Acad Sci U S A **106**(4): 1261-1266.
Haynes, S. E., et al. (2006). The P2Y12 receptor regulates microglial activation by extracellular nucleotides. Nat Neurosci **9**(12): 1512-1519.
Henry, L. C., et al. (2011). Acute and chronic changes in diffusivity measures after sports concussion. J Neurotrauma **28**(10): 2049-2059.
Heppner, F. L., et al. (2005). Experimental autoimmune encephalomyelitis repressed by microglial paralysis. Nat Med **11**(2): 146-152.
Holbourn, A. H. S. (1943). Mechanics of head injuries. Lancet **242**: 438-441.
Holtzman, D. M., et al. (1999). Expression of human apolipoprotein E reduces amyloid-beta deposition in a mouse model of Alzheimer's disease. J Clin Invest **103**(6): R15-R21.
Homsi, S., et al. (2009). Minocycline effects on cerebral edema: relations with inflammatory and oxidative stress markers following traumatic brain injury in mice. Brain Res **1291**: 122-132.

Homsi, S., et al. (2010). Blockade of acute microglial activation by minocycline promotes neuroprotection and reduces locomotor hyperactivity after closed head injury in mice: a twelve-week follow-up study. J Neurotrauma **27**(5): 911-921.
Horsburgh, K. and J. A. Nicoll (1996). Selective alterations in the cellular distribution of apolipoprotein E immunoreactivity following transient cerebral ischaemia in the rat. Neuropathol Appl Neurobiol **22**(4): 342-349.
Hosmane, S., et al. (2012). Toll/interleukin-1 receptor domain-containing adapter inducing interferon-beta mediates microglial phagocytosis of degenerating axons. J Neurosci **32**(22): 7745-7757.
Hua, X. Y., et al. (2005). Intrathecal minocycline attenuates peripheral inflammation-induced hyperalgesia by inhibiting p38 MAPK in spinal microglia. Eur J Neurosci **22**(10): 2431-2440.
Huang, Y., et al. (2001). Apolipoprotein E fragments present in Alzheimer's disease brains induce neurofibrillary tangle-like intracellular inclusions in neurons. Proc Natl Acad Sci U S A **98**(15): 8838-8843.
Hylin, M. J., et al. (2013). Repeated mild closed head injury impairs short-term visuospatial memory and complex learning. J Neurotrauma **30**(9): 716-726.
Ikonomovic, M. D., et al. (2004). Alzheimer's pathology in human temporal cortex surgically excised after severe brain injury. Exp Neurol **190**(1): 192-203.
Israelsson, C., et al. (2009). Closed head injury in a mouse model results in molecular changes indicating inflammatory responses. J Neurotrauma **26**(8): 1307-1314.
Iverson, G. L. (2005). Outcome from mild traumatic brain injury. Curr Opin Psychiatry **18**(3): 301-317.
Iverson, G. L., et al. (2004). Cumulative effects of concussion in amateur athletes. Brain Inj **18**(5): 433-443.
Iverson, G. L., et al. (2000). Prevalence of abnormal CT-scans following mild head injury. Brain Inj **14**(12): 1057-1061.
Iwata, A., et al. (2004). Traumatic axonal injury induces proteolytic cleavage of the voltage-gated sodium channels modulated by tetrodotoxin and protease inhibitors. J Neurosci **24**(19): 4605-4613.
Jellinger, K. A. (2004). Head injury and dementia. Curr Opin Neurol **17**(6): 719-723.
Jiang, Y. and D. L. Brody (2012). Administration of COG1410 reduces axonal amyloid precursor protein immunoreactivity and microglial activation after controlled cortical impact in mice. J Neurotrauma **29**(13): 2332-2341.
Johansson, B., et al. (2009). Mental fatigue and impaired information processing after mild and moderate traumatic brain injury. Brain Inj **23**(13-14): 1027-1040.
Johnson, V. E., et al. (2013a). Inflammation and white matter degeneration persist for years after a single traumatic brain injury. Brain **136**(Pt 1): 28-42.
Johnson, V. E., et al. (2013b). Axonal pathology in traumatic brain injury. Exp Neurol **246**: 35-43.
Jordan, B. D., et al. (1997). Apolipoprotein E epsilon4 associated with chronic traumatic brain injury in boxing. JAMA **278**(2): 136-140.
Kanayama, G., et al. (1996). The effects of repetitive mild brain injury on cytoskeletal protein and behavior. Methods Find Exp Clin Pharmacol **18**(2): 105-115.
Kay, K. R., et al. (2013). Studying synapses in human brain with array tomography and electron microscopy. Nat Protoc **8**(7): 1366-1380.
Kigerl, K. A., et al. (2009). Identification of two distinct macrophage subsets with divergent effects causing either neurotoxicity or regeneration in the injured mouse spinal cord. J Neurosci **29**(43): 13435-13444.
Kim, H. S. and Y. H. Suh (2009). Minocycline and neurodegenerative diseases. Behav Brain Res **196**(2): 168-179.

Kim, J. H., et al. (1996). A re-examination of sex differences in axon density and number in the splenium of the rat corpus callosum. Brain Res **740**(1-2): 47-56.
Klawiter, E. C., et al. (2011). Radial diffusivity predicts demyelination in ex vivo multiple sclerosis spinal cords. Neuroimage **55**(4): 1454-1460.
Klemenhagen, K. C., et al. (2013). Repetitive concussive traumatic brain injury interacts with post-injury foot shock stress to worsen social and depression-like behavior in mice. PLoS One **8**(9): e74510.
Koffie, R. M., et al. (2012). Apolipoprotein E4 effects in Alzheimer's disease are mediated by synaptotoxic oligomeric amyloid-beta. Brain **135**(Pt 7): 2155-2168.
Koffie, R. M., et al. (2009). Oligomeric amyloid beta associates with postsynaptic densities and correlates with excitatory synapse loss near senile plaques. Proc Natl Acad Sci U S A **106**(10): 4012-4017.
Konsman, J. P., et al. (2000). Diffusion and action of intracerebroventricularly injected interleukin-1 in the CNS. Neuroscience **101**(4): 957-967.
Koo, E. H., et al. (1990). Precursor of amyloid protein in Alzheimer disease undergoes fast anterograde axonal transport. Proc Natl Acad Sci U S A **87**(4): 1561-1565.
Kopeikina, K. J., et al. (2011). Tau accumulation causes mitochondrial distribution deficits in neurons in a mouse model of tauopathy and in human Alzheimer's disease brain. Am J Pathol **179**(4): 2071-2082.
Kopeikina, K. J., et al. (2013). Synaptic alterations in the rTg4510 mouse model of tauopathy. J Comp Neurol **521**(6): 1334-1353.
Kutner, K. C., et al. (2000). Lower cognitive performance of older football players possessing apolipoprotein E epsilon4. Neurosurgery **47**(3): 651-657; discussion 657-658.
Lalancette-Hebert, M., et al. (2007). Selective ablation of proliferating microglial cells exacerbates ischemic injury in the brain. J Neurosci **27**(10): 2596-2605.
Lamantia, A. S. and P. Rakic (1990). Cytological and quantitative characteristics of four cerebral commissures in the rhesus monkey. J Comp Neurol **291**(4): 520-537.
Langlois, J. A., et al. (2006). The epidemiology and impact of traumatic brain injury: a brief overview. J Head Trauma Rehabil **21**(5): 375-378.
Laskowitz, D. T., et al. (2007). COG1410, a novel apolipoprotein E-based peptide, improves functional recovery in a murine model of traumatic brain injury. J Neurotrauma **24**(7): 1093-1107.
Laskowitz, D. T., et al. (2010). Traumatic brain injury exacerbates neurodegenerative pathology: improvement with an apolipoprotein E-based therapeutic. J Neurotrauma **27**(11): 1983-1995.
Laurer, H. L., et al. (2001). Mild head injury increasing the brain's vulnerability to a second concussive impact. J Neurosurg **95**(5): 859-870.
Le Bihan, D. (2007). The 'wet mind': water and functional neuroimaging. Phys Med Biol **52**(7): R57-90.
Liaquat, I., et al. (2002). Effect of apolipoprotein E genotype on hematoma volume after trauma. J Neurosurg **96**(1): 90-96.
Lieberman, D. M., et al. (1995). Convection-enhanced distribution of large molecules in gray matter during interstitial drug infusion. J Neurosurg **82**(6): 1021-1029.
Lipton, M. L., et al. (2008). Multifocal white matter ultrastructural abnormalities in mild traumatic brain injury with cognitive disability: a voxel-wise analysis of diffusion tensor imaging. J Neurotrauma **25**(11): 1335-1342.
Loane, D. J., et al. (2014). Progressive neurodegeneration after experimental brain trauma: association with chronic microglial activation. J Neuropathol Exp Neurol **73**(1): 14-29.
Longhi, L., et al. (2005). Temporal window of vulnerability to repetitive experimental concussive brain injury. Neurosurgery **56**(2): 364-374; discussion 364-374.

Lund, S., et al. (2005). Inhibition of microglial inflammation by the MLK inhibitor CEP-1347. J Neurochem **92**(6): 1439-1451.
Lynch, J. R., et al. (2002). Apolipoprotein E affects the central nervous system response to injury and the development of cerebral edema. Ann Neurol **51**(1): 113-117.
Mac Donald, C. L., et al. (2007a). Diffusion tensor imaging reliably detects experimental traumatic axonal injury and indicates approximate time of injury. J Neurosci **27**(44): 11869-11876.
Mac Donald, C. L., et al. (2007b). Detection of traumatic axonal injury with diffusion tensor imaging in a mouse model of traumatic brain injury. Exp Neurol **205**(1): 116-131.
Mahley, R. W. (1988). Apolipoprotein E: cholesterol transport protein with expanding role in cell biology. Science **240**(4852): 622-630.
Mannix, R., et al. (2013). Clinical correlates in an experimental model of repetitive mild brain injury. Ann Neurol **74**(1): 65-75.
Mannix, R. C., et al. (2011). Age-dependent effect of apolipoprotein E4 on functional outcome after controlled cortical impact in mice. J Cereb Blood Flow Metab **31**(1): 351-361.
Margulies, S. S., et al. (1990). Physical model simulations of brain injury in the primate. J Biomech **23**(8): 823-836.
Marmarou, A., et al. (1994). A new model of diffuse brain injury in rats. Part I: Pathophysiology and biomechanics. J Neurosurg **80**(2): 291-300.
Maxwell, W. L. and D. I. Graham (1997). Loss of axonal microtubules and neurofilaments after stretch-injury to guinea pig optic nerve fibers. J Neurotrauma **14**(9): 603-614.
Maxwell, W. L., et al. (1995). Cytochemical evidence for redistribution of membrane pump calcium-ATPase and ecto-Ca-ATPase activity, and calcium influx in myelinated nerve fibres of the optic nerve after stretch injury. J Neurocytol **24**(12): 925-942.
Mayeux, R., et al. (1995). Synergistic effects of traumatic head injury and apolipoprotein-epsilon 4 in patients with Alzheimer's disease. Neurology **45**(3 Pt 1): 555-557.
Mazerolle, E. L., et al. (2013). Intra-individual variability in information processing speed reflects white matter microstructure in multiple sclerosis. Neuroimage Clin **2**: 894-902.
McCrea, M., et al. (2003). Acute effects and recovery time following concussion in collegiate football players: the NCAA Concussion Study. JAMA **290**(19): 2556-2563.
McCrory, P., et al. (2009). Consensus statement on concussion in sport - the Third International Conference on Concussion in Sport held in Zurich, November 2008. Phys Sportsmed **37**(2): 141-159.
McKee, A. C., et al. (2009). Chronic traumatic encephalopathy in athletes: progressive tauopathy after repetitive head injury. J Neuropathol Exp Neurol **68**(7): 709-735.
McKee, A. C., et al. (2013a). The spectrum of disease in chronic traumatic encephalopathy. Brain **136**(Pt 1): 43-64.
McKee, A. C., et al. (2013b). The spectrum of disease in chronic traumatic encephalopathy. Brain **136**(Pt 1): 43-64.
Meehan, W. P., 3rd, et al. (2012). Increasing recovery time between injuries improves cognitive outcome after repetitive mild concussive brain injuries in mice. Neurosurgery **71**(4): 885-891.
Micheva, K. D. and S. J. Smith (2007). Array tomography: a new tool for imaging the molecular architecture and ultrastructure of neural circuits. Neuron **55**(1): 25-36.
Milman, A., et al. (2005). Mild traumatic brain injury induces persistent cognitive deficits and behavioral disturbances in mice. J Neurotrauma **22**(9): 1003-1010.
Mittl, R. L., et al. (1994). Prevalence of MR evidence of diffuse axonal injury in patients with mild head injury and normal head CT findings. AJNR Am J Neuroradiol **15**(8): 1583-1589.
Mizuno, T., et al. (2003). Production and neuroprotective functions of fractalkine in the central nervous system. Brain Res **979**(1-2): 65-70.

Monif, M., et al. (2009). The P2X7 receptor drives microglial activation and proliferation: a trophic role for P2X7R pore. J Neurosci **29**(12): 3781-3791.
Moretti, L., et al. (2012). Cognitive decline in older adults with a history of traumatic brain injury. Lancet Neurol **11**(12): 1103-1112.
Morganti-Kossmann, M. C., et al. (2007). Modulation of immune response by head injury. Injury **38**(12): 1392-1400.
Mortimer, J. A. (1985). Epidemiology of post-traumatic encephalopathy in boxers. Minn Med **68**(4): 299-300.
Mortimer, J. A., et al. (1991). Head trauma as a risk factor for Alzheimer's disease: a collaborative re-analysis of case-control studies. EURODEM Risk Factors Research Group. Int J Epidemiol **20 Suppl 2**: S28-35.
Mouzon, B., et al. (2012). Repetitive mild traumatic brain injury in a mouse model produces learning and memory deficits accompanied by histological changes. J Neurotrauma **29**(18): 2761-2773.
Mouzon, B. C., et al. (2014). Chronic neuropathological and neurobehavioral changes in a repetitive mild traumatic brain injury model. Ann Neurol **75**(2): 241-254.
Movsesyan, V. A., et al. (2004). MGLuR5 activation reduces beta-amyloid-induced cell death in primary neuronal cultures and attenuates translocation of cytochrome c and apoptosis-inducing factor. J Neurochem **89**(6): 1528-1536.
Namjoshi, D. R., et al. (2013). The Liver X Receptor Agonist GW3965 Improves Recovery from Mild Repetitive Traumatic Brain Injury in Mice Partly through Apolipoprotein E. PLoS One **8**(1): e53529.
Newton, M. R., et al. (1992). A study comparing SPECT with CT and MRI after closed head injury. J Neurol Neurosurg Psychiatry **55**(2): 92-94.
Nicoll, J. A., et al. (1995). Apolipoprotein E epsilon 4 allele is associated with deposition of amyloid beta-protein following head injury. Nat Med **1**(2): 135-137.
Nilsson, P., et al. (1990). Changes in cortical extracellular levels of energy-related metabolites and amino acids following concussive brain injury in rats. J Cereb Blood Flow Metab **10**(5): 631-637.
Niogi, S. N. and P. Mukherjee (2010). Diffusion tensor imaging of mild traumatic brain injury. J Head Trauma Rehabil **25**(4): 241-255.
Niogi, S. N., et al. (2008). Extent of microstructural white matter injury in postconcussive syndrome correlates with impaired cognitive reaction time: a 3T diffusion tensor imaging study of mild traumatic brain injury. AJNR Am J Neuroradiol **29**(5): 967-973.
Nolin, P. and L. Heroux (2006). Relations among sociodemographic, neurologic, clinical, and neuropsychologic variables, and vocational status following mild traumatic brain injury: a follow-up study. J Head Trauma Rehabil **21**(6): 514-526.
North, R. A. (2002). Molecular physiology of P2X receptors. Physiol Rev **82**(4): 1013-1067.
O'Jile, J. R., et al. (2006). Information processing following mild head injury. Arch Clin Neuropsychol **21**(4): 293-296.
Oddo, S., et al. (2003). Triple-transgenic model of Alzheimer's disease with plaques and tangles: intracellular Abeta and synaptic dysfunction. Neuron **39**(3): 409-421.
Oehmichen, M., et al. (1999). Is traumatic axonal injury (AI) associated with an early microglial activation? Application of a double-labeling technique for simultaneous detection of microglia and AI. Acta Neuropathol **97**(5): 491-494.
Ohkubo, N., et al. (2003). Apolipoprotein E and Reelin ligands modulate tau phosphorylation through an apolipoprotein E receptor/disabled-1/glycogen synthase kinase-3beta cascade. FASEB J **17**(2): 295-297.
Ojo, J. O., et al. (2013). Repetitive mild traumatic brain injury augments tau pathology and glial activation in aged hTau mice. J Neuropathol Exp Neurol **72**(2): 137-151.

Okonkwo, D. O., et al. (2003). Dose-response of cyclosporin A in attenuating traumatic axonal injury in rat. Neuroreport **14**(3): 463-466.
Okonkwo, D. O., et al. (1998). Alteration of the neurofilament sidearm and its relation to neurofilament compaction occurring with traumatic axonal injury. Brain Res **784**(1-2): 1-6.
Olivares, R., et al. (2001). Species differences and similarities in the fine structure of the mammalian corpus callosum. Brain Behav Evol **57**(2): 98-105.
Omalu, B. I., et al. (2006). Chronic traumatic encephalopathy in a national football league player: part II. Neurosurgery **59**(5): 1086-1092; discussion 1092-1083.
Omalu, B. I., et al. (2005). Chronic traumatic encephalopathy in a National Football League player. Neurosurgery **57**(1): 128-134; discussion 128-134.
Oppenheimer, D. R. (1968). Microscopic lesions in the brain following head injury. J Neurol Neurosurg Psychiatry **31**(4): 299-306.
Orlovska, S., et al. (2013). Head Injury as Risk Factor for Psychiatric Disorders: A Nationwide Register-Based Follow-Up Study of 113,906 Persons With Head Injury. Am J Psychiatry.
Paolicelli, R. C., et al. (2011). Synaptic pruning by microglia is necessary for normal brain development. Science **333**(6048): 1456-1458.
Parkhurst, C. N., et al. (2013). Microglia promote learning-dependent synapse formation through brain-derived neurotrophic factor. Cell **155**(7): 1596-1609.
Perry, V. H. and C. Holmes (2014). Microglial priming in neurodegenerative disease. Nat Rev Neurol.
Pierpaoli, C., et al. (2001). Water diffusion changes in Wallerian degeneration and their dependence on white matter architecture. Neuroimage **13**(6 Pt 1): 1174-1185.
Plassman, B. L., et al. (2000). Documented head injury in early adulthood and risk of Alzheimer's disease and other dementias. Neurology **55**(8): 1158-1166.
Polfliet, M. M., et al. (2001). A method for the selective depletion of perivascular and meningeal macrophages in the central nervous system. J Neuroimmunol **116**(2): 188-195.
Polydoro, M., et al. (2013). Reversal of neurofibrillary tangles and tau-associated phenotype in the rTgTauEC model of early Alzheimer's disease. J Neurosci **33**(33): 13300-13311.
Ponomarev, E. D., et al. (2011). MicroRNA-124 promotes microglia quiescence and suppresses EAE by deactivating macrophages via the C/EBP-alpha-PU.1 pathway. Nat Med **17**(1): 64-70.
Pooler, A. M., et al. (2013). Tau-amyloid interactions in the rTgTauEC model of early Alzheimer's disease suggest amyloid-induced disruption of axonal projections and exacerbated axonal pathology. J Comp Neurol **521**(18): 4236-4248.
Prabhu, S. S., et al. (1998). Distribution of macromolecular dyes in brain using positive pressure infusion: a model for direct controlled delivery of therapeutic agents. Surg Neurol **50**(4): 367-375; discussion 375.
Raghupathi, R., et al. (2004). Traumatic axonal injury is exacerbated following repetitive closed head injury in the neonatal pig. J Neurotrauma **21**(3): 307-316.
Ramlackhansingh, A. F., et al. (2011). Inflammation after trauma: microglial activation and traumatic brain injury. Ann Neurol **70**(3): 374-383.
Reeves, T. M., et al. (2005). Myelinated and unmyelinated axons of the corpus callosum differ in vulnerability and functional recovery following traumatic brain injury. Exp Neurol **196**(1): 126-137.
Rimel, R. W., et al. (1982). Moderate head injury: completing the clinical spectrum of brain trauma. Neurosurgery **11**(3): 344-351.
Roberts, G. W., et al. (1990). The occult aftermath of boxing. J Neurol Neurosurg Psychiatry **53**(5): 373-378.
Roberts, G. W., et al. (1991). beta A4 amyloid protein deposition in brain after head trauma. Lancet **338**(8780): 1422-1423.

Roberts, G. W., et al. (1994). Beta amyloid protein deposition in the brain after severe head injury: implications for the pathogenesis of Alzheimer's disease. J Neurol Neurosurg Psychiatry **57**(4): 419-425.
Saatchi, S., et al. (2012). Three-dimensional microstructural changes in murine abdominal aortic aneurysms quantified using immunofluorescent array tomography. J Histochem Cytochem **60**(2): 97-109.
Saatman, K. E., et al. (2010). Calpain as a therapeutic target in traumatic brain injury. Neurotherapeutics **7**(1): 31-42.
Sabo, T., et al. (2000). Susceptibility of transgenic mice expressing human apolipoprotein E to closed head injury: the allele E3 is neuroprotective whereas E4 increases fatalities. Neuroscience **101**(4): 879-884.
Sanchez Mejia, R. O., et al. (2001). Minocycline reduces traumatic brain injury-mediated caspase-1 activation, tissue damage, and neurological dysfunction. Neurosurgery **48**(6): 1393-1399; discussion 1399-1401.
Saunders, R. L. and R. E. Harbaugh (1984). The second impact in catastrophic contact-sports head trauma. JAMA **252**(4): 538-539.
Sayed, N., et al. (2013). Clinical phenotype of dementia after traumatic brain injury. J Neurotrauma **30**(13): 1117-1122.
Schafer, D. P., et al. (2012). Microglia sculpt postnatal neural circuits in an activity and complement-dependent manner. Neuron **74**(4): 691-705.
Scheff, S. W. and P. G. Sullivan (1999). Cyclosporin A significantly ameliorates cortical damage following experimental traumatic brain injury in rodents. J Neurotrauma **16**(9): 783-792.
Selwyn, R., et al. (2013). Mild traumatic brain injury results in depressed cerebral glucose uptake: An (18)FDG PET study. J Neurotrauma **30**(23): 1943-1953.
Sherriff, F. E., et al. (1994). Early detection of axonal injury after human head trauma using immunocytochemistry for beta-amyloid precursor protein. Acta Neuropathol **87**(1): 55-62.
Shitaka, Y., et al. (2011). Repetitive closed-skull traumatic brain injury in mice causes persistent multifocal axonal injury and microglial reactivity. J Neuropathol Exp Neurol **70**(7): 551-567.
Shultz, S. R., et al. (2012). Repeated mild lateral fluid percussion brain injury in the rat causes cumulative long-term behavioral impairments, neuroinflammation, and cortical loss in an animal model of repeated concussion. J Neurotrauma **29**(2): 281-294.
Simard, A. R., et al. (2006). Bone marrow-derived microglia play a critical role in restricting senile plaque formation in Alzheimer's disease. Neuron **49**(4): 489-502.
Smith, C., et al. (2006). Association of APOE e4 and cerebrovascular pathology in traumatic brain injury. J Neurol Neurosurg Psychiatry **77**(3): 363-366.
Smith, D. H., et al. (2003a). Amyloid beta accumulation in axons after traumatic brain injury in humans. J Neurosurg **98**(5): 1072-1077.
Smith, D. H., et al. (2003b). Diffuse axonal injury in head trauma. J Head Trauma Rehabil **18**(4): 307-316.
Smith, D. H., et al. (1999). High tolerance and delayed elastic response of cultured axons to dynamic stretch injury. J Neurosci **19**(11): 4263-4269.
Song, S. K., et al. (2003). Diffusion tensor imaging detects and differentiates axon and myelin degeneration in mouse optic nerve after retinal ischemia. Neuroimage **20**(3): 1714-1722.
Spain, A., et al. (2010). Mild fluid percussion injury in mice produces evolving selective axonal pathology and cognitive deficits relevant to human brain injury. J Neurotrauma **27**(8): 1429-1438.
Stone, J. R., et al. (2001). Intra-axonal neurofilament compaction does not evoke local axonal swelling in all traumatically injured axons. Exp Neurol **172**(2): 320-331.
Strich, S. J. (1970). Lesions in the cerebral hemispheres after blunt head injury. J Clin Pathol Suppl (R Coll Pathol) **4**: 166-171.

Strittmatter, W. J., et al. (1994). Isoform-specific interactions of apolipoprotein E with microtubule-associated protein tau: implications for Alzheimer disease. Proc Natl Acad Sci U S A **91**(23): 11183-11186.
Strittmatter, W. J., et al. (1993). Apolipoprotein E: high-avidity binding to beta-amyloid and increased frequency of type 4 allele in late-onset familial Alzheimer disease. Proc Natl Acad Sci U S A **90**(5): 1977-1981.
Sullivan, P. M., et al. (1997a). Targeted replacement of the mouse apolipoprotein E gene with the common human APOE3 allele enhances diet-induced hypercholesterolemia and atherosclerosis. J Biol Chem **272**(29): 17972-17980.
Sullivan, P. M., et al. (1997b). Targeted replacement of the mouse apolipoprotein E gene with the common human APOE3 allele enhances diet-induced hypercholesterolemia and atherosclerosis. Journal of Biological Chemistry **272**(29): 17972-17980.
Tang-Schomer, M. D., et al. (2012). Partial interruption of axonal transport due to microtubule breakage accounts for the formation of periodic varicosities after traumatic axonal injury. Exp Neurol **233**(1): 364-372.
Tang-Schomer, M. D., et al. (2010). Mechanical breaking of microtubules in axons during dynamic stretch injury underlies delayed elasticity, microtubule disassembly, and axon degeneration. FASEB J **24**(5): 1401-1410.
Tang, Y. P., et al. (1997a). A concussive-like brain injury model in mice (I): impairment in learning and memory. J Neurotrauma **14**(11): 851-862.
Tang, Y. P., et al. (1997b). A concussive-like brain injury model in mice (II): selective neuronal loss in the cortex and hippocampus. J Neurotrauma **14**(11): 863-873.
Tashlykov, V., et al. (2007). Apoptotic changes in the cortex and hippocampus following minimal brain trauma in mice. Brain Res **1130**(1): 197-205.
Teasdale, G. and B. Jennett (1974). Assessment of coma and impaired consciousness. A practical scale. Lancet **2**(7872): 81-84.
Teasdale, G. M., et al. (2005). The association between APOE epsilon4, age and outcome after head injury: a prospective cohort study. Brain **128**(Pt 11): 2556-2561.
Teasdale, G. M., et al. (1997). Association of apolipoprotein E polymorphism with outcome after head injury. Lancet **350**(9084): 1069-1071.
Tesseur, I., et al. (2000a). Prominent axonopathy and disruption of axonal transport in transgenic mice expressing human apolipoprotein E4 in neurons of brain and spinal cord. Am J Pathol **157**(5): 1495-1510.
Tesseur, I., et al. (2000b). Expression of human apolipoprotein E4 in neurons causes hyperphosphorylation of protein tau in the brains of transgenic mice. Am J Pathol **156**(3): 951-964.
Thurman, D. J., et al. (1998). The epidemiology of sports-related traumatic brain injuries in the United States: recent developments. J Head Trauma Rehabil **13**(2): 1-8.
Tran, H. T., et al. (2011a). Controlled cortical impact traumatic brain injury in 3xTg-AD mice causes acute intra-axonal amyloid-beta accumulation and independently accelerates the development of tau abnormalities. J Neurosci **31**(26): 9513-9525.
Tran, H. T., et al. (2011b). Distinct temporal and anatomical distributions of amyloid-beta and tau abnormalities following controlled cortical impact in transgenic mice. PLoS One **6**(9): e25475.
Uryu, K., et al. (2007). Multiple proteins implicated in neurodegenerative diseases accumulate in axons after brain trauma in humans. Exp Neurol **208**(2): 185-192.
Uryu, K., et al. (2002). Repetitive mild brain trauma accelerates Abeta deposition, lipid peroxidation, and cognitive impairment in a transgenic mouse model of Alzheimer amyloidosis. J Neurosci **22**(2): 446-454.

van der Naalt, J., et al. (1999). One year outcome in mild to moderate head injury: the predictive value of acute injury characteristics related to complaints and return to work. J Neurol Neurosurg Psychiatry **66**(2): 207-213.
Varvel, N. H., et al. (2012). Microglial repopulation model reveals a robust homeostatic process for replacing CNS myeloid cells. Proc Natl Acad Sci U S A **109**(44): 18150-18155.
Venkatesan, C., et al. (2010). Chronic upregulation of activated microglia immunoreactive for galectin-3/Mac-2 and nerve growth factor following diffuse axonal injury. J Neuroinflammation **7**: 32.
Verghese, P. B., et al. (2011). Apolipoprotein E in Alzheimer's disease and other neurological disorders. Lancet Neurol **10**(3): 241-252.
Viano, D. C., et al. (2009). Concussion in professional football: animal model of brain injury--part 15. Neurosurgery **64**(6): 1162-1173; discussion 1173.
Wang, Y., et al. (2012). IL-34 is a tissue-restricted ligand of CSF1R required for the development of Langerhans cells and microglia. Nat Immunol **13**(8): 753-760.
Wang, Y., et al. (2011). Quantification of increased cellularity during inflammatory demyelination. Brain **134**: 3587-3598.
Watkins, L. R., et al. (1997). Evidence for the involvement of spinal cord glia in subcutaneous formalin induced hyperalgesia in the rat. Pain **71**(3): 225-235.
Wilde, E. A., et al. (2008). Diffusion tensor imaging of acute mild traumatic brain injury in adolescents. Neurology **70**(12): 948-955.
Yaghmai, A. and J. Povlishock (1992). Traumatically induced reactive change as visualized through the use of monoclonal antibodies targeted to neurofilament subunits. J Neuropathol Exp Neurol **51**(2): 158-176.
Yan, Q., et al. (2003). Anti-inflammatory drug therapy alters beta-amyloid processing and deposition in an animal model of Alzheimer's disease. J Neurosci **23**(20): 7504-7509.
Ye, S., et al. (2005). Apolipoprotein (apo) E4 enhances amyloid beta peptide production in cultured neuronal cells: apoE structure as a potential therapeutic target. Proc Natl Acad Sci U S A **102**(51): 18700-18705.
Zhan, Y., et al. (2014). Deficient neuron-microglia signaling results in impaired functional brain connectivity and social behavior. Nat Neurosci **17**(3): 400-406.
Zhang, B., et al. (2012). The microtubule-stabilizing agent, epothilone D, reduces axonal dysfunction, neurotoxicity, cognitive deficits, and Alzheimer-like pathology in an interventional study with aged tau transgenic mice. J Neurosci **32**(11): 3601-3611.
Zhang, K., et al. (2010). Are functional deficits in concussed individuals consistent with white matter structural alterations: combined FMRI & DTI study. Exp Brain Res **204**(1): 57-70.
Zhang, L., et al. (2006). Diffusion anisotropy changes in the brains of professional boxers. AJNR Am J Neuroradiol **27**(9): 2000-2004.
Zhao, P., et al. (2007). Extracellular signal-regulated kinase-regulated microglia-neuron signaling by prostaglandin E2 contributes to pain after spinal cord injury. J Neurosci **27**(9): 2357-2368.
Zohar, O., et al. (2003). Closed-head minimal traumatic brain injury produces long-term cognitive deficits in mice. Neuroscience **118**(4): 949-955.

APPENDIX

TABLE A1: REVIEW OF EXPERIMENTAL MODELS OF MILD TRAUMATIC BRAIN INJURY AND CONCUSSION IN RAT AND MOUSE

Reference	Organism	Injury Description	Endpoints	Main findings
Nilsson et al. 1990	rat	Single mild 1.5 or 2.5 mm controlled cortical impact (piston)	240 minutes	Performed microdialysis and measured energy metabolites after injury, GABA, taurine, glutamate and aspartate were all altered over 240 minute timecourse.
Kanayama et al. 1996	rat	7x daily 1.0 atm fluid percussion injuries	1 week, 1 month	Abnormal MAP2, tau, and neurofilament (IHC) in perikarya and impaired behavior (novel environment)
Tang et al. 1997	mouse	Single weight drop injury	12 hours—3 weeks	46% mortality, 23% skull fracture, edema, impaired MWM performance, cell loss (Cresyl violet)
Han et al. 2000	mouse	Single weight drop (Tang et al.)		Widespread neurodegeneration in CA2/3 and increased GFAP in APOE-/- mice
Laurer et al. 2001	mouse	2x daily pneumatic impacts with rubber tip	3, 7, 14, 21, 28, 56 days	Impaired rotarod, no change in MWM. Reduced neuroscore that recovered by 14 days. APP in thalamus at 28 days, no cell loss or MAP2 loss
DeFord et al. 2002	mouse	1-4x weight drop injuries (50 g, 100 g, 150 g masses)	3 hours, 2 and 12 days	Determined weight drop parameters that resulted in 100% survival, no skull fractures, no cell loss (cresyl violet), repetitive injury produced MWM impairments
Uryu et al. 2002	mouse	2x daily pneumatic impacts with rubber tip (Laurer et al.)	2 days, 9 or 16 weeks	Repetitive injury increased amyloid deposition in Tg2576 mice. Slight MWM deficits 16 weeks after repetitive injury but not single injury. No cell loss, sparse GFAP.
Zohar et al. 2003	mouse	20, 25, or 30 g single weight drop injury	7, 30, 60, or 90 days	Injury impaired MWM performance in all groups that last to 90 days. No histological abnormalities (MRI)
Creeley et al. 2004	mouse	3x 21 g daily weight drop injuries		Contra-coup argyrophilic injury. Small group differences in MWM (increased path length to platform)
Conte et al. 2004	mouse	2x daily pneumatic impacts with rubber tip (Laurer et al.)	8 weeks	Vitamin E supplementation for 8 weeks post injury reduced MWM deficits and amyloid deposition in Tg2576 mice.
Longhi et al. 2005	mouse	1x or 2x pneumatic impacts with rubber tip, 3, 5, or 7 day interval (Laurer et al.)	72 hours and 1 week	Mice have MWM deficits with up to a 5 day injury interval between 2 hits, not in the single hit group. Fluorojade B in ipsilateral cortex, increased APP in white matter (semiquantitative analysis), reduced MAP2

Reference	Organism	Injury Description	Endpoints	Main findings
Milman et al. 2005	mouse	30 g single weight drop injury (Zohar et al.)	7, 30, 60, 90 days	Deficits in swimming T maze, forced swim tests, and passive avoidance at sporadic intervals post-injury
Tashlykov et al. 2007	mouse	15,20,25,30 g weight drop (Zohar et al.)	72 hours	Apoptosis after injury
Abdel Baki et al. 2009	rat	Single controlled cortical impact (1.0 mm, 3 m/s or 2.5 mm, 4 m/s)	7 days or 3 weeks	No difference in open field and passive avoidance. Increasingly difficult avoidance tests were used to discriminate sham, mild, and moderate TBI groups.
Hamberger et al. 2009	rat	1x or 3x ballistic weight impactor, unfixed, helmeted head (Viano et al.)	10 days	Multiple injuries produced NF200 accumulation, increased gfap, hemorrhages and edema.
Israelson et al. 2009	mouse	Single 30 g weight drop (Zohar et al.)	4, 22 hours, 3 and 7 days	Increased transcription of genes involved in inflammation (qPCR)
Viano et al. 2009	rat	1x or 3x (every 6 hours) ballistic weight impacts, unfixed, helmeted head	1, 4 or 10 days	11-33% of rats had focal brain injury or hemorrhage and increased bleeding after 3 hits. Head acceleration reached 450g to 1750g without skull fracture.
Spain et al. 2010	mouse	Single mild (0.9 atm) fluid percussion injury	4, 24, 72 hours, 4 and 6 weeks	No difference in MWM performance, few injured neurons (H&E), increased APP in external capsule at 24 hours and in thalamus at 4 and 6 weeks. No clear changes in myelin
Creed et al. 2011	mouse	Single pneumatic impact with 5mm metal tip, midline between lambda and bregma	24 hours, 3, 7, 14 days	MWM deficits on days 1-3 post-injury but not 4-6. Increased APP in corpus callosum and external capsule at 24 hours and 3 days, increased SMI-32 at 24 hours. Increased axonal Fluorojade B at 7 and 14 days. Reduced myelinated axon CAP amplitude at 24 hours and 14 days. Increased unmyelinated axon refractoriness at 14 days.
Davidsson et al. 2011	rat	Single rotational acceleration (0.3-2.1 Mrad/s	2 hours-7 days	1.0 Mrad/s^2 or above produced axonal injury (APP, silver), upregulated Cox2, elevated serum S100β

Reference	Organism	Injury Description	Endpoints	Main findings
Goldstein et al. 2012	mouse	Single blast injury, unfixed head	2 weeks	Increased GFAP, SMI-31, tau labeling in cortex and hippocampus
Kane et al. 2012	mouse	5x or 10x daily weight drop in unrestrained mouse	4 hours, 5 and 30 days	Increased GFAP, increased tau phosphorylation at 30 days (Western Blot), mixed results in rotarod testing
Meehan et al. 2012	mouse	1x, 3x, 5x, or 10x 54 g weight drop, unfixed head	24 hours, 1 month, 1 year	Mice that received weekly impacts performed worse on MWM but mice that received monthly impacts did not. Deficits were apparent when testing began at 24 hours or 1 month post-injury. Small n per group.
Mouzon et al. 2012	mouse	1x or 5x electromagnetic impact with 5mm metal tip every 48 hrs	24 hours, 10 days	1x and 5x injuries had impaired rotarod and Barnes maze performance, increased APP, GFAP, microglia in corpus callosum and brainstem.
Shultz et al. 2012	rat	1x, 3x, or 5x (1-1.5 atm) fluid percussion injury every 5 days	24 hours or 8 weeks	5x group had impaired elevated plus maze and forced swim test, 3x and 5x had impaired MWM. No changes in beam walk, open-field or social behavior tasks. 3x and 5x had more microglia in injured cortex. Large areas of cortical damage in 3x and 5x groups.
Hylin et al. 2013	rat	Single mild (1-1.5 atm) fluid percussion injury	5 days	1.0 atm injury did not cause motor or MWM deficits. 1.5 atm had mild motor deficits, impaired MWM, altered cerebral perfusion, reduced FA in cingulum, increased silver staining, APP, iba-1, and GFAP in corpus callosum.
Mannix et al. 2013	mouse	1x, 5x, 7x 54 g weight drop unfixed head, daily, weekly, biweekly, or monthly	2 days, 2 months, 6 months or 1 year	Daily and weekly impacts resulted in impaired MWM performance but biweekly or monthly did not. No T2-weighted MRI abnormalities. No effect of ApoE4 allele in MWM performance
Ojo et al. 2013	mouse	1x or 5x EM impact with 5mm metal tip every 48 hrs (Mouzon et al.)	3 weeks	5x but not 1x injury appeared to increase tau pathology in human tau knock-in mouse line (immunohistochemistry, CP13, RZ3, PHF1). Increased GFAP and CD45. Neuronal injury in CA3 (cresyl violet).
Selwyn et al. 2013	rat	Single mild (1.2 atm) fluid percussion injury	3, 24 or 72 hours, 5, 7, 9, 14, 16 or 21 days	Injury resulted in transient reduction in glucose uptake between 24 hours and 5 days (PET). Motor impairments in beam walk and peg walk. No change in Barnes maze. Possible axonal loss or white matter damage 10 days post-injury. Reduces MAPs in cortex at 10 and 21 days.

Reference	Organism	Injury Description	Endpoints	Main findings
Mouzon et al. 2014	mouse	1x or 5x electromagnetic impact with 5mm metal tip every 48 hrs	6, 12, or 18 months	5x injury mice performed poorly on Barnes maze at all timepoints. No difference in rotarod or elevated plus maze. Iba-1, gfap, and occasional APP was present in corpus callosum at 12 months post-injury. No Aβ or tau changes.

TABLE A2: TRANSGENIC MOUSE LINES FOR MICROGLIAL DEPLETION

Mouse line	Refs	Experimental Model	Result	Mechanism	Specificity
CD11b-TK (Zurich, Switzerland)	(Heppner et al. 2005; Grathwohl et al. 2009; Varvel et al. 2012)	Mouse EAE, Alzheimer's mice (APP_{swe}/PS1 & APP23)	Reduced EAE symptoms, reduced number of microglia by up to 90%, did not alter Aβ	Herpes simplex virus thymidine kinase induces toxicity in CD11b cells after valganciclovir administration	Yes, will selectively deplete monocytes
CD11b-TK (Quebec, Canada)	(Gowing et al. 2006; Simard et al. 2006; Lalancette-Hebert, et al. 2007)	Nerve axotomy, cortical stab, ischemia, Alzheimer's mice (APP_{swe}/PS1)	Reduced EAE symptoms, reduced number of microglia by up to >75%, bone marrow microglia reduced Aβ plaques	Herpes simplex virus thymidine kinase induces toxicity in CD11b cells after ganciclovir administration	Yes, will selectively deplete monocytes
IL34 -/-	(Wang, et al. 2012)		Mice have ~80% fewer microglia	IL34 is required for normal microglial development	Langerhans cells are also affected
CSF1R -/-	(Ginhoux, et al. 2010)		Mice fail to develop microglia	CSF1R is required for microglial development	Osteoclasts are all affected
MAFIA	(Burnett et al. 2004)		70% loss of macrophage in blood, spleen, lung and thymus, >90% loss in bone marrow and peritoneum	FKBP-fas induces apoptosis in Csf1r expressing cells after administration of AP20187	Will deplete macrophage and dendritic cells.
P2Y12 -/-	(Haynes, et al. 2006)	Microglial culture, in vivo cortical laser ablation injury	Microglia failed to extend processes towards nucleotides or injured areas	P2Y12 signaling is required for microglial chemotaxis in response to nucleotides	No, also found on platelets but not found on peripheral macrophage
p38α -/-	(Bachstetter, et al. 2013)	Mouse controlled cortical impact	Microglia do not have altered morphology after brain injury but do have upregulated cytokine production.	Lack of phospho-p38α inhibits microglia activation	No, p38α is ubiquitously expressed
CX_3CR1^{CreER}	(Parkhurst et al. 2013)		99% reduction of microglia (by flow cytometry and iba-1 immunohistochemistry) by day 1 after diphtheria toxin	Tamoxifen-inducible cre recombinase drives expression of diphtheria toxin receptor. Administration of diphtheria toxin depletes microglia	Yes

TABLE A3: PHARMACOLOGICAL COMPOUNDS USED TO MANIPULATE MICROGLIA

Compound	Refs	Experimental Model	Result	Mechanism	Specificity
Mac-1-Saporin	(Dommergues et al. 2003; Garcia-Alloza et al. 2007; Zhao et al. 2007)	Rat spinal cord injury, cortical stab, PSAPP mice	Application of Mac-1-Sap reduced microglial number	Binds to CD11b and toxin is internalized	Yes, will only bind to monocytes
Minocycline	(Bye et al. 2007; Kim et al. 2009)	TBI, ischemia, ALS, etc.	Reduced microglial activation by histology and ELISA	No clear mechanism, thought to act through P38 but could be indirect	No, may work through neurons
CHPG	(Movsesyan, et al. 2004; Byrnes et al. 2009a; Byrnes et al. 2009b)	Rat spinal cord injury	Treatment reduced TNFα, NO, ROS	Agonist of mGluR5, blocks expression of NADPH oxidase in microglia	No, mGluR5 present on other cell types
Brilliant Blue G	(North 2002; Monif et al. 2009)	Primary microglial cultures, spinal cord injury	Reduced microglial markers, TNFα, iNOS, NADPH oxidase	Selective P2X7 receptor antagonist	Primarily expressed in macrophage
miR-124	(Ponomarev et al. 2011)	Mouse EAE	Peripheral miR-124 suppressed EAE	Inhibition of C/EBP-α and PU.1 (transcription factors)	No, miR-124 regulates many pathways
CX3CL1	(Mizuno, et al. 2003)	LPS activated microglial cell cultures	Fractalkine suppressed TNFα, NO, IL-6	Not clear, may be NF-κB	Yes
D-JNKI1	(Benakis, et al. 2010)	MCAo	No effect on microglial activation, contrary to in vitro results	No clear mechanism, could be indirect	No
COG1410	(Laskowitz et al. 2007)	Mouse TBI	Reduced microglial activation	No clear mechanism, could be indirect	No
Ibuprofen	(Yan, et al. 2003)	Tg2576 mice	Reduced CD45, CD11b	Multiple targets	No
CEP-1347	(Lund, et al. 2005)	LPS stimulated cell cultures and mice	Reduced TNFα after LPS in vitro and in vivo	MLK inhibitor seems to work through P38/JNK	No
Fluorocitrate	(Hassel, et al. 1992; Watkins, et al. 1997)	Formalin hyperalgesia	Injected into spinal cord, blocked hyperalgesia	Inhibits glial Krebs cycle enzyme	NA
Chlodronate Liposomes	(Polfliet, et al. 2001; Hawkes, et al. 2009)	Wild-type rats, TgCRND8 mice	Injected into lateral ventricle, reduced perivascular macrophage	Ingested by phagocytic cells to induce toxicity	Yes, but limited penetration in brain

PROTOCOL: RE-SECTIONING BRAIN SLICES FOR HISTOLOGY

Adapted from (Crawford, et al. 2009a)

Gelatin Recipe (for 100 mls)

7.5g gelatin

15g sucrose

to 100ml with ddH2O

1) Heat to 50℃ to dissolve gelatin and sugar. Ali quot in plastic conicals and store at 4℃.
2) To use gelatin, reheat to 35-40℃.
3) Place drop of warm gelatin in a cryomold (cat#62534-25, E.M.S.) and immediately place the slice on top of the gelatin. Use a paintbrush to smooth the surface of the section so that it is flat—it helps to do this over ice so that the gelatin will start to firm up and adhere to the slice.
4) Cover with a second layer of gelatin—do not allow the first layer to completely set before doing this as the layers will separate later.
5) Allow gelatin blocks to cool for 1 hour at 4℃. Then remove the cryomolds and trim some of the excess gelatin from around the slice with a razor blade.
6) Once blocks have chilled, remove from cryomolds and place in 4% PFA overnight
7) Transfer to 30% sucrose PBS overnight.
8) Section on a freezing microtome you normally would, taking care to line up the face of the section as best as you can with the blade—this should yield 3-4 good 50 micron sections per 300-400 micron slice.